Physico-chemistry of zirconia to titanium brazing using pure gold : wetting and interfacial reactivity

Marie Fischer

THÈSE

Pour obtenir le grade de

DOCTEUR DE L'UNIVERSITÉ GRENOBLE ALPES

Spécialité : 2MGE : Matériaux, Mécanique, Génie civil, Electrochimie

Arrêté ministériel : 25 mai 2016

Présentée par

Marie FISCHER

Thèse dirigée par **Fiqiri HODAJ**, Professeur des Universités, Université Grenoble Alpes
et co-encadrée par **Valérie CHAUMAT**, Docteure-Ingénieure de recherche, Université Grenoble Alpes, CEA Grenoble

préparée au sein du **Laboratoire de Conception et Assemblages du CEA/LITEN/DTCH/SCPC** et du **Laboratoire Science et Ingénierie des Matériaux et Procédés**
dans **l'École Doctorale I-MEP2 - Ingénierie - Matériaux, Mécanique, Environnement, Energétique, Procédés, Production**

Physico-chimie du brasage zircone / titane par l'or pur : mouillage et réactivité interfaciale

Physico-chemistry of zirconia to titanium brazing using pure gold: wetting and interfacial reactivity

Thèse soutenue publiquement le **25 mars 2022**,
devant le jury composé de :

Monsieur Fiqiri HODAJ
PROFESSEUR DES UNIVERSITES, Grenoble INP, Directeur de thèse
Madame Marie-Laurence GIORGI
PROFESSEURE DES UNIVERSITES, CentraleSupélec, Rapportrice
Monsieur Luis Filippe MALHEIROS
PROFESSEUR, Universidade do Porto, Rapporteur
Monsieur Christophe GIRARDEAUX
PROFESSEUR DES UNIVERSITES, Aix-Marseille Université, Examinateur
Monsieur Jean-Michel MISSIAEN
PROFESSEUR DES UNIVERSITES, Grenoble INP, Président
Madame Valérie CHAUMAT
DOCTEURE-INGENIEURE DE RECHERCHE, Université Grenoble Alpes, CEA Grenoble, Co-encadrante de thèse, Invitée
Monsieur Guillaume TOURREL
INGENIEUR, Société Oticon Medical, Invité

Remerciements

J'ai eu l'immense chance d'avoir été encadrée par deux personnes aussi compétentes sur les plans scientifique et pédagogique, qui ont su me transmettre le goût de la recherche et d'innombrables connaissances et compétences que je mettrai à profit dans ma carrière d'ingénieure-chercheuse. Alors merci, Fiqiri et Valérie, pour votre dévouement dans vos rôles respectifs de directeur et d'encadrante, avec tant de bienveillance et toujours dans la bonne humeur. Merci Fiqiri pour votre patience et pour les centaines d'heures que vous avez consacré à nos discussions scientifiques enrichissantes dans le but de me faire progresser tout au long de la thèse. Merci Valérie de m'avoir transmis ton impressionnant savoir-faire et ta rigueur, avec une humanité inégalable qui me manque déjà …

Je remercie également chaudement Guillaume, mon encadrant industriel, sans qui cette thèse n'aurait jamais vu le jour, et sans qui je n'aurais jamais eu le courage de me lancer dans un doctorat ! Merci Guillaume de m'avoir fait confiance depuis mon école d'ingénieur jusqu'à aujourd'hui puisque nous sommes maintenant collègues !

Je tiens à remercier tous les membres du jury de m'avoir fait l'honneur de juger mon travail de thèse. Premièrement, le président M. Missiaen et le rapporteur M. Girardeaux, pour la discussion scientifique enrichissante sans perdre de vue la problématique industrielle. Ensuite, les rapporteurs Mme. Giorgi et M. Malheiros pour leur lecture approfondie du manuscrit et leurs remarques pertinentes.

J'adresse ensuite mes remerciements à tous les membres du laboratoire LCA, en particulier au chef de laboratoire Philippe Emonot, et mes collègues avec qui j'ai partagé quatre années de thèse dans la bonne humeur et qui ont tous participé, d'une manière ou d'une autre, à la réussite de ce doctorat : Isabelle C, Carole, Isabelle M, Thierry, Bruno, Julien, Lisa, Olivier, Sebastien, Laurent, Emmanuel, Jean-Marie, José, Willy, Fabien, Matthieu, Rayissa, PEF, Laurence et Mattias. Je remercie particulièrement Valérie Merveilleau pour son aide précieuse et quotidienne, son professionnalisme, sa bienveillance, sa gentillesse, son humour et son écoute lors de nos longues discussions ! Pour la bonne ambiance quotidienne, je remercie tous mes collègues stagiaires, thésards, alternants et post-doc, en particulier Agathe, Sarah, Lucas, Marie, Oualid, Camille, Maxime, Clara et big up à mes précieux amis Meryem et Simon. Meryem, je n'oublierai jamais l'accueil que tu m'as fait en arrivant dans la team brasage, et tout ce que tu m'as transmis.

Je remercie les spécialistes de la caractérisation, en particulier ceux de la PFNC : François et Camille pour leurs analyses MEB-FEG et TEM (et les superbes images !) et Olivier pour la DRX, ainsi que les spécialistes du SIMAP Stéphane et Thierry pour la DRX, Gregory pour l'XPS et Hervé le spécialiste du capricieux four sans qui toutes mes manip de goutte déposée seraient tombées à l'eau !

Ces quatre années, bien qu'elles soient passées vite, ont été longues loin de ma famille et de mes amis. Je remercie mes parents d'avoir fondé une famille (parfaite) si unie, que même la distance n'a pu, et ne pourra éloigner. Merci aussi à tous mes chers amis d'avoir rendu ma vie plus belle. Et surtout, merci à mon soleil Lilie d'avoir été le bébé le plus sage, souriant et adorable de la terre pendant mes longues journées de rédaction ; merci de me combler d'amour.

Arnaud, je te dédie ce manuscrit, car il met ENFIN fin à mes longues années d'études, durant lesquelles tu as toujours été là. Merci de m'avoir suivi à Grenoble (après Limoges et Antibes), de m'avoir toujours soutenu dans mes choix et d'avoir fait tant de sacrifices pour qu'on partage notre quotidien. Merci d'avoir pris soin de nous lorsque je vivais « rédaction », et merci d'avoir supporté ma fatigue ! Tu rends mon quotidien meilleur, et je suis honorée de partager ta vie, toi qui es la plus belle personne que je connaisse.

Contents

General introduction and industrial context

What would be our perception of the world without our ability to hear ? A world without the song of birds, a world devoid of words, laughter and music. A world deaf to our vital need for communication. And yet, one child in a thousand is born deep deaf, and at three years old, three out of a thousand children have severe or deep deafness, impacting language development. Since 1976, a medical device revolutionized the treatment of severe or deep deafness : the cochlear implant. Since its creation, more than one million of cochlear implants were implanted, allowing deaf people to access the world of sound. This implant is intended for both deaf-born children and also people who have lost hearing because of an infectious disease or a major sound trauma for instance.

This electronic medical device transforms sounds into electrical signals which are directly sent to the auditory nerve. A cochlear implant consists of two components presented in Figure 1 : an external part and an internal cochlear implant.

The external part is composed of a sound processor placed behind the ear, and a lead which connects the processor to an antenna. This antenna is magnetically tied to the skin exactly over the internal cochlear implant.

The internal part is a receiver that is surgically slid underneath the skin on the temporal bone. This electronic stimulating device generates electrical impulses that are transmitted to the auditory nerve via an electrode array implanted in the cochlea. In order to protect the electronic receiver from chemical and physical stresses, it is encapsulated in a hermetic housing (Figure 1b).

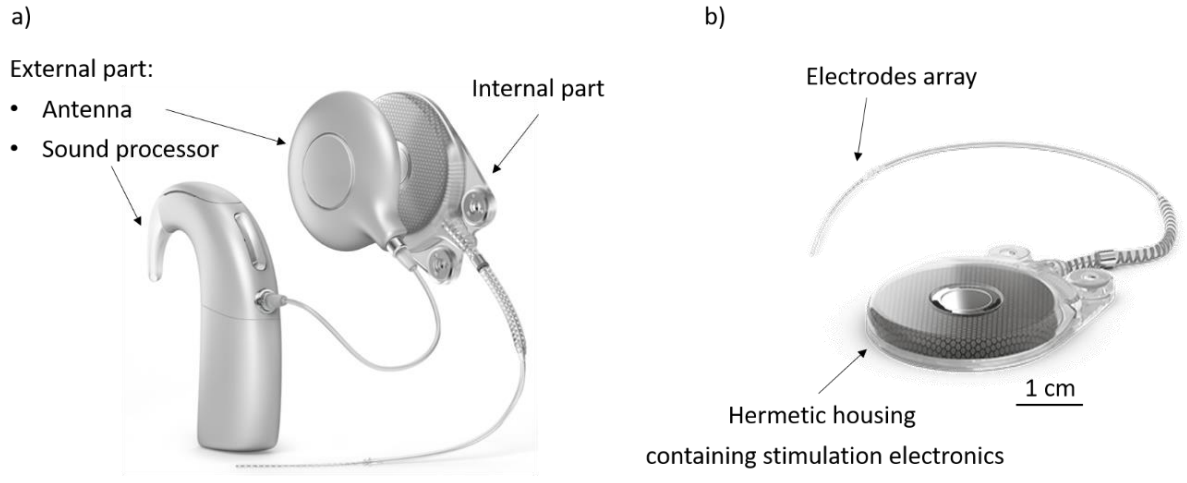

Figure 1: Pictures of a cochlear implant from Oticon Medical : a) the whole system composed of the external and internal parts, b) internal part.

The upper part of the implant casing is in ceramic. This material is used for its transparency to electromagnetic field radio frequency permeability and to reduce magnetic interactions during

medical examinations (such as magnetic resonance imaging). The lower part of the implant housing is made of pure titanium for its fineness, its excellent mechanical and corrosion resistance. Indicatively, the implant housing has a diameter ϕ = 29.2mm, and a thickness h = 3.8 mm.

The solution used to joint ceramic to titanium is brazing. This technique consists of melting a filler metal between the two substrates to be assembled. Two categories of brazed assemblies are distinguished : *similar brazing* when the materials to be brazed are of the same nature (metal / metal, ceramic / ceramic, etc…) and *dissimilar brazing* when materials are of different natures (metal / ceramic, metal / composite, metal / glass, etc…). In the specific case of this cochlear implant housing, we talk about dissimilar brazing. As substrates, the filler metal must be biocompatible, thus it consists of noble metals such as Au or Ag.

The success of brazing depends on several conditions. In order to obtain a good adhesion between the materials to be assembled and the filler metal, a good *wetting* is necessary. On the other hand, the bonds formed at the interfaces, by chemical interactions, must be strong. Finally, at the end of the thermal cycle used to join, when the temperature is decreased from the brazing temperature to room temperature, thermomechanical stresses are generated as soon as the brazing alloy solidifies due to the difference in coefficient of thermal expansion between the materials to be assembled (especially in the case of dissimilar brazing), and also with the brazing alloy.

In the case of similar brazing of metals, wetting occurs by forming strong metal bondings, leading to a good adhesion between the assembled metals. This is more complex when ceramic is involved in the brazed assembly (ceramic / ceramic or ceramic / metal brazing). Indeed, ceramics such as alumina or zirconia are not wetted by noble metals (Au, Cu, Ag, etc …). Two approaches are considered to address this challenge :

- The metallization of ceramic by an active element (Ti or Zr for instance).
- The use of a reactive brazing alloy consisting of a noble metal and a reactive element (Ti, Zr, etc…) to ensure ceramic wetting thanks to the formation of a reaction product layer, wettable by the braze.

Historically, in the field of electronic medical device (such as defibrillators, neurostimulators, cochlear implants, etc…), the ceramic usually used is high purity alumina, so that the older Oticon Medical generation of cochlear implant housing was made of alumina 99.5%. Recently, new standards raised the threshold requirement of mechanical resistance for cochlear implant, in particular by imposing an impact test. In general, ceramics have low elasticity (high Young's modulus) compared with metals, so a moderate resistance to mechanical shocks. Thus, alumina found its limits since its fracture toughness (i.e. its ability to resist cracking due to an impact wave) is quite low (K_{IC} ~ 4 – 5 MPa.$m^{1/2}$). Therefore,

zirconia, and particularly the Yttria Tetragonal Zirconia Polycrystal (YTZP), having excellent resistance to mechanical shocks with a fracture toughness four times greater than that of alumina (K_{IC} ~ 16 MPa.$m^{1/2}$), was considered.

Concerning this new implant generation, joining of the titanium and zirconia parts of the implant housing is performed in two steps (see Figure 2). First, two titanium ferrules are brazed to zirconia cover by melting and flowing a filler metal into the joint (Figure 2a).

The work of this thesis concerns this sandwich brazed joint.

Then, both Ti ferrules of this brazed assembly are laser-welded to the Ti cover, leading thus to a hermetical closing of the implant housing containing the electronic board (Figure 2b). Notice that hermeticity is a necessary property of the brazed joint ; any loss of hermeticity can damage the electronic board and thus the overall operation of the implant.

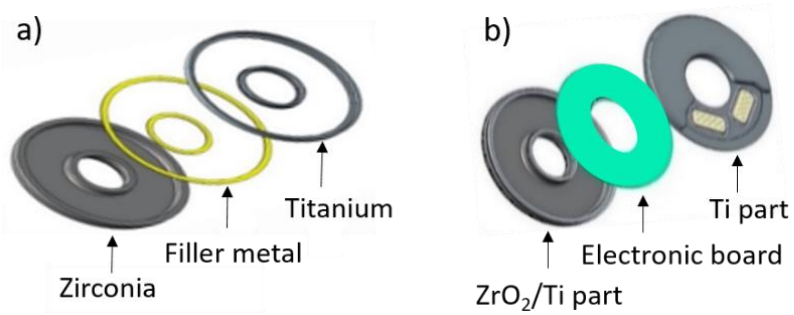

Figure 2: Joining of the implant housing a) zirconia to titanium brazing with preforms of filler metal, b) joining of the zirconia and titanium parts by Ti / Ti laser welding.

Concerning the alumina-to-titanium brazing of the older implant generation, wetting of alumina by the braze was performed thanks to a metallization by Ti active element.

In this study, reactive brazing of zirconia-to-titanium will be investigated: the active element is directly provided by the filler metal, forming at the zirconia / braze interface, a wettable reaction product layer.

The objectives of this study are therefore, on the one hand, to select brazing alloys suitable for the zirconia-to-titanium active brazing, and on the other hand to recommend brazing conditions in order to achieve a hermetic and mechanically strong dissimilar joint. Two reactive elements are investigated: titanium and zirconium.

To reach these objectives, the envisaged methodology is as follows :

- Studies of wetting and reactivity of zirconia (substrate 1) by biocompatible active alloys ; selection of a relevent candidate.
- Wetting and reactivity studies of titanium (substrate 2) by this selected candidate.
- Zirconia-to-titanium brazing : selection of the brazing parameters that lead to a successful joint without defects.
- Deep study of this successfull joint through fine microstructural characterizations and preliminary mechanical tests.

This manuscript consists of four chapters.

The first one is a literature review of wetting, interfacial reactivity and brazing of the two substrates to be assembled : zirconia and titanium.

The second chapter describes zirconia and titanium substrates, the metallic alloys, the experimental methods used to perform the wetting and brazing experiments as well as the hermeticity and mechanical tests.

The third chapter deals with wetting and reactivity studies of both zirconia and titanium substrates.

The last chapter presents the entire zirconia-to-titanium brazing study, composed of a parametric study, a detailed investigation of the reactivity in the selected brazing conditions, and a mechanical characterization of the joint.

Finally, a summary of the main results of this work and some key conclusions and prospects are presented.

Chapter 1 : State of the art

Contents

1. Introduction

This literature review first presents some general aspects of wetting, reactivity and brazing processes. The fundamental equations and dynamic aspect of wetting are described. Then, zirconia interactions with metals and liquid alloys, as well as interfacial interaction between gold and titanium are presented. Finally, a literature review of zirconia brazing is exposed, in both cases of zirconia-to-zirconia joining and dissimilar brazing with titanium.

2. General aspects of wetting and brazing

2.1. General aspect of brazing and relationship with wetting

Brazing is a joining process by melting a metal or filler alloy (braze) with a melting temperature below the melting temperatures of the materials to be joined. The liquid metal or alloy flows over surfaces to form a fillet between components and into the gap between the components, and then solidifies to form a permanent bonding. Joining by brazing is only possible when the liquid braze allows wetting of the components to be assembled (i.e. the contact angle θ is less than 90° (Figure 3b)). Indeed, in the case of bad wetting (i.e. the contact angle θ is higher than 90° (Figure 3a)), the intimate contact between the braze and the substrates to be assembled is not established.

Thus a good wetting of the surfaces to be assembled is a necessary condition to provide an effective brazing. Moreover, in order to obtain a good adhesion, the bonds created at the braze / substrate interfaces have to be mechanically strong. Controlling the interfacial reactivity allows to manage these interfaces, in particular the morphology and thickness of the interfacial reaction product.

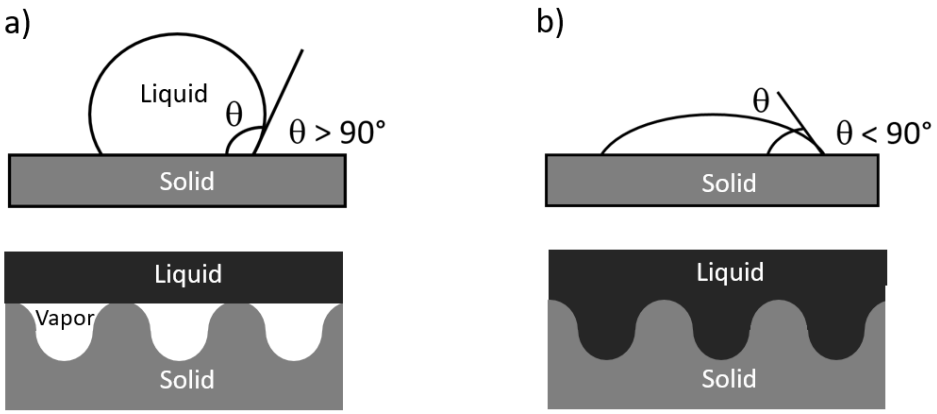

Figure 3: Wetting and brazing, a) Contact angle Θ > 90°, b) Contact angle Θ < 90°.

Notice that the term “brazing” is used when melting temperatures of the filler alloys (brazes) are higher than 450°C, whereas the term “soldering” is preferred for filler alloys (solders) with melting temperature lower than 450°C.

Two brazing configurations are possible: sandwich brazing (Figure 4a), and capillary brazing (Figure 4b). In sandwich brazing configuration, the brazing alloy is placed between the two materials to be assembled. In capillary configuration, the braze is placed nearby the gap between the two materials to be assembled. Liquid braze flows to infill the space by capillary attraction, which is exerted by the substrates.

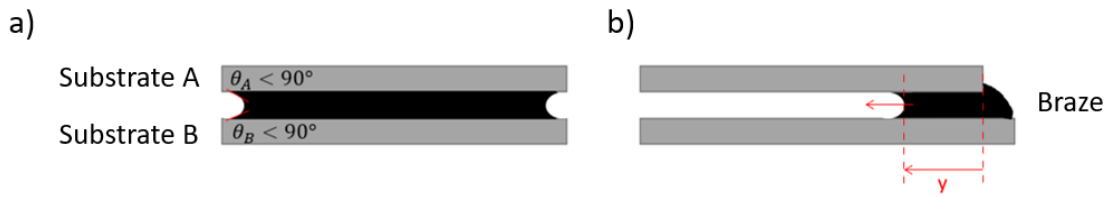

Figure 4: Brazing configurations: a) sandwich brazing, b) capillary brazing (y is the infiltration distance).

The thermodynamic condition of spontaneous infiltration of a liquid metal in a planar capillary gap formed between two solids A and B is $\theta_A + \theta_B < 180°$. For clean metal surfaces, the contact angle θ_{Met} is usually lower than about 50°. Consequently, in the case of metal / ceramic joining (Figure 5), the thermodynamic condition for spontaneous infiltration of a planar metal / ceramic gap is that the contact angle of the liquid metal on the ceramic substrate θ_{Cer} should be lower than about 130°. However, for practical cases of capillary brazing of real rough solid surfaces, the condition $\theta_{Cer} < 90°$ is recommended and even necessary in order to avoid formation of numerous voids on the ceramic side[1]. Indeed, as discussed above, a bad wetting of the ceramic does not assure an intimate ceramic / braze contact (Figure 3a) at atomic scale, inducing thus defects at the ceramic / braze interface like voids.

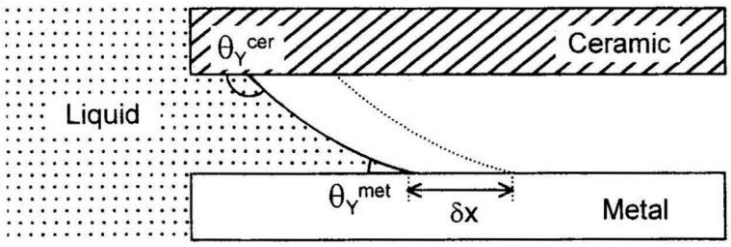

Figure 5: Infiltration of a liquid into a gap between metal and ceramic components[2].

Two categories of brazed assemblies can be discerned: similar and dissimilar brazing. Similar brazing involves assembling two materials with the same nature (metal / metal, ceramic / ceramic, …). Dissimilar brazing consists of assembling two materials with different nature (metal/ceramic,

metal/composite, metal/glass, …). Successfully assembling two types of materials is more difficult because of the difference of the respective physico-chemical and mechanical properties. Upon cooling, after the isothermal holding (brazing), thermomechanical stresses are generated, causing the embrittlement of the brazed assembly, especially for brazes with high melting temperature.

Generally, wetting study precedes brazing study, in order to ensure a good wetting of the surfaces to be assembled, and a good adhesion at the braze / substrate interface. Valuable data are also extracted from the wetting study such as the nature and mechanisms of the occurring phenomena.

Wetting and brazing atmosphere

Wetting study and brazing can be carried out under different controlled atmospheres, in order to reduce, to stop, or in some case, to promote the formation of oxides at the surface of the substrate or the liquid alloy. The possible atmospheres are as follows:

- Chemically inert atmospheres (helium, argon): inert gas prevents the volatilization of some components during brazing.
- Chemically active atmospheres (carbon monoxide, dihydrogen): reducing atmospheres limit the formation of oxides.
- Under air or oxidized atmosphere (controlled partial oxygen pressure): repair of brazed parts, brazing with oxide braze.
- Under vacuum: dissociates some oxides, eliminates impurities initially present or degassing during heat treatment.

In the case of active brazing, with Ti or Zr in the alloy, most of the wetting and brazing experiments are carried out under high vacuum (10^{-5} to 10^{-6} mbar).

2.2. Fundamental equations of wetting and adhesion

2.2.1. Ideal solid surface

The wettability phenomenon is illustrated by the spreading of a liquid drop on a solid surface. In the ideal case there is no chemical reaction between the solid surface (S), the liquid (L) and the vapor phase (V), and the gravitational forces are negligible (i.e. for a drop of liquid of very low mass, typically less than 100 mg). The suitability of the drop for wetting is determined by the contact angle θ formed at the triple line, where solid, liquid and vapor phases are in contact (Figure 6). A liquid is said to be not wetting when the contact angle exceeds 90° (Figure 6a) and wetting when the angle is less than this

value (Figure 6b). In both cases, wetting is said to be partial. Perfect wetting is characterized by a zero contact angle, where the liquid fully spreads over the surface of the solid (Figure 6c).

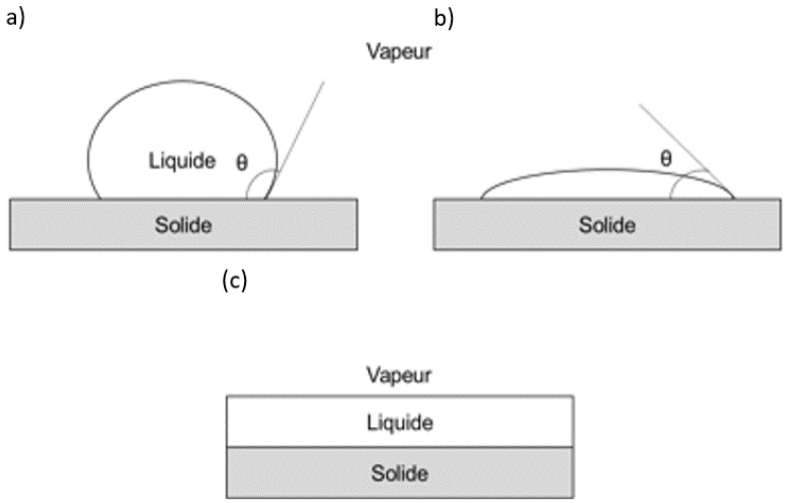

Figure 6: Contact angle configurations: (a) Θ > 90°: non-wetting liquid, (b) Θ < 90°: wetting liquid, (c) Θ = 0°: perfect wetting.

At thermodynamic equilibrium, the relationship between contact angle, surfaces and interfaces energies (Figure 7) can be expressed by the Young's equation:

$$cos\,\theta = \frac{\sigma_{SV}-\sigma_{SL}}{\sigma_{LV}} \qquad (1)$$

In this relation σ_{SV} is the surface energy of the solid in equilibrium with the vapor phase, σ_{SL} the interfacial energy between the liquid and the solid and σ_{LV} the surface energy of the liquid in equilibrium with its vapour. Generally σ_{ij} is defined by the work required to create an additional i/j interface per unit area (in J/m²).

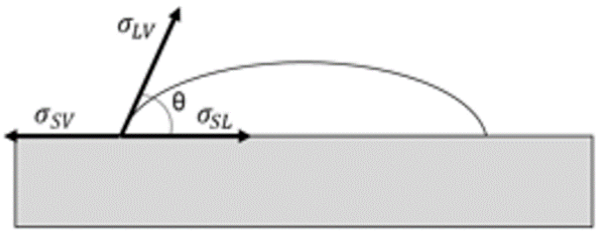

Figure 7: Surface and interface tensions of the liquid, solid and vapor system.

The Young equation *(1)* can also be expressed considering the work of adhesion W_a and the liquid cohesion work W_c.

W_a is the work required to separate a solid/liquid interface in order to create two solid/vapor and liquid/vapor free surfaces:

$$W_a = \sigma_{LV} + \sigma_{SV} - \sigma_{SL} \qquad (2)$$

The liquid cohesion work W_c depends on interaction intensities in the liquid phase, and represents the work required to create two liquid/vapor interfaces from the liquid :

$$W_C = 2\sigma_{LV} \qquad (3)$$

Combining equations *(1)* to *(3)*, the equation giving the contact angle becomes :

$$\cos\theta = 2\frac{W_a}{W_C} - 1 \qquad (4)$$

Therefore, according to equation *(4)* wetting in liquid/solid/vapor system results from the competition between adhesion forces at liquid/solid interface and cohesion forces within the liquid. The adhesion forces promote wetting while the cohesion forces tend to decrease the solid/liquid interface and thus are detrimental to wetting.

Consequently, to obtain an excellent wetting (i.e. contact angle θ ≈ 0°, cos θ = 1), adhesion work value must be equal or almost equal to cohesion work value : $W_a \approx W_c = 2\sigma_{LV}$. This condition can be satisfied only if solid/liquid interfacial bonding are strong (for instance metallic or covalent bonding).

Generally, the surface energies (or surface tensions) of liquid metals increase with the melting temperature (Figure 8). Figure 8 gives a correlation between the surface tension of liquid metals and their molar evaporation enthalpy ΔH_{evap} (J/mol) and molar volume V_m (m^3/mol).

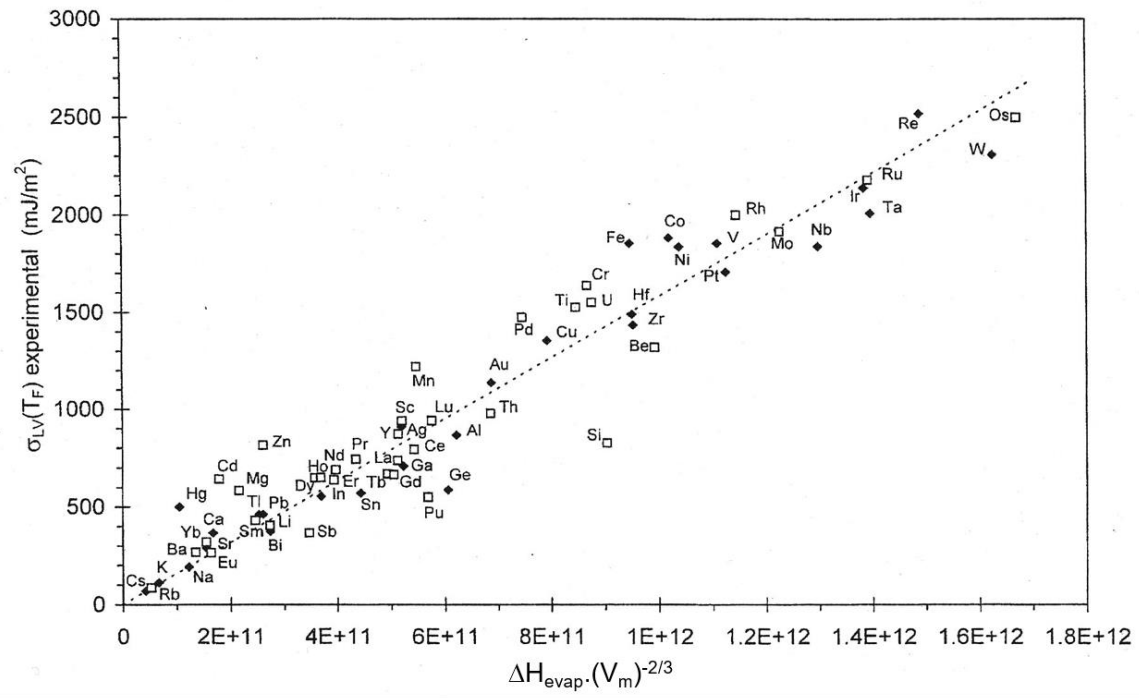

Figure 8: Correlation between liquid metal surface energies and $\Delta H_{evap}.(V_m)^{-2/3}$ (σ = 2.5x10^{-9} $\Delta H_{evap}.(V_m)^{-2/3}$)[1].

2.2.2. Real solid surface

The determination of the thermodynamic contact angle requires special experimental conditions. Substrates must be smooth, flat, perfectly horizontal, chemically homogeneous and inert in relation to the products used in the experiments, and must have an invariable behaviour under the test conditions. Under practical conditions, the measured contact angle θ is between the interval $[\theta_r; \theta_a]$, with θ_a the advancing contact angle and θ_r the receding contact angle (Figure 9).

$$\theta_r < \theta < \theta_a \qquad (5)$$

This phenomenon is called contact angle hysteresis. It is expressed by the difference between the extreme contact angles $\Delta\theta = \theta_a^{max} - \theta_r^{max}$, and results from surface defects such as chemical or topological heterogeneities (roughness, porosity, etc.).

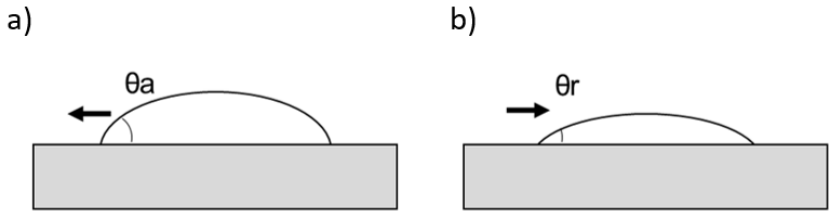

Figure 9: The advancing angle θ_a and the receding contact angle θ_r for a liquid on a non-ideal solid surface.

a) Effect of roughness

Surface roughness of the solid changes the contact angle because of surface irregularities or asperities which slow the movement of the triple line. Indeed, according to Shuttleworth and Bailey[3], the triple line remains blocked by surface defects from the point at which the local contact angle is equal to Young's contact angle (Figure 10). This phenomena is called pinning of the triple line. The measured advancing contact angle θ_a is overestimated (higher than Young's contact angle θ_Y) because it is measured relative to the horizontal plane of the substrate surface. At the microscopic scale, the real contact angle corresponds to θ_Y. In the same way, the receding contact angle θ_r, measured at the macroscopic scale, is underestimated.

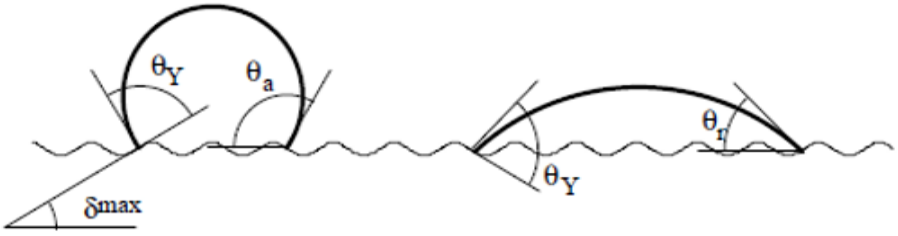

Figure 10: Schematic representation of the roughness impact on the contact angle according to the model of Shuttleworth and Bailey[3].

Notice that Diallo recently studied the pinning phenomena, in the case of wetting on heterogeneous metal-oxides (iron and silica) by a non-reactive liquid metal (lead)[4].

According to recent study from Wu et al.[5], the mechanisms governing the effects of roughness on non-reactive and reactive systems are different.
In the first case of non-reactive systems with a contact angle lower than 90°, roughness significantly improves wetting due to the appearance of additional driving forces when liquid flows over surface roughness microcavities. Thus, the final contact angle obtained is lower than that on a flat surface and therefore the wetting is better.
In the second case of reactive systems, spreading on a rough surface leads to a very low spreading rate because of liquid blocking in surface cavities (pinning of the triple line) resulting in a less good wettability compared to the wetting on a flat surface [5].

In the literature, very few studies describe the influence of surface roughness of the substrate on reactive spreading kinetics. Therefore, the role of roughness is not well established. For instance, Voytovych et al.[6] show that when the alumina roughness varies between 4 nm and 1.3 µm, the spreading kinetics of the reactive alloy Cu – Ag – Ti on alumina at 900°C remains mostly unchanged.
However, Nalagatla[7] shows that the spreading kinetics of the reactive alloys Sn-Pb on a Cu substrate decreases significantly when the roughness increases from 3.8 nm to 180 nm. In the same way, Chen et al.[8] show that the reactive spreading kinetics of a liquid alloy Sn - Bi on a Cu substrate decreases when the roughness increases from 50 nm to 1.8 µm. In addition, the final contact angle increases from 45° to 65° when the roughness R_a increases.

b) Effect of surface heterogeneity

The presence of chemical heterogeneities due to surface contamination, segregation, metal or alloy inclusions on the solid surface, may have effects similar to the surface roughness effects.
Surface heterogeneities may result from oxidation or deoxidation of the substrate surface, occurring in a reductive or oxidizing atmosphere. This concerns metallic substrates as for example in the Pb/Fe system[9] or ceramic substrates as in the case of the TiC/Al system[10]. Substrate phase transformation may also be at the origin of surface modifications, i.e. the diamond graphitization in the Sn/diamond system[11].
That is why working with single-crystal or amorphous substrates with a very high purity is recommended.

Until then, we have discussed static wetting, the case of simple contact between a liquid and a solid surface. One must also consider the spreading of the liquid drop from its initial form to its final equilibrium form. Considering these phenomena, the dynamic aspect of wetting is rather treated.

2.3. Dynamic aspects of wetting

There are two distinct types of wetting :

(i) Non-reactive wetting, when the reactions between the solid and the liquid drop are negligible and the interfacial energies remain constant throughout the wetting process.

(ii) Reactive wetting, when the liquid reacts with the solid by altering the nature and/or morphology of the liquid / solid interface.

2.3.1. Non-reactive wetting

In general, the wetting kinetics is determined by measuring the triple line velocity when the contact angle decreases to its equilibrium value. In order to obtain reproducible results, some conditions must be satisfied, such as: (a) measurements at constant temperature, (b) non-polluted solid and liquid surfaces, (c) controlled roughness of the solid substrate, and (d) neglected external forces.
In the case of non-reactive wetting for spontaneous wetting experiments, i.e. in the absence of external forces, spreading time of a drop depends on its viscosity.

a) Effect of viscosity on spreading rate and shape of liquid metal drop

For a non-wetting system, when a drop of liquid metal is spread on a solid substrate, two shapes of drops are observed.
In the first configuration of inertia spreading (Figure 11a), the drop shape is not spherical. The instantaneous contact angle quickly approaches the final contact angle. Spreading consists of increasing the area of contact of the drop with the solid substrate, while the triple line configuration remains almost unchanged. Thus the spreading rate depends on the speed of the moving mater from the center of the drop to the triple line.

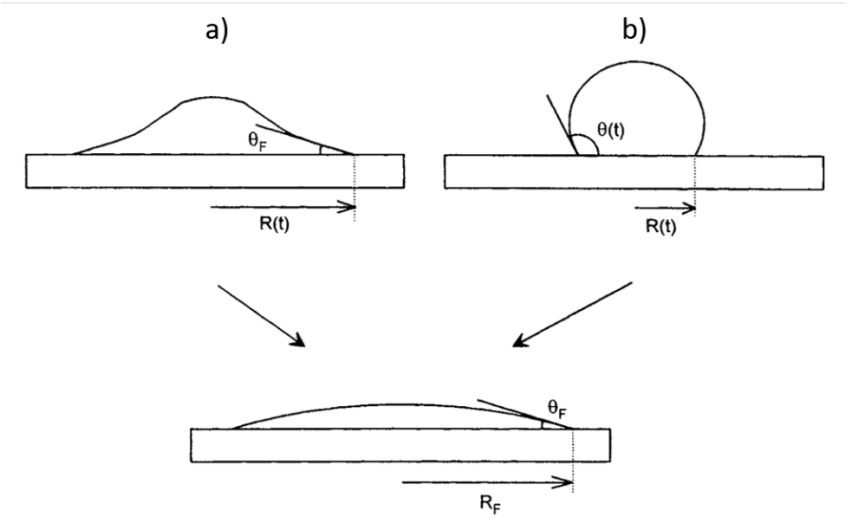

Figure 11: a) Inertial spreading, b) Viscous spreading of a liquid drop of metal in a non-wettable solid/liquid system[1].

This type of spreading is characteristic of low viscosity (η) systems like liquid metals (η ~ 10^{-3} à 10^{-2} Pa.s, see Table 1). This results in a high spreading rate at the triple line. The spreading is controlled by the inertia forces which are responsible for the non-spherical shape of the drop.

Metal	**Au**	**Ag**	**Ga**	**Sn**	**Pb**	**Ni**	**Fe**	**Ti**
Viscosity η (10^{-3} Pa.s)	4.84	4.20	1.95	1.81	4.22	4.61	5.03	2.2
Melting temperature (°C)	1064	962	30	232	327	1453	1576	1668

Table 1: Some metal viscosities at their melting temperature[12].

The wetting study of metal / metal non-reactive systems like Pb/α-Fe[13], Sn/Mo [14]or Sn / Ge [15], and ceramic/metal systems such as Cu/Al_2O_3[1], has shown that the spreading time of the liquid metal drop is in the order of 10^{-2} seconds. This corresponds to spreading rates between 0.5 m/s and 1 m/s[1].

In the second configuration of viscous spreading (Figure 11b) the base radius R varies with time, while the shape of the drop remains spherical. This corresponds to a viscous spreading where the energy dissipation occurs mainly in the liquid near the triple line while the rest of the liquid can move easily, thus maintaining a spherical drop shape.

This type of spreading applies to systems where the liquid material has a high viscosity, for example the ternary liquid SiO_2-Na_2O-TiO_2 which has a viscosity of about 10^2-10^3 Pa.s[16]. Wetting experiments for SiO_2-Na_2O-TiO_2/Pt system show that spreading time is of the order of 100 s and that spreading rate is slow[16].

In general, the spreading time of a millimetric drop with a high viscosity (η > 10 Pa.s) is greater than 100 seconds and the drop keeps a spherical shape throughout the experiment[17]. This indicates the presence of a balance of pressures inside the drop at every moment.

b) Effect of gravity on the spreading kinetics of the liquid drop

In all the above, the effect of gravity on the spreading of the liquid drop is neglected, considering drops with very small size and negligible mass (< 100 mg).

For relatively larger drops, gravity can affect spreading rate in two ways[18]:

- By increasing the value of the final base radius Rf compared to cases where gravity is neglected (Figure 12).
- By decreasing the spreading time, which increases the spreading rate of the drop.

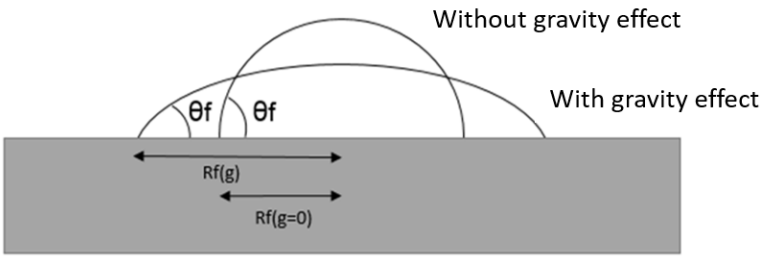

Figure 12: Drop shape with and without gravity effect[1].

Generally, gravity effect on spreading is significant only if the mass of the liquid drop exceeds 100 mg[1]. To sum up, for high viscosity liquids, the spreading rate is very low, it is controlled by the viscosity, and the drop shape remains spherical throughout the test. On the contrary, in the case of low viscosity liquids (such as liquid metals), spreading rate is very high and is controlled by inertial forces.
Gravity can also change the shape and the spreading rate of the liquid drop, generally when the mass of the drop exceeds 100 mg.

2.3.2. Reactive wetting

There are two types of reactivity in the case of reactive wetting: wetting by dissolving solid substrate in liquid metal, and wetting by the formation of a compound at the liquid metal/solid substrate interface by chemical reaction.

2.3.2.1. Dissolutive wetting

The dissolution process of a solid A in a liquid B is illustrated in Figure 13. When a liquid drop of metal B is in contact with a solid A, at a temperature T_0 above the melting temperature of B and below that of A (see Figure 13), solid A will dissolve in liquid B until the A content of the liquid reaches the liquidus of A (C_A^{eq}).

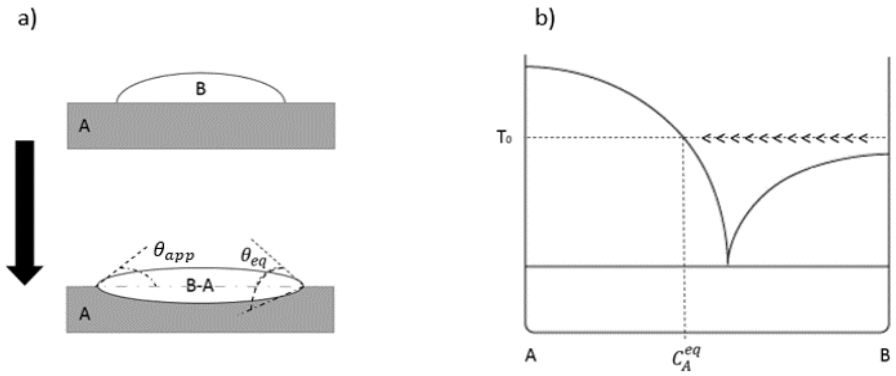

Figure 13: a) Dissolution process of a solid A in a liquid B, b) Schematic phase diagram of the binary A-B system.

The wetting is described as dissolutive when wetting and spreading of the liquid on the solid surface occur at the same time as the dissolution of the solid in the liquid. This phenomenon occurs in many metal/metal systems. It can also happen in some ceramic/metal systems, such as Ni/C[1], Ni/HfB_2 [19] and Ni/SiC [20].

In general, dissolution leads to a decrease in the contact angle through two effects[21]:

- Decrease in surface tension of the liquid, when the surface tension of the solid is lower than the liquid one ($\sigma_{sv} < \sigma_{Lv}$).
- The formation of a "crater" under the drop, so that the apparent contact angle θ_{app} is less than the local equilibrium angle θ_{eq}, formed at the triple line (Figure 13b).

An example of a system where wetting occurs by dissolution of the substrate is shown in Figure 14.

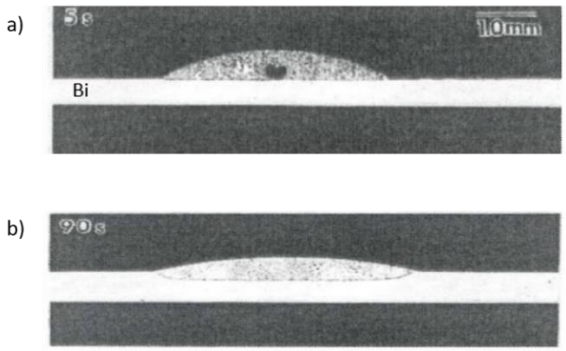

Figure 14: Cross sections of Bi - 20 wt% Sn drops on pure Bi substrates at 245°C, quenched at different times (a) t = 5s, (b) t = 90s [22].

Dissolutive wetting occurs in three characteristic steps (Figure 15)[22]:

Step 1 : Spreading of the liquid on solid is representative of a non-reactive system as described above. The equilibrium contact angle close to Young's angle (Figure 15b) is attained in approximately $t_1 \approx 10^{-2}$ s. There is no change in the morphology of the solid/liquid interface.

Step 2 : The dissolution of the solid in the liquid begins. The geometry of the system is changed at the triple line (the characteristic angle is the apparent angle θ_{app} and the base radius R_2) after $t_2 \approx 10^2$s. For example, in the Bi – 20 wt% Sn system on pure Bi, the interface modification started from times lower than 90s (Figure 14). This step is followed by the diffusion process, induced by the difference in concentrations between the liquid at the solid/liquid interface and the drop bulk.

Step 3 : Afterwards, the shape of the liquid/solid interface is modified to obtain a liquid / solid interface with the same curvature radius everywhere: $t = t_3$ corresponds to the total equilibrium (Figure 15). This last step can be attained after hours, even thousands of hours.

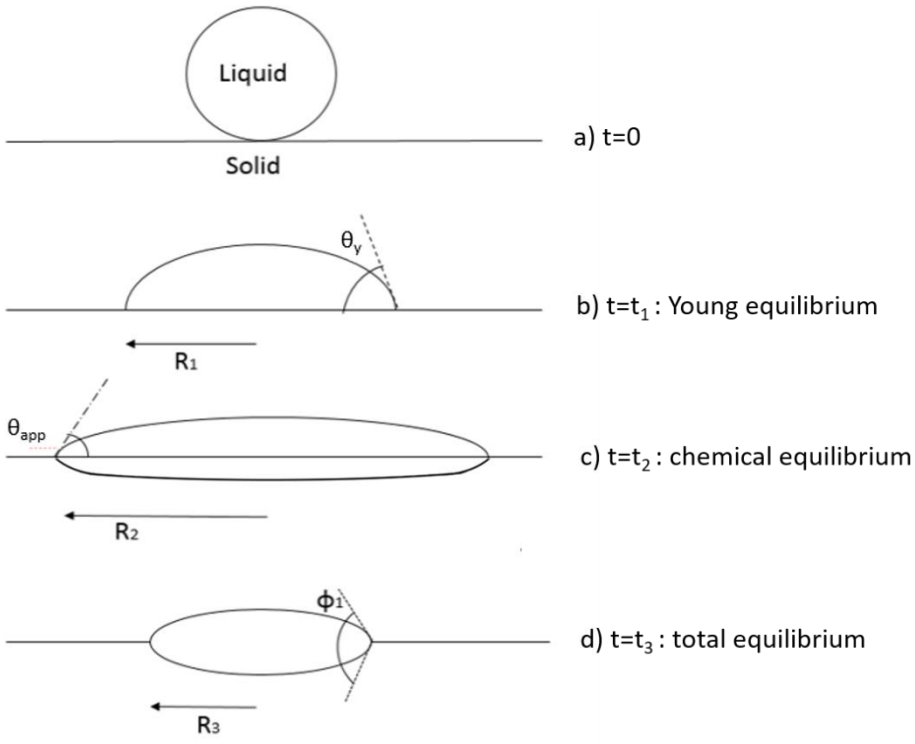

Figure 15: Kinetics of dissolutive wetting according to Warren's et al model[22].

2.3.2.2. Reactive wetting with formation of three-dimensional compounds at the solid/liquid interface

a) Generalities

Interfacial reactions between a liquid alloy containing a reactive element A and a solid substrate S may lead, under certain conditions, to the formation of a new three-dimensional compound A_mS_n at the liquid/solid interface (Figure 16). In general, this reactive compound is a continuous layer and is formed according to the following reaction :

$$m((A)) + n<S> \rightarrow <A_mS_n> \qquad (6)$$

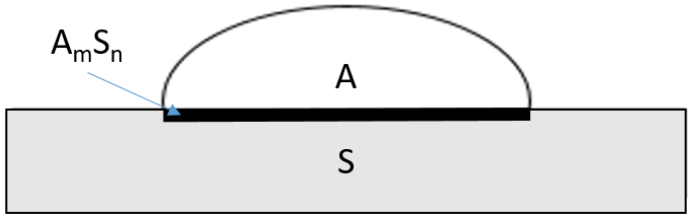

Figure 16: Reaction between a liquid drop of an alloy containing an active element A and the substrate S, forming an interfacial compound A_mS_n.

((A)) refers to the element A dissolved in the liquid alloy. <S> and $<A_mS_n>$ refer to the pure constituents S and A_mS_n at solid state.

From a thermodynamic point of view, this reaction can take place only if the molar fraction of A (x_A) in the liquid alloy is higher than a certain value x_A^*, called the limit molar fraction of A for reactivity between solute A and substrate S.

This limit molar fraction x_A^* can be calculated by writing the thermodynamic equilibrium conditions of the reaction (6), given by the following relation:

$$\Delta G° - mRT\ln a_A = 0 \qquad (7)$$

$\Delta G°$ is the standard Gibbs free energy of formation of the A_mS_n compound from pure liquid A and pure solid S at temperature T, R the universal gas constant (8,314 $J \cdot mol^{-1} \cdot K^{-1}$), and $a_A = \gamma_A x_A$ the thermodynamic activity of the active element A in the liquid alloy, γ_A being its activity coefficient.

A number of studies have been carried out on reactive wetting mechanisms in the case of formation of a three-dimensional layer. Thus different models have been established to describe this type of reactive wetting. The most relevant model for our study is the RPC model (Reaction Product Control). It mainly describes the wetting in ceramic / metal systems where interfacial reactions lead to the formation of a wettable and continuous layer of a reaction product at the interface.

Based on the model developed by K. Landry and N. Eustathopoulos[23], the final contact angle and spreading rate are both controlled by the reaction leading to the formation of the compound at the triple line.

Thus, in the RPC model, the initial contact angle θ_0 is the contact angle formed on the substrate surface before reaction (Figure 17a). After a transient phase, a quasi-stationary configuration is established at the triple line. The progress of the liquid is blocked by the presence of the non-wettable substrate in front of the triple line. Thus the progress is made by lateral growth of the wettable reaction product until the macroscopic contact angle θ_F reaches the final equilibrium contact angle θ_P of the liquid on the reaction product ($\theta_F = \theta_P$), (Figure 17c).

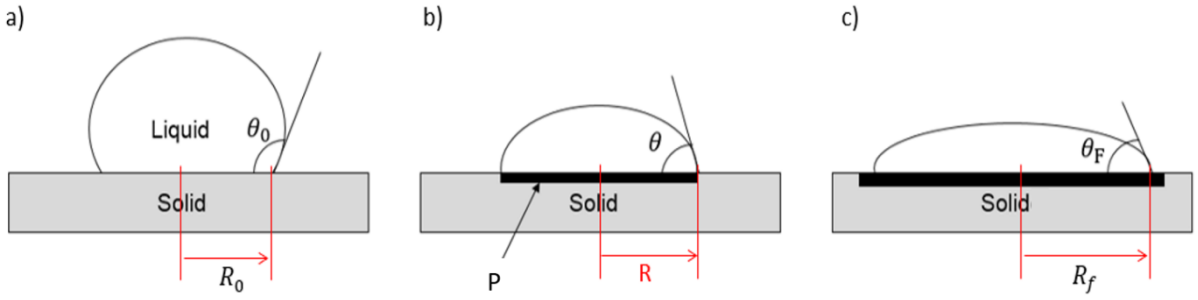

Figure 17: The RPC model (when the reaction product is better wetted than the base substrate), R is the base radius of the drop[23].

Thus, when the reaction product formed at the liquid / solid interface is better wetted than the substrate, the interfacial reaction improves the wetting of the system. On the contrary, if the reaction product is less wettable than the substrate, the reactivity reduces the wettability of the system.
Below, we will develop the reactive spreading mechanisms in the case when the interfacial reactivity improves wetting since this case interests us within the framework of our study.

b) Reactive wetting mechanisms : when the reaction product is better wetted than the substrate

Very often, the reaction product formed at the interface by interaction between the solid substrate and the liquid metal significantly improves the wetting. In such reactive systems, spreading time is about 10-10^4 s (much higher than that of a non-reactive system ~ 10^{-2} s). According to the RPC model, the reactive spreading rate becomes equal to the radial growth rate of the reaction product at the triple line.
The radial growth rate of the reaction product at the triple line may be limited by one of the following processes:

- The transport by diffusion of reactive species from the center of the liquid drop to the triple line.
- The reaction kinetics of the reaction (6) to the triple line.

Thus, the spreading rate of the drop, v = dR/dt, is controlled by the slowest of the two phenomena. R is the base radius of the drop (Figure 17).

Below, we present the two limit cases of reactive spreading control.

a) Reactive spreading limited by diffusion of reactive element A

When reaction rates are high, the lateral growth rate of the reaction product at the triple line is limited by the diffusion of the reactive element A, from the center of the drop to the triple line (Figure 18).

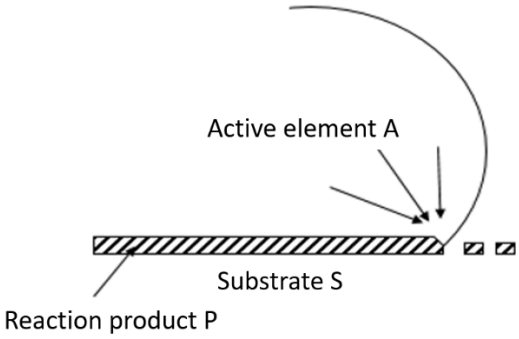

Figure 18: Reactive spreading limited by diffusion of reactive element from the center of the drop to the triple line.

This type of reactive spreading has been described in detail by Mortensen et al. [24], by considering the diffusion of reactive species A in the volume of the drop, and assuming that reaction (6) is in thermodynamic equilibrium at the triple line. This model leads to a simple analytical expression of the spreading rate v = dR/dt :

$$\frac{dR}{dt} = \frac{2DF_{(t)}}{en_v}(C_0 - C_e)\theta \qquad (7)$$

D is the diffusion coefficient of the active element in the liquid (m²/s), n_v the mole number of the active element per unit volume of the reaction product, e the thickness of the reaction product at the triple line, C_0 the nominal concentration of the active element of the drop, C_e the active element concentration at equilibrium with the reaction product (at the triple line) and $F_{(t)}$ is a function that depends very little on time and can be considered constant (≈ 0.04). According to this model, the spreading rate is proportional to the instantaneous contact angle of the drop.

Cu-Cr / C_v [25] and Cu-Sn-Ti / C_v [26] systems, in which the active elements are respectively Cr and Ti, have been studied to verify the validity of this model.

Dezellus et al. [26] results are in agreement with the Mortensen et al.[24] model, the spreading rate is directly proportional to the instantaneous contact angle. The same results were found in the study of the Cu-Cr / C_v system by Voytovytch et al. [25]. However, the intersection of the line given by V = dR/dt as a function of θ does not pass through the origin of the axis (θ = 0), but rather through an angle (θ = 40°), as shown in Figure 19.

This shift is explained by the presence of chemical reactions between the metallic drop and the substrate behind the triple line. The active element is consumed not only at the triple line but also along the liquid / solid interface, thus reducing the flux of active element(s) reaching the triple line. Indeed, the formed chromium carbide layer grows a lot during spreading and therefore there is a variation in the thickness of this layer from the center of the drop to the triple line.

On the contrary, in the case of the Cu-Sn-Ti / Cv system, the titanium carbide layer is very thin and its growth is extremely slow. As a result, there is no significant difference in TiC thickness between the center of the drop and the triple line.

To account for the growth of the reaction product behind the triple line (as in the case of chromium carbide), a semi-analytical model was developed by Hodaj et al. [27]. In this model, the effect of the interfacial reaction behind the triple line on the spreading rate was taken into account and the model has been validated by the spreading description in the Cu-Cr / Cv reactive system (Figure 19).

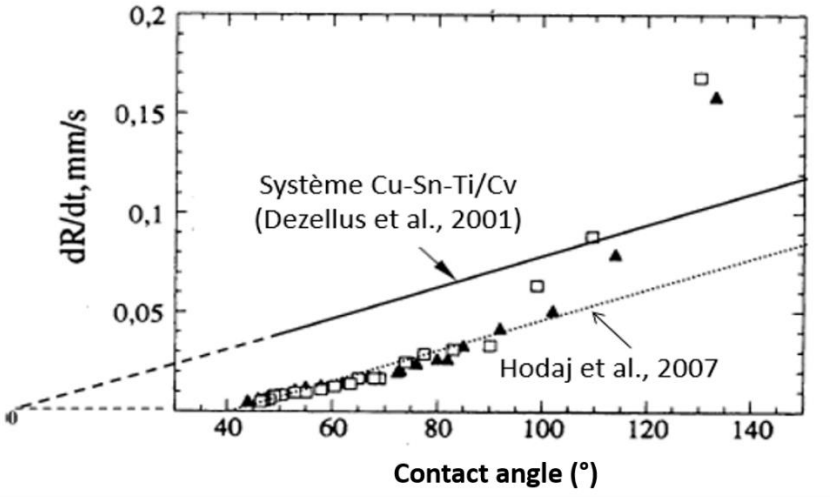

Figure 19: Triple line speed depending on the instantaneous contact angle for the Cu-1 at % Cr/vitreous carbon system at 1150°C [24]. Spreading rate according to the model of Hodaj et al.[27].

b) Reactive spreading limited by the reaction kinetics at the triple line

When the diffusion of reactive element in the liquid alloy is very fast compared to reaction kinetics at the triple line, spreading is limited by the reaction kinetics at the triple line. In this case, the concentration of the reactive element at the triple line is substantially equal to the concentration C_0 in the drop center.

The chemical reaction rate, proportional to $C_0 - C_{eq}$, is fairly constant and therefore the spreading rate is almost constant. C_{eq} is the concentration of reactive species A when the reaction (6) is at thermodynamic equilibrium.

In this case, the reaction rate noted V_r (mole.m^{-2}.s^{-1}) is assumed to be constant over time if:

- The reaction does not change the composition of the drop in such a way that the chemical environment of the triple line is constant over time, and
- A stationary configuration is obtained at the triple line during wetting.

In Cu-Si / SiC [28] and Ni-Si / C [29] systems, after a transient state where the contact angle decreases quickly, the spreading rate keeps decreasing slightly (quasi-linear spreading) and tends to a constant value (Figure 20). This quasi-linear spreading shows that spreading rate is not limited by the diffusion of the reactive element, but rather by the kinetics of the local reactions at the triple line.

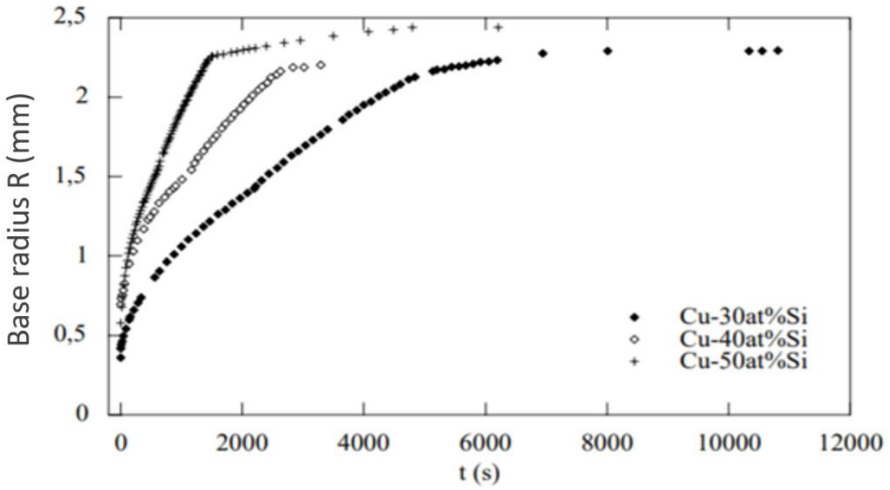

Figure 20: Variation of the base radius (R) of the drop over time in the case of reactive wetting limited by the reaction kinetics at the triple line. Cu-Si / vitreous carbon system at 1150°C [30].

In some cases, the two phenomena mentioned above (dissolution and formation of three-dimensional compound at the interface) can occur in the same system. Some parameters such as temperature, the presence and/or the content of element(s) in the alloy are responsible for these phenomena.

To sum up, reactive wetting involves wetting by dissolution or by formation of three-dimensional compound at the drop/liquid interface. This compound may be more or less wettable than the substrate. If the reaction product is better wetted by the liquid alloy than the substrate, the spreading rate is limited either by the diffusion of the active element from the center of the drop to the triple line, or by chemical reactions at the triple line. Generally, substrate roughness has no impact on reactive wetting[6].

2.4. Mechanical characterization of the brazed joints

The mechanical characterization of brazed assemblies is quite difficult because it depends on two factors: residual stresses that develop during the manufacturing of the brazed specimens on the one hand, and on the properties of the joint on the other hand. Internal stresses are generated, during cooling, mainly by the difference of thermal expansion coefficient between the brazed materials. Moreover, the residual stress rate generated during the manufacture of the test pieces is induced by the specimen's design. This value is very difficult to quantify, so the comparison of mechanical strengths found in the literature is complex.

However, several methods, presented in Figure 21, exist to measure the mechanical strength of the brazed joint by evaluating the maximum stress σ_{max} or the fracture toughness K_c but the manufacture of the test specimens and the test tool are rarely well detailed. Some authors were inspired by ceramic rupture tests such as 3-point or 4-point bending [31].

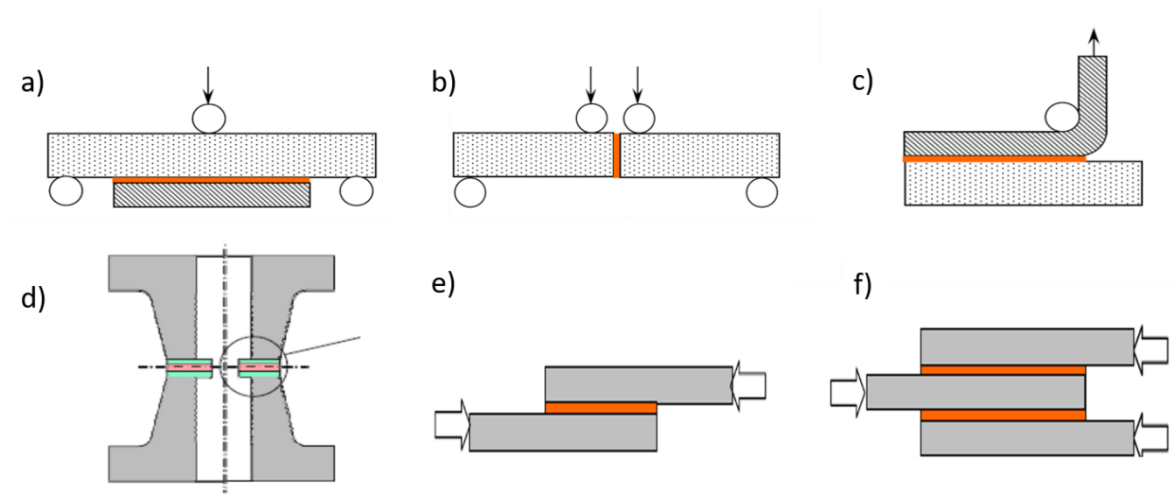

Figure 21: Examples of mechanical tests performed to quantify the joint strength: a) three-point-bending, b) four-point-bending, c) peel test, d) tensile test, e) shearing test, f) symmetrical shearing test by compression.

The majority of mechanical tests carried out on brazed joints are the shearing tests. A brazed specimen and the tool test are presented in Figure 22.

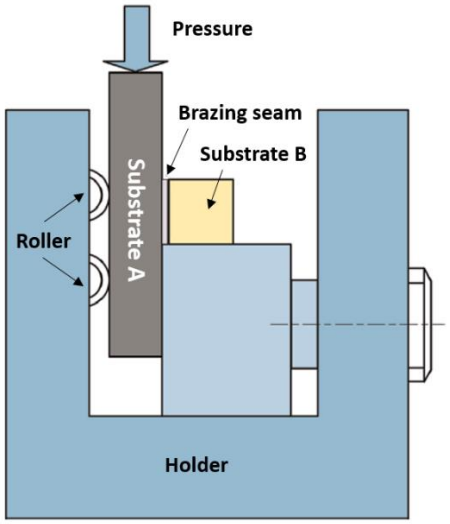

Figure 22: Schematic description of shear test configuration[32]

A standard tensile test (ASTM F19-64) has been developed for brazed assemblies. The sample design is presented in Figure 21d. Yet, this standard is rarely used in the literature. The problem of this test is that crack initiates in the most fragile material of the brazed assembly which is often ceramic substrate, so the tensile stress measured is that of ceramic and not that of joint. In particular, it could be the case for alumina-to-metal brazed assembly when strong interfaces are formed after brazing. However, this standard tensile test is adapted for advanced zirconia like Y-TZP, which has a high tensile rupture strength.

Most of the authors only present a rupture stress average in a few brazing conditions with varying holding time and brazing temperature. The goal of these tests is to identify the potential of the brazed pieces and to support the chemical analysis of the joint. To our knowledge, only one mechanical study of ceramic brazed joints was carried out, in order to propose a failure criteria[33].

2.5. Conclusion

In this section, the general aspects of wetting and brazing processes were presented.

First, the relation between wetting and brazing was exposed: wetting, that is the ability of the filler metal to wet the substrates to be assembled, is a necessary condition to perform a good brazing. Moreover, in order to obtain a good adhesion, the bonds formed at the braze / substrate interfaces have to be mechanically strong. Wetting of a solid by a liquid metal was addressed in a general way, in order to define the main variables involved in the wetting study, such as contact angle, surface and interfacial energies, works of adhesion and cohesion which are linked by the Young relation. The effect of surface roughness and surface heterogeneity of a solid on its wetting by a liquid alloy has also been presented.

Then, dynamic aspects of wetting were addressed. When considering the spreading of a liquid droplet on a solid substrate, from its initial state to its final equilibrium state, wetting can be either non-reactive or reactive. In the case of non-reactive wetting, viscosity and gravity can have a significant impact on spreading kinetics of the liquid alloy. In the case of reactive wetting, two types of reactivity are distinguished: *dissolutive wetting* occurring when liquid metal dissolves the bulk substrate, and *reactive wetting* with the formation of a reaction product layer at the liquid / solid interface. Several models were established in order to describe the spreading kinetics of wetting. In this literature review, we were only interested in the research study most relevant to this present work: the RPC (Reaction Product Control) model. According to this model, the reactive spreading kinetics can be either limited by the reaction kinetics at the triple line, or by the diffusion of the reactive element from the droplet bulk to the triple line.

Finally, the main methods to determine the mechanical strength of the brazed joints, especially by evaluating the maximum stress σ_{max} or the fracture toughness K_c were reported.

3. Zirconia interactions with metals and liquid alloys

3.1. Introduction

Since zirconia is one of the substrates studied in wetting and brazing condition in this thesis, zirconia and in particular the Yttria-Tetragonal Zirconia Polycrystal (Y-TZP) will be presented in this section. Then, we will focus on the wetting and reactivity of zirconia with liquid alloys containing Zr and Ti active elements, as well as on the wetting of Ti oxide by liquid alloys (Ti oxide being the reaction product formed at the reactive liquid alloys containing Ti / zirconia interface).

First of all, we are interested in the binary phase diagram of the oxygen-zirconium system at 1 bar, presented in Figure 23. At about 1100°C (i.e. an average temperature of our study), the solubility of oxygen in the bcc terminal solid solution (βZr) is ~3 at% and the solubility of oxygen in the cph terminal solid solution (αZr) is ~30 at%. In other words, a very high oxygen content can be dissolved in solid Zr without forming zirconium oxide. Thus, zirconium is an excellent candidate to play the role of oxygen getter, that is a gas trap in vacuum furnace to decrease the oxygen partial pressure.

Figure 24 shows the three stable crystallographic structures of zirconium oxide: monoclinic α-ZrO_2, tetragonal β-ZrO_2 and cubic γ-ZrO_2. α-ZrO_2 and β-ZrO_2 oxides are sub stoichiometric compounds (the ratio O/Zr is very close but lower than 2) while γ-ZrO_2 oxide exists in a large composition range. In the

following paragraph, a special attention is paid to ZrO_2 and a detailed description of its different allotropic crystalline structures will be given since it is the chosen ceramic substrate studied in the entire present work.

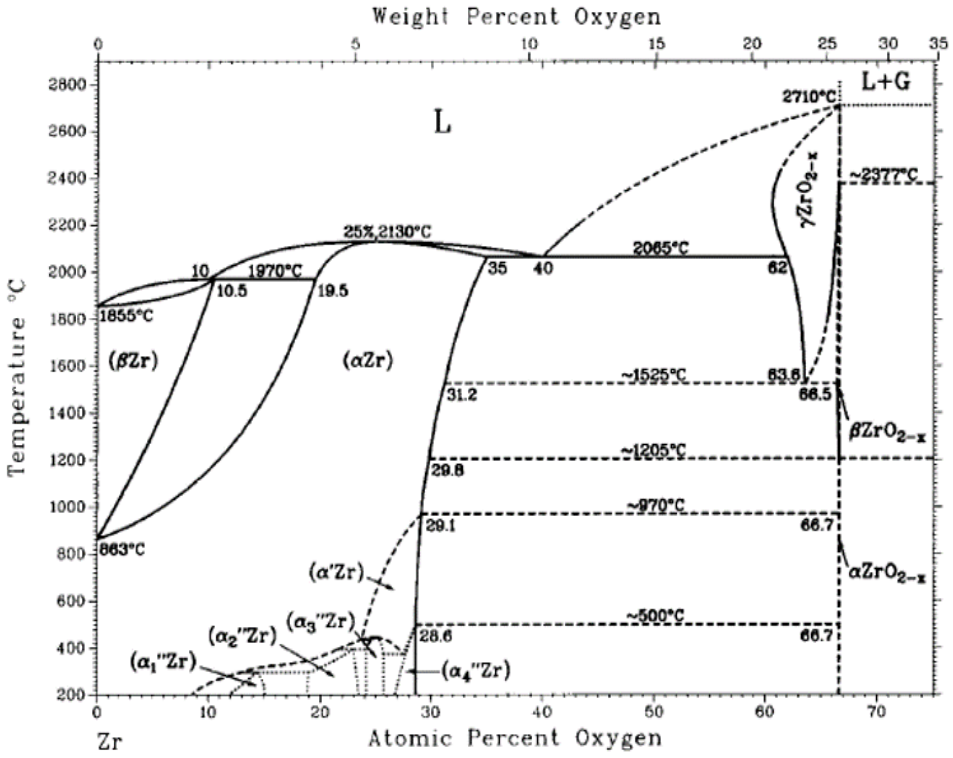

Figure 23: The O-Zr binary phase diagram[34].

3.2. Zirconia

ZrO_2 zirconium oxide, also named zirconia, is an advanced ceramic usually provided by sintering. This ceramic has a wide applications range, due to its excellent physical and electrical properties (solid electrolyte, fuel cell, etc …) and mechanical properties. Biomedical field continues to use this bio-inert ceramic for its excellent mechanical properties, especially friction resistance and very high toughness (i.e. crack propagation resistance).

In this section, we will present the different crystallographic structures of zirconia, the way to stabilize this ceramic at room temperature, and then, a greater importance will be attached to zirconia used for this research work: the 3 mol% yttria-stabilized tetragonal zirconia polycrystal (3Y-TZP).

3.2.1. The zirconia phases

At atmospheric pressure, pure zirconia can exist in three phases: monoclinic, quadratic and cubic depending on temperature:

- The monoclinic phase (figure 24c) is stable at low temperature, below 1170°C. It is described in the space group P21/c. In this structure (distorted structure near CaF_2), Zr^{4+} cations are in coordination 7 with O^{2-} anions (coordination 8 in CaF_2 structure).
- The tetragonal phase (*quadratique in french*) (figure 24b) is stable in the temperature range 1170 - 2360°C. It is a distorted fluorite structure (CaF_2, Fm3m cubic face centered) described in the space group $P4_2/nmc$.
- The cubic phase (figure 24a) is stable at high temperature in the range 2360 – 2680°C (which is the zirconia melting point). It is a fluorite structure in which oxygen ions are moved slightly from the position (¼,¼,¼).

The crystallographic parameters are illustrated in Figure 24 and specified in Table 2.

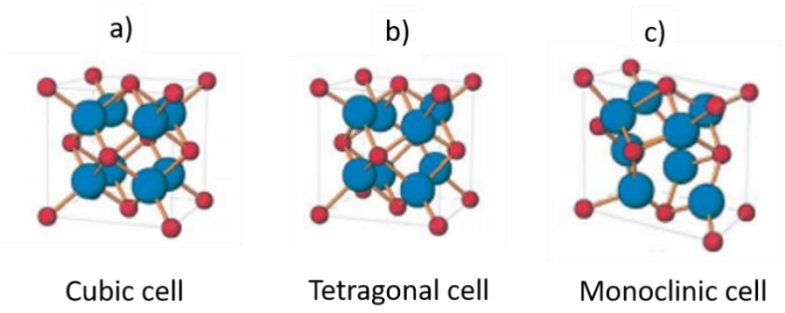

Figure 24: The three structures of pure zirconia, with O^{2-} anions in blue and Zr^{4+} cations in red [35].

Phase	JCPDS data sheet	Lattice parameters
Monoclinic	00-037-1484	a = 5.313 Å b = 5.212 Å c = 5.147 Å β = 99.22°
	00-036-0420	a = 5.146 Å b = 5.213 Å c = 5.311 Å β = 99.13°
Tetragonal	00-017-923	a = 3.598 Å c = 5.152 Å
	50-0089	a = 3.6 Å b = 3.6 Å c = 5.15 Å
Cubic	00-027-997	a=5,09 Å

Table 2: Crystallographic parameters of the three structures of pure zirconia [35].

The tetragonal-monoclinic (t-m) martensitic transformation, occurring during heating (m-t) and cooling (t-m) stages when zirconia sintering, is widely studied because it is responsible for disintegration of pure zirconia pieces after sintering. Indeed, during this phase transformation, a significant shear deformation and an increase in volume of about 4-5 % lead to important internal stresses.

In order to avoid the (t-m) transformation occurring during cooling, it is necessary to stabilize tetragonal or cubic phases at room temperature thanks to the addition of another oxide in the zirconia composition. The most common oxides are yttrium, cerium, magnesium and calcium oxide. Their use conducts to three main types of microstructures, named Fully Stabilized Zirconia (FSZ), Partially Stabilized Zirconia (PSZ) and Tetragonal Zirconia Polycrystal (TZP). The FSZ, exclusively composed of cubic phase, is the most common zirconia used for oxygen sensor and solid oxide fuel cell electrolytes (SOFC). PSZ are composed of a cubic matrix containing nanometric tetragonal or monoclinic precipitates. TZP is considered as tetragonal phase monolith even if it also includes a low content of cubic phase.

3.2.2. Yttria Tetragonal Zirconia Polycrystal YTZP

In biomedical field, the most commonly used zirconia is the 3-YTZP, a TZP stabilized with 3 mol% yttria and sintered at about 1500°C, for its excellent mechanical properties (especially fracture toughness) at room temperature. Some YTZP phase diagrams are presented in Figure 25. Since Duwez[36] introduced the first zirconia - yttria phase diagram in 1951, successive versions were proposed. Figure 25 presents the most recent phase diagram (a), the most used (b), and the metastable phase diagram (c). As cations diffusion is extremely slow (about one month is necessary to homogenize the composition of a 3 µm-grain at 1500°C), referring to metastable phase diagram is necessary, knowing that zirconia sintering is performed during at most a couple of hours at 1500°C. On this diagram (Figure 25c), the dotted lines, showing T_0(t-m) and T_0(c-t) indicate t-m and c-t phase change temperatures depending on the yttrium content in each phase (and not the yttrium content in the whole material).

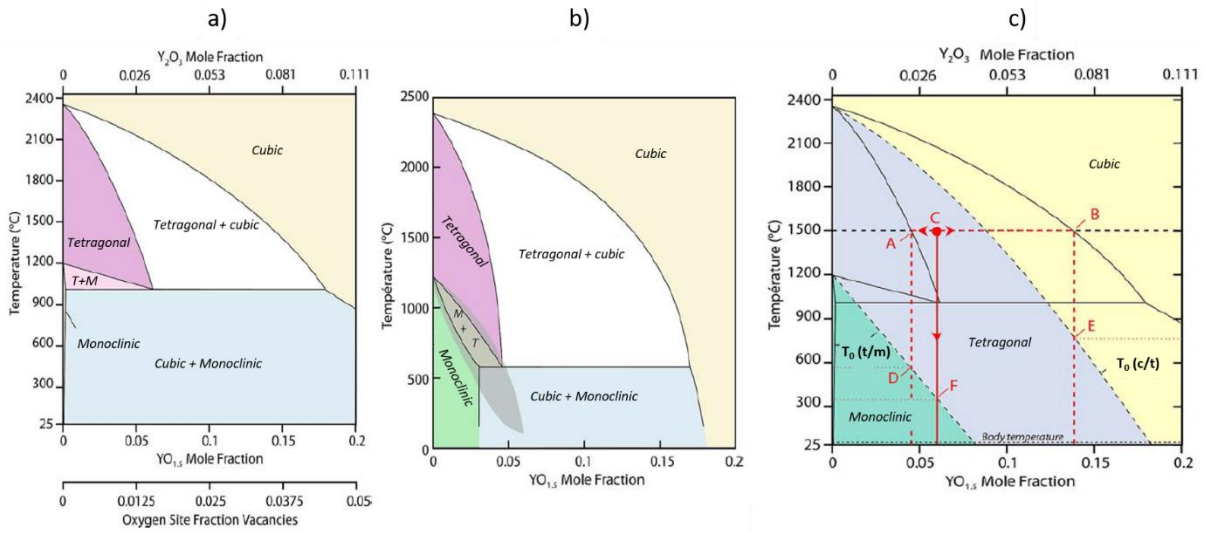

Figure 25: Zirconia - yttria phase diagrams: a) the most recent, b) the most used, c) a stable (full lines) and metastable (dotted lines) phase diagram[37].

Gremillard[37] explains how to read this diagram with the example of a 3Y-TZP. From a nanometric powder of homogeneous composition, during sintering, temperature is increased up to 1500°C, the powder has the composition of point C (see Figure 25c). For a long sintering (several hours even days), equilibrium is attained and phases at 1500°C are indicated by point A (tetragonal phase containing 2.4 mol% of Y_2O_3) and point B (cubic phase containing 7.5 mol% of Y_2O_3). Knowing the very low Zr^{4+} cation diffusion at T < 1500°C, any cooling rate is considered as quenching. The phases follow vertical lines in the phase diagram from points A and B. At about 750 and 600°C, the vertical lines cross respectively the T_0 (c-t) and T_0 (t-m) lines (point E and D). Thus, the stable phase below 750°C with a yttria content of 7.5 mol% is tetragonal, and the stable phase below 600°C with a yttria content of 2.4 mol% is monoclinic. However, the energy barriers implemented in the c-t and t-m transformations at 750°C and 600°C are too high to be crossed, so zirconia is composed of a mix of two metastable phases: the cubic phase containing 7.5 mol% of Y_2O_3 and the tetragonal phase containing 2.4 mol% of Y_2O_3. In the case of a very short sintering process, equilibrium at 1500°C is not attained so the system remains at point C containing the only tetragonal phase with 3 mol% of yttria.

The stabilization of zirconia with yttrium oxide allows to obtain, at room temperature, a material composed of a very high content of metastable tetragonal phase. This metastable material exhibits high fracture toughness thanks to the tetragonal-to-monoclinic (t-m) phase transformation occurring locally during crack propagation, schematically presented in Figure 26. Indeed, tensile stresses are important near crack, leading thus to local destabilization of metastable tetragonal grains, resulting in local transformation in monoclinic phase. The increase of grain volume providing the (t-m) transformation allows to close the crack front.

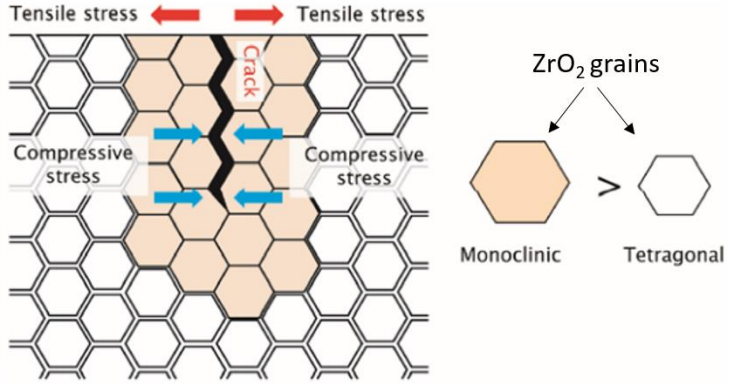

Figure 26: Schematic transformation toughening (t-m) in crack propagation process of zirconia showing the decrease in grain volume during monoclinic - tetragonal (m-t) transformation of zirconia[38].

Figure 27 presents fracture toughness of different zirconia depending on their yttria content in the range 0 - 12 mol% Y_2O_3. This graph shows that fracture toughness strongly depends on zirconia structure in the range 1.7 – 6.4 MPa.m$^{1/2}$. Zirconia with the higher mechanical property are tetragonal zirconia polycrystal (TZP), especially those stabilized with a low Y_2O_3 content, typically 3 mol%.

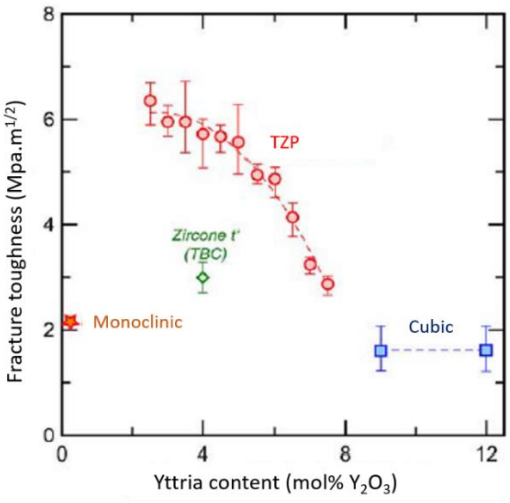

Figure 27: Fracture toughness of different zirconia[37].

3.3. Interfacial interactions of ZrO_2 and Ti oxides with liquid alloys

3.3.1. Introduction

A necessary condition to achieve a successful brazing is a good wetting of the substrates to be joined. It is well known that liquid noble metals like Cu, Ag or Au do not wet zirconia. For example, Chatain et al.[39] measured a final contact angle of 124° of liquid Au on zirconia at 1100°C. To improve the wetting, addition of Zr or Ti as reactive element in the filler metal is often investigated in the literature. In this work, wetting and reactivity of zirconia substrate by reactive alloys are investigated. Moreover, we

also study wetting and reactivity of titanium oxide by these alloys. Indeed, as it will be seen later, in the case of ZrO_2 / Au / Ti brazing, there is formation of a titanium oxide layer at the braze / ZrO_2 interface.

3.3.2. Wetting and reactivity of ZrO_2 with liquid alloys containing Zr and Ti

3.3.2.1. Zr reactive element

There is a shortage of studies on zirconia wetting by alloys containing zirconium as active element. Typically, the addition of Zr in the alloy reduces the contact angle θ, leading to a good wetting of zirconia by the Zr-alloys.

Iwamoto et al.[40] investigated zirconia wetting by Zr-Cu alloys under vacuum with different Zr contents in the alloy in the range 47-79 at% Zr. The temperature dependence of the contact angle of Zr-Cu alloys on zirconia is presented in Figure 28a. For 79, 53 and 47 wt% Zr, the contact angles decrease with temperature in the range 900-1050°C then kept constant, respectively at 80°, 60° and 45°. The contact angle of the 63Zr-Cu alloy on zirconia keeps decreasing with temperature until θ ~ 20°. The zirconia/Zr-Cu interface is not described in sessile drop configuration, but in zirconia/zirconia brazing configuration. Figure 28b shows a SEM micrograph of a ZrO_2 / 53Zr-Cu alloy interface joined at 1000°C for 30 min (1273 K for 1.8 ks). At 1000°C for 30 min, the 53Zr-47Cu/zirconia interface is composed of two successive layers: Cu_xZr_y (~ 2 µm) and zirconium oxide (~ 3 µm). According to the EPMA analysis, the possible phases are Cu_5Zr_2, Cu_3Zr_2 for the reaction layer in contact with zirconia substrate (marked B), and $ZrO_{1.63}$ for the topping layer (marked C). In the joint, zones D and E are two different Cu-Zr compounds.

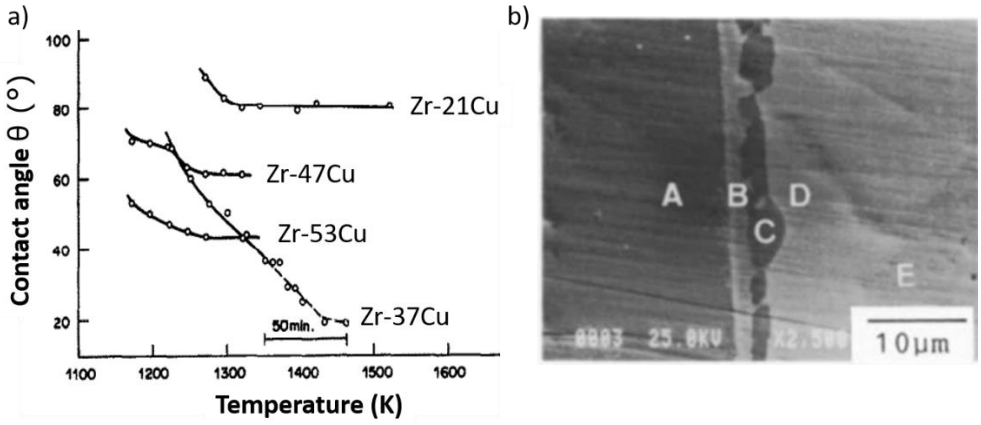

Figure 28: a) Temperature dependence of the contact angle of liquid Zr-Cu alloys on zirconia, b) SEM micrograph of the ZrO_2 / 53at%Zr-Cu alloy interface joined at 1273 K for 1.8 ks[40].

Xue et al[41] have turned their attention on zirconia wetting by liquid silver-indium base alloy between 842°C and 927°C. With 1.1 and 4.8 at% Zr in $Ag_{65}In_{35}$, zirconia is not wetted by the liquid alloys (the contact angles are respectively about 140°and 118°). However, with 2.4, and 3.7 at% Zr in the alloy, zirconia is wetted (about 80° and 60° respectively). Thus zirconia can be wetted by AgInZr alloys only in the zirconium content ranging from 2 to 3.7 at%. The AgIn-3.2Zr/ZrO_2 interface formed at 900°C for 30 min was examined by XRD [41]. The reaction layer is entirely composed of ZrO_2.

Lastly, the wetting of zirconia by the (Cu-17.5Ga)-Zr and (Cu-16.9Ge)-Zr alloys was studied by Durov et al.[42]. For Cu-Ga-Zr, the minimal contact angle is 30° at 1150°C with 15 at% of Zr. The final contact angle of Cu-Ge-5Zr on zirconia reaches 40° at 1150°C. At the Cu-Ga-Zr/zirconia interface, zirconium is adsorbed and EDX analyses reveals the presence of a ZrO layer. Authors proposed the following reaction, processing at the interface: $ZrO_2 + x_{Zr} \rightarrow ZrO_{2-x} + x\text{ZrO}$.

3.3.2.2. Ti reactive element

Zirconia wetting by Ti active element, meanwhile, was investigated by using different matrix (M). Table 3 sums up the best contact angles obtained on zirconia by the M-Ti-alloys studied in the literature.

However, to the best of our knowledge, there are no published studies in the literature on the wetting of zirconia by the Au-Ti alloys.

Brazing alloy	Temperature (°C)	Contact angle θ (°)	Reference
Sn0.3Ag0.7Cu-xTi (2<x<5wt%)	1050	10-20	[43]
SnAgCu-4Ti (wt%)	1000	10	[44]
Sn-4Ti (at%)	1000	20	[45]
Ag-27Cu-3Ti (wt%)	950	30	[46]
Ag60Cu40-5Ti (at%)	950	22	[47]
Ag65In35-4,7Ti (at%)	1150	25	[48]
Ag-86Sn-4Ti (wt%)	950	55	[46]
Sn-4Ti and Sn-8Ti (at%)	1000	20	[49]
(Cu-17.5Ga)-15Ti (at%)	1150	60	[42]
(Cu-16.9Ge)-5Ti (at%)	1150	75	[42]

Table 3: Contact angles of the Ti-active brazing alloys / zirconia systems.

Very good wetting in the M-Ti alloys / zirconia systems was obtained. Chuang et al.[46] have investigated the wetting of zirconia by the Ag27Cu3Ti active filler metal under a vacuum of 10^{-4} Torr. They showed that the alloy does not wet zirconia at 800°C, but the contact angle decreases to 34° at 900°C and remains constant at higher temperature. Luigia et al.[47] have studied the wetting of Ag-Cu-Ti alloy on zirconia under vacuum (10^{-5}.Pa), by adding 5 at% Ti in an eutectic Ag60-Cu40 at% alloy. Figure 29a presents the spreading kinetics in this system at 950°C. The final contact angle obtained is about 22°. Figure 29b presents a micrograph of the Ag-Cu-Ti / zirconia interface. At least three layers are detected at this interface: a layer of Ti oxide 4µm thick at zirconia side (the O/Ti ratio in this layer varies from 66/33 to 46/54 at%), a second layer (~2µm thick) of Ti40-Cu30-O30 (at%) and a third layer (3-5 µm thick) of Ti54-Cu27-O19 (at%) on the alloy side are detected.

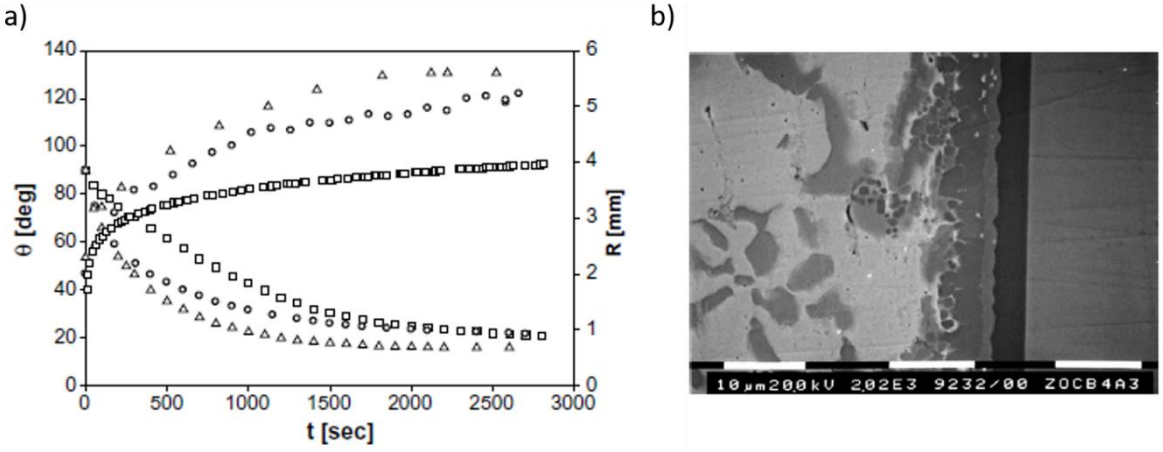

Figure 29: a) Kinetics of spreading of Ag-Cu-Ti (5 at% Ti) alloy on ZrO_2 at 950°C (open square) : Radius R and contact angle θ as a function of time (open cercles and triangles concern Al_2O_3-ZrO_2 and IN738 substrates respectively), b) SEM micrograph of the Ag-Cu-Ti / ZrO_2 interface [47].

Numerous studies in the literature reported the darkening of zirconia after wetting experiments under vacuum when both Zr and Ti active elements are used. In some cases, zirconia substrate turned fully black during contact with liquid metal at high temperature. It is the case of the wetting of zirconia by the Zr6Cu alloy investigated by Iwamoto et al.[40] XRD analysis of the substrate shows that change of color does not imply a transformation of the crystalline phase, but the EPMA analysis reveals that black zirconia is sub-stoichiometric, possibly $ZrO_{1.67}$. In other studies, the darkening of zirconia is localized around the active metal droplet, as it is showed in Figure 30. Zirconia can lose oxygen when joined with active alloys under vacuum. ZrO_2 provides O^{2-} anions which react with active elements (Ti or Zr for instance), forming non-stoichiometric phases in zirconia[42]. According to Durov et al.[42], the F-centers of zirconia (anions, vacancies or held electrons) are responsible for the darkening of zirconium oxide. Authors have investigated the kinetics of dark zone spreading in the case of (Cu-17,5Ga)-10Ti/ZrO_2 contact at 1050°C by measuring the dark zone diameter around the droplet for contact times from

5min to 90min (Figure 30). They showed that the width of the dark zone (x) follows a parabolic law $x^2=2Dt$ where t is the holding time, and D the diffusion coefficient of F-centers from the ceramic-metal interface to the bulk ceramic.

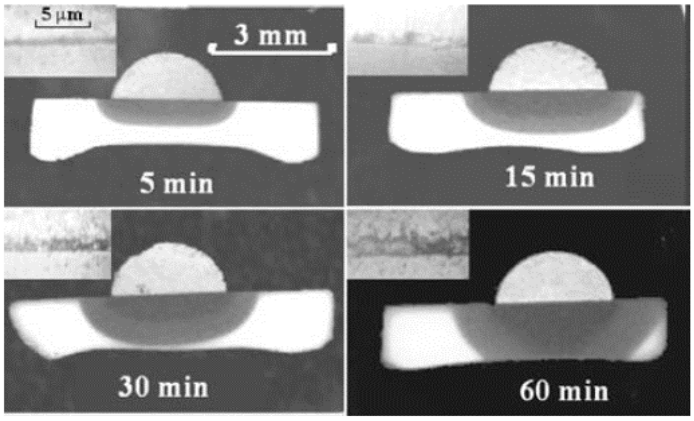

Figure 30: Kinetics of dark zone spreading at ZrO_2-(Cu-17.5Ga)-10Ti contact, 1150°C [42].

Durov et al.[42] and Chatain et al.[39] studied the effect of zirconia stoichiometry on wetting. The non-stoichiometric zirconia (black zirconia) is slightly better wetted by metals (gold for instance) than stoichiometric zirconia (white zirconia). According to Durov et al.[42], zirconium atoms of ZrO_{2-x} substrate may pass in liquid metal, reacting with metal. This phenomena makes disappear the oxygen deficit of this sub-stoichiometric zirconia (they observed black zirconia becoming white). Thus, the proposed reactional mechanism occurring at the black zirconia / noble metal interface studied is :

$ZrO_{2-x} \rightarrow ZrO_2 + x\ Zr$.

3.3.3. Wetting of Ti oxide by liquid alloys

Figure 31 gives the binary Ti-O phase diagram[50] showing the formation of numerous Ti oxides. All oxides are stoichiometric compounds except γ-TiO oxide which is stable for temperatures higher than 460°C. The oxygen content in γ-TiO oxide at 1100°C (i.e. an average temperature of our study), varies between about 50 and 55 at% oxygen. Note that for temperature lower than 920°C there is another stable TiO oxide (α-TiO) which is stoichiometric. Note also that the solubility limit of oxygen in α-Ti solid solution is very high in all temperature range (~33 at% O) while its solubility in β-Ti solid solution at 1100°C is much lower (~3 at% O).

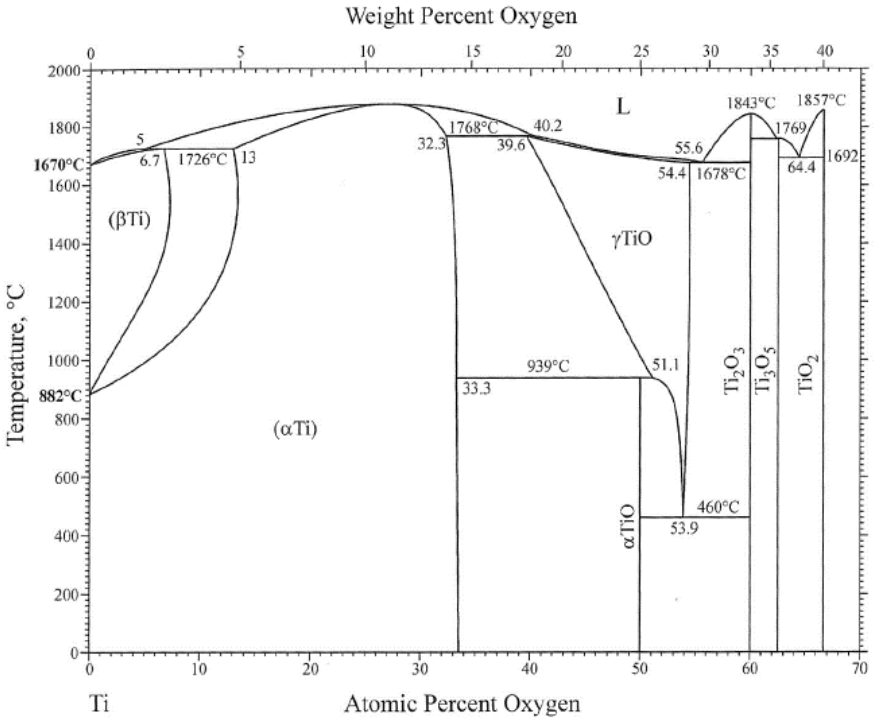

Figure 31: The binary O-Ti phase diagram[50].

Chatain et al.[39] studied gold wetting on pre-elaborated titanium oxides TiO_2, TiO and Ti_4O_7. The contact angles measured just after gold melting are respectively 122°±5°, 120°±6° and 88° ±10°. They showed that wetting of pure metal on titanium oxide depends on its stoichiometry. They also noticed that in the case of TiO substrate, the contact angle of liquid gold decreased to 28° in 45 min. The SEM analysis proved that, at the substrate / gold interface, the solid phase changed into the $TiAu_4$ intermetallic compounds due to a quick saturation of Au in Ti, leading thus to a decrease of the chemical interfacial gradient between liquid and solid phases.

However, other authors found lower contact angles on TiO product layer formed in situ at the Al_2O_3 / alloy interface.

Voytovych et al.[6] studied the wetting of alumina by Ag-Cu-0.7Ti at% alloy and found that a $Ti_{1.75}O$ reaction product layer is formed at the interface. The contact angle, on this oxide layer obtained at 900°C under vacuum (10^{-5} Pa) is 60-65°.

These results are in a good agreement with Kritsalis et al.[51] work, who studied the wetting of alumina by Ni-Pd-Ti alloys and reported that the contact angle decreases from about 100° to 50° when the Ti content increases from 2 to 25 at% (Figure 32). This team established a relation between titanium oxide stoichiometry formed at the ceramic / metal interface and metal wetting on this TiO_x reaction product layer. They attributed the high contact angles on Ti_3O_5 and Ti_5O_9 to the low titanium activity

a_{Ti} in liquid alloy due to strong interactions between Ni-Ti and Pd-Ti. When a_{Ti} increases, the titanium oxide layer formed at the interface (Ti_2O_3) has a higher Ti molar fraction. This oxide is the best wetted by the metallic alloys (contact angle about 50°).

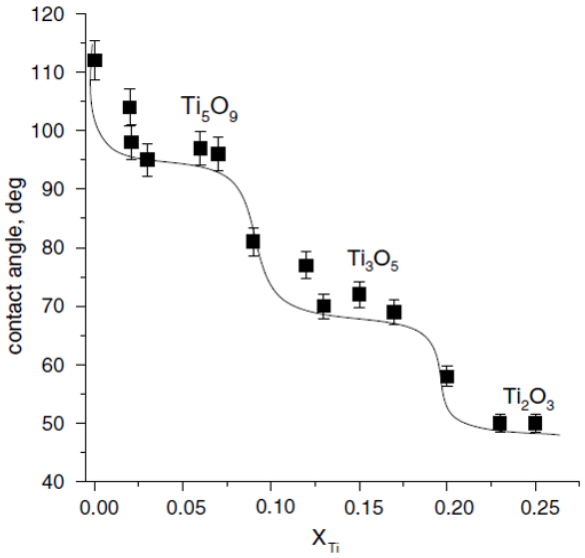

Figure 32: Variation of the contact angle of NiPd-Ti alloys on Al_2O_3 as a function of the molar fraction of Ti [51].

Wan et al.[52] investigated the wetting of alumina by Ni-14 at%Ti alloy and Ni-based alloys containing 16 at% Ti. At the reactive Al_2O_3 / alloy interface, a titanium oxide layer is formed. They reported that wetting of Ni-14Ti alloy on Al_2O_3 leads to a contact angle of about 62° attributed to the contact angle on the reaction product formed at the interface, i.e. the semi-metallic Ti_2O_3 oxide. Increasing the Ti activity in Ni-Ti alloy, by adding Fe and Cr in the alloy, leads to a decrease of the contact angle down to about 37°. Furthermore, adding Si in the Ni-Fe-Cr-Ti alloy decreases the melting temperature and above all allows to obtain a very low contact angle θ ~ 21°. In the case of Ni-based-Ti alloys with Fe-Cr and Fe-Cr-Si, the reaction product layers formed at the Al_2O_3 / alloy interface are respectively the metallic oxides TiO_{1+x} and TiO_{1-x}. TiO is a non-stoichiometric oxide, so that its metallic character evolves with its composition, resulting in different contact angles on this oxide. Figure 33 gives a SEM micrograph of a (Ni-19.3Fe-20.7Cr)-10Si-16Ti at% alloy / Al_2O_3 interface showing the TiO reaction product layer formed at 1463 K for 30 min.

The main conclusion of these studies is that when the metallic character of the titanium oxide increases (i.e. the fraction molar of Ti in the oxide increases), the wetting of this product layer by molten metals increases as well.

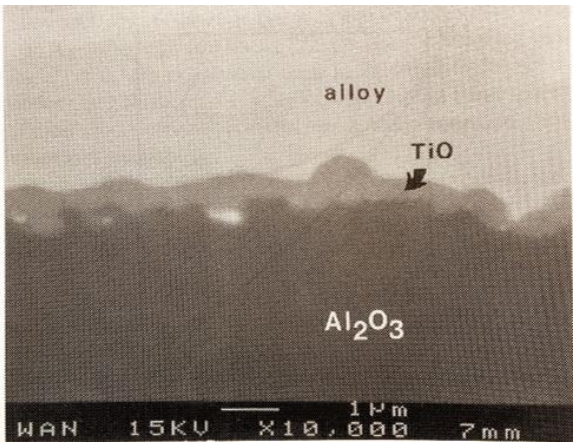

Figure 33: SEM micrograph of the cross-section of (Ni-19.3Fe-20.7Cr)-10Si-16Ti (at%) alloy / Al_2O_3 interface showing TiO_{1+x} reaction product at the interface (holding time of 30 min at 1463K). The final contact angle is about 21° [52].

3.4. Conclusion

Nowadays, interactions between zirconia and metals are more and more studied because of the good properties of this ceramic. Zirconia is not wetted by noble metals, but the addition of an active element such as Zr or Ti in the metal provides spreading of the liquid alloy on zirconia (reactive wetting). Reactive wetting of zirconia is related, especially in the case of Ag-Cu-Ti alloys, with the formation of a wettable product layer at the ceramic / active alloy interface. However, at the best of our knowledge, no study is reported in the literature on wetting and interfacial reactivity in the Au-Ti alloys / zirconia substrate system. Wetting of the titanium oxides by molten metals is well established in the literature, in particular in the case of alumina wetting by Ti-active alloys. The addition of Ti in metal allows the wetting of ceramic substrate, with a drastic decrease of the contact angle from ~125° to ~20°, thanks to the formation of the wettable Ti_xO_y reaction layer at braze / ceramic interface. Oxygen atoms are provided by the zirconia substrate, becoming thus sub-stoichiometric. Wetting of titanium oxide strongly depends on its stoichiometry. When the metallic character of the titanium oxide increases (i.e. the fraction molar of Ti in the oxide increases), the wetting of this product layer by molten alloys increases as well. The contact angle on TiO_2 is ~122° while those of TiO range from ~37° to ~21°, depending of its stoichiometry.

4. Interfacial reaction between gold and titanium

4.1. Introduction

To the best of our knowledge, there is no study available in the literature describing wetting and interfacial reactivity in the liquid gold / solid titanium system. However, there are two studies of

reactivity between gold and titanium at solid state, relating the formation of four Ti-Au intermediate intermetallic layers.

In this section, we will first present the Ti-Au binary phase diagram and some mechanical and physico-chemical properties of the Ti/Au intermetallic compounds. Then a generic phase growth model in the case of the formation of one intermediate phase will be presented. Finally we will sum up the two studies of Au/Ti interdiffusion performed at solid-state.

4.2. Au-Ti phase diagram

In the continuation of this work, some phase diagrams will be used several times, especially the Ti-Au phase diagram, presented in Figure 34.

In the titanium rich domain, two phenomena are notable. First, pure titanium is the seat of an allotropic transformation α-Ti → β-Ti occurring at 882°C. The crystal structure of titanium at room temperature is close-packed hexagonal (cph) α phase with a c/a ratio of 1.587. At about 882°C, the titanium undergoes a transformation to a body-centered cubic (bcc) β phase which remains stable up to the melting temperature of Ti (1670°C). Secondly, the high solubility of gold in β-Ti until 15 at% is notable, while the maximal solubility of gold in α-Ti is only 1.7 at%.

In the gold-rich side of this diagram, the Au-based solid solution (δ-Au) presents a face-centered cubic (fcc) crystal structure and a significant variation of Ti solubility from about 2 at% Ti at 500°C to 12 at% Ti at 1123°C.

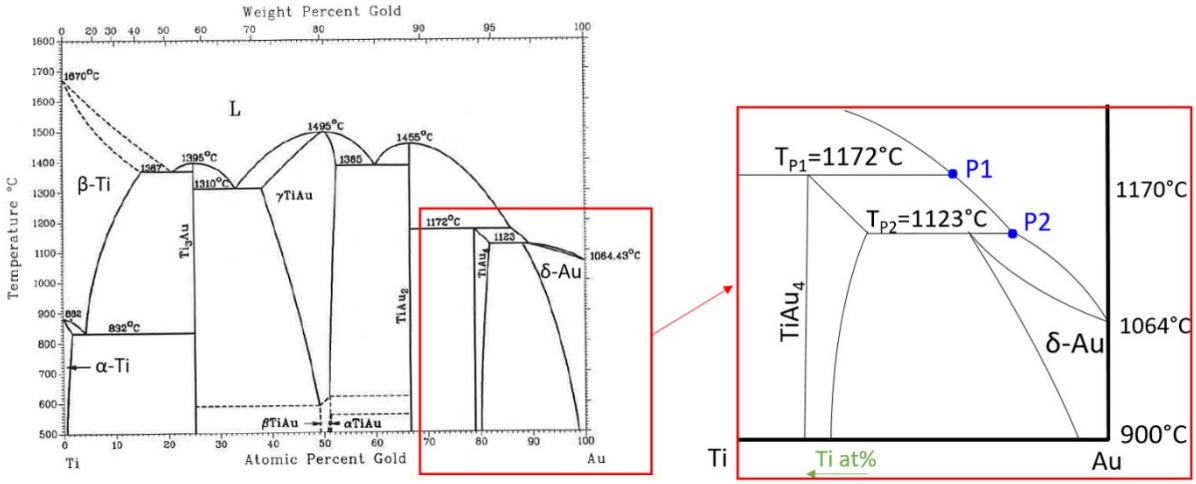

Figure 34: Binary phase diagram of the Ti-Au system[53].

This phase diagram presents 4 intermetallic compounds (IMCs), including two stoichiometric IMCs (Ti_3Au and $TiAu_2$) and two non-stoichiometric IMCs (TiAu and $TiAu_4$). The TiAu phase has a wide range of composition depending on the temperature, while the $TiAu_4$ composition range is 1-3 at%. Ti_3Au, TiAu and $TiAu_2$ are congruently melting compounds, and their melting points are respectively 1395°C, 1495°C and 1455°C. $TiAu_4$ is an incongruently melting compound, with a peritectic decomposition at 1172°C. The melting points of all Ti / Au IMCs are higher or much higher than the melting temperature of gold (1064.43°C).

This phase diagram presents numerous invariant transformations (three-phase equilibria). Here below only invariant transformations for temperatures lower than 1200°C will be presented.

In the Ti-rich domain, at 832 ± 2°C, the eutectoid transformation β-Ti → α-Ti + Ti_3Au occurs, with α-Ti and β-Ti compositions being 1.7 ± 0.1 and 4.2 ± 0.2 at% Au respectively.

In the Au rich domain, the Ti-Au phase diagram presents 2 peritectic transformations. At T_{P1}= 1172°C, the reaction $TiAu_2$ + Liquid (L) → $TiAu_4$ occurs, with $TiAu_2$, L and $TiAu_4$ compositions being respectively 66.7, 86 and 80 at% Au. The second peritectic reaction, $TiAu_4$ + Liquid (L) → δ-Au, occurs at T_{P2}= 1123°C, with $TiAu_4$, L and δ-Au compositions being 82, ~89 and ~88 at% Au respectively.

Some other useful binary phase diagrams such as Au-Zr, Ag-Zr and Ag-Ti diagrams are given in appendix 1.

4.3. Mechanical and physico-chemical properties of the Ti-Au intermetallic compounds

In this paragraph, some mechanical and physico-chemical properties of the Ti/Au intermetallics compounds are given[54] and compared with those of pure Ti and pure Au[53]. The intermetallic phases are typically ordered compounds, conferring a fragile character. On the contrary, gold is considered as the most ductile metal, meaning it can withstand a significant plastic deformation without breaking.

Table 4 summarizes the crystal structure, the molar volume, the mass density and the Vickers hardness of these phases. Notice that crystal structure of the juxtaposed phases Ti / Ti_3Au, and TiAu /$TiAu_2$ are different. The hardness of TiAu, $TiAu_2$ and $TiAu_4$ are quite similar, about 250 HV (Vickers Hardness) and close to Ti hardness, whereas Ti_3Au is much harder (~800 HV).

Phase	Crystal structure	Molar volume x10^{-6} (m^3/mol)	Mass density (g/cm^3)	Vickers Hardness (HV)
Ti	HCP (α- Ti) BCC (β-Ti)	10.55	4.5 ± 0.5	200 ± 10
Ti_3Au	Cubic (Cr_3Si)	9.93	8 ± 0.5	800 ± 50
TiAu	Cubic (CsCl)	10.34	11 ± 0.5	250 ± 50
$TiAu_2$	Tetragonal ($MoSi_2$)	10.05	13 ± 0.5	250 ± 50
$TiAu_4$	Tetragonal ($MoNi_4$)	6.99	15 ± 0.5	250 ± 50
Au	FCC	10.19	19± 1	20 -58

Table 4: Mechanical and physico-chemical properties of Ti, Ti-Au IMCs and Au [54] [53].

4.4. Phase growth model

Physico-chemical growth models of one or two reactive layers in a binary A-B system are relatively well established in the case of growth limited by diffusion of reactive element through the reaction product layer (see for instance[55] [56]). However, to the best of our knowledge, there is no simple model describing analytically the growth kinetics of four intermediate phases, as it is the case in the Ti / Au system studied in this thesis.

In this paragraph, a model based on the growth of a single δ phase between A and B components is presented. It corresponds for instance to a simple diffusion couples such as Ag/Sn, where the single intermediate phase Ag_3Sn is formed and grows at the interface.

Figure 35 gives a schematic phase diagram of the binary A-B system, and the concentration profile of the B constituent through the system, in the case of a single intermediate phase (δ). In the case of growth kinetics limited by diffusion process, the thermodynamic equilibrium is reached at the reactional interfaces, thus concentrations at these interfaces are given by the phase diagram.

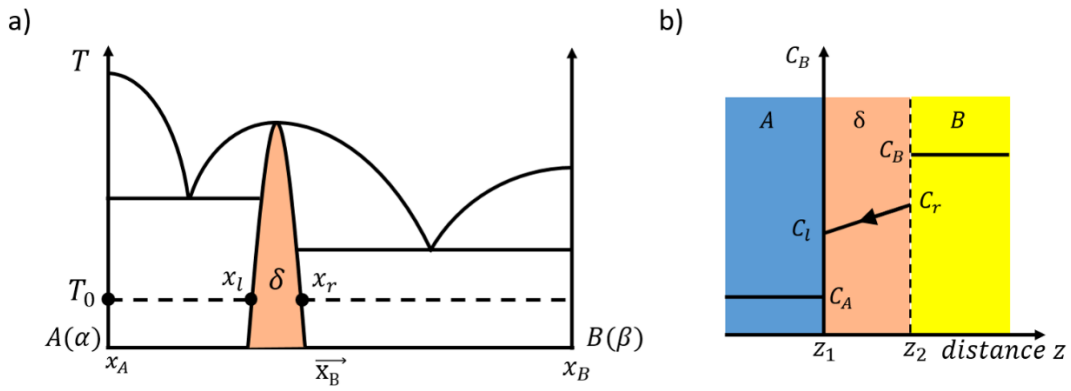

Figure 35: a) Schematic phase diagram of a binary A-B system, with formation of a single intermediate δ phase, b) schematic representation of the concentration variation of B constituent through the A / δ / B system.

To simplify the calculations, the mutual solubilities between A (β phase) and B (α phase) at solid state are assumed almost equal to zero. Concerning the δ phase which represents the A_xB_y intermediate phase, its concentration is defined by two limit concentrations : C_l at the interface with α(A) phase, and C_r at the interface with β(B) phase. C_i gives the concentration of constituent B at left and right interfaces, and z the space coordinate.

In order to express the variation with time of the thickness (e) of the δ phase, a mass balance for the constituent B is established at both interfaces 1 and 2 (at the left and the right of the δ phase).

At interface 1: $$(C_l - C_A)\frac{dz_1}{dt} = J_\delta - J_A = J_\delta \quad (1)$$

At interface 2: $$(C_B - C_r)\frac{dz_2}{dt} = J_B - J_\delta = -J_\delta \quad (2)$$

The diffusion fluxes in the α(A) and β(B) phases are assumed equal to zero ($J_A = J_B = 0$).

We note $\Delta C_\delta = C_r - C_l$ and $e = z_2 - z_1$ (see Figure 35b).

The diffusion flux of B through the δ phase (J_δ) is given by the Fick law:

$$J_\delta = -D_\delta \frac{\partial C_\delta}{\partial z} \approx -D_\delta \frac{\Delta C_\delta}{e} \quad (3)$$

D_δ is the diffusion coefficient of B component in the δ phase.

From the equations (1) to (3), we obtain:

$$\frac{d(z_2 - z_1)}{dt} = -\left(\frac{1}{C_B - C_r} + \frac{1}{C_l - C_A}\right) J_\delta = \left(\frac{1}{C_B - C_r} + \frac{1}{C_l - C_A}\right) D_\delta \frac{\Delta C_\delta}{e}$$

Thus : $$\frac{de}{dt} = \left(\frac{1}{C_B - C_r} + \frac{1}{C_l - C_A}\right) D_\delta \frac{\Delta C_\delta}{e} \quad (4)$$

By integrating equation (4) from $e = e_0$ (t = 0) to e(t), the expression of the variation of the thickness of δ phase with time is obtained (parabolic growth law):

$$e^2 - e_0^2 = k.t \quad (5)$$

with $$k = 2\left(\frac{1}{C_B - C_r} + \frac{1}{C_l - C_A}\right) D_\delta . \Delta C_\delta \quad (6)$$

k is the growth rate constant in m^2/s.

In the simple case where the partial molar volumes (V_m) of A and B are considered constant and equal, the expression of the growth constant k as a function of the molar fraction x (= $C.V_m$) of the B constituent is obtained:

$$k = 2\left(\frac{1}{x_B - x_r} + \frac{1}{x_l - x_A}\right).\Delta x_\delta . D_\delta \quad (7)$$

Moreover, if the A and B constituents are considered as pure (i.e. $x_A = 0$ and $x_B = 1$) and the δ phase is almost stoichiometric ($x_l = x_r = x_\delta$), a simple equation of the growth constant k is obtained, depending only on the molar fraction and the diffusion coefficient of B constituent in the δ phase:

$$k = 2\frac{\Delta x_\delta}{x_\delta(1 - x_\delta)} D_\delta \quad (8)$$

4.5. Growth kinetics of Au-Ti intermetallic compounds

The growth kinetics of Au-Ti intermetallic compounds between liquid Au and solid Ti, with bulk Au and Ti materials, is not studied in the literature. Some Ti/Au interdiffusion studies are conducted on thin film couple, and only two published papers deal with interdiffusion in bulk Ti/Au diffusion couple at solid state. Taguchi et al.[57] investigated the growth kinetics of the Ti-Au intermetallic compounds (IMCs) in the Au/Ti diffusion couple in the temperature range 837 – 877 °C for reaction times up to 72h. Kumar et al.[58] studied the growth kinetics of IMCs in this system at 900°C for 120h. Both studies report the formation of four successive layers at the Ti / Au interface corresponding to the four Ti-Au intermetallic compounds given by the binary Ti-Au phase diagram (Ti_3Au, TiAu, $TiAu_2$ and $TiAu_4$). Moreover, Taguchi et al. [57] reported the formation of the β-Ti solid solution layer situated between α-Ti and Ti_3Au layers. According to both teams, the growth kinetics of all these Ti-Au IMCs (and β-Ti phase) obey a parabolic law, suggesting that the growth is controlled by diffusion process. A SEM micrograph presented in Figure 36 shows wavy interfaces between IMCs layers. According to Kumar et al[58], this wavy shape is due to high anisotropy in diffusion of the intermediate phases because of crystal orientations, as well as to the very complex process of growth in this system. Indeed, while a given phase grows thanks to the consumption of one or two neighboring phases, at the same time, this phase may also be consumed by one or two neighboring phases (growth and regress at reactive interfaces).

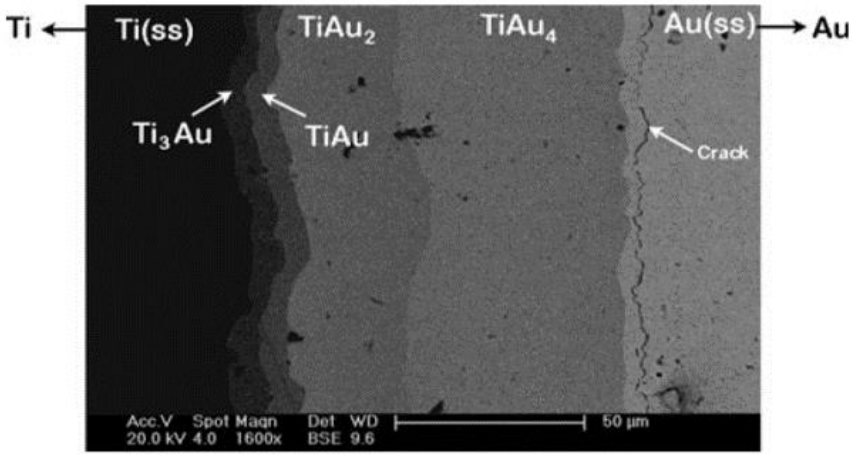

Figure 36: Interdiffusion zone developed in the Au/Ti diffusion couple annealed at 900°C for 120h[58].

The growth kinetics of the intermetallic and β-Ti layers follows the diffusion law

$e^2 = k_p.t$, with e the thickness of the layer, k_p the growth rate constant and t the time.

Taguchi et al.[57] and Kumar et al.[58] determined the diffusion parameters of the Ti /Au diffusion couple, especially the parabolic growth rate constant k_p presented in Figure 37. Both teams found similar results: the growth rates of $TiAu_2$ and $TiAu_4$ compounds are much higher than those of Ti_3Au and TiAu compounds at 877 – 900 °C.

Taguchi et al.[57] found that the growth rate constants of the IMC layers vary with temperature following the Arrhenius equation with very high activation energies, in the range 450 - 737 kJ/mol (respectively for the AuTi and Au_2Ti phases). At 877°C (1150K), they found the k_p parabolic growth constants equal to ~ 5.5, 3.5, 17 and 20.10^{-16} m^2/s respectively for the $AuTi_3$, AuTi, $AuTi_2$ and $AuTi_4$ phases.

Extrapolating the temperature dependence of k_p curves plotted by Taguchi et al.[57] at T = 900°C = 1173K (i.e. $10^{-4}/T = 8.5\ K^{-1}$, see Figure 37a), the obtained k_p values are between 100 and 900.10^{-17} m^2/s, i.e. of the same order of magnitude as those reported by Kumar et al.[58] (Figure 37b).

Note finally that at the best of our knowledge, there is no data in the literature concerning the diffusion coefficients of Ti and Au in Ti-Au intermetallics.

a)

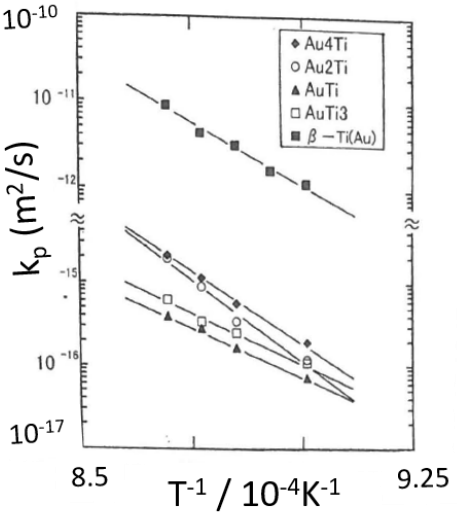

b)

Phase	$k_p \times 10^{-17}$ (m^2/s)
Ti_3Au	5.4
AuTi	4.7
$TiAu_2$	140
$TiAu_4$	405

Figure 37: a) Temperature dependence of growth constant rate k_p of five phases formed at Au/Ti interface in the temperature range 827-877°C.[57] and b) parabolic growth constant (k_p) at 900°C[58] for Au_4Ti, Au_2Ti, AuTi and $AuTi_3$ phases.

4.6. Conclusion

In this section, the Ti-Au binary phase diagram, that we will frequently refer to in the following work, is presented. It contains 4 intermetallic compounds (IMCs), including two stoichiometric IMCs (Ti_3Au and $TiAu_2$) and two non-stoichiometric IMCs (TiAu and $TiAu_4$) with melting points higher or much higher

than the melting temperature of Au (1064.43°C). These IMCs have a fragile character, in contrast with pure Au which is considered as the most ductile metal.

A generic phase growth model in the case of the formation of one intermediate phase is presented. The growth kinetics of 4 intermediate phases, as in the Ti-Au system, is complex and no simple analytical solution has been presented in the literature.

To the best of our knowledge, no reactivity study between liquid gold and solid titanium are reported in the literature. However, two studies of interdiffusion between Ti and Au at solid state at 900°C and 837-877°C show a parabolic growth kinetics of the four Ti-Au intermetallic compounds given by the Ti-Au phase diagram (Ti_3Au, TiAu, $TiAu_2$ and $TiAu_4$). The IMCs growth follows the Arrhenius equation, with very high activation energies (in the range 450 - 737 kJ/mol).

5. Literature review for zirconia brazing

5.1. Introduction

Zirconia is an advanced ceramic of great importance for its notable physical properties and in particular those of electrical and electronic conduction. For its remarkable chemical and thermal refractory properties, zirconia deserves to be assembled with metals such as titanium for various applications. Brazing is one of the best technique to join Ti to zirconia.

In this section, brazed assemblies reported in the literature for zirconia-to-zirconia (similar brazing) and zirconia-to-titanium brazing (dissimilar brazing) will be presented, as well as the interfacial reactivity and mechanical characterization of the joint (if they were studied).

5.2. Similar brazing of zirconia (zirconia-to-zirconia brazing)

Several studies deal with zirconia-to-zirconia brazing, using a wide range of brazing alloys and most of them explore the Ti and Zr active elements. Another method is the use of mixture of Ag powders and oxide (SiO_2, CuO) powders as potential filler for zirconia-to-zirconia brazing at high temperatures[59 60].

Table 5 summarizes experimental conditions (active element content or brazing mixture, holding time and temperature) and the mechanical strength of the joint for some cases of zirconia-to-zirconia brazing reported in the literature.

Brazing alloy or brazing mixtures*	Temperature (°C)	Holding time (min)	Mechanical strength	Reference
Sn-4Ti	1000	10	shear strength : 22-28 MPa	49
Ag27Cu3Ti Sn10Ag4Ti	900°C	10	Flexural strengths: 227 MPa 137 MPa	46
Zr-47Cu	900	5	3-point bending strength: 350 MPa	40
Ag57Cu38Ti5	850	30	Shear strength: 150 MPa	61
Ni-Ti	1350	30	shear strength 100MPa	32
63Ag-35.25Cu-1.75Ti	850	5	4-point bending strength: 280 MPa	62
Ag-35Cu-1.65Ti	900	10	-	63
Au-Ti with sputtered Ti	1080	1	-	64
Ag-2SiO_2*	1050	30	Shear strength: 47 MPa	59
Ag-2CuO*	1000	60	4 point bend strength 157 ± 24 MPa	60

Table 5: Summary of the ZrO_2 / ZrO_2 brazed assemblies using active filler metals.

For the whole examples cited in Table 5, zirconia is successfully brazed. In the cases where Ti is used as active element, these good results are due to the formation of reaction layer(s) at the zirconia / braze interface. For instance, two SEM micrographs of a ZrO_2 / Ag27Cu3Ti alloy interface and a ZrO_2 / Ni-Ti interface, respectively brazed at 900 and 1350°C for 10 and 30 min, are presented in Figure 38. Chuang et al.[46] reported the formation of two layers at the zirconia / Ag27Cu3Ti alloy (Figure 38a). Next to zirconia, a thin TiO layer of about 2 µm, and juxtaposed, a thicker layer (~10 µm) which consists of Ti_2Cu compounds with small TiAg strips. Zhang et al.[32], who are interested in ZrO_2 / Ni-Ti brazing, also revealed the formation of two reactive layers (Figure 38b). Near zirconia, a discontinuous TiO layer of about 5 µm (marked as C) is analyzed, and on this reaction product, a thicker layer of about 28 µm, is identified as Ni_2Ti_4O (marked as D).

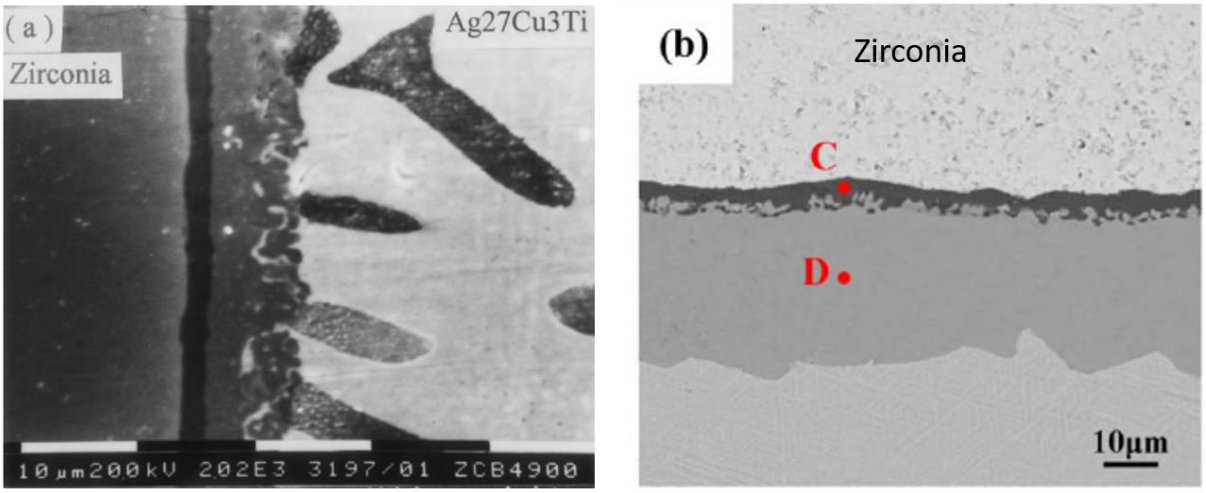

Figure 38: SEM micrographs of zirconia / braze interfaces of the systems: a) ZrO_2 / Ag27Cu3Ti/ZrO_2 brazed at 900°C for 10 min [46],b) ZrO_2 / Ni–Ti / ZrO_2 brazed at 1320°C for 30 min[32].

Among all the studies given in Table 5, only one paper intends to consider a biocompatible solution [64]. Agathopoulos et al.[64] studied the zirconia brazing with Ti-Au system in different conditions with Ti coating layer on an Au foil (25µm) or on sputtered Au (100-500nm), to achieve 1-8 at% Ti in the Ti / Au layer stacking. The successful brazing experiments were carried out under dynamic vacuum (oxygen pressure $P_{O2} < 2.10^{-3}$ Pa) at 1080°C for 1 min, in the configuration zirconia / Au foil (25µm) / Au (10nm) / Ti (260-530nm) / Au (20nm) / Δ, were Δ indicates a symmetry plane. Joints with 1 at% and 2 at% of Ti were analysed by SEM and EDX, and no difference on interfacial microstructure was identified. Both joints are composed of a thick Au layer with small Ti oxide particles. Ti is dissolved in the metal, but poor wetting of zirconia is obtained, and the liquid phase did not fill the gap between the ceramic substrates.

5.3 Dissimilar brazing zirconia / titanium

Since the 2000s, zirconia to titanium (or Ti6Al4V) brazing has been widely studied for various types of applications, such as electronic or biomedical, especially since their thermal expansion coefficient are quite similar (YTZP 3mol%: $9,6x10^{-6}K^{-1}$, Ti: $9,0x10^{-6}K^{-1}$ and TA6V: $9,4x10^{-6}K^{-1}$).

To braze zirconia and titanium, the standard method consists of using a foil of an active brazing alloy containing a reactive element like Zr or Ti. Active element can also be directly deposited on ceramic surface, by sputtering or mechanical metallization[65].

Ag-Cu-Ti reactive alloys with various Ag, Cu and Ti contents are widely investigated in the literature [63,66–71]. Wei et al.[71] have brazed zirconia to Ti with Ag68.8Cu26.7Ti4.5 filler at 900°C under vacuum

(~ 10^{-3} Pa) for 0.1 - 6h. After brazing during 0.1h, they observed four intermetallic compounds (IMCs) at Ti / braze interface, and TiCu and TiO layers at braze / ZrO_2 interface. These active filler metals are also used to the zirconia-to-zirconia brazing.

Others studies describe zirconia to titanium joining, with active alloys containing Zr and Ti as active elements, such as Zr-Ti-Ni-Cu, Zr-Cu-Al-Ni[72] or Ag-Cu-In-Ti[67].

Table 6 summarizes some cases of the zirconia / titanium joints investigated in the literature. Only their best brazing conditions (active element content, contact time and temperature) are indicated. When reaction layers are described and mechanical strength is tested, information is reported in Table 6.

Since metallic substrate is constituted of titanium which is an active element, it is also possible to use, as braze, a single metal or an alloy which does not contain any active element. In this case, Ti is provided by the substrate from dissolution and diffusion through the braze alloy, enriching it in Ti active element and reacting with zirconia. Table 7 summarizes the zirconia / titanium assemblies reported in the literature, with non-reactive filler metals. Their best brazing conditions (active element content, contact time and temperature) are indicated. When reaction layers are described and mechanical strength of the joints are given, information is reported in the table 7.

Brazing alloy or brazing mixture*	Brazing Conditions	Zirconia / braze interface	Braze / Ti interface	Mechanical strength	Ref
59Ag-27.25Cu-12.5In1.25Ti 63Ag-35.25Cu-1.75Ti 68.8Ag-26.7Cu-4.5 Ti. (wt%)	850-1000°C 5-30 min	Ti_xO_y < 2 µm	-	4-point-flexure: 63Ag-35.25Cu-1.75Ti, (850°C for 5 min) 225 ± 8 MPa	67
Ag-28Cu-2Ti Filler Reinforced with Cerium Oxide Nanoparticles (0<x<0.1 wt%)*	980°C 10 min	-	Cu_2Ti + Cu_4Ti	Shear stress 20-23 MPa	68
Metallized zirconia with Ti, Au-18Ni	980 °C, 10 min	TiO_x	Ti-Au, Ti-Al-Ni-V, Ti-Al-Ni	3-point flexure 62 ± 24 MPa	65
63Ag-35,25Cu-1,75Ti	840°C 5 min	-	-	3-point flexure 242 ± 18 MPa	66
Zr54Ti22Ni16Cu8	860°C 60 min	-	-	shear strength ~186 MPa	73
63Ag-35.25-Cu-1.75 Ti	850°C 5 min	TiOx ~3 µm	CuTi and $CuTi_2$ ~10 µm	3-point bend test 246 MPa	69
Au-Ti (différentes configurations de métallisation)	1065-1100°C 1 min to 60 min	TiO_2	$TiAu_6$ / $TiAu_2$ / TiAu / Ti_3Au / alpha-Ti[O]	-	64
Cu-40Ag-5Ti	870°C 5 min	Cu_2(Ti, Ag)O ~2 µm	Ti_3Cu_4, TiCu and Ti_2Cu	tensile strength 150 ± 50 MPa	74
$Ti_{47}Zr_{28}Cu_{14}Ni_{11}$	850°C 30 min	TiO+TiO2 ~10 µm	α-Ti+(Ti,Zr)2(Cu,Ni) eutectic / acicular Widmanstäten structure	Shear strength 63 MPa	75 76
Ag-Cu-Ti / N-Cu foam / Ag-Cu	870°C 10 min	-	-	Shear strength 96 MPa	70
$Ti_{33}Zr_{17}Cu_{50}$	900°C 10 min	Cu_2Ti_4O+(Ti, Zr)$_2$Cu ~6 µm TiO+TiO_2 ~4 µm	Ti-Cu IMCs	Shear strength 162 MPa 10 min at 900°C	77
68,8Ag26,7Cu4,5Ti	900°C 6 min	TiCu and TiO	Ti-Cu IMCs	-	71
68,8Ag-26,7Cu-4,5Ti	900°C 1 h	Ti_3Cu_3O and Ti_2O	Ti-Cu IMCs	-	71
Ni / Ti / Ni	1035°C 5 min	Ti_2Ni, Ni_2Ti_4O	Ti2Ni, Ni2Ti4O	3-point flexure 261 ± 64 MPa Tensile test 169 ± 33 N	78
Ag-35Cu-1.65Ti	900°C 1 min	Ti_2O and Cu-Ti-O	Ti-Cu IMCs	Flexure 445 ± 50 MPa	63
Zr55Cu30Al10Ni5	900°C 10 min	-	-	shear strength 95 MPa at 900°C, 10 min	72

Table 6: Summary of the ZrO_2 / Ti brazed assemblies with active filler metals.

Brazing alloy	Brazing Conditions	Zirconia / braze interface	Braze / Ti interface	Mechanical strength	Ref
Ag (35 µm)	980C° 30 min	Ti_3O_2 thick layer (~40 µm), large holes	-	-	79
Ag-28Cu	820°C 10 min	TiO_x ~ 3µm	CuTi and $CuTi_2$	3-point flexure 32 ± 9 MPa	66
NiCrSiB	1025°C 10 min	TiO	-	shear strength 285 MPa	80
Au	1150°C 10 min	TiO	The 4 Ti-Au IMCs ~35 µm	shear strength ~35.0 MPa	81
Au (25 µm)	1065°C-1100°C 1 min to 60 min	TiO_2	$TiAu_6$ / $TiAu_2$ / TiAu / Ti_3Au / alpha-Ti[O]	-	64
AgCu	870°C 10 min.	TiO 0.5-1 µm	Ti-Cu IMCs ~15 µm	shear strength 52 MPa	82

Table 7: Summary of the ZrO_2 / Ti brazed assemblies using non-active alloys as filler metal: Ti active element is provided by the substrate.

The majority of the filler metals studied in the literature are composed of toxic elements such as Cu or Ni which prevent their use for implantable device. To our knowledge, there are only two published papers that deal with zirconia / titanium brazing with gold as filler metal.

Agathopoulos et al.[64] joined Ti and zirconia with a gold foil 25µm thick under vacuum (~2.10^{-3} Pa) at 1065-1100°C. They observed formation of a Ti_xO_y layer at the zirconia interface and four Ti-Au IMCs at the Ti side. No Zr was detected in the reaction zone.

Recently, Lei et al.[81] studied the effect of brazing temperature and holding time on the interfacial microstructure of the ZrO_2 / Au / Ti joint, with an Au-foil 50µm thick under vacuum ($1.3x10^{-3}$ Pa) in the temperature range 1110-1190°C for 5 - 30 min. The joint, presented in Figure 39 is composed of five layers: at the Ti side, an overlay of the four Ti-Au intermetallic compounds layer given by the Ti-Au phase diagram Ti_3Au, TiAu, $TiAu_2$, $TiAu_4$ (respectively named *I,II,III and IV* in Figure 39) and at ZrO_2 side, a thin (< 5 µm) TiO layer (named *V* in Figure 39). Titanium oxide layer is formed thanks to Ti diffusion from the metallic substrate through the joint following, at zirconia side, the reaction:

$$Ti + ZrO_2 \rightarrow TiO_x + ZrO_{2-x}$$

The global thickness of the Ti_3Au-TiAu-$TiAu_2$ layer varies with time and temperature in the range ~ 19-30 µm, whereas the morphology and the thickness of TiO layer do not significantly change. An optimal shear strength of 35 MPa is obtained for a joint brazed at 1150°C for 10 min.

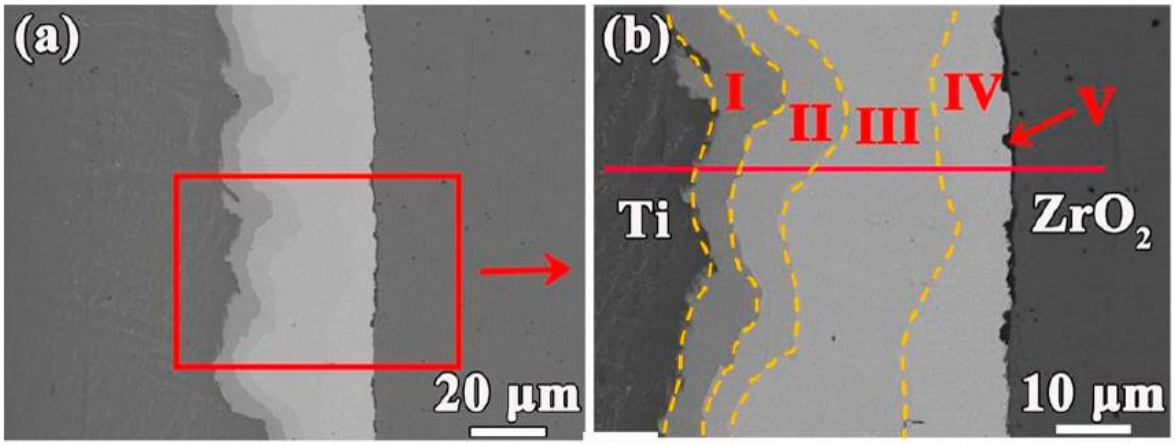

Figure 39: Typical microstructures and elemental distribution of titanium / Au / ZrO_2 joint at 1150 °C for 10 min[81].

Many authors have reported that zirconia turns grey or black near the joint, after a zirconia / titanium brazing under high vacuum. Zirconia substrate becomes darker as the distance from the braze decreases. The parameters influencing zirconia darkening are, among other, the chemical nature of the metallic substrate, the active element (Ti or Zr) content in the filler metal, the brazing temperature and dwell time at liquid state. Hanson et al.[67] have measured the thickness of dark zirconia zone as a function of dwell time for different brazing temperatures, in the case of zirconia-to-zirconia brazing with 63Ag-35.25Cu-1.75Ti alloy. They have shown that the width of the dark zone increases from 1.8mm to 3mm, when brazing temperature increases from 850 to 1000°C. Under these conditions, for dwell times between 5 and 30 min, the width of the dark zone does not progress.

5.4. Summary/conclusion

Zirconia-to-zirconia (similar) brazing and zirconia-to-titanium (or TA6V alloy) brazing (dissimilar brazing) are widely investigated in the literature.

Concerning dissimilar brazing, active alloys containing Ti and/or Zr active elements are often used, although filler metals without active element are also usable since titanium substrate dissolves and diffuses in the liquid alloy. Several studies are reported using Ag-Cu based alloys or nickel which are toxic and non-biocompatible, preventing their use for zirconia-to-titanium brazing in a view of biomedical application. To our knowledge, only two papers deal with Ti / ZrO_2 brazing with pure gold.

In any case, titanium dissolved in the liquid alloy reacts with oxygen from zirconia substrate, leading to the formation of a Ti oxide (or sometimes mixed oxide like TiCu oxide) reaction product layer at the zirconia / joint interface.

6. Conclusions

In this literature review, wetting and brazing process are presented. The relation between brazing process and wetting properties of the system is reported. The necessary condition to perform a good brazing is the ability of the liquid braze to wet the substrates to be assembled.

The wetting of solids by liquid metals is addressed in a general way, in order to define the main physico-chemical properties involved in the wetting study, especially the contact angle, the surface and interfacial energies, and the work of cohesion and adhesion which are linked by the Young relation.

When considering the spreading of a liquid droplet from its initial position to its final equilibrium position, we are talking about dynamic wetting, which can be non-reactive or reactive wetting. In the case of non-reactive wetting, viscosity and gravity can have a significant impact on spreading kinetics of the liquid metal. In the case of reactive wetting, two types of reactivity are distinguished, dissolution and chemical reaction. Dissolutive wetting occurs when liquid metal dissolves the bulk substrate. On the other hand, reactive wetting is concerned by the formation of a reaction product layer at the liquid / solid interface. This reaction product can be more wettable than the substrate, improving the spreading of liquid metal, or, on the contrary less wettable and thus limiting or stopping the spreading of the liquid droplet.

A state of the art of the zirconia wetting by liquid alloys is performed. While zirconia is not wetted by noble metals, the addition of an active element in the metal, such as Zr or Ti provides reactive wetting of zirconia thanks to the formation of zirconium oxide or titanium oxide product layer at the interface. Oxygen atoms are provided by the zirconia substrate, becoming thus sub-stoichiometric. The contact angle on this reactive layer strongly depends on the stoichiometry of the oxide formed at the interface, reaching ~20° on TiO layer.

The Ti-Au system is investigated, firstly by presenting the Ti-Au binary phase diagram. 4 intermetallic compounds (IMCs) are revealed, including two stoichiometric IMCs (Ti_3Au and $TiAu_2$) and two non-stoichiometric IMCs (TiAu and $TiAu_4$), all having melting points higher or much higher than Au melting temperature. These IMCs have a fragile character, in contrast with pure Au which is considered as the most ductile metal. A generic phase growth model in the case of the formation of one intermediate phase is also presented. While the formation of 4 intermediate phases is complex, as in the Ti-Au system, no simple analytical solution for the growth kinetics has been presented in the literature.

Reactivity between liquid gold and solid titanium is neither reported in the literature. Some studies of interdiffusion between Ti and Au at solid state show a parabolic growth kinetics of the four Ti-Au IMCs given by the Ti-Au phase diagram.

Finally, a literature review for similar brazing of zirconia and dissimilar brazing of zirconia-to-titanium is presented. Active alloys containing Ti (and/or Zr) active elements are often used. In the case of dissimilar brazing, it is also possible to use non-active alloys since titanium substrate dissolves and diffuses in the joint. Several brazing studies are performed by using Ag-Cu based alloys or nickel which are toxic and non-biocompatible, preventing their use for zirconia-to-titanium brazing in a view of biomedical application.

To the best of our knowledge, there are only two published works in the literature which study the brazing of titanium with zirconia by using pure gold.

In any case, titanium reacts with oxygen from zirconia substrate, leading to the formation of a Ti oxide (or mixed oxide like TiCu oxide) reaction product layer at the zirconia / joint interface. This product layer is wettable by molten metals, providing successful brazing.

References of chapter 1

1. N. Eustathopoulos, M.G. Nicholas & B. Drevet. *Wettability at high temperatures*. (Pergamon materials series, 1999).

2. N. Eustathopoulos, F. Hodaj & O. Kozlova, The wetting process in brazing. in *Advances in Brazing* 3–30 (Elsevier, 2013). doi:10.1533/9780857096500.1.3.

3. R. Shuttleworth & G.L.J. Bailey. The spreading of a liquid over a rough solid. *Discussions of the Faraday Society*, **3**, 16–22 (1948).

4. M. Diallo. Wetting on heterogeneous metal-oxides regular patterned surfaces by a non-reactive liquid metal. Materials. [PhD Thesis, Université Paris-Saclay] (2019).

5. M. Wu, L. Chang, L. Zhang, X. He & X. Qu. Effects of roughness on the wettability of high temperature wetting system. *Surf Coat Technol* **285,** 145–152 (2016).

6. R. Voytovych, F. Robaut & N. Eustathopoulos. The relation between wetting and interfacial chemistry in the CuAgTi/alumina system. *Acta Mater.* **54**, 2205–2214 (2006).

7. D. R. Nalagatla, Influence of surface roughness of copper substrate on wetting behaviour of molten solder alloys (2007). University of Kentucky Master's Theses. 488. https://uknowledge.uky.edu/gradschool_theses/488

8. Y.-Y. Chen, J.-G. Duh, & B.-S. Chiou. The effect of substrate surface roughness on the wettability of Sn-Bi solders. *J Mater Sci Mater Electron.* **11***,* 279–283 (2000).

9. P. Protsenko, A. Terlain, M. Jeymond & N. Eustatopoulos. Wetting of Fe-7.5%Cr steel by molten Pb and Pb-17Li. *Nucl Mater* **307-311,** 1396–1399 (2002).

10. N. Frumin. Wettability and phase formation in the TiCxAl system. *Scr. Mater.* **37**, 1263–1267 (1997).

11. K. Nogi, Y. Okada, K. Ogino & N. Iwamoto. Wettability of diamond by liquid pure metals. *Mater Trans JIM.* **35**, 156–160 (1994).

12. E. A. Brandes, *Smithells metals reference book*. (Butterworth-Heinemann, 1998).

13. S.I. Popel, B.V. Tsarevskii & V.G. Babkin. Wetting of refractory oxides by metal and slag melts. *Refractories* **15**, 577–582 (1974).

14. Y. V. Naidich, V. V. Zabuga, & V. M. Perevertailo. Temperature dependance of spreading kinetics in systems with different types of interaction of contaction phases. *Adgez. Rasplav. Paika Mater.* **27**, 23–24 (1992).

15. Y. V. Naidich, V. M. Perevertailo & G.M. Nevodnik, Kinetics of spreading of molten metals on solid surfaces. *Sov. Powder Metall. Met. Ceram.* **11**, 555–558 (1972).

16. L. M. Hocking & A. D. Rivers, The spreading of a drop by capillary action. *J. Fluid Mech.* **121**, 425 (1982).

17. N. Ebrill. (University of Newcastle, 1999).

18. M. Denesuk, J.P. Cronin, B.J.J. Zelinski, N.J. Kreidl & D.R. Uhlmann. Predictive modelling of liquids spreading on solid surfaces. *Phys. Chem. Glas.* **34**, 203–211 (1993).

19. A. Passerone, M. Muolo, F. Valenza, F. Monteverde & N. Sobczak. Wetting and interfacial phenomena in Ni-HfB2 systems. *Acta Mater.* **57**, 356–364 (2009).

20. C. Rado, S. Kalogeropoulou & N. Eustatopoulos. Wetting and adhesion in metal-silicon carbide systems: the effect of surface polarity of SiC. *Scr Mater.* **47***,* 203–208 (1999).

21. Eustathopoulos, N. & Voytovych, R. The role of reactivity in wetting by liquid metals: a review. *J. Mater. Sci.* **51**, 425–437 (2016).

22. Warren, J. A., Boettinger, W. J. & Roosen, A. R. Modeling reactive wetting. *Acta Mater.* **46**, 3247–3264 (1998).

23. K. Landry & N. Eustathopoulos. Dynamic of wetting in reactive metal / ceramic systems: linear spreading. *Acta Mater.* **40**, 3923–3932 (1996).

24. A. Mortensen, B. Drevet & N. Eustathopoulos. Kinetics of diffusion-limited spreading of sessile drop in reactive wetting. *Scr Mater* **36**, 645–651 (1997).

25. R. Voytovytch, A. Mortensen, F. Hodaj & N. Eustathopoulos. Diffusion-limited reactive wetting: study of spreading kinetics of Cu-Cr alloys on carbon substrate. *Acta Mater.* **47**, 1117–1128 (1999).

26. O. Dezellus, F. Hodaj, A. Mortensen, & N. Eustathopoulos. Diffusion-limited reactive wetting: spreading of Cu-Sn-Ti alloys on vitreous carbon. *Scr Mater.* **44***,* 2543–2549 (2001).

27. F. Hodaj, O. Dezellus, J.N. Barbier, A. Mortensen, & N. Eustathopoulos. Diffusion-limited reactive wetting: effect of interfacial reaction behind the advancing triple line. *J Mater Sci.* **44**, 8071–8082 (2007).

28. O. Dezellus, F. Hodaj, C. Rado, J.N. Barbier, & N. Eustathopoulos. Spreading of Cu-Si alloys on oxidized SiC in vacuum: experimental results and modelling. *Acta Mater.* **50**, 979–991 (2002).

29. V. Bougiouri, R. Voytovych, O. Dezellus, & N. Eustathopoulos. The role of the chemical reaction in the infiltration of porous carbon by NiSi alloys. *J Mater Sci.* **42***,* 2016–2021 (2007).

30. O. Dezellus. Contribution à l'étude des mécanismes de mouillage réactif. Matériaux. [PhD, Institut National Polytechnique de Grenoble - INPG], (2000). ⟨tel-00009773⟩

31. F. Moszner, M.O. Gustavo, M. Chiodi, J. Janczak-Rusch, G. Blugan and J. Kuebler. Mechanical behavior of SiC joints brazed using an active Ag-Cu-In-Ti braze at elevated temperatures. *Int. J. Appl. Ceram. Technol.* **14**, 703–711 (2017).

32. Zhang, Q., Wang, J., Zheng, K., Lu, Y. & Yang, H. Microstructure evolution and mechanical properties of ZrO_2 / ZrO_2 joints brazed with Ni–Ti filler metal. *Mater. Res. Express.* **6**, 126547 (2019).

33. Minh, N. L. Caractérisation mécanique de jonctions brasées SiC / BraSiC® / SiC et critère de dimensionnement à la rupture, [PhD, Université Pierre et Marie Curie] (2011).

34. J.P. Abriata & J. Garces. The O-Zr system. *Bull. Alloy Phase Diagr.* **7**, 116–123 (1986).

35. R.H. Hannink, P.M. Kelly & B.C. Muddle. Transformation toughening in zirconia-containing ceramics. *J. Am. Ceram. Soc.* **83**, (2000).

36. P. Duwez, F.H. Brown & F. Odell, The Zirconia-Yttria System. *J. Electrochem. Soc.* **98**, 356 (1951).

37. L. Gremillard. Biocéramiques des monolithes aux composites. [HDR, MATEIS - Matériaux, ingénieurie et science, Villerbanne] (2009).

38. J. Chevalier, L. Gremillard, A.V. Virkar & D.R. Clarke. The Tetragonal-Monoclinic Transformation in Zirconia: Lessons Learned and Future Trends. *J. Am. Ceram. Soc.* **92**, 1901–1920 (2009).

39. D. Chatain, F. Chabert, V. Ghetta & J. Fouletier. New Experimental Setup for Wettability Characterization under Monitored Oxygen Activity: I, Role of Oxidation State and Defect Concentration on Oxide Wettability by Gold. *J. Am. Ceram. Soc.* **76**, 1568–1576 (1993).

40. N. Iwamoto & H. Yokoo. Joining of zirconia to metals using Zr-Cu alloy. *Eng. Fract. Mech.* **40**, 931–940 (1991).

41. X. M. Xue, Z. T. Sui & J.T. Wang, Effect of zirconium on wettability of alumina and zirconia by silver-indium base alloy. *J. Mater. Sci. Lett.* **11**, 1514–1517 (1992).

42. A. V. Durov, Y.V. Naidich & B. D. Kostyuk. Investigation of interaction of metal melts and zirconia. *J. Mater. Sci.* **40**, 2173–2178 (2005).

43. H. Bian, W. Fu, Y. Z. Lei, X. G. Song, D. Liu, J. Cao & J.C. Feng . Wetting and low temperature bonding of zirconia metallized with Sn0.3Ag0.7Cu-Ti alloys. *Ceram. Int.* **44**, 11456–11465 (2018).

44. H. Bian, Y. Zhou, X. Song, S. Hu, B. Shi, J. Kang & J. Feng. Reactive wetting and interfacial characterization of ZrO2 by SnAgCu-Ti alloy. *Ceram. Int.* **45**, 6730–6737 (2019).

45. W. Fu, A. Passerone, H. Bian, S. Hu, Y. Zhao, & X. Song, M. Wang & F. Valenza. Wetting and interfacial behavior of Sn–Ti alloys on zirconia. *J. Mater. Sci.* **54**, 812–822 (2019).

46. T. H. Chuang, M.S. Yeh & Y. H. Chai. Brazing of zirconia with AgCuTi and SnAgTi active filler metals. *Metall. Mater. Trans. A* **31**, 1591–1597 (2000).

47. M. Luigia Muolo, E. Ferrera, L. Morbelli & A. Passerone. Wetting, spreading and joining in the alumina–zirconia–Inconel 738 system. *Scr. Mater.* **50**, 325–330 (2004).

48. X. M. Xue, J. T. Wang & Z. T. Sui. Wettability and interfacial reaction of alumina and zirconia by reactive silver-indium base alloy at mid-temperatures. *J. Mater. Sci.* **28**, 1317–1322 (1993).

49. W. Fu, X. Song, A. Passeronne, S. Hu, H. Bian, Y. Zhao, M. Wang & F. Valenza. Interactions, joining and microstructure of Sn-Ti/ZrO2 system. *J. Eur. Ceram. Soc.* **39**, 1525–1531 (2019).

50. H. Okamoto. O-Ti (Oxygen-Titanium). *J. Phase Equilibria* **22**, 515–517 (2001).

51. P. Kritsalis, B. Drevet, N. Valignat, N. Eustathopoulos. Wetting transitions in reactive metal/oxide systems. **30**, 6. (1994).

52. C. Wan, P. Kritsalis, B. Drevet, & N. Eustatopoulos. Optimization of wettability and adhesion in reactive nickel-based alloys/alumina systems by a thermodynamic approach. *Mater. Sci. Eng.* **207**, 181–187 (1996).

53. J. L. Murray, The Au-Ti (Gold-Titanium) system. *Bull. Alloy Phase Diagr.* **4**, 278–283 (1983).

54. E. Svanidze, T. Besara, M. F. Ozaydin, C. S. Tiwary, K. Wang, S. Radhakrishnan, S. Mani, Y. Xin, K. Han & E. Morosan, High hardness in the biocompatible intermetallic compound β-Ti_3Au. *Sci. Adv.* **2**, (2016).

55. J. Philibert. Reactive diffusion in thin films. *Applied Surface Science*. **53**, 74–81 (1991).

56. A. M. Gusak, T. V. Zaporozhets, Y. O. Lyashenko, S. V. Kornienko, M. O. Pasichnyy & A.S. Shirinyan. Diffusion-controlled Solid State Reactions: In Alloys, Thin Films and Nanosystems. *John Wiley & Sons* (2011).

57. O. Taguchi, T. Watanobe, Y. Yamazaki & Y. Iijima. Reaction diffusion in the Au-Ti System between 1110K and 1150K. in *Defect and diffusion forum*. **194–199** 1569–1574 (2001).

58. A. K. Kumar A. & Paul. Interdiffusion studies in bulk Au–Ti system. *J. Mater. Sci. Mater. Electron.* **21**, 1202–1206 (2010).

59. Z. Wang, C. Li, X. Si, B. Yang, Y. Huang, J. Qi, J. Feng & J. Cao. Brazing YSZ ceramics by a novel SiO2 nanoparticles modified Ag filler. *Ceram. Int.* **46**, 16493–16501 (2020).

60. J. T. Darsell & K. S. Weil. Effect of Filler Metal Composition on the Strength of Yttria Stabilized Zirconia Joints Brazed with Pd-Ag-CuO x. *Metall. Mater. Trans. A* **39**, 2095–2105 (2008).

61. H. Q. Hao, Y. L. Wang, Z. H. Jin & X. T. Wang. Joining of zirconia to zirconia using AgCuTi filler metal. *J. Mater. Process. Technol.* **52**, 238–247 (1995).

62. W. B. Hanson, K. I. Ironside & J. A Fernie. Active metal brazing of zirconia. *Acta Mater.* **48**, 4673–4676 (2000).

63. J. V. Emiliano, R.N. Correia, P. Moretto & S. D. Peteves. Zirconia-Titanium Joint Interfaces. *Mater. Sci. Forum* **207–209**, 145–148 (1996).

64. S. Agathopoulos, R. N. Correia, E. Joanni & J. R. A. Fernandes. Interactions at Zirconia-Au-Ti Interfaces at High Temperatures. *Key Eng. Mater.* **206–213**, 487–490 (2001).

65. J. S. Pimenta, A. J. A. Buschinelli, R. M. Nascimento, A. E. Martinelli & J. Remmel. Joining of zirconia mechanically metallized with titanium. *Cerâmica* **56**, 212–221 (2010).

66. J. S Pimenta, A. J. A. Buschinelli, R. M. do Nascimento, A. E. Martinelli & J. Remmel. Brazing of zirconia to titanium using Ag-Cu and Au-Ni filler alloys. *Soldag. Insp.* **18**, 349–357 (2013).

67. W. B. Hanson, K. I. Ironside & J. A. Fernie. Active metal brazing of zirconia. *Acta Mater.* **48**, 4673–4676 (2000).

68. A. Sharma & B. Ahn. Brazeability, Microstructure, and Joint Characteristics of ZrO_2 / Ti-6Al-4V Brazed by Ag-Cu-Ti Filler Reinforced with Cerium Oxide Nanoparticles. *Adv. Mater. Sci. Eng.* **2019**, 1–11 (2019).

69. O. Smorygo, J. S. Kim, M. D. Kim & T. G. Eom. Evolution of the interlayer microstructure and the fracture modes of the zirconia/Cu–Ag–Ti filler/Ti active brazing joints. *Mater. Lett.* **61**, 613–616 (2007).

70. C. Li, Joining of yttria stabilised zirconia to Ti6Al4V alloy using novel CuO nanostructure reinforced Cu foam interlayer. *Mater. Lett.* **253**, 105–108 (2019).

71. Wei, S.-H. & Lin, C.-C. Microstructural evolution and bonding mechanisms of the brazed Ti/ZrO_2 joint using an $Ag_{68.8}$ $Cu_{26.7}$ $Ti_{4.5}$ interlayer at 900 °C. *J. Mater. Res.* **29**, 684–694 (2014).

72. Liu, Y., Hu, J., Shen, P., Guo, Z. & Liu, H. Effects of Fabrication Parameters on Interface of Zirconia and Ti-6Al-4V Joints Using Zr55Cu30Al10Ni5 Amorphous Filler. *J. Mater. Eng. Perform.* **22**, 2602–2609 (2013).

73. S. W. Park, H. Lee, B. H. Lee, T. H. Kim, K. I. Kim, S. A. Hong, M. Kim, S. Hyun, G. H. Ryu & K. T. Kim, Effect of Interface Microstructure on Joint Strength of Zirconia/Titanium Alloy Brazed with Amorphous Zr-Ti-Ni-Cu Active Filler Metal. *Metals* **10**, 718 (2020).

74. C. Peytour, P. Berthet, F. Barbier & A. Revcolevschi, Interface microstructure and mechanical behaviour of brazed TA6V/zirconia joints. *J. Mater. Sci. Lett.* **9**, 1129–1131 (1990).

75. Y. Liu, J. Hu, Y. Zhang & Z. Guo, Interface microstructure of the brazed zirconia and Ti-6Al-4V using Ti-based amorphous filler. *Sci. Sinter.* **45**, 313–321 (2013).

76. Y. Liu, J. Hu, Y. Zhang & Z. Guo, Joining of Zirconia and Ti-6A1-4V Using a Ti-based Amorphous Filler. *J. Mater. Sci. Technol.* **27**, 653–658 (2011).

77. Y. H. Liu, J. D. Hu, P. H. Shen, X. Han & J. C. Li, Microstructural and mechanical properties of jointed ZrO2/Ti–6Al–4V alloy using Ti33Zr17Cu50 amorphous brazing filler. *Mater. Des.* **47**, 281–286 (2013).

78. G. Jiang, D. Mishler, R. Davis, J. P. Mobley & J. H. Schulman, Zirconia to Ti-6Al-4V braze joint for implantable biomedical device. *J. Biomed. Mater. Res. B Appl. Biomater.* **72B**, 316–321 (2005).

79. S. Agathopoulos, S. Pina & R.N. Correia. A review of recent investigations on zirconia joining for biomedical applications. in *Advances in joining of Ceramics* 135–147 (Charles A. Lewinson, Mrityunjay Singh and Ronald Loehman, 2003).

80. J. Cao, X. G. Song, C. Li, L. Y. Zhao & J. C. Feng, Brazing ZrO2 ceramic to Ti–6Al–4V alloy using NiCrSiB amorphous filler foil: Interfacial microstructure and joint properties. *Mater. Charact.* **81**, 85–91 (2013).

81. Y. Lei, H. Bian, W. Fu, X. Song, J. Feng, W. Long & H. Niu, Evaluation of Biomedical Ti/ZrO2 Joint Brazed with Pure Au Filler: Microstructure and Mechanical Properties. *Metals* **10**, 526 (2020).

82. X. Dai, J. Cao, J. Liu, D. Wang & J. Feng, Interfacial reaction behavior and mechanical characterization of ZrO2/TC4 joint brazed by Ag–Cu filler metal. *Mater. Sci. Eng. A* **646**, 182–189 (2015).

Chapter 2 : Materials and experimental methods

Contents

1. Introduction

This chapter presents, in a first part, the selected materials for the present study, namely the substrates (zirconia and titanium) and the filler metals.

Then, two experimental techniques used to conduct the wetting study will be exposed: the sessile drop and dispensed drop methods. Finally, brazing sample set up and experimental equipment (especially the furnaces) will be presented.

Once wetting and brazing samples are manufactured, they are characterized. In this second part, methods used to prepare and to characterize the samples are detailed. These methods make it possible to study the physico-chemical properties of the samples in order to understand the phenomena occurring during the wetting and brazing processes and to propose the relevant reaction mechanisms. Lastly, the mechanical characterization of the brazed specimens will be described.

2. Materials

Materials used for the present wetting and brazing studies are classified into two categories: the substrates and the brazing alloys or metals. The raw materials properties and their characterizations are detailed in this first part.

2.1. Substrates

Remember that the goal of this work is to study the zirconia to titanium brazing for the cochlear implant application. For this reason, the two substrates are imposed by the industrial application.

2.1.1. Zirconia YTZP

In this study, two shapes of zirconia samples (detailed in paragraph 3.2.) are used: zirconia discs for wetting and basic brazing experiments, and zirconia samples in a complex form used for brazing of tensile test specimens. The two types of samples are sintered following the same manufacturing process, so that pieces have identical composition and surface state.

a) General presentation

Zirconia used in the present study is an Yttria-stabilized Tetragonal Zirconia Polycrystal (YTZP) with adjunction of 3 mol% yttria (Y_2O_3). This advanced ceramic has a wide range of applications but is specifically employed for biomedical applications since it is a bioinert ceramic with an extremely high fracture toughness.

This ceramic is formed by hot isostatic pressing (HIP), with a post HIP heat treatment. The composition of the fired zirconia is given in Table 8.

Oxides	$ZrO_2 + HfO_2 + Y_2O_3$	Y_2O_3	HfO_2	Al_2O_3	Other oxides
Composition (wt %)	99.6	5.35	1.9	0.24	0.16

Table 8: Composition of the YTZP provided by the supplier [1].

b) Microstructural characterization

X-ray diffraction analysis of the raw zirconia sample was performed before and after a brazing thermal cycle at 1077°C for 3 min under high vacuum (~5.10^{-6} mbar). X-ray diffraction patterns are presented in Figure 40. Zirconia consists of a mix of polycrystalline phases. Before brazing heat treatment, a major phase of tetragonal zirconia $(ZrO_2)_{0.96}(Y_2O_3)_{0.04}$, and two minor phases of monoclinic ZrO_2 and cubic $Y_{0.425}Zr_{0.5}7O_{1.788}$ are detected. After brazing heat treatment, the general composition of zirconia does not change. However we notice a disappearance of the minor monoclinic phase.

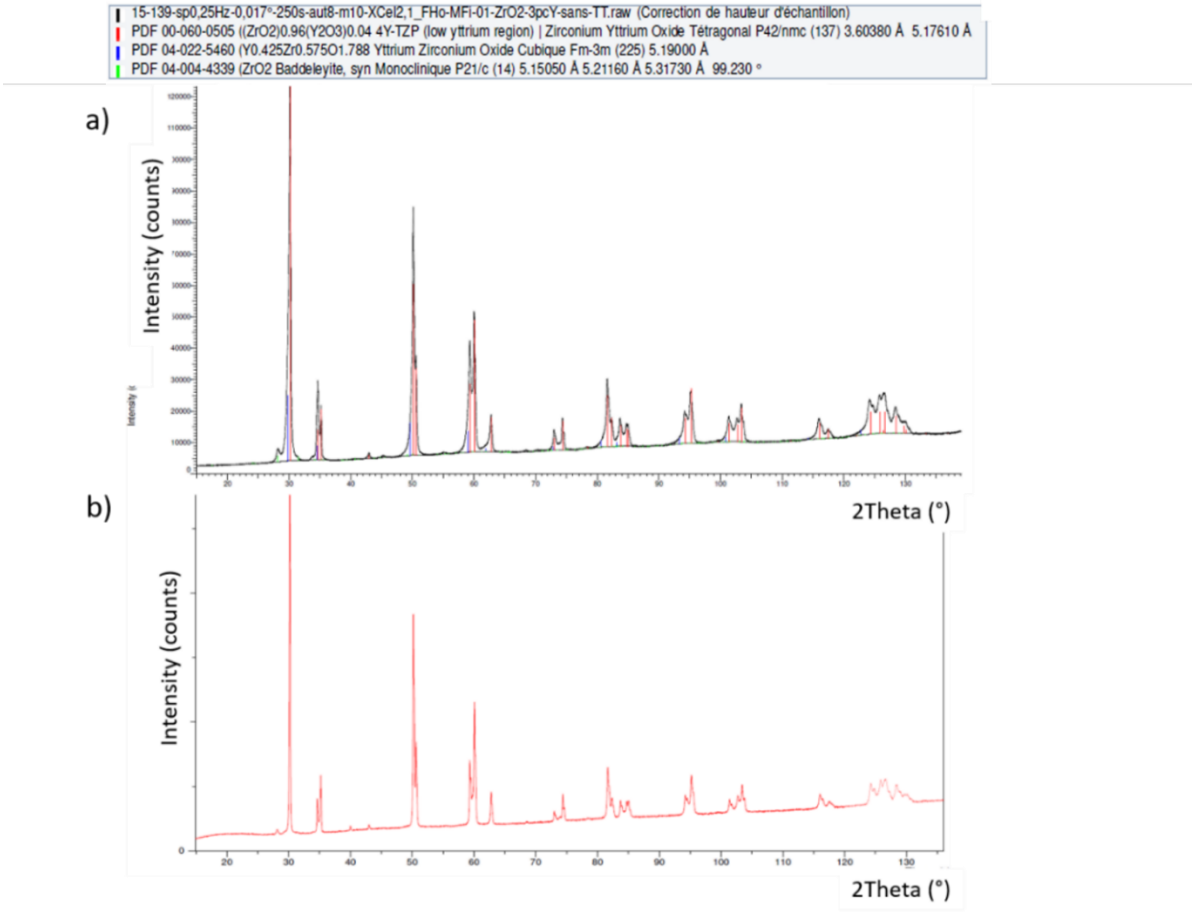

Figure 40: X-ray diffraction patterns of zirconia disc a) before and b) after brazing heat treatment at 1077°C for 3 min under high vacuum.

Some microstructural characterizations are provided by the supplier[1]. The bulk density of zirconia is 6.08 g/cm^3. The linear intercept grain size is 0.391 µm with a standard deviation of 0.156 µm. The amount of monoclinic phase is 0.29%.

c) Mechanical properties

Some physico-mechanical properties of the Y-TZP, provided by the supplier, are presented in Table 9.

Thermal expansion coefficient (30 - 1100°C)	Mean 4-point bending strength	Weibull Modulus (4-point bending strength)	Young's Modulus	Vickers Hardness
11.8.10^{-6} K^{-1}	1356 MPa	9.5	212 GPa	13.1 GPa

Table 9: Some physico-mechanical properties of the Y-TZP provided by the supplier[1].

d) Surface state

For the wetting and brazing studies, it is important to control the cleanliness of the raw (as received) substrates surfaces because spreading kinetics and wetting properties can be altered due to surface pollution. A surface analysis of zirconia was performed by X-ray photoelectron spectroscopy (XPS) to control the surface state of the substrate. The general spectra presented in Figure 41 reveals only the presence of Zr, O, Y and C chemical elements. Thus, zirconia substrates have no chemical pollution on their surface.

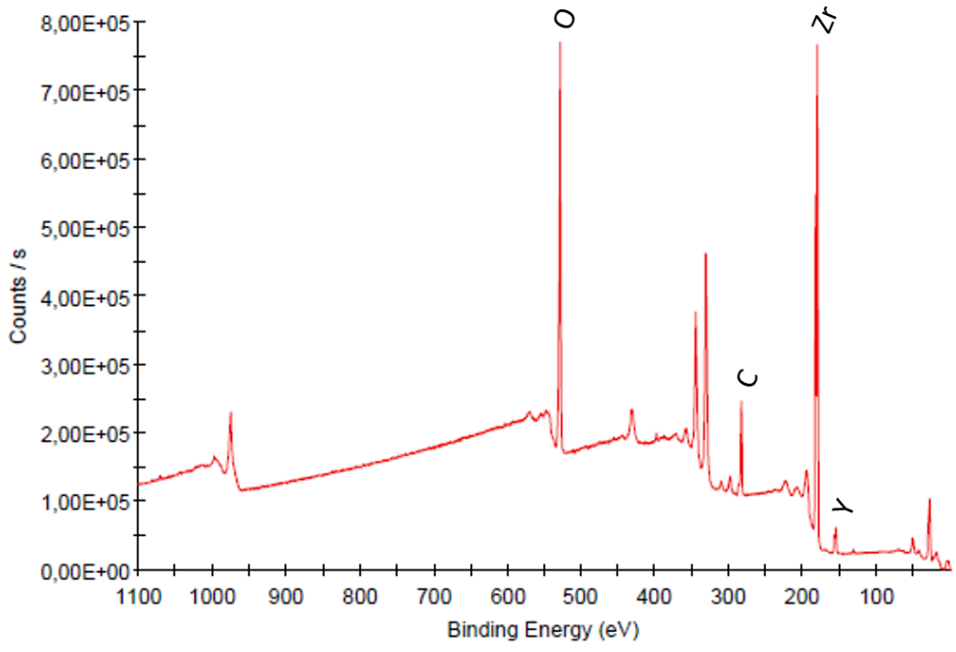

Figure 41: XPS spectra of the raw YTZP zirconia disc.

Since the raw zirconia surface “as received” from the ceramist manufacturer is clean, no particular surface preparation (except cleaning in acetone and ethanol in an ultrasonic bath) is needed to perform the wetting and brazing study. The majority of wetting experiments, and the whole brazing experiments, are carried out with raw zirconia as received. The wetting study of zirconia by some alloys is performed also on polished zirconia in order to study the impact of substrate roughness on wetting and spreading kinetics. Thus, two levels of mechanical polishing were carried out: a basic polishing until the SiO_2 colloidal suspension 6 µm, and a precision polishing until the SiO_2 colloidal suspension 0.25 µm. The resulting substrates are respectively named “polished zirconia” and “mirror polished zirconia”. Roughness measurement on the three types of zirconia samples was performed using the InfiniteFocus Alicona equipment. Figure 42 presents the roughness profiles for the three types of zirconia substrates and the Ra (arithmetic average of profile heinght deviations from the main line), Rq (quadratic average of profile height deviations from the mean line) and Rz (mean value of the five Rzi values, which corresponds to the maximum roughness depth). The Ra values are 530, 220 and 20 nm for raw, polished and mirror zirconia respectively.

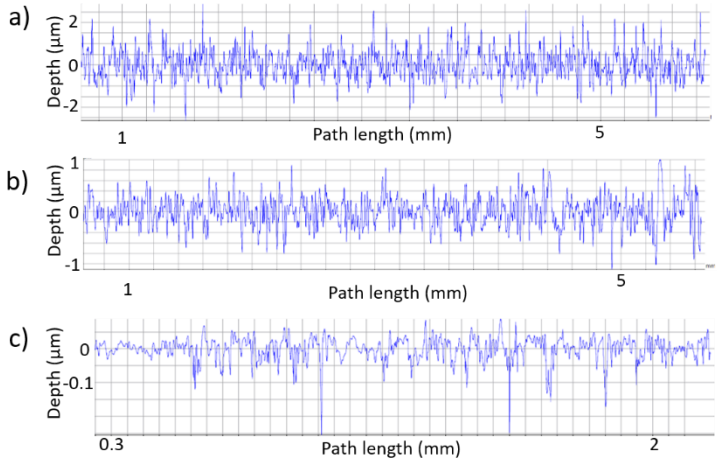

d)

	Raw ZrO_2	Polished ZrO_2	Mirror polished ZrO_2
R_a (µm)	0.53	0.22	0.02
R_q (µm)	0.68	0.28	0.03
R_z (µm)	4.65	1.64	0.25

Figure 42: Roughness profiles of the three zirconia surface states: a) raw zirconia, b) polished zirconia, c) mirror polished zirconia, and d) roughness values of the three zirconia surface states.

2.1.2. Titanium Grade 2 (T40)

Two shapes of titanium substrate (detailed in paragraph 3.2.) are used in this study: titanium discs for wetting and basic brazing experiments, and titanium rings for tensile test specimens. The two types of samples consist of Grade 2 Titanium, also known as T40, with identical composition and surface state.

a) General presentation

Grade 2 titanium (T40) is pure titanium used in different fields of industry, and in particular in aeronautic and medical applications. This pure titanium has a low density, a good biocompatibility and an excellent corrosion resistance.

b) Physical properties

Some typical physical properties of T40 are given in Table 10.

Density	Vickers hardness	Expensive thermal coefficient (20-200°C)	Young's modulus at 20°C
4.5 $g.cm^3$	145 HV	$8.7.10^{-6}$ m/m.°C	105.10^3 N/mm^2

Table 10: Physical properties of Grade 2 Titanium (T40)[2]

c) Surface state

The roughness measurements, performed with a mechanical sensor and the roughness meter Mahr Pocket Surf, averaged on 8 samples, allow to determine $R_a = 0.8 \pm 0.1$ µm for both Ti samples (disc and ring).

It is well known that titanium surface is covered by a native and stable oxide layer. An XPS analysis of the titanium substrate (disc) was carried out to evaluate the nature of the Ti oxide(s) and its thickness layer. The deconvolution of the Ti spectrum envelope presented in Figure 43 reveals the presence of 3 components: Ti_m, Ti^{3+} and Ti^4, which correspond respectively to metallic Ti, Ti_2O_3 and TiO_2. This Ti oxide layer is covered by a thin carbon layer. An XPS model of Ti substrate with the two top layers is presented in Figure 43b. Since Ti oxide layer (composed of Ti_2O_3 and TiO_2) may have an impact on metal spreading on Ti substrate, two methods to remove/reduce the layer thickness were experimented and performed a few hours (~3h) before the XPS analyses: manual polishing and chemical etching in acid solution. The thickness (e) of Ti oxide layer (noted D in Figure 43b), estimated from the deconvolution of Ti spectrum envelope, and that of the C layer (noted d), are given in Figure 43c.

a)

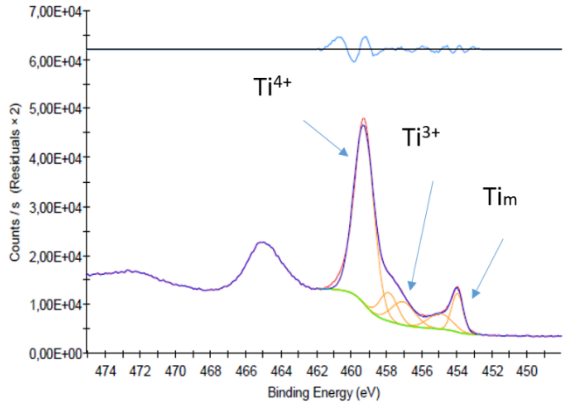

b)

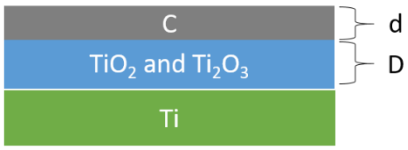

c)

	Raw Ti	Etched Ti	Polished Ti
e(d) (nm)	3.0	3.0	2.3
e(D) (nm)	6.4	1.5	0.8

Figure 43: a) EDX spectrum of Ti disc, b) EDX model of Ti substrate, c) thickness of the two top layers (D and d) of Ti substrate

The polishing and etching of Ti substrate have an impact on the thickness of Ti oxide layer e(D), which decreases from 6.4 nm for the raw Ti to 1.5 and 0.8 nm respectively for the etched Ti and polished Ti. On the contrary, whatever the treatment carried out on Ti substrate, the carbon layer thickness e(d) varies only slightly in the range 2.3 - 3.0 nm.

2.2. Metals and brazing alloys

In this study, noble metals (Au, Ag) and Au-20wt%Sn alloy are used in wetting and brazing configurations. These metals and Au-Sn alloy are also employed to process active brazing alloys, classified in two categories: brazing alloys containing Zr active element and brazing alloys containing Ti active element.

2.2.1. Pure metals and Au-Sn alloy

Some characteristics of the pure metals (Au, Ag) and Au-20wt%Sn alloy used in wetting conditions and brazing conditions are presented in Table 11. Notice that the Au-20wt%Sn (29 at%Sn) is an eutectic alloy with a low melting point (278°C). This alloy was furnished by Wesgo. The lineal temperature expansion coefficient of gold is 14. 10^{-6} $(°C)^{-1}$ [3].

Metals, purity and Au-Sn alloy	Melting temperature	Shape	Dimension
Au Grade 99.99	1064°C	Washers for tensile specimens	ϕ_{int}=9mm ϕ_{ext}=11.25mm Thickness: 100 µm
Au Grade 99.99	1064°C	Ribbon	Width: 15mm Thickness: 25, 50, 100, 150 µm

Au Grade 99.99	1064°C	Logs	ϕ=3mm Length:6mm
Ag 99.99	962°C	Ribbon	Thickness: 125 µm
Ag 99.99	962°C	Wire	ϕ=0.5 mm
Au-20wt%Sn	278°C	Foil	Thickness: 50 µm

Table 11: Noble metals and Au-Sn alloy studied in wetting and brazing configurations, and used to prepare the active brazing alloys.

2.2.2 Active brazing alloys containing Zr active element

Active alloys containing Zr active element are investigated in wetting conditions with the Au, Ag and Au-Sn matrix. These alloys are not commercially available, so they are prepared in situ during wetting experiments or lab-made by cold crucible induction melting.

a) In-situ elaborated alloys

The active brazing alloys Au+4wt%Zr and Au-Sn+3wt%Zr are elaborated *in-situ* during the wetting experiments.

b) Ag-3Zr alloy processed by cold crucible induction melting

Ag-3wt%Zr alloy was elaborated in ribbon-shaped at the ICMPE CNRS laboratory of the Material and Chemical Institute, Paris-Est.

The method is composed of the three steps described below: first the cold crucible induction melting of the alloy in ball-shaped, then the elongation of the alloy in the shape of an ingot, and finally the ribbon shaping by melt spinning.

First, the Ag-3wt%Zr alloy elaboration was performed by metal melting by induction heating (see Figure 44). Silver and zirconium are placed in a BN crucible contained itself in a Cu crucible surrounded by an inductor coil. Heat is generated by up and down induced currents which stir the molten metal, leading to a homogeneous mixture. This process leads to a ball-shaped alloy.

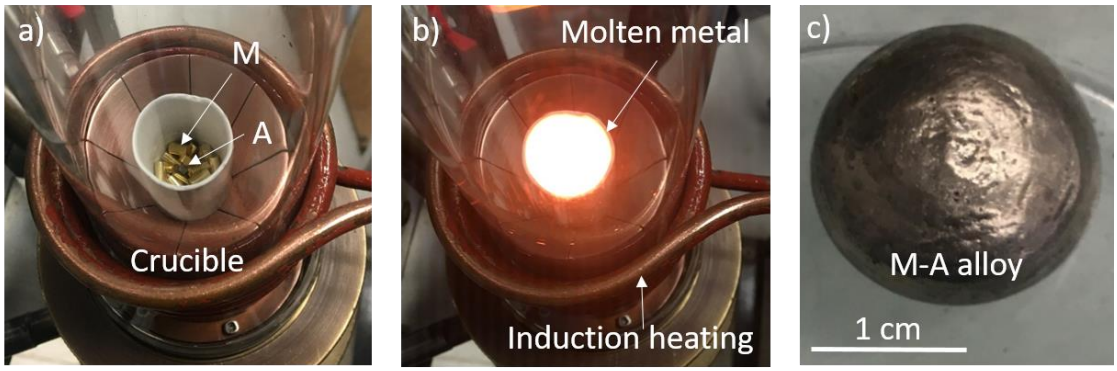

Figure 44: Elaboration of M-A alloy (M = matrix Au or Ag, A = Zr or Ti active element) by cold crucible induction melting. a) set up before heating, b) set up during metal melting, c) resulting active alloy in ball-shaped.

Then, the ball-shaped alloy is elongated in the shape of an ingot by induction heating on two Cu tubes covered by BN. The resulting Ag-3Zr alloy is an ingot of ϕ~6-8 mm in diameter and ~40mm long (Figure 45).

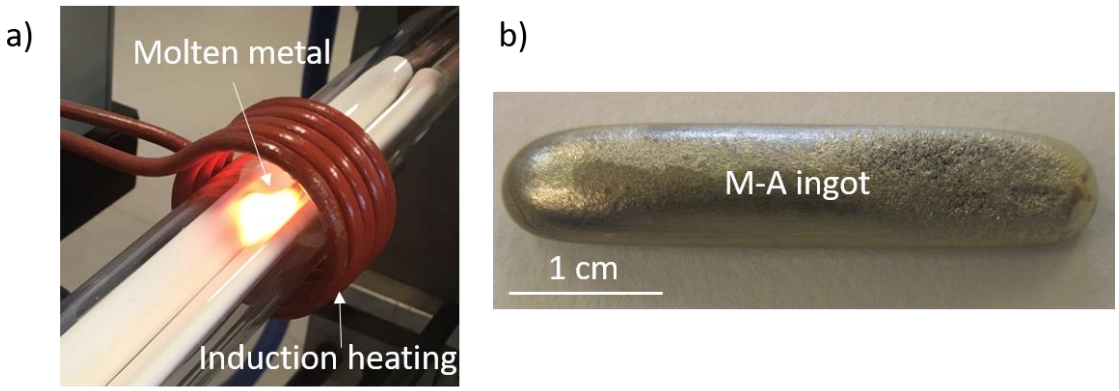

Figure 45: a) Elongation of the M-A alloy (M = matrix Au or Ag, A = Zr or Ti active element) by induction heating, b) resulting ingot of M-A alloy.

Finally, a ribbon is manufactured by melt-spinning from the ingot. The latter is melted by induction in a glass nozzle situated at 150 µm of a Cu wheel that turns at 20 m/s (see Figure 46a). The liquid alloy is ejected on the wheel and solidifies in a ribbon-shaped of about 11 mm wide, and 2 m long. The thickness of the Ag-3Zr ribbon, measured with an electronic micrometer, ranges from 81 to 111 µm. The roughness of the two faces are different : R_a=5.6 ± 0.5 µm for the « rough side » (Figure 46b) and R_a=1.2 ± 0.7 µm for the « smooth side » (Figure 46c)

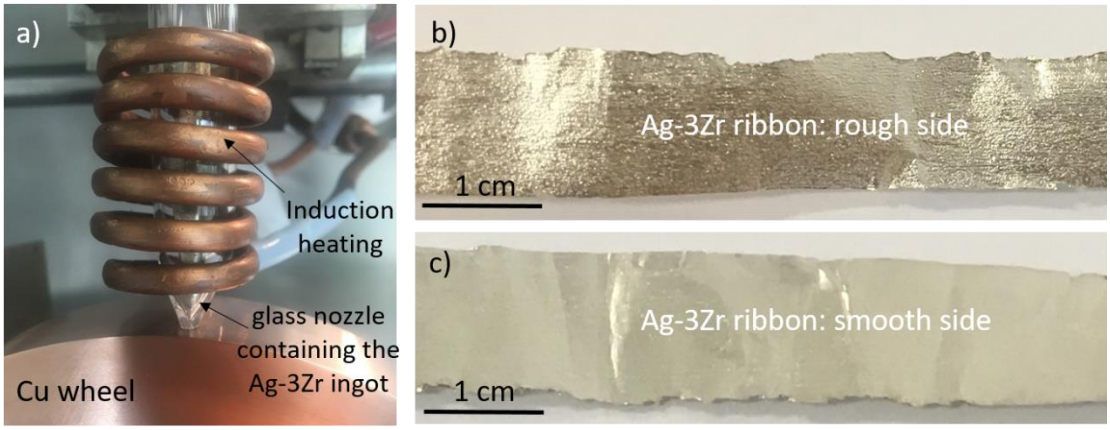

Figure 46: a) Melt-spinning set up, resulting ribbon of Ag-3wt%Zr alloy : b) « rough side » and c) « smooth side».

2.2.3 Active brazing alloys containing Ti active element

Active alloys containing Ti active element are investigated in wetting conditions with the Au, Ag and Au-Sn matrix. A commercial Active Brazing Alloy (ABA) with composition Au-3wt%Ni- 0.6 wt%Ti (Gold-ABA®) is studied. The Au-Ti, Ag-Ti and Au-20Sn-Ti alloys are not commercially available, so they are prepared in situ during wetting experiments or lab-made by cold crucible induction melting.

a) Industrial brazing alloy Gold-ABA® (Au-3Ni-0.6Ti)

Gold-ABA® is a high-purity active brazing alloy of gold, nickel and titanium, developed by Morgan Advanced Materials, Wesgo, for direct application to ceramic surfaces. The nominal composition by weight provided by the supplier is 96.4% Au, 3.0% Ni and 0.6% Ti (impurities < 0.01 wt%). The Ti and O contents of Gold-ABA® were verified by ICP plasma emission spectroscopy (Ti content) and dry combustion coupled with infrared detection (O content). These analyses give respectively 0.6wt%Ti and 0.01wt%O, which is in a good agreement with the expected values. The liquidus and solidus temperatures of this alloy are respectively 1030 and 1003°C. Some physical properties, provided by the supplier, are given in Table 12.

Coefficient of thermal expansion (CTE) at 20-850°C	Density	Tensile Strength	Recommended Brazing Temperature
16.1 x 10^{-6} $°C^{-1}$	1830 kg/m^3	334 MPa	1025 – 1030°C

Table 12: Physical properties of Gold-ABA® alloy (Au-3wt%Ni-0.6wt%Ti) provided by the supplier

b) In situ elaborated alloys

Au + 3wt%Ti, Ag + 4wt%Ti and Au-20Sn + 3wt%Ti alloys are prepared in situ during wetting experiments, by directly melting a piece of Ti over a sheet of metal (Au, Ag and Au-Sn) placed on the ceramic substrate.

c) Alloy processed by cold crucible induction melting

Three lab-made Au-xTi alloys (Au-1Ti, Au-2Ti and Au-4Ti (wt%)) were processed by the ICMPE CNRS laboratory using the cold crucible induction melting method already presented in section 2.2.2. According to the Ti-Au phase diagram (Figure 34 chapter 1), the liquidus temperatures of these alloys are respectively about 1080°C, 1110°C and 1170°C. Figure 47 gives representative optical and SEM micrographs and EDX analyses of polished surfaces of the Au-xTi alloys. The compositions of the three alloys are homogeneous everywhere in the analyzed zone of 36 mm^2. In the Au-1Ti alloy, Ti is dissolved in solution. The bulk microstructure of Au-2Ti is composed of Au with Au-Ti precipitates of about 50 µm. The Au-4Ti microstructure consists of a Au-Ti solid solution with $TiAu_4$ primary dendrites of about 100 µm.

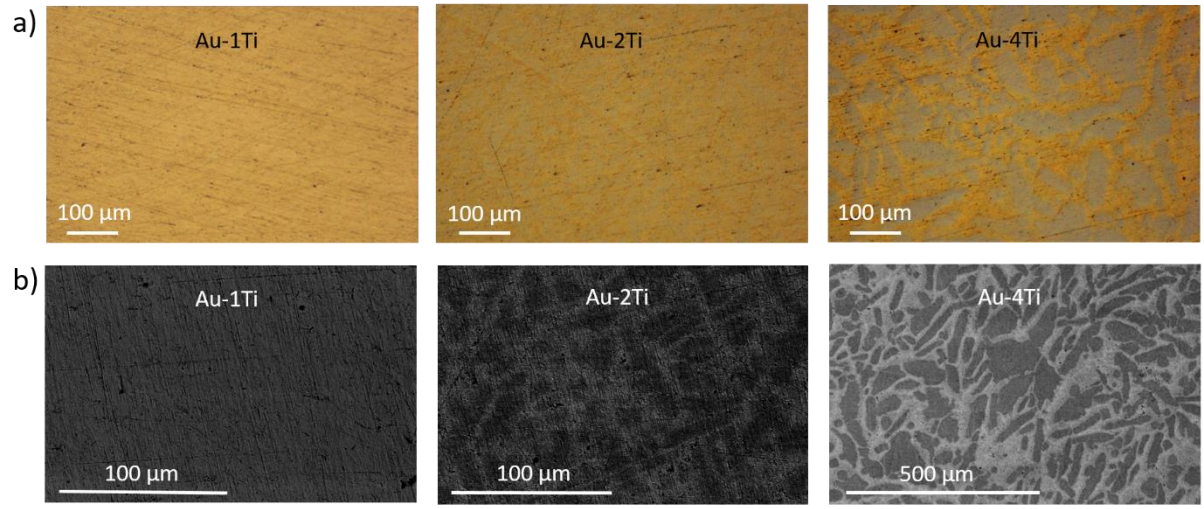

c)	Au-1Ti	Au-2Ti	Au-4Ti	Precipitates of the Au-4Ti alloy
wt%Ti	0.6	1.6	3.3	4.1
at%Ti	2.6	6.3	12.2	14.8

Figure 47: a) Optical and b) SEM micrographs of polished surfaces of the Au-xTi alloys (x = 1, 2 and 4 wt%), c) EDX analyses giving the Ti content in the alloys and in the precipitates of Au-4Ti alloy.

The Ti content in the three Au-xTi alloys are precisely determined by ICP plasma emission spectroscopy, and the O content is analyzed by dry combustion and infrared detection. The Ti and O contents are presented in Table 13.

	Ti (wt%)	O (wt%)
Au-1Ti	1.0	0.011
Au-2Ti	1.98	0.007
Au-4Ti	3.99	0.011

Table 13: Ti and O contents in the Au-xTi (x = 1, 2, 4 wt%) alloys elaborated by the ICMPE laboratory.

3. Experimental methods

In this section, the different experimental methods employed, firstly for the wetting study of zirconia and titanium substrates by liquid metals, and secondly for the brazing experiments in sandwich configuration, will be described. Finally, the experimental equipment used for the wetting and brazing studies, that is the furnaces and the acquisition system, will be presented.

3.1. Wetting experiments

Wetting experiment consists of following the spreading of a liquid metal or alloy droplet on a solid substrate, in order to quantitatively describe the wetting process. The measured parameters of the liquid droplet are its height h, its base diameter d_B and especially its contact angles θ_L and θ_R, respectively measured at the left and the right side of the droplet profile (Figure 48).

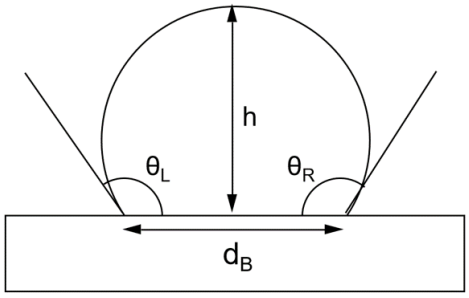

Figure 48: Characteristic parameters of a droplet obtained with the sessile drop method

Two different approaches are experienced in this work: the sessile drop and the dispensed drop techniques.

3.1.1. The sessile drop method

The most classic method to study the wetting behavior of a liquid on a solid substrate is the sessile drop technique. This experimental method consists of depositing a solid piece of metal (or some small pieces) on a solid substrate in the vertical metallic furnace LPA at the CEA. In this study, the droplet is either a pure metal, a pre-elaborated alloy or an alloy which is elaborated *in-situ* during the sessile

drop experiment (see Figure 49). Notice that the mass of the metal must be less than 100 mg in order to neglect the gravity effect. The LPA brazing furnace, equipped with a window, allows to observe and record, thanks to a video system, the melting and the spreading of the metal (or alloy) during heating from melting temperature to the experimental temperature and during isothermal holding at desired temperatures.

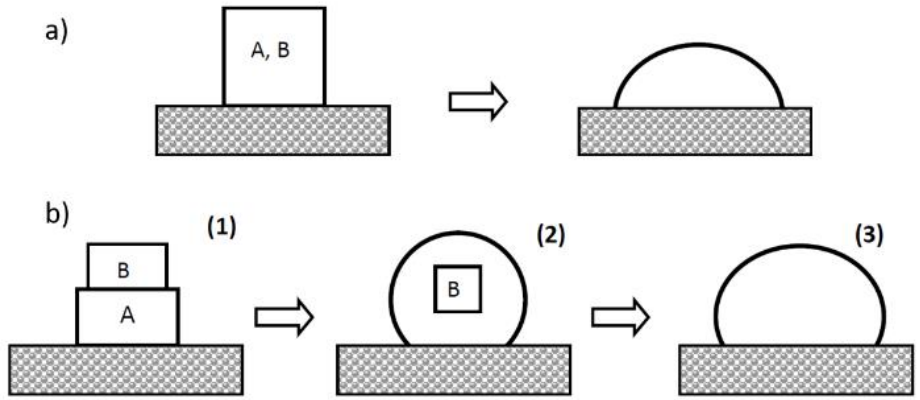

Figure 49: Classic sessile drop method: a) an A,B alloy prepared before wetting experiment; b) in situ elaboration of an A,B alloy (1) initial configuration, (2) dissolution of B in liquid A (melting temperature of B higher than that of A), (3) formation of the homogeneous droplet over the substrate.

3.1.2. The dispensed drop method

This method was carried out in the metallic furnace of the SIMAP laboratory. The experimental method, schematically represented in Figure 50, consists of deposing liquid metal or alloy droplets on small substrates (1 to 3 substrates having a surface of 1 cm^2) on a turning table inside the furnace, thanks to a piston. The metal or alloy to be studied is previously inserted in an alumina crucible situated over the substrate. The crucible is linked to a thin alumina capillary (1 mm outer diameter and 0.6 mm inner diameter). When the study temperature is reached, the piston allows to push the liquid out of the crucible through the capillary. Thus, a spontaneous spreading of the drop over the substrate occurs.

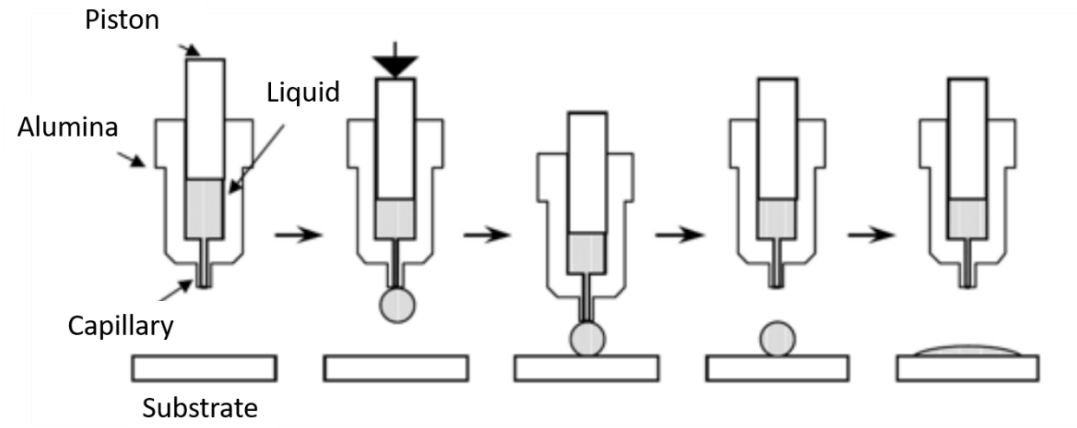

Figure 50: Different stages of the droplet deposition by the dispensed drop technique.

This specific experiment allows to separate the melting and spreading processes, so fully isothermal experiments can be performed. Indeed, with the classic sessile drop technique, substrate and metal or alloy are in contact during the entire thermal cycle including heating from room temperature to study temperature, thus interfacial reactions and spreading can occur during the temperature rise from the melting temperature to the experimental temperature.

3.2. Brazing experiments

The joining of substrates is performed by brazing in sandwich configuration, which consists of directly placing a braze foil between the substrates to be assembled. Two designs of samples are used in this study: a basic sandwich sample and a tensile brazed specimen.

The two substrates composing the basic sandwich sample are zirconia and titanium discs with a diameter ϕ = 15mm and a height h = 2mm. The filler metal or alloy (Au, Ag, Au-Sn, Au-3Ni-0.6Ti) is cut in a sheet with the dimensions ϕ ~ 12 mm and 25 µm < h < 150 µm. Before brazing, a tungsten weight of 20 g is placed on the assembly to ensure a homogeneous contact between filler metal and substrates during the brazing process. A draw of a basic sandwich assembly with the W weight is presented in Figure 51a.

The shape and dimensions of materials (substrates and filler metal) constituting the tensile specimens are inspired of the ASTM F19 - 64 standard. A cross-section of the specimen is represented in Figure 51b. Two massive parts of zirconia (ϕ_{max} = 24mm, h = 11.1mm) are brazed to a titanium ring (ϕ_{int} =9mm, ϕ_{ext} = 11.25mm, h = 0.5mm) with two preformed rings of filler metal (ϕ_{int} = 9mm, ϕ_{ext} = 11.25mm, h = 0.1mm), so that a specimen is composed of two brazed joints with a brazed interface area of 35.8mm^2.

Before heat treatment, the five circular parts (ZrO_2, Au preform, Ti ring, Au preform and ZrO_2) are assembled thanks to a graphite tool which consists of a base and a circular shaft. The five parts are successively stacked around the graphite shaft, thereby aligning the zirconia parts.

The samples are placed in the brazing furnace under high vacuum and undergo a thermal cycle. The thermal cycle is composed of a temperature rise until the brazing temperature, an isothermal holding and a cooling stage until room temperature. Pictures of a basic sandwich assembly placed in the LPA furnace, and four tensile specimens simultaneously brazed in this furnace, are respectively presented in Figure 51c and d.

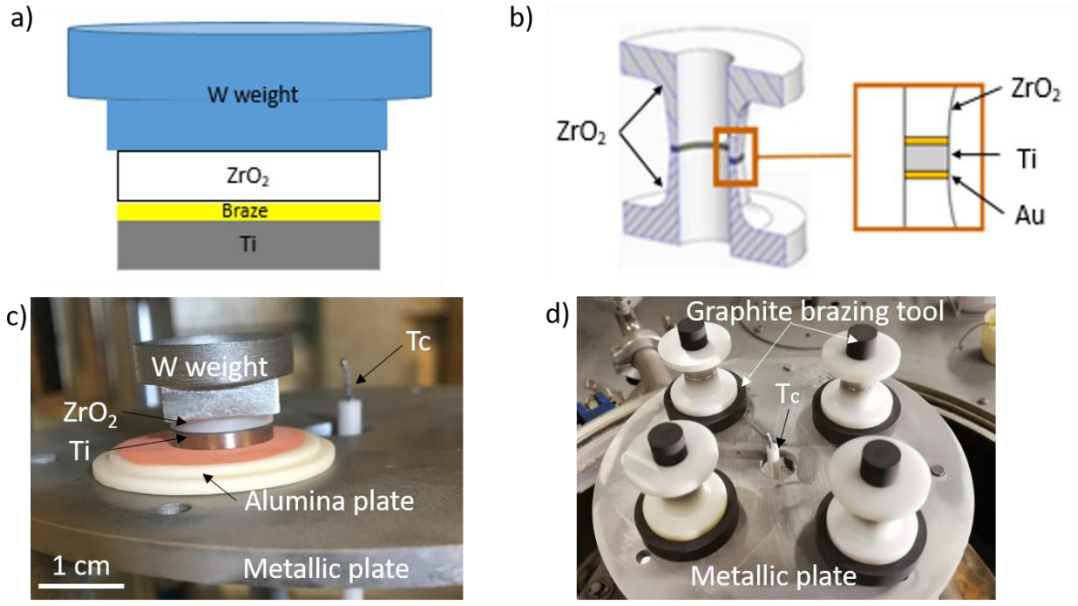

Figure 51: Schematic representation of a) a basic sandwich brazed sample, b) a cross section of a brazed tensile specimen, and pictures of c) a sandwich brazed sample in the furnace and d) four tensile specimens simultaneously brazed in the LPA furnace.

3.3. Experimental equipments

The wetting study was performed in two different metallic furnaces. The sessile drop experiments were carried out in the LPA metallic furnace at the CEA Grenoble, whereas the dispensed drop experiments were performed in the horizontal metallic furnace at the SIMAP laboratory in Grenoble.

The brazing study was realized in two different furnaces. Most of the samples (the whole basic sandwich samples and most of the tensile specimens) were brazed in the LPA metallic furnace. In order to investigate the impact of the partial pressure of oxygen on the mechanical properties of the joints, some tensile specimens were brazed in a graphite furnace, which imposes a very low partial pressure of oxygen.

Before each thermal cycle, the substrates and the filler metals are cleaned in acetone then ethanol for five minutes in an ultrasonic bath.

3.3.1. Furnaces

a) LPA metallic furnace at the CEA

The LPA metallic furnace, presented in Figure 52, is constituted of a cylindrical chamber in stainless steel with double walls cooled thanks to a water cooling system. This chamber consists of two parts, a movable lid and a fixed base. A window allows the observation of samples placed inside the furnace on the molybdenum plate. The useful dimensions of the enclosure are a diameter ϕ = 120 mm and a hight h = 200 mm. The thermal shields placed near the enclosure are in molybdenum (Mo), and the inner thermal shields (near the resistor) are in tungsten (W). The heating is performed thanks to a metallic resistor in tungsten.

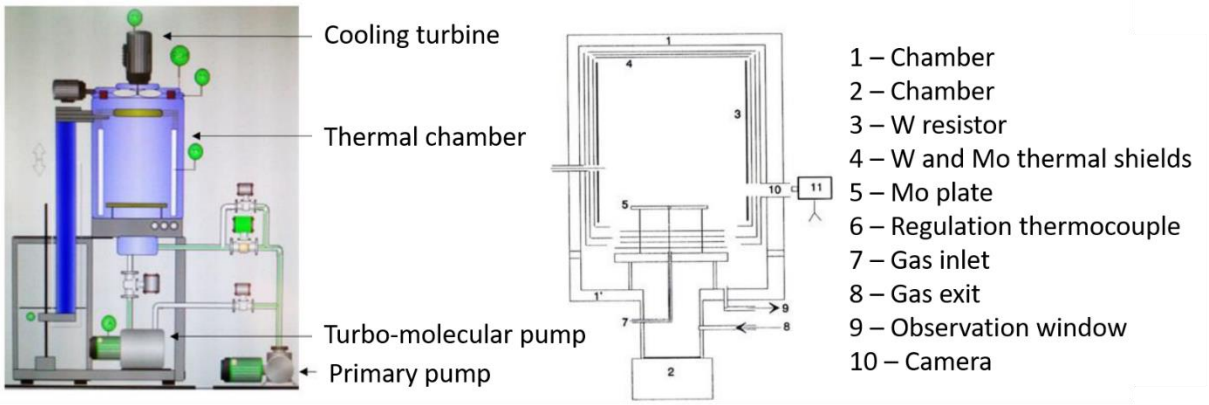

Figure 52: a) Outer and b) inner schematic representations of the LPA furnace.

The chamber is linked to a pumping system which is composed of a dry primary pump and a turbo-molecular secondary pump, leading to a vacuum level reaching at most 2.10^{-4} Pa. The temperature regulation is ensured by a W – Re thermocouple placed in the middle of the Mo plate, that is about 5-20 mm from the sample. The maximal set temperature of this furnace is 2000°C.

b) Metallic furnace of the SIMAP laboratory

The metallic furnace of the SIMAP laboratory, presented in Figure 53, is constituted of a horizontal cylindrical chamber in stainless steel with double walls cooled thanks to a water cooling system. The heating is ensured by a molybdenum resistor surrounded by thermal shield. The substrates (from 1 to 3 square-shape substrates with the dimensions 10x10 mm^2) are placed in the furnace on a turning plate in alumina. Alumina crucible containing metal or alloy to be deposited on the substrates is placed above the turning place, in order to accurately deposit, successively, the liquid metal on the different

substrates. Three windows allow to simultaneously illuminate, observe and record with a camera the deposit drop experiment.

The pumping system of the furnace, composed of a primary pump and a turbo-molecular pump, allows to reach a high vacuum level of 10^{-5} Pa.

The temperature regulation is ensured by a PID controller thanks to two Pt – Pt 10% Rh thermocouples, placed at about 10 mm of the sample. The maximal set temperature of this furnace is 1500°C.

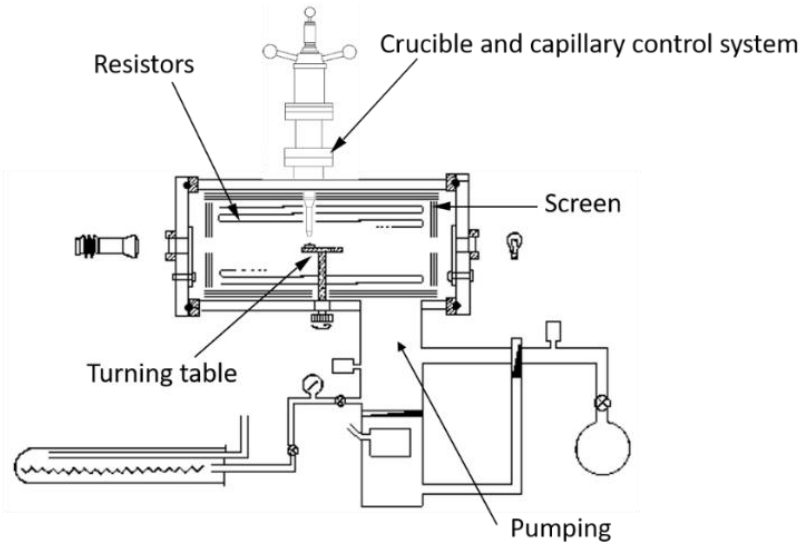

Figure 53: Schematic representation of the metallic furnace of the SIMAP laboratory.

3.3.2. Acquisition system

In order to record the profile of the droplet required for the wetting study, a camera is placed in front of the furnaces window. The samples are illuminated by a light source placed in front of a second window in the case of the horizontal furnace, and in front of the single window in the case of the LPA metallic furnace.

The acquisition system of the LPA furnace allows to record 1 frame per second (fps).

At the horizontal furnace of the SIMAP laboratory, two different cameras are used. A classic CCD camera is able to record at most 50 fps. A high speed camera is used to record the early stage of wetting at 1500 fps. The contact angle θ of the drop was measured with an accuracy of ±3°.

4. Sample preparation and characterization

4.1. Metallographic preparation

Samples from wetting and brazing experiments are prepared in order to be characterized. The metallographic preparation consists of encapsulating samples in epoxy resin, then cutting them in cross-section with a diamond circular saw (Accutom saw provided by STRUERS). The cross-sections are then polished with colloidal silica suspension until 1 µm. Before SEM observation, samples are metallized with carbon.

4.2. Physico-chemical characterizations

The physico-chemical characterization consists first of an optical observation with the InfiniteFocus equipment (ALICONA), which is an optical 3D measurement system. Then, cross-sections are analyzed by scanning electron microscopy (SEM) and FEG-SEM (Field Emission Gun). SEM provides high resolution images of the cross sections by rastering an electron beam which is focused on the sample surface. SEM is linked to an Energy Dispersive X-Ray Analyzer (EDX) providing semi-quantitative information of the analyzed sample.

Some selected samples are analyzed by Transmission Electron Microscopy (TEM). This technique is based on the transmission of an electron beam through a specimen to form images with a very high resolution and diffraction patterns. This technique requires specific sample preparation at nanometric scale thanks to the Focused Ion Beam (FIB) technology under SEM.

4.3. Hermeticity and mechanical characterization

Several methods allow to quantify the mechanical properties of the brazed joints (see chapter 1). The mechanical test selected in this work is the tensile test based on the ASTM F19-64 standard. The main reason which made our choice on this type of test is the part geometry (Figure 51b), which allows testing both hermeticity and mechanical strength of the brazed joint. Indeed, they are two key parameters of the brazing study for the implantable device application.

4.3.1. Leak test

In order to verify the hermeticity of the brazed joints, the helium spraying method is used thanks to the ADIXEN ASM 142D equipment. A draw and a picture of the leak test device are presented in Figure 54. This fine leak testing allows to detect and measure a leak rate (mbar.L.s^{-1}). This technique involves

vacuuming (10^{-6} Pa) inside the brazed tensile specimen which is closed thanks to seals and a cover. The sample is then sprayed with helium. If there is a leak, helium penetrates the sample and the flow of helium is measured by the He detector.

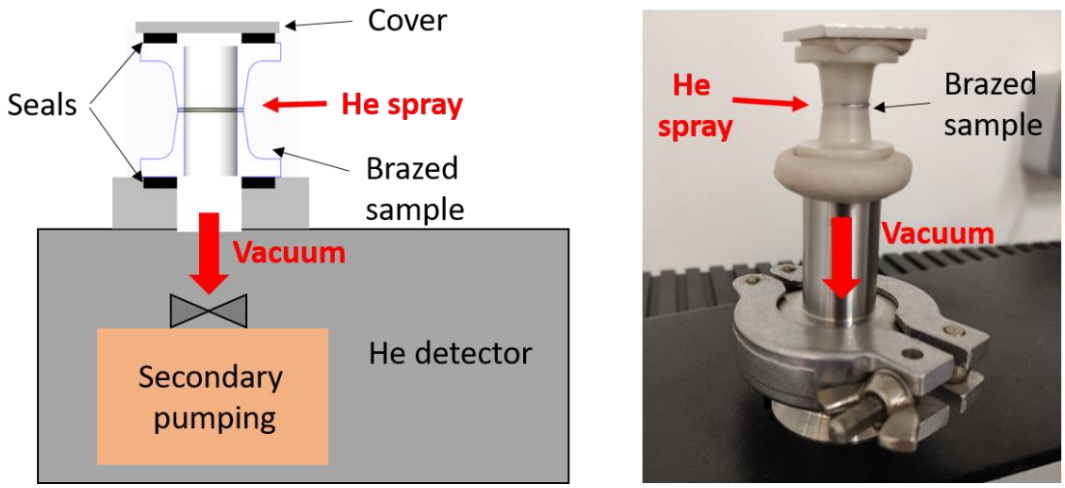

Figure 54: a) Schema and b) picture of leak test device of the brazed specimens.

4.3.2. Tensile test

The tensile test is performed by a hydraulic traction machine MTS with a 10 kN cell having an accuracy of ± 0.025 kN. The brazed specimen is placed in the tensile tool presented in Figure 55. The force applied to the test piece by the traction machine over displacement is recorded, giving the maximal force (N) supported by the sample. From this value, knowing the brazed surface (35.2 mm^2), the rupture stress of the specimen (in MPa) is calculated.

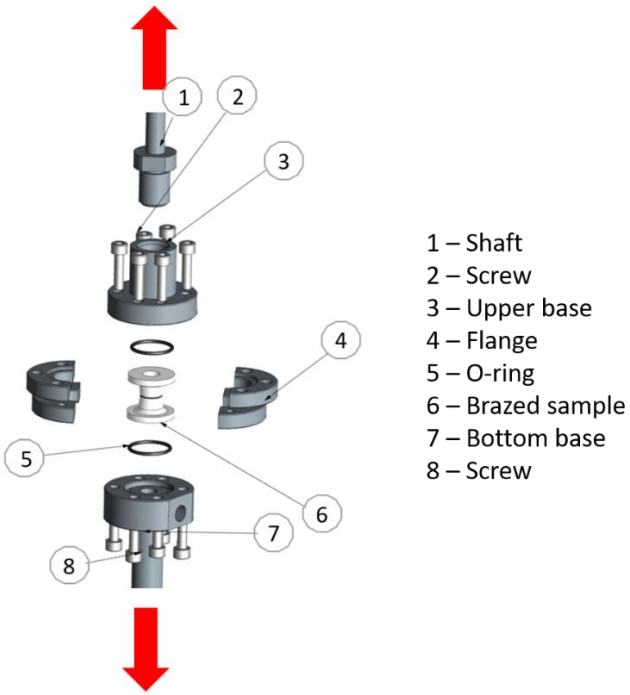

Figure 55: Exploded view of a brazed specimen and the tensile tool for tensile test

5. Conclusion

In this chapter, the materials used for the wetting and brazing studies are presented: ZrO_2 and Ti substrates, as well as filler metals and alloys (Au, Au-20wt%Sn, Ag and active alloys containing Zr and Ti active elements).

Afterwards, the experimental methods of sessile drop and dispensed drop are described. These techniques will be used to study the wetting of zirconia by different alloys containing Zr and Ti active elements, and the wetting of titanium by pure Au, presented in chapter 3.

The apparatus used to performed sessile drop experiments and brazing experiments under high vacuum (~5.10^{-6} mbar) is the LPA metallic furnace in the CEA. The dispensed drop experiments were performed under high vacuum (10^{-6} mbar) in the metallic furnace of the SIMAP laboratory. Most of the in-situ images of metal spreading on substrates were recorded with a CCD camera (50 frames/s). Some specific experiments were recorded by a rapid camera (up to 1500 frames/s).

Brazing experiments are performed in sandwich configuration with two shapes of sample: the basic sandwich assemblies and the tensile specimens consisting of two brazed joints.

Finally, the physico-chemical and mechanical characterizations of the samples are exposed. The interfacial reactivity of the polished cross-sections (substrate/droplet samples and brazed samples) are analyzed by microscopy (optical, SEM, FEG-SEM and TEM) and EDX. Control of hermeticity and tensile test set-up of the tensile specimens are presented.

References of chapter 2

1. Supplier Material Certificate of YTZP for ISO 13356:2015. (2018).

2. Y. Combres, Propriétés du titane et de ses alliages. *Tech. Ing.* **20** (2010).

3. G.W.C. Kaye & T.H. Laby. *Tables of Physical and Chemical Constants and Some Mathematical Functions*, 8th Edition, Longmans Green and Co., London, (1936).

Chapter 3 : Wetting and reactivity in the ZrO_2 / reactive liquid alloys and Ti / liquid Au systems

Contents

1. Introduction

This thesis deals with zirconia to titanium brazing for a biomedical application. In this case, the common filler alloys used are based on noble metals (Au, Cu, Ag, etc…). Wetting is a necessary condition to perform a satisfying brazing; that is why, in this chapter, we investigate the interfacial interactions (wetting and reactivity) between both substrates (zirconia and titanium) and liquid Au, Ag and their active alloys.

In the absence of barriers to wetting such as oxide films on the liquid or the solid, molten metals wet metallic substrates (contact angle lower than 90°) whatever the intensity of interactions between the liquid and the solid[1].

The first part of this chapter presents zirconia wetting. Noble metals like Au, Cu, Ag do not wet zirconia. The addition of a few percent of an active element (Zr or Ti) into the filler metals allows zirconia wetting [2–6]. Two different types of active alloys are investigated in this chapter. First, we study spreading kinetics and interfacial reactivity of zirconium active alloys on zirconia substrate. Then, wetting of zirconia by titanium reactive alloys is presented and discussed. Based on zirconia wetting study, the best candidate alloy to perform the continuation of the work is selected.

In the second part of this chapter, wetting study of the second substrate (titanium) to be brazed is conducted with the chosen filler metal. Moreover, the interfacial reactivity between these metals is investigated.

The entire experimental study of this chapter was carried out in two metallic furnaces under a high vacuum of about 10^{-6} mbar. Sessile drop experiments were performed in the LPA furnace (CEA) and deposited drop experiments were performed in the horizontal furnace (SIMAP laboratory). The contact angles θ of the drop were measured with an accuracy of ±3°.

2. Wetting and reactivity of zirconia by liquid alloys containing Zr and Ti as reactive elements

2.1. Introduction

In this work, three metallic matrix are selected to study the wetting of zirconia: pure silver with a melting point T_m = 962°C, gold-tin eutectic alloy with low melting point (T_m = 278°C), and pure gold (T_m = 1064°C).

In the present study, two active elements, which have a different behavior with zirconia substrate, are explored:

- Zirconium active element, leading to the formation of a wettable sub-stoechiometric zirconia layer while in contact with the zirconia substrate[2,3,7].
- Titanium reactive element, forming Ti oxides which are wettable by liquid metals[4–6,8].

Firstly, wetting and reactivity of zirconia by zirconium active alloys are presented. In a second time, wetting study of zirconia by titanium active alloys is described. The experimental study was performed by the sessile drop method, except some selected experiments which were carried out by the dispensed drop technique.

2.2. Zr reactive element

In this section, wetting of zirconia by M-Zr alloys (M = Ag, Au-20wt%Sn and Au) is investigated. Interfacial reactivity of the three systems (zirconium reactive alloys / zirconia) is presented with fine characterization of the interfaces. Moreover, for alloys which are not selected for the brazing study (chapter 4), some preliminary brazing tests are performed and described in this section.

2.2.1. Wetting of zirconia by Ag-3Zr alloy and preliminary brazing tests

Silver is a noble metal widely studied for ceramic / metal brazing, in particular associated with copper. In this study, silver matrix is worth investigating in wetting configuration in the aim of zirconia-to-titanium brazing, for its intermediate melting temperature (962°C). The Ag-Zr brazing alloy selected to perform the zirconia wetting study is a ribbon of Ag-3wt%Zr (melting point ~ 960°C). Indeed, this alloy has already been successfully elaborated, and studied by Kolstsov et al.[9] in the case of AlN wetting.

Wetting experiments were carried out in order to determine the temperature range of wetting and spreading on the zirconia substrate. A piece of Ag-3Zr alloy is placed on zirconia substrate inside the furnace and the process is recorded with a camera installed ahead the furnace window.

Figure 56 presents in situ images of the sample during heating at 5°C/min up to 980°C. The saturated vapor pressure of silver at 980°C being relatively high, the wetting study is limited to a short duration, similar to brazing time (a few minutes in liquid state): an isothermal holding of 1 minute is carried out at 980°C, then temperature is rapidly decreased up to room temperature (20°C/min).

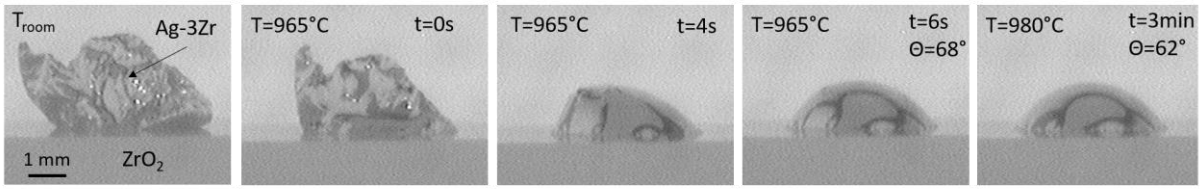

Figure 56: Some selected images of the Ag-3wt% alloy / zirconia substrate system during melting and spreading of the alloy.

We can observe the piece of alloy changing shape with temperature from 965°C. After 10 seconds, the Ag-3Zr alloy takes the form of a spherical cap droplet, and the contact angle θ is relatively low (θ = 62°). Afterwards, the contact angle does not evolve with time during the isothermal holding of 1 min at 980°C.

Another experiment shows that during heating to 980°C, the same contact angle θ ~ 62° is obtained at 980°C. Afterwards, during a long holding time (4h) at this temperature, the droplet radius remains constant but the droplet height continuously decreases. Moreover, a significant mass loss of the alloy was measured after the heat treatment. These two experimental facts prove that a significant silver evaporation occurs under vacuum at 980°C.

Top views of Ag-3Zr on zirconia samples after different isothermal holdings at 980°C (1min, 45min and 4h), presented in Figure 57, show that zirconia (originally white), turns grey after contact with the liquid Ag-Zr alloy. This grey color intensifies with duration of contact of zirconia with the liquid phase. This is due to the fact that ZrO_2 substrate becomes sub-stoichiometric ZrO_{2-x} while reacting with Zr active alloy at the droplet / substrate interface. Indeed, the link between grey color and the change in stoichiometry is well established in the literature and is recurring in zirconia wetting and brazing[10–13].

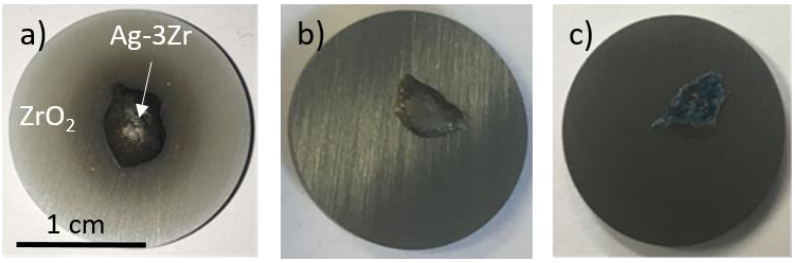

Figure 57: Top views of Ag-3wt%Zr / zirconia samples after different isothermal holdings at 980°C: a) 1min, b) 45min and c) 4h.

A cross section of the Ag-3Zr/zirconia sample held for 1 min at 980°C is presented in Figure 58. The droplet adheres to the substrate and no defect is observed at the interface. The SEM micrographs show the formation of a reaction layer containing Zr and O, of about 2-3 µm thick on the ceramic

substrate (see Figure 58b). EDX analyses of the droplet reveals that a very low Zr content of the Ag-3Zr alloy is consumed to react at the zirconia / alloy interface. The observation of this interface in the region close to the triple line (Figure 58c) clearly shows that the reaction layer (2-3 µm thick) is situated over the initial surface of zirconia substrate marked by a yellow dotted line. This means that the zirconia substrate is not consumed during the formation of the reaction layer. This point will be discussed in detail in section 2.2.3 in the case of reaction between zirconia and Au-3Zr alloy.

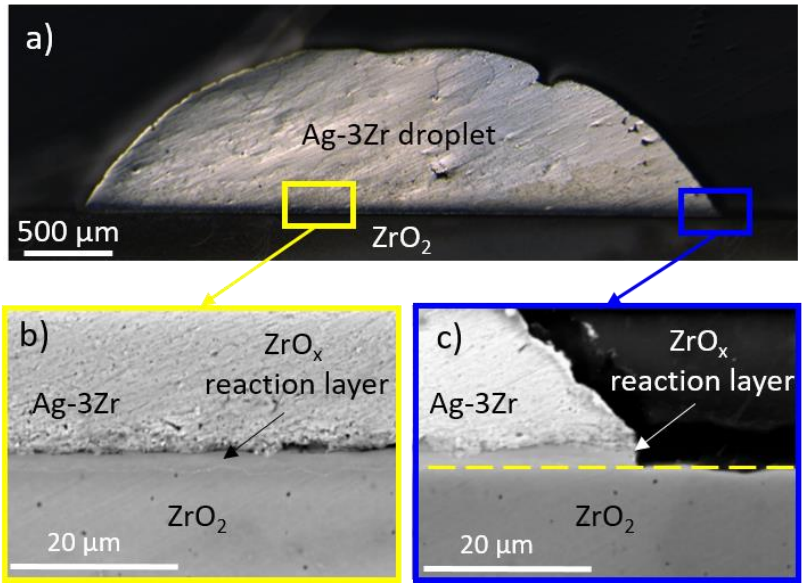

Figure 58: SEM micrographs of a cross section of the Ag-3wt% Zr/zirconia sample held for 1 min at 980°C.

Previous experiments show a good wetting of zirconia by the Ag-3Zr alloy at 980°C (θ ~ 60°), and a good mechanical adhesion of the solidified droplets on zirconia, without defect like voids or cracks. Thus, a zirconia to titanium brazing test was carried out with the Ag-3Zr ribbon.

At this stage, it is important to point out that in the brazing configuration, Ti substrate will dissolve in the liquid alloy and react with zirconia at liquid / zirconia interface. However, given the fact that the activity coefficient of Ti at infinite dilution in liquid Ag referred to liquid Ag at 1000°C is very high (γ_{Ti}^{∞} = 4)[14], the thermodynamic activity of Ti (a_{Ti}) in liquid Ag is also very high: $a_{Ti} = \gamma_{Ti}^{\infty} x_{Ti} = 0.16$ for Ti molar fraction x_{Ti} = 0.04 (4 at%Ti). This could lead to a very strong reactivity between dissolved Ti and ZrO_2, and thus to the formation of a thick reaction layer at liquid alloy / zirconia interface. Therefore, the brazing thermal cycle was defined with a holding time as low as possible (1 min at 980°C) in order to limit significant titanium diffusion from the titanium substrate through the liquid silver towards the zirconia.

Figure 59a gives a cross section of the ZrO_2 / Ag-3Zr / Ti joint. Despite the short duration in liquid state, titanium from the substrate dissolves and diffuses into the liquid silver and reacts with zirconia to form a very thick reactive layer of about 32 µm at the zirconia / braze interface (Figure 59a-b). EDX analyses of the reaction layer indicate that this layer consists of Ti oxide. Notice that zirconia substrate turns fully black (Figure 59c), resulting from a strong interaction between zirconia and reactive elements (Zr and especially Ti) at the ceramic / filler metal interface. As it was specified in chapter 1, very thick reaction layers are detrimental to the mechanical properties of the joint. Therefore, the Ag-3Zr reactive alloy, and in particular the silver matrix are not selected in the following study of zirconia/titanium brazing.

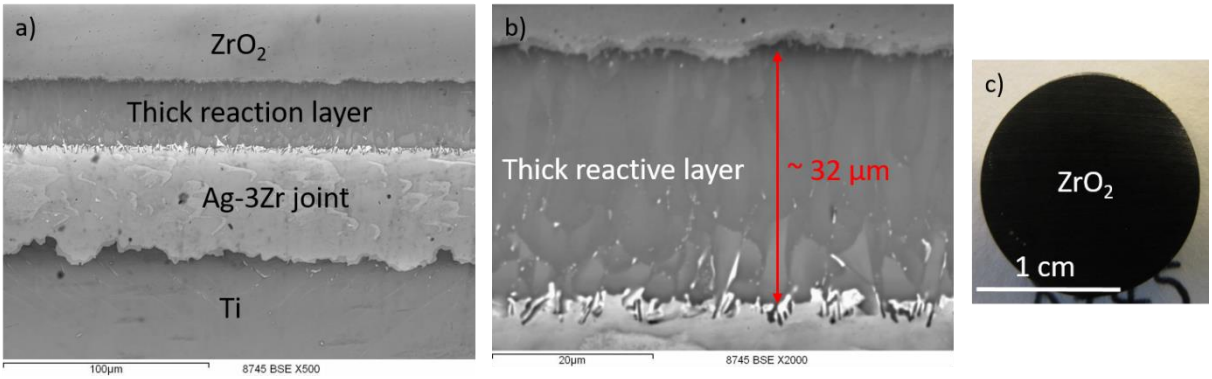

Figure 59: SEM micrographs of a *cross section of the ZrO_2/ Ag-3Zr / Ti joint performed at 980°C for 1 min (a and b) Optical top view of the sample after the experiment showing that zirconia substrate turns fully black (c).*

However, note that Ag-3Zr brazing alloy seems to be adapted to the zirconia brazing by itself according to a preliminary brazing test performed at 1010°C for 5 min. Figure 60 gives two optical micrographs of a cross section of the ZrO_2 / Ag-3Zr / ZrO_2 system after the brazing process. The joint has a homogeneous thickness and no defect like voids or cracks are observed under the optical microscope (Figure 60a). At both zirconia / braze interfaces, a sub-stoichiometric zirconia (ZrO_{2-x}) layer of 2-5 µm is formed on the ceramic substrate (Figure 60b). After brazing, the zirconia substrates turned grey, sign of the formation of a reaction product at the interfaces.

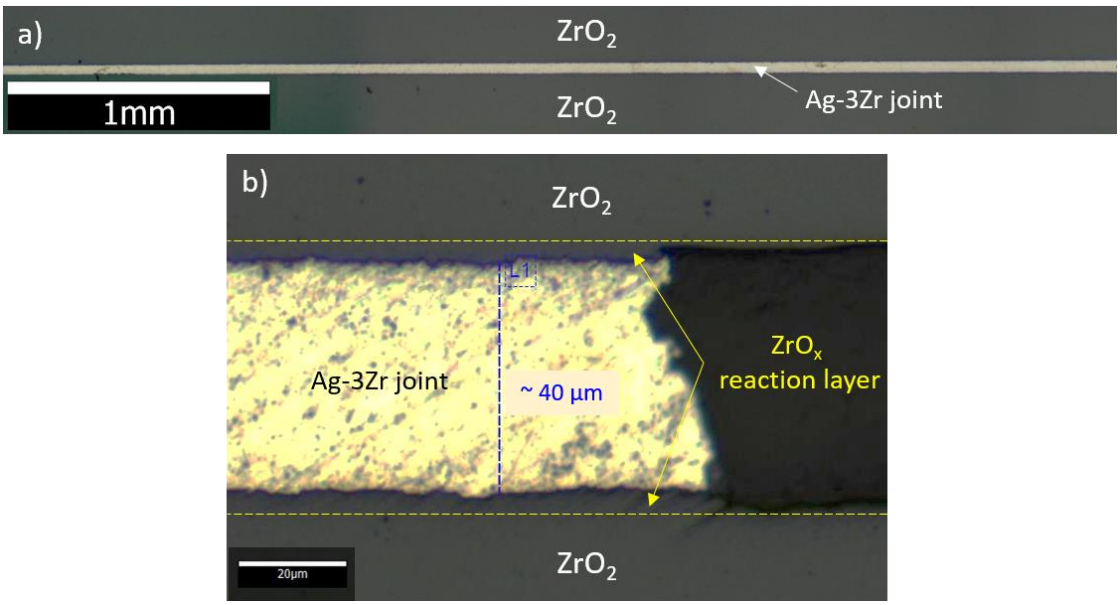

Figure 60: Optical micrographs of a *cross section of the ZrO_2 / Ag-3Zr / ZrO_2 joint performed at 1010°C for 5 min.*

2.2.2. Zirconia wetting by Au-Sn-Zr alloy

The eutectic Au-20wt%Sn alloy is considered as matrix since its very low melting point (276°C) could allow to drastically decrease the brazing temperature in order to control the interfacial reactivity, and also to reduce the thermomechanical stresses generated in the joint during the brazing process at the cooling stage.

A wetting experiment was carried out using the Au-20Sn-3Zr alloy prepared in-situ by directly melting a piece of Zr placed between several Au-20Sn foils on the zirconia substrate. The sample is heated up to 1064°C at the heating rate of 10°C/min. The melting and spreading of the alloy are followed during heating, and Figure 61a presents some images of the sample in the furnace at different temperatures.

During heating, a continuous change in shape of the Au-Sn alloy is observed from 290°C to 970°C. However, a *spherical cap droplet is observed only when the temperature attains about 970°C despite the fact* that the melting point of Au-20Sn alloy is 278°C. This is due to the fact that in this temperature range (278-970°C), the melted Au-Sn foils are covered with a Sn oxide layer. The elimination of this oxide layer under vacuum becomes possible with increasing temperature. This leads first to a partial communication of liquid metal between different foils and an obvious change in the alloy form (see Figure 61a, from 400°C to 750°C). It is only at about 970°C that the alloy looks like a liquid spherical cap drop: the oxide layer covering the liquid droplet surface breaks and/or is eliminated under vacuum. The very high contact angle (θ=170°) observed at 970°C could be due to the fact that the liquid alloy is

covered by an oxide layer which acts as a barrier to wetting and spreading of Au-Sn-Zr alloy over zirconia substrate; this oxide layer is destroyed under vacuum at about 970°C.

As soon as a spherical cap droplet is formed, an isothermal holding is achieved at 980°C in order to observe the liquid droplet spreading on the zirconia. First, the contact angle decreases rapidly from 170° to 60° in about 1 min, corresponding to a reactive wetting (formation and lateral growth of a wettable sub-stoichiometric ZrO_{2-x} layer at the triple line). Then, the contact angle decreases more slowly, from 60° to 50° during 20 min. Afterwards the temperature is raised up to 1064°C and is maintained during 10 min. The final contact angle is 28°. Thus, a very good wetting of zirconia by the Au-20Sn-3Zr alloy is obtained at high temperature (980-1064°C).

At the end of this experiment, the solidified droplet is adherent to the zirconia substrate (Figure 61b).

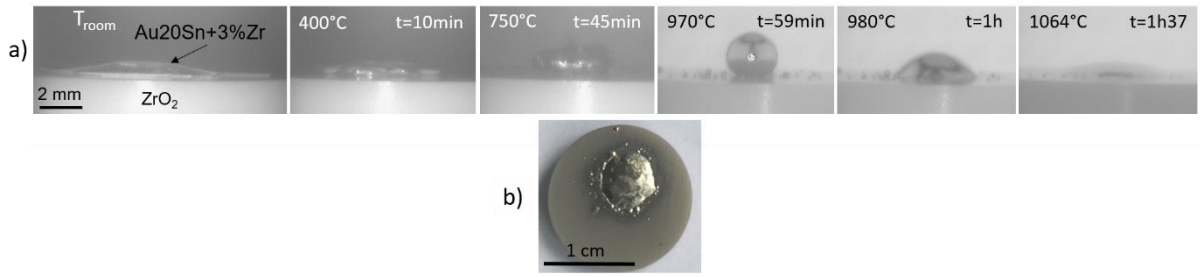

Figure 61: a) Some selected images of the Au-20Sn-3Zr/zirconia substrate during heating up to 1064°C. b) Top view of Au-20Sn-3Zr/zirconia sample after the wetting experiment.

The cross section of the Au-20Sn-3Zr drop on zirconia is observed by SEM and presented in Figure 62a. No crack or failure is observed at the metal / zirconia interface. The bulk microstructure of the drop is homogeneous and is composed of AuSn primary dendrites (δ phase) and eutectic structure (δ + ζ phases) - see the Au-Sn binary phase diagram in Figure 62b. At the zirconia / drop interface, an island-shape reaction layer is observed. This non-continuous layer measures up to 12µm thick. According to the EDX analysis, the Zr/O ratio is 38/62 at%, which suggests that, the reactive layer formed at zirconia/Au-20Sn-3Zr alloy could be ZrO_2 oxide.

The interest of studying this low melting point alloy (278°C) is to decrease the zirconia-to-titanium brazing temperature compared to Ag and Au matrix. However, the stable Sn oxide layer at the surface of the alloy in the temperature range 280-970°C would cause serious problems for brazing so we decided not to elaborate the Au-Sn-Zr alloy for brazing tests.

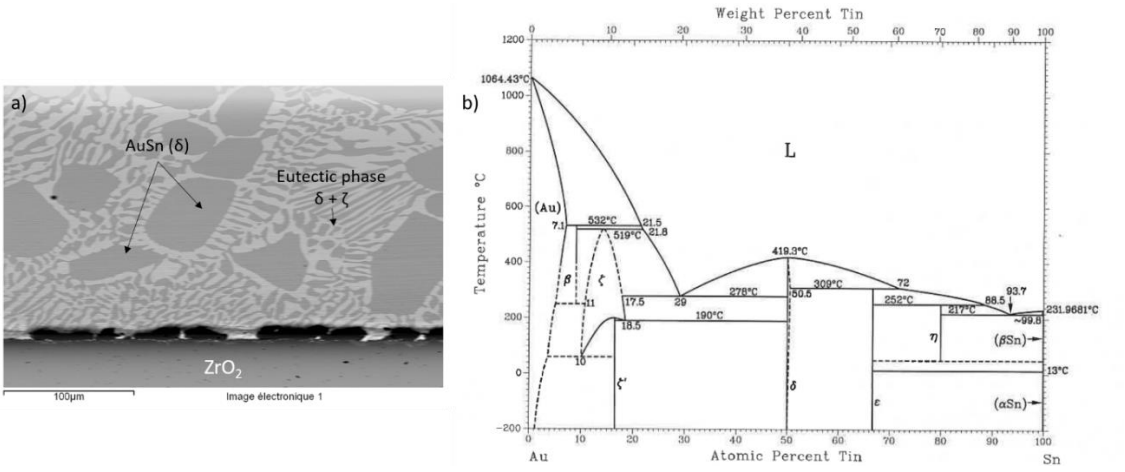

Figure 62: a) SEM micrograph of a cross section of the Au-20Sn-3Zr drop on zirconia. b) Binary Au-Sn phase diagram[15].

2.2.3. Wetting and reactivity studies of zirconia by Au-3Zr alloy

Wetting experiments were carried out using Au-3Zr alloy prepared in situ on zirconia. A massive Zr piece is placed on Au foil thus there is no contact between Zr element and ceramic substrate before gold melting. The sample is heated up to 1070°C with a heating rate of 10°C/min. The melting point of Au-3wt%Zr alloy is about 1064°C (see appendix 1). Figure 63 gives some selected images of the sample at room temperature and during isothermal holding at 1070°C. It can be noted that when the temperature attains 1070°C (higher than the melting point of Au and Au-3Zr alloy) the sample has not the form of a spherical cap droplet. This is due to the formation of a Zr oxide layer at the surface of the alloy which breaks or is removed after about 30 seconds at 1070°C, i.e. when a spherical cap droplet is obtained. The observation of different values of right and left contact angles of about 94° and 103° respectively, clearly indicates pinning of the triple line (the triple line is blocked). Then, the contact angle decreases down to 66° after 7 minutes at 1070°C by reactive wetting (formation and lateral growth of a wettable reaction layer at the triple line). Afterwards the contact angle remains constant with time and temperature, during heating up to 1250°C for 1h30 min.

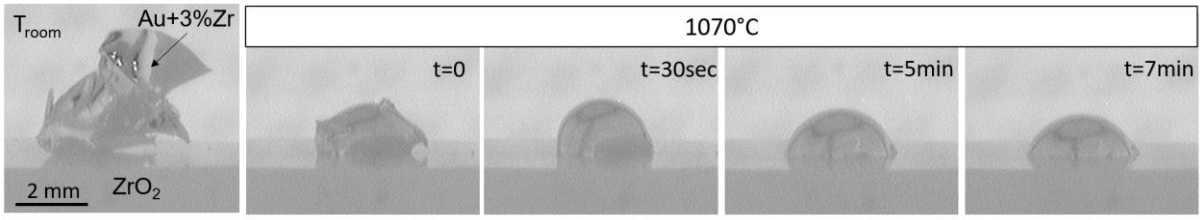

Figure 63: Selected images of the Au+3wt%Zr / zirconia sample at room temperature and during isothermal holding at 1070°C.

Figure 64 gives cross section images of the Au-3Zr droplet on zirconia, after 45 min in liquid phase in the temperature range 1064-1150°C. The bulk microstructure of the droplet is homogeneous (Figure

64a) and EDX analysis shows that the Zr content in the droplet is about 2.5 wt%Zr. At the zirconia / Au-3Zr alloy interface, a thick (~ 12 µm) and facetted reaction layer is formed. According to the EDX analysis, the reaction product layer is composed of about 66 at%O and 34 at%Zr which suggests that the reactive layer formed at zirconia / Au-3Zr alloy is the ZrO_2 oxide.

Note that, as it is indicated by the Zr-O phase diagram (Figure 23), zirconia is not a stochiometric compound. In the following, in order to distinguish the zirconia substrate from the zirconia reaction layer, they are respectively noted by ZrO_{2-x} and ZrO_{2-y} (with x << 1 and y << 1) – see Figure 9.

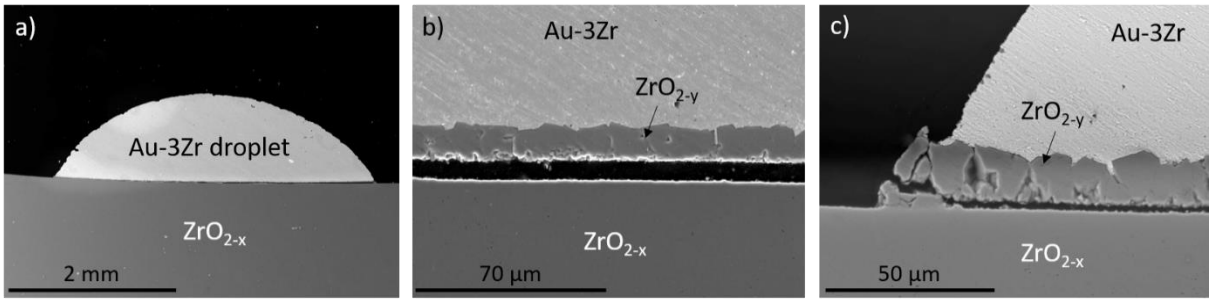

Figure 64: SEM images of cross section of Au-3Zr droplet on zirconia, after 45 min in liquid phase in the temperature range 1064-1150°C.

Figure 64c clearly shows that the zirconia substrate (ZrO_{2-x}) / reaction layer (ZrO_{2-y}) interface is situated at the same horizontal level as the zirconia substrate surface (on the left side of the triple line). Thus, it can be concluded that the growth of the reaction layer takes place at the interface 2 (alloy / ZrO_{2-y} reaction layer interface) by reaction between zirconium (diffusing from the bulk alloy) and oxygen diffusing through the reaction layer from the interface 1 (ZrO_{2-x} / ZrO_{2-y} interface) to the interface 2 (ZrO_{2-y} / alloy interface). This result is in full agreement with the fact that the diffusion coefficient of oxygen in zirconia is several orders of magnitude higher than that of Zr [16–20]. This means also that an oxygen diffusion profile exists through the zirconia substrate, i.e., the stoichiometry of zirconia varies from ZrO_2 in the bulk zirconia (far from the interface 1) to ZrO_{2-x} at interface 1.

Note that this mechanism could be applied also to other M-Zr / zirconia systems (M= Ag, Au-20Sn). The overall chemical reaction occurring at the substrate / alloy interface can be written as:

$$(2-y)O_d + (Zr)_{Au} \rightarrow ZrO_{2-y} \qquad (1)$$

where O_d denotes oxygen atoms diffusing through ZrO_{2-y} reaction layer, and reacting at ZrO_{2-y} / Au-Zr alloy interface with Zr atoms contained in the liquid alloy, noted $(Zr)_{Au}$.

The diffusing oxygen atoms are liberated from zirconia substrate which becomes sub-stoichiometric according to the following relation:

$$ZrO_2 \rightarrow ZrO_{2-x} + xO_d \qquad (2)$$

From these chemical reactions, two simple calculations allow to estimate in one hand the Zr consumption of the alloy leading to the formation of the ZrO_{2-y} reaction layer (reaction 1), and in the other hand the deviation from stoichiometry of zirconia substrate (from ZrO_2 to ZrO_{2-x}) caused by the reaction 2. We assume that ZrO_{2-y} is a dense layer without porosities and thus its density is equal to that of zirconia: ρ_{ZrO2} = 6.08 g/cm^3 (see chapter 2 – section 2.1.1). The molar masses of oxygen and Zr are 16 and 91.2 g/mol respectively.

First, a mass balance of Zr was performed in order to evaluate the zirconium consumption due to the formation of ZrO_{2-y} reaction layer at the substrate / alloy interface. From the droplet / ZrO_2 contact area (7.4 mm^2) and the reactive layer thickness (12 µm), we calculate the volume (V_{RL} = 8.88.10^{-5} cm^3) and the mass of ZrO_{2-y} reaction layer (m_{RL} = 5.10^{-4} g = 0.5 mg). Thus with y << 1, the corresponding mass of Zr contained in the reaction layer is about 0.37 mg. Knowing the initial mass of Zr contained in the Au-3wt%Zr alloy (2.7mg), we can conclude that less than about 16wt% of zirconium active element of the alloy is consumed to form the ZrO_{2-y} reaction product layer. This result is in agreement with EDX analysis showing that the content of Zr in the droplet is ~2.5wt%Zr (close to the initial Zr content equal to 3wt%).

Second, an oxygen mass balance allows to estimate the deviation from the stoichiometry (x) of zirconia substrate ZrO_{2-x} (disc Ø = 15 mm, h = 2 mm) with a volume $V_{substrate}$ = 0.58 cm^3 caused by the formation of the ZrO_{2-y} reaction layer with a volume V_{RL} = 8.88.10^{-5} cm^3. By assuming an isotropic variation of stoichiometry of zirconia (from ZrO_2 to ZrO_{2-x}) in the entire substrate, the value of x can be calculated from the following relation:

$$x \approx 2\frac{V_{RL}}{V_{substrate}} = 3.10^{-4} \qquad (3)$$

This means that the value of deviation (x) from stoichiometry of zirconia would be of the order of 3.10^{-4}.

Note finally that, from a mechanical point of view, the faceted shape of the reaction layer is not recommended for brazing because, in this case, failure initiation could occur predominantly at the

braze / reaction layer interface. Moreover, as we had some trouble with the Au-Zr ribbon shaping, we decided not to continue the study with the Au-Zr alloys.

2.2.4. Conclusion

Zirconium active element was investigated in wetting configuration in the three matrix Ag, Au-20Sn and Au in view to consider zirconia / titanium brazing with the M-Zr alloys (M = Ag, Au-20Sn and Au). A good wetting of zirconia by the three M-Zr alloys was obtained. Table 14 summarizes the final contact angles of M-Zr alloys on zirconia with associated temperatures.

Zirconium active alloy (wt%)	**Temperature**	**Final contact angle θ**
Ag-3Zr	980°C	62°
Au-20Sn-3Zr	1064°C	28°
Au-3Zr	1070°C	66°

Table 14: Final contact angles of active alloys containing Zr on zirconia substrate.

Unfortunately, we encountered different issues with these filler metals:

- The high thermodynamic activity of titanium in liquid silver does not allow to successfully braze zirconia to titanium with Ag-3Zr. Indeed, a very thick reaction layer is formed at the ZrO_2 / Ag-3Zr interface even with a short duration of the braze in liquid state.
- The oxidation of Au-20Sn-3Zr alloy prevents wetting of zirconia at low temperatures. Thus, the temperature must be raised at least at 970°C (that means 700°C above the Au-20Sn melting point) for the zirconia to be wetted by the Au-Sn-Zr alloy. Note moreover that in the 270-970°C temperature range, the liquid alloy (trapped under the oxide crust) could react with the substrates, and may form thick reaction layers in the ZrO_2 / Ti brazing configuration.
- At the Au-3Zr / zirconia interface, a faceted reaction layer is formed. This shape could be detrimental to the mechanical behavior of the joint. Moreover, we had difficulty to elaborate Au-Zr ribbons.

Therefore, we chose to not pursue the study of zirconium active element in order to focus our research on titanium active element.

2.3. Ti active element

This section deals with wetting of zirconia by liquid alloys containing titanium as reactive element. By using the same approach as in the previous section, the active element Ti is investigated in the three-selected matrix Ag, Au-20Sn and Au.

First, wetting of zirconia by Ag-4Ti and Au-20Sn-3Ti alloys as well as the reactivity at the zirconia substrate / active alloys are presented and discussed.

Then, wetting and interfacial reactivity of zirconia by Au-xTi alloys ($0.6 < x < 4$ wt%) are studied in detail.

These experiments were conducted in order to select the filler metal, which would be studied in both wetting configuration on titanium substrate, and zirconia-to-titanium brazing configuration.

2.3.1. Wetting of zirconia by Ag-Ti and Au-20Sn-Ti alloys and preliminary brazing tests

a) Ag-Ti alloy

Zirconia wetting by the Ag-4wt%Ti alloy was studied during an isothermal holding at 980°C. The alloy was prepared in situ by placing a piece of Ti on a twisted wire of Ag, wrapped in a thin Ag foil. The heating rate was fixed at 10°C/min. Figure 65 shows some selected images during melting and spreading of the alloy on zirconia at 980°C. During the 2 min before the isothermal holding, in the temperature range 962-980°C, the thin Ag foil completely melts and the Ag wire begins to melt. During the first minutes at 980°C, the piece of Ti dissolves in the liquid Ag. However, after 4 min of contact, a part of the massive Ti piece is still detected on the right side of the liquid alloy, resulting in the pinning of the triple line with two different contact angles θ on the left (θ_l ~ 70°) and on the right side (θ_r ~ 102°) of the drop. A good wetting of zirconia is obtained at 980°C: the final contact angle, measured after 10 min of contact in liquid phase is 65°. Afterwards, the contact angle remains constant up to 30 min at 980°C. Note that when the temperature increases to 1000°C, the triple line does not move anymore during 30 min despite the fact that the height of the drop decreases due to Ag evaporation (i.e. pinning of the triple line).

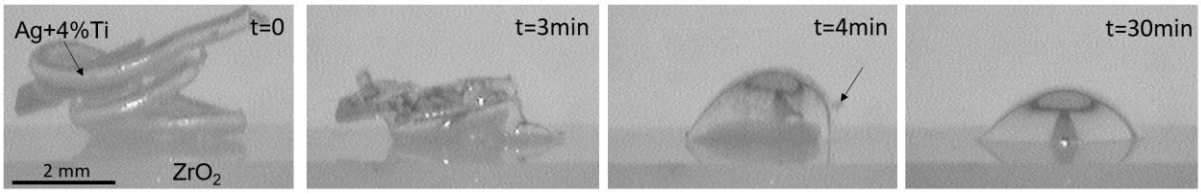

Figure 65: Some selected images during melting and spreading of the Ag+4wt%Ti alloy on zirconia substrate at 980°C.

Some SEM images of the cross section of the Ag-4Ti droplet on zirconia after about 1h in liquid state, in the temperature range of 962-1000°C are presented in Figure 66. Note that the contact angle of the solidified droplet is lower than the measured contact angle in situ at 980°C because silver evaporated during 30 min at 1000°C. The bulk microstructure of the drop is homogeneous and it is composed of AgTi precipitates dispersed in a silver matrix. EDX analysis of the droplet clearly indicates that there is no trace of Zr content.

A very thick and homogeneous Ti_xO_y reactive layer of about 50 µm is formed at the zirconia / alloy interface. Thus the final contact angle of the alloy corresponds to the equilibrium contact angle on Ti_xO_y compound. A decohesion of the solidified droplet is observed at the reactive layer / zirconia interface.

It is well established in the literature that most of Ti_xO_y titanium oxides are wetted by titanium active alloys [21,22]. Voytovych et al.[22] studied the wetting of mono and polycrystalline alumina substrates by the eutectic Ag-72wt%Cu alloy containing 3 to 8 at%Ti. While Cu-Ag alloy does not wet alumina (the contact angle being higher than 140°), the addition of some wt%Ti leads to a drastic decrease of the contact angle (lower than 20°) in less than 10 min. Moreover, the wetting behavior was found to be practically independent of the surface roughness of the samples varying from 4 nm to 1.5 µm. Kristalis et al.[21] studied the wetting of alumina by Ni-45at%Pd azeotropic alloy containing up to 30at%Ti. They show that the contact angle θ on Ti_xO_y layer (formed at the alloy / substrate interface), strongly depends on the molar fraction of Ti in the formed oxide: θ decreases with Ti/O ratio ($\theta \approx 95°$, 70 and 50° on Ti_5O_9, Ti_3O_5 and Ti_2O_3 respectively).

Note that the goal of the isothermal holding at 1000°C for 30min is to exacerbate the reaction at the zirconia / alloy interface in order to determine the growth mechanism of the reaction layer. Indeed, in this case the Ti_xO_y reaction layer formed is very thick (about 50 µm).

Figure 66a clearly shows that the zirconia substrate / reaction layer interface is situated at the same horizontal level as the zirconia substrate surface. It can thus be concluded that the growth of the reaction layer takes place at the alloy / reaction layer (Ti_xO_y) interface by reaction between titanium (diffusing from the bulk alloy) and oxygen diffusing through the reaction layer following the reaction:

$$yO_d + x(Ti)_{Ag} \rightarrow Ti_xO_y \qquad (4)$$

with O_d referring to oxygen diffusing in the reaction layer and $(Ti)_{Ag}$ referring to the dissolved titanium in the liquid Ag-Ti alloy. As it has been discussed above, O_d is liberated from zirconia which changes its stoichiometry.

This reactive mechanism is in agreement with the fact that no trace of Zr was detected in the droplet, i.e. the growth of Ti_xO_y mainly occurs by reaction (4) and not by reaction $ZrO_2 + (Ti)_{Ag} \rightarrow Ti_xO_y + (Zr)_{Ag}$, where $(Zr)_{Ag}$ denotes Zr atoms dissolved in liquid Ag.

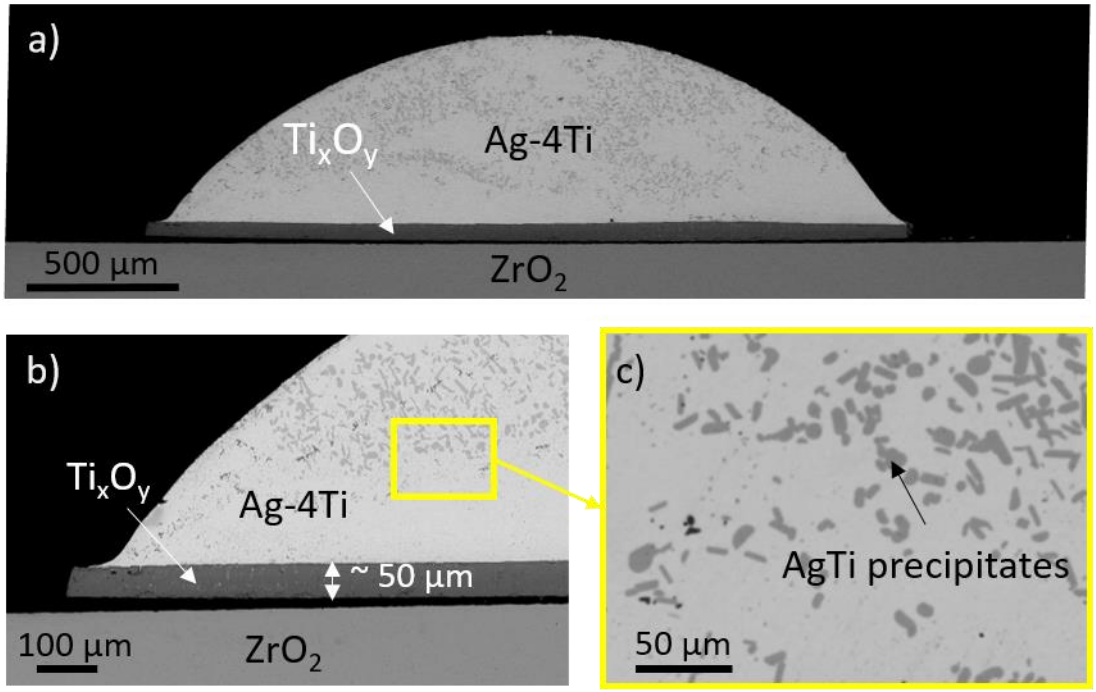

Figure 66: SEM images of the cross section of the Ag-4Ti droplet on zirconia after about 1h in liquid state between 980 and 1000°C.

Despite the fact that the thermodynamic activity of titanium in liquid silver is very high (see section 2.2.1), zirconia to titanium brazing was tested just to verify if the mechanical behavior of the system would be as it was expected or not. Therefore, a thick Ag foil was used (125 µm thick) and the thermal cycle was chosen with a short duration in liquid state: 970°C for 1 min, with a heating rate of 10°C/min. Resulting from this thermal cycle, a successful assembly of zirconia to titanium was obtained (substrates do not detach manually).

Microscopic images of a cross section of the sample show a homogeneous joint. However, large failures of millimeter length are detected at the interface (Figure 67a).

A thick Ti_xO_y reaction layer of about 15 µm is formed at the zirconia side (Figure 67b) despite the fact that the contact time in liquid state is very low. Figure 67c shows that the large failures are located at the oxide layer / joint interface. Thus, as it was expected, this thick oxide layer does not allow a good mechanical strength of the assembly. Note that this type of failure in brazing configuration occurring at the Ti_xO_y / Ag interface is different from that observed in sessile drop configuration which takes place at the Ag-Ti solidified droplet / zirconia interface (see Figure 66). This difference could be due to the fact that stress distribution occurring during the cooling process is very different between sessile drop configuration and brazed assembly configuration.

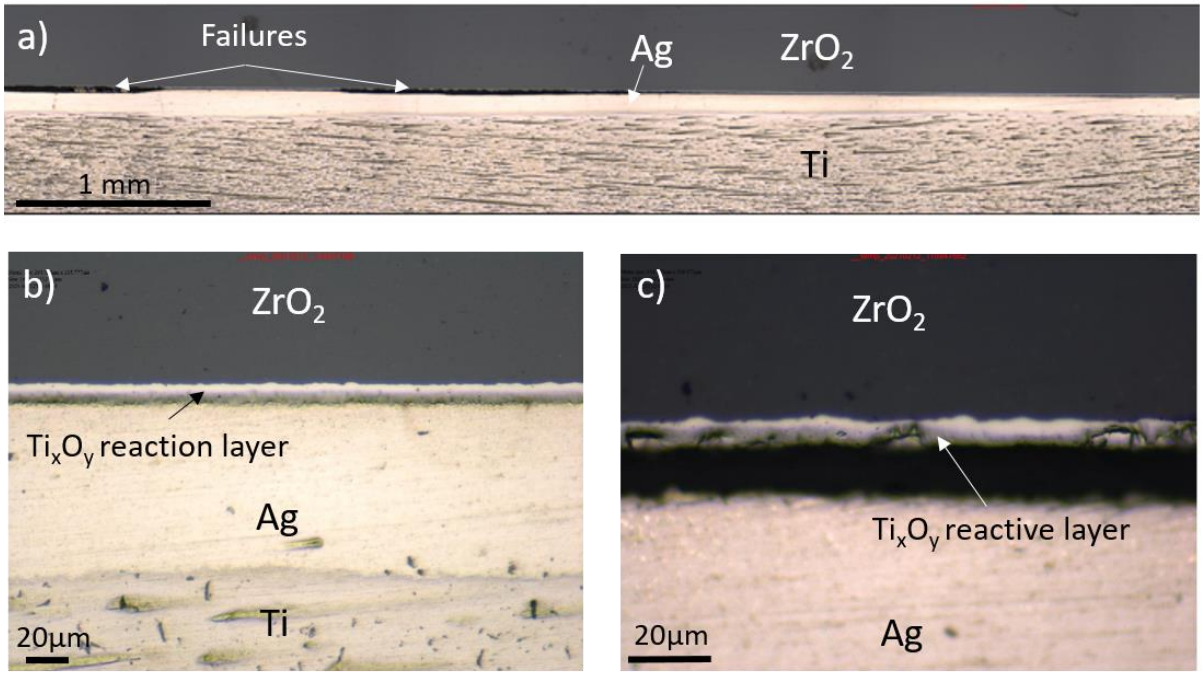

Figure 67: SEM images of a cross section of ZrO_2 / Ag / Ti assembly performed at 970°C for 1min.

b) Au-Sn-Ti alloy

Wetting of zirconia by the Au-20Sn-3Ti alloy, prepared in situ is also investigated. Figure 68b presents sample before heat treatment, composed of a massive Ti piece trapped inside a sheet stacking of Au-20Sn alloy, placed on a zirconia substrate.

This sample is heated up to 1064°C with a heating rate of 10°C/min. Figure 68a presents some selected in situ pictures taken during the heating process. During heating, a continuous change in the shape of the alloy is detected in the temperature range 280 - 985°C until the formation of a droplet with a spherical shape *at about 985°C*. The contact angle θ at this temperature is higher than 90°. This phenomenon is due to the formation of a Sn surface oxide crust at room temperature and also during heating, preventing the formation of a spherical drop after melting. This oxide layer is destroyed under

vacuum at high temperature, at about 900 - 1000°C. Note that for temperatures higher than the melting point of the eutectic Au-Sn alloy (278°C), titanium can dissolve in the alloy but the contact between the piece of Ti and the liquid could be only punctual and thus the dissolution process becomes negligible. Once the droplet takes the form of a spherical cap at about 985°C, the titanium piece is surrounded by the liquid and thus it dissolves in liquid Au-Sn alloy. Afterwards Ti diffuses towards ZrO_2 / alloy interface and reacts with zirconia leading to the formation of a Ti_xO_y wettable compound at the interface. Thus the liquid alloy spreads over zirconia surface by reactive wetting process. At 1020°C the massive Ti piece is not visible anymore which means that a significant proportion of titanium is dissolved in the liquid alloy. The evolution of contact angle θ and drop base radius (Figure 68a) shows that spreading continues during heating up to 1064°C (θ decreases down to 30°) as well as during isothermal holding for 10 min at 1064°C (θ decreases from 30° to the final contact angle 15-20°). Spreading kinetics is not presented here because the obtained in situ images are not of good quality, causing high measurement uncertainty of the contact angle.

As a conclusion, a very good wetting of zirconia by the Au-20Sn-3Ti is observed at high temperature (T > 1020°C).

At the end of this experiment, solidified droplet adheres to zirconia substrate. Comparison of the aspect of ceramic surface before and after the wetting experiment (Figure 68b-c) clearly shows the color change of the substrate from white to black. This color change is due to the change in the stoichiometry of zirconia from ZrO_2 (white color) to ZrO_{2-x} (black color) as it is reported in the literature by several studies [10–13] on reactivity between active alloys and zirconia.

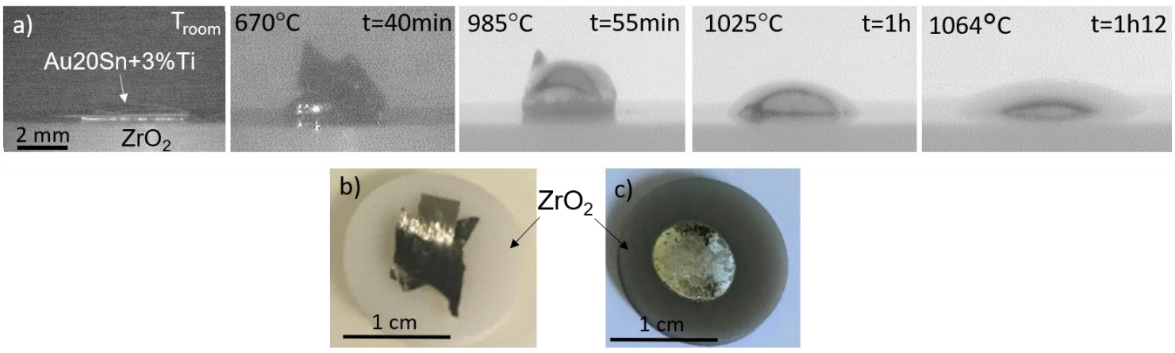

Figure 68: Selected images of Au-Sn + 3wt%Ti / zirconia system during heating from room temperature to 1064°C (a). Top view images of the sample at room temperature before (b) and after wetting experiment (c).

Figure 69 shows that the solidified droplet is composed of two distinct zones. The interface between these two zones is indicated by a red dotted curved line. The center of the drop is rich in Au-Ti precipitates, whereas the periphery of the drop is poor in Au-Ti precipitates.

At the drop / zirconia interface, a faceted, not-continuous, and highly irregular reaction layer is observed. This faceted layer is composed of particles in the shape of whiskers up to 10 µm in length. EDX analysis of these particles shows that they are composed of titanium oxide.

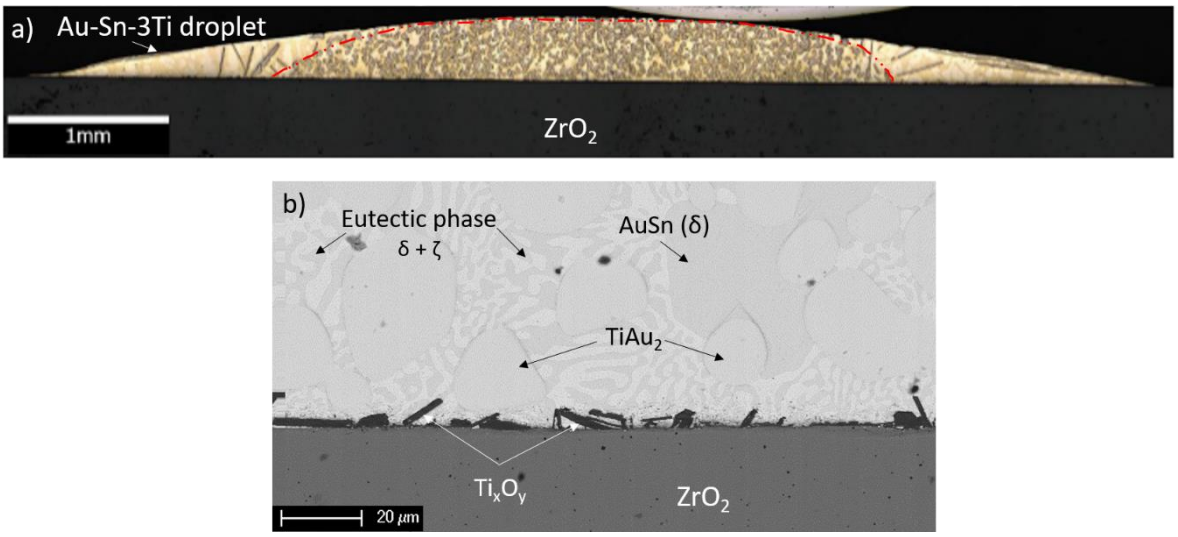

Figure 69: Optical image of a cross section of Au-20Sn + 3 wt%Ti / zirconia system after a wetting experiment at 1064°C (a). SEM image of the interface (b).

Despite the oxidation issue of the Au-Sn alloy, a Ti / ZrO_2 brazing experiment was carried out with a Au-20Sn foil of 125 µm thick. In fact, the assembly configuration may be conducive to surface deoxidation of the filler metal given the fact that Ti can form very stable intermetallic compounds (IMC) with both Au and Sn. Indeed, for thin oxide films, wetting is strongly improved by IMC formation reactions at the interface leading to replacement of the oxidized surface by a clean surface of an IMC: the thin and continuous Sn oxide layer would be splitted in small particles due to the IMC reaction formation[23].

However, this brazing test, performed at 1020°C for 15 min, was inconclusive: ceramic and titanium substrate were not successfully assembled (they are separated after the brazing test). The top view of the zirconia substrate after heat treatment presented in Figure 70a, shows light grey and dark grey zones. The dark grey parts correspond to the areas where titanium has reacted with zirconia. At the light grey area, titanium did not react with ceramic. SEM micrograph of a cross section of the titanium substrate (Figure 70b) shows the formation of uneven successive layers. Two thin layers formed at

titanium side are not continuous, and the thicker layer formed on the Au-Sn side is dotted with defects like porosities and cracks.

EDX analyses of the thick layer clearly indicate that, the entire Au-Sn joint has reacted with Ti substrate during brazing process. This reaction leads to the formation of Ti-Au and Ti-Sn-Au intermetallic compounds, which are solid at the brazing temperature (1020°C). The discontinuous top layer in Figure 70b corresponds to a Ti_xO_y layer formed by reaction between Ti and zirconia substrate.

As a conclusion, the Au-20Sn filler metal is not adapted for Ti / ZrO_2 brazing. In some places along the joint, the surface oxidation of Au-Sn alloy prevents Ti reaction at ZrO_2 / joint interface. In other areas, all the Au-Sn joint has reacted with Ti substrate during the liquid phase duration (more than 1h from melting temperature of Au-Sn alloy to 1020°C), leading thus to a total solidification of the joint at the brazing temperature.

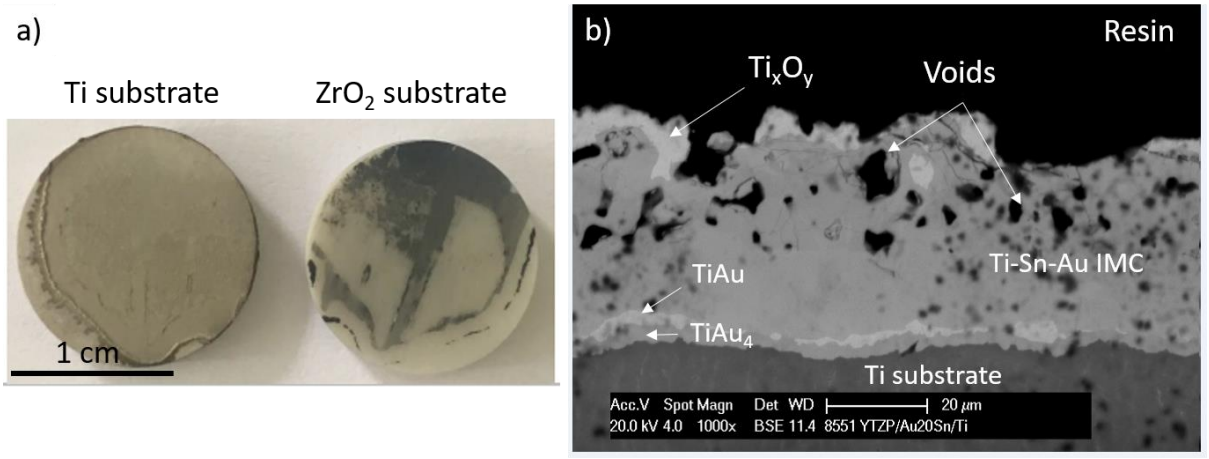

Figure 70: Top view of Ti and zirconia substrates (a) and SEM micrograph of a cross section of the Ti substrate after an isothermal holding at 1020°C for 15 min.

c) Conclusion

To conclude, Ag and Au-20Sn matrix were investigated in wetting and brazing configurations. Good wetting of zirconia by the Ag-4Ti and Au-20Sn-3Ti (wt%) alloys was obtained, with the respective final contact angles θ_f = 65°at 980°C and θ_f = 15-20° at 1064°C. However, preliminary brazing tests clearly showed that Ag and Au-20Sn matrix are not interesting for zirconia-to-titanium brazing. Indeed, the thermodynamic activity of titanium in liquid silver is very high, leading thus to the formation of a thick reaction product layer at the braze / zirconia interface, even with a short liquid phase duration.

Regarding Au-20Sn alloy, its surface oxide layer, stable at temperatures below 950-1000°C, does not allow its use neither at middle temperature range (300 - 900°C) nor at higher temperature (T > 900°C). Indeed, this native oxide prevents good local intimate contact especially with zirconia substrate leading thus to unreacted zones in the Ti / Au-Sn / ZrO_2 joint.

2.3.2. Interfacial interactions between zirconia and liquid Au-Ti alloys

In this section, wetting study of zirconia by Au-xTi alloys (x represents the mass percent of Ti in Au-xTi alloy) is investigated in detail, mainly using the sessile drop method but also using the dispensed drop technique. In order to identify the titanium content impact on spreading kinetics and on reactivity with zirconia, five titanium contents are selected, ranging from 0.6 to 4 wt%. The Au-xTi alloys investigated in this section as well as their processing method are summarized in Table 15.

Ti content (wt%)	**Processed in situ**	**Elaborated alloys**
0.6	Au-0.6Ti	Au-3Ni-0.6Ti commercial alloy (GOLD-ABA®)
1	Au-1Ti	Au-1Ti
2	-	Au-2Ti
3	Au-3Ti	-
4	-	Au-4Ti

Table 15: Au-xTi (wt%) alloys used in the wetting study and their processing method.

The binary Ti-Au phase diagram, to which we refer throughout the following work, is given in Figure 71. Concerning the wetting of zirconia by liquid Au-Ti alloys, we focus on the Au-rich side of this diagram, where low Ti contents (in wt% and at%) are indicated by red vertical lines.

Note that, contrary to the silver matrix, the thermodynamic activity of titanium in liquid gold is very low. Indeed, the activity coefficient of Ti at infinite dilution in liquid Au referred to liquid Au at 1100°C is extremely low (γ_{Ti}^{∞} = 2.10^{-4})[24] compared to γ_{Ti}^{∞} = 4 for Ag matrix. Thus the thermodynamic activity

of Ti (a_{Ti}) in liquid gold is also extremely low : $a_{Ti} = \gamma_{Ti}^{\infty} x_{Ti} = 4.8.10^{-6}$ to $2.9.10^{-5}$ when the molar fraction of Ti (x_{Ti}) increases from about 0.024 (0.6wt%) to 0.15 (4wt%).

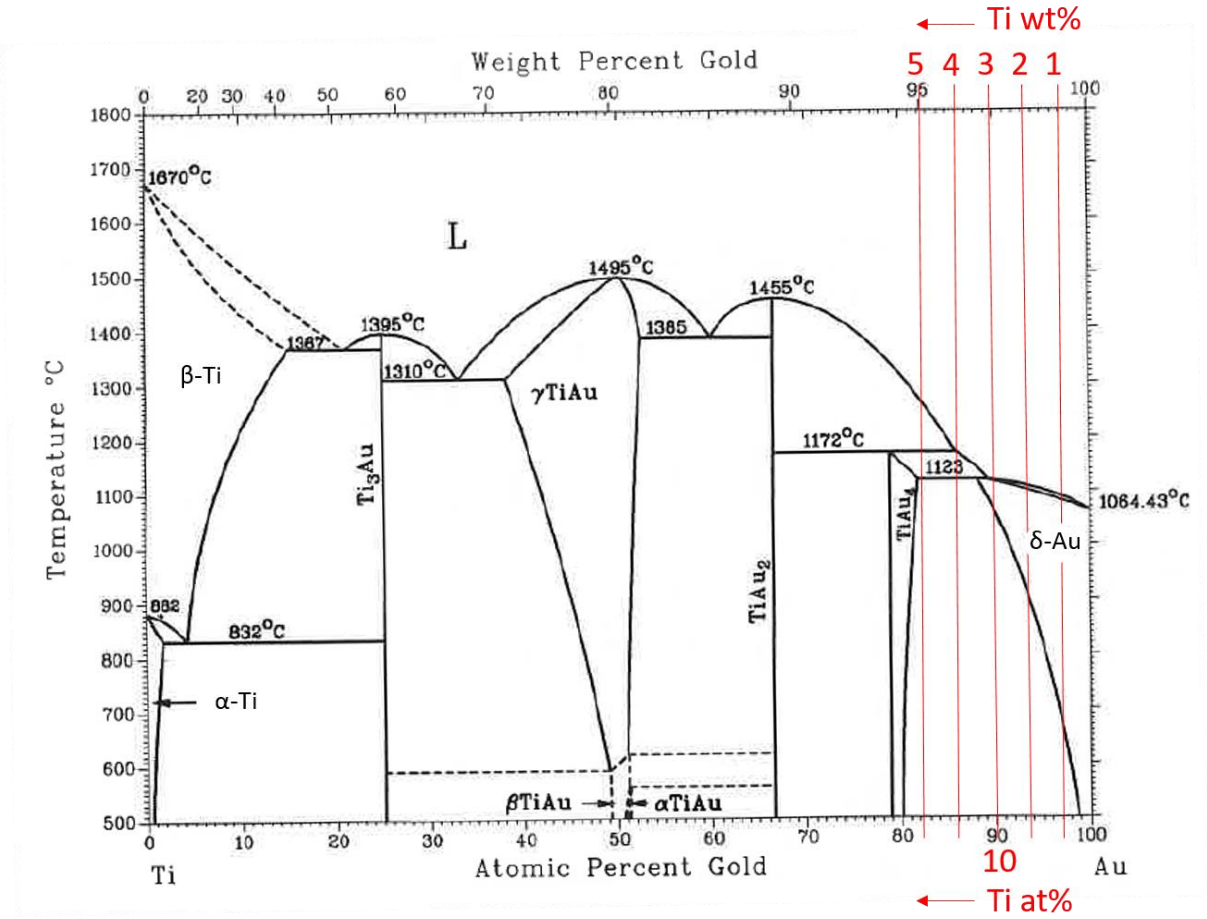

Figure 71: Binary Ti-Au phase diagram[25].

First, wetting experiments of zirconia by the Au-xTi alloys in the temperature range 1040-1250°C are detailed. In situ images, spreading kinetics, SEM and optical micrographs, as well as analyses of the samples are presented in the order of increasing Ti content.

Then, the reaction layer formation at the Au-xTi alloy / zirconia interface is investigated, as a function of reaction time and titanium content.

2.3.2.1. Wetting study of zirconia by the Au-xTi alloys (0.6 < x < 4 wt%)

Wetting experiments of the Au-xTi alloys on zirconia were carried out both on raw zirconia substrates (surface roughness R_a = 0.5 µm), and on polished zirconia substrates (R_a = 0.2 µm). In some particular cases described below, mirror polished zirconia (R_a < 30 nm) were used in order to study the effect of surface roughness on reactive wetting process.

Figure 72 shows that pure gold does not wet zirconia. Indeed, a contact angle of liquid gold on zirconia of 123° was observed at 1100°C. This value is in agreement with the value reported in the literature[26].

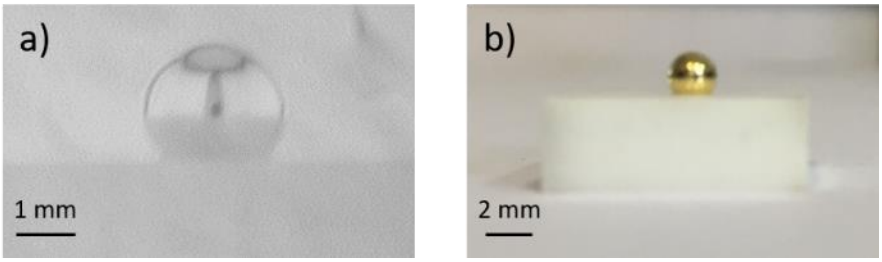

Figure 72: In situ image of liquid gold on zirconia substrate (a) and optical image of Au / ZrO_2 sample after a wetting experiment at 1100°C (b).

In order to improve zirconia wetting by liquid gold, titanium active element is added. Indeed, while the Ag-Cu alloys do not wet zirconia, a very good wetting by the active Ag-Cu-Ti alloys is obtained[5,6,8,27]. Thus, zirconia wetting by the Au-Ti active alloys with different Ti contents from 0.6 to 4wt% is studied and described in this section.

a) Wetting of zirconia by the commercial Gold-ABA® alloy (Au-3Ni-0.6Ti)

The first experiment was performed on polished zirconia (R_a = 0.2 µm) with the commercial active alloy Gold-ABA® containing 0.6 wt%Ti. Note that Gold-ABA® liquidus temperature is 1030°C. Figure 73a shows the variation of the contact angle θ as a function of time and temperature between 1040°C and 1170°C. Remember that the contact angle θ of the drop was measured with an accuracy of ±3° (see chapter 2). The heating rate for this experiment is 16°C/min and a liquid droplet is formed at about 1040°C. Figure 73b gives some selected images of the droplet during its spreading from the initial to the final contact angle. The initial observed contact angle (θ = 125°) remains constant during about 1 min and afterwards it decreases from 125° to 86° in about 7 min during heating up to 1170°C. Finally, the contact angle remains constant at 86° during the isothermal holding for 4 min at 1170°C.

The initial contact angle of 125° corresponds to the contact angle of pure liquid gold on zirconia substrate. This means that during this time the reaction between the active alloy and zirconia is not yet sufficient to lead to a reactive wetting or a pinning of the triple line can occur. After 1 min of contact, the reactive spreading process starts which is due to the formation of a wettable reactive layer at the zirconia / alloy interface as it will be seen below.

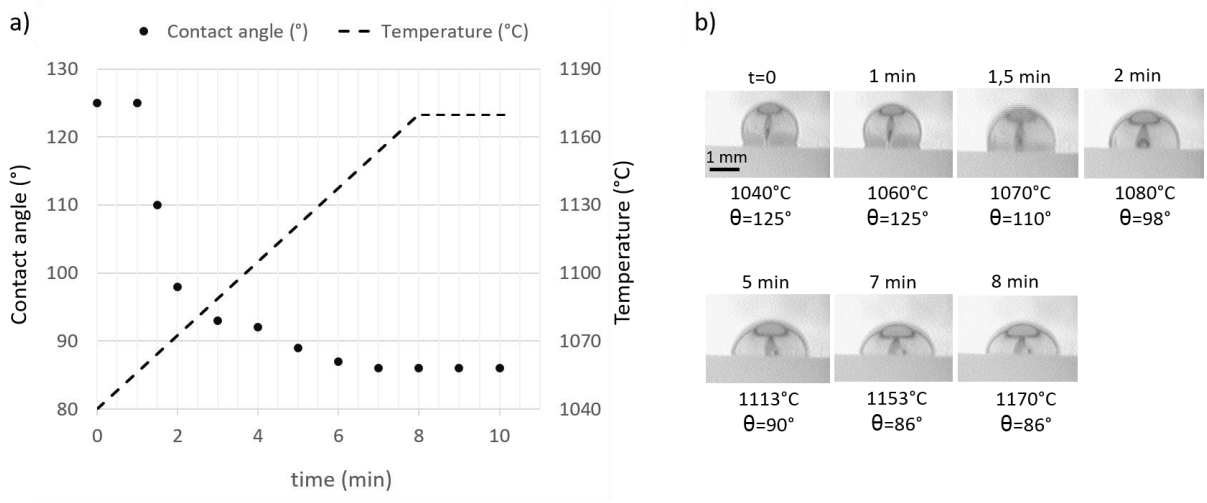

Figure 73: Variation of the contact angle θ as a function of time and temperature during wetting of Gold-ABA® alloy containing 0.6 wt%Ti on polished zirconia substrate (R_a = 0.2 µm) (a). Some selected images of the droplet during heating from 1040 to 1170°C (b).

Three wetting experiments of Gold-ABA® on raw zirconia (R_a = 0.5 µm) were repeated up to 1250°C. In two cases, the liquid alloy does not spread over zirconia substrate below 1200°C, the contact angle being about 170° after a long time in liquid state (20 min and 1h30 respectively). During heating above 1200°C, a sudden spreading occurs at 1202°C and 1212°C respectively. The contact angle θ decreases from 170° to 110° in a split second, corresponding to a jump of the triple line. During the third experiment (up to 1250°C), alloy does not spread on ceramic substrate at all and the contact angle remains constant at 170°: the triple line stays blocked (pinning of the triple line). Figure 74a shows two images of liquid alloy on zirconia sample, taken at one-second interval, before and after the sudden spreading at 1212°C. Note that the allotropic transformation of zirconia at 1205°C (monoclinic → tetragonal) could be at the origin of the depinning of the triple line phenomena occurring twice around this temperature. This phenomenon of pinning of the triple line during spreading, well known in the case of non-reactive systems, is not so often observed in reactive systems and especially in reactive metal / ceramic systems.

Figure 74b presents two top-views of zirconia substrate after wetting experiments with Gold-ABA® alloy stayed 20 min (left) and 1h30 (right) in liquid state. We observe that, in the case of short contact duration of liquid alloy on zirconia, the substrate surface remains globally white, and turns grey on a limited area close to and in contact with the Au-Ti droplet; whereas zirconia turns fully dark grey when duration in liquid state is 1h30 long. As it is already mentioned before, the darkening of zirconia is due to its loss of oxygen leading to the formation of sub-stoichiometric zirconia ZrO_{2-x}.The dark zone area of zirconia grows with reaction time between the liquid Au-Ni-Ti alloy and zirconia. Note also that the

droplet is detached from the substrate after wetting experiment only for the long duration in liquid state. That may correspond to a significant reaction at the zirconia / Au-3Ni-0.6Ti alloy interface.

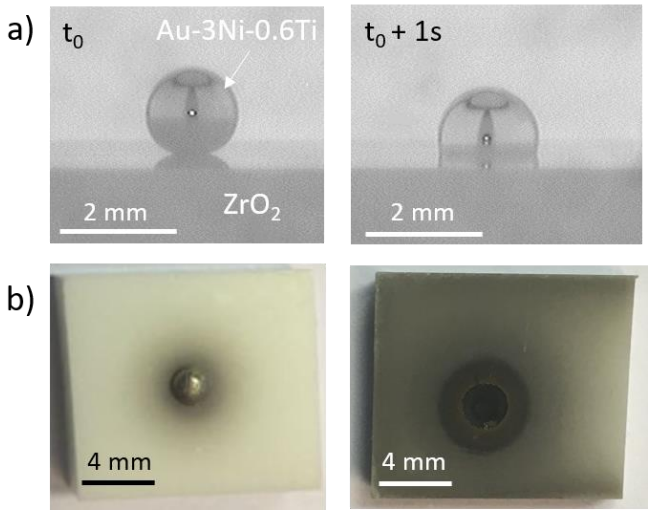

Figure 74: Two images of liquid Gold-ABA® alloy on raw zirconia, taken at one-second interval, before and after the sudden spreading at 1212°C (a). Top-views of zirconia substrate after a contact with Gold-ABA® alloy in liquid state for 20 min (left) and 1h30 (right) (b).

Figure 75 gives SEM micrographs of a cross section of a Gold-ABA® (Au-3Ni-0.6Ti alloy) droplet on zirconia substrate after 20 min of contact in liquid state in the temperature range 1030-1250°C. The formation of a reaction product at the Au-Ni-Ti alloy / zirconia interface is observed. The interfacial layer has a homogeneous thickness of about 1-2 µm and EDX analysis shows that this layer consists of Ti_xO_y phase. The mechanism of formation of this reactive layer will be described below, in the case of Au-1Ti alloy.

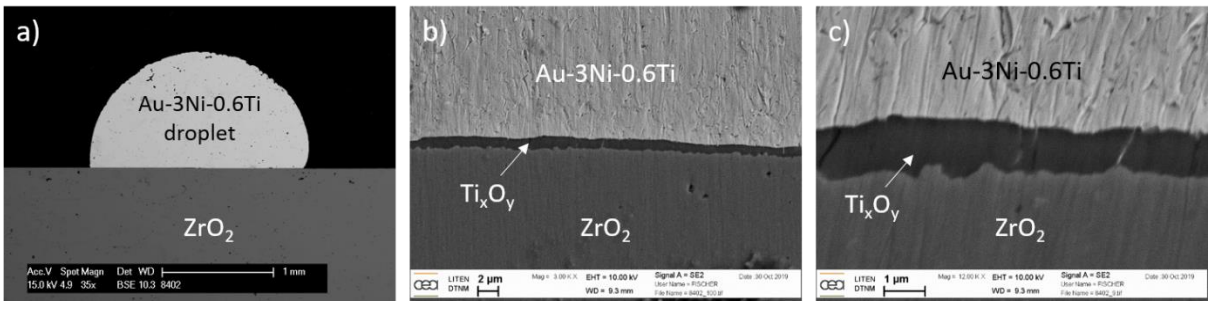

Figure 75: SEM micrograph of a cross section of a Gold-ABA® (Au-3Ni-0.6Ti alloy) droplet on zirconia substrate after 20 min of contact in liquid state in the temperature range 1030-1250°C.

Wetting and reactivity of Gold-ABA® with zirconia substrate are of great interest for the brazing applications, and this low Ti content into gold matrix deserves further study. However, for industrial reason with a view to biomedical application, it is suitable to study the wetting of zirconia by Au-Ti alloys without Ni found in the Gold-ABA® (Au-3Ni-0.6Ti) commercial alloy.

b) *Wetting of zirconia by Au-1wt%Ti alloy*

A preliminary study of wetting of raw zirconia (R_a = 0.5 µm) by the Au-1Ti alloy, prepared in situ during sessile drop experiment, was investigated. Selected images of alloy / substrate sample during heating up to 1112°C are presented in Figure 76. In this case, the massive Ti piece seems to be dissolved in liquid gold during a few minutes of heating from melting temperature of gold (1064°C) to about 1070°C. The value of the contact angle θ = 104±3° obtained at 1070°C was found to be almost equal to the contact angle of Gold-ABA® alloy at the same temperature. This contact angle remains constant even if the temperature is increased up to 1270°C, for 1h in liquid state.

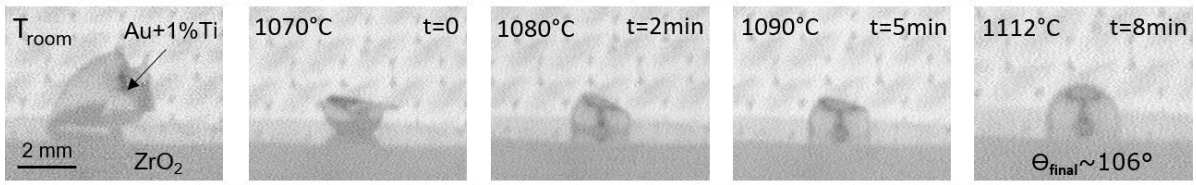

Figure 76: Selected images of Au+1Ti alloy / zirconia sample during up to 1112°C.

Afterwards, wetting experiments with a pre-prepared Au-1Ti alloy by melt-spinning were performed. Figure 77 gives some selected images of two Au-1Ti / raw zirconia (R_a = 0.5µm) samples, heated simultaneously up to 1250°C with a heating rate of 20°C/min. The two pieces of alloy melt rapidly between 1110 and 1113°C and, for both samples, a spherical cap is observed at 1113°C (which is close to the liquidus temperature of the alloy). Although the Au-1Ti alloy is a reactive alloy with zirconia, the observed contact angles are extremely high (160°-170°) in the temperature ranges 1113°C-1140°C for the first sample (Figure 77a) and 1113°C-1166°C (Figure 77b) for the second sample respectively. This delay at wetting clearly indicates a pinning of the triple line on zirconia substrates, even for very high contact angles. One of the droplet (Figure 77a) spreads over zirconia ceramic when the temperature increases from 1140°C to 1166°C, the contact angle decreases down to 105° and afterwards it remains constant during heating up to 1250°C. The other droplet (Figure 77b) remains blocked (θ = 170°) during heating up to 1250°C and then during cooling a sudden and significant jump of the droplet was observed (but the corresponding temperature and contact angle were not noted). The final contact angle measured on the solidified drop is evaluated to about 105°.

This pinning phenomenon of the triple line does not allow to establish the spreading kinetics of Au-1Ti on zirconia or to determine the equilibrium contact angle of this system. We can only confirm that the lower observed contact angle of Au-1Ti alloy on zirconia is 105°, which suggests that the equilibrium contact angle might be lower.

It is well known in the literature that pining phenomena is reinforced with increasing surface roughness of the substrate [1]. In order to determine if the roughness of zirconia substrate has an influence on its reactive wetting by Au-1Ti alloy, wetting experiments were performed on polished zirconia (R_a = 0.2 µm) and on mirror polished zirconia (R_a < 30 nm). In both cases, we observed also pinning of the triple lines and very high values of contact angles (θ ~ 170°) at temperature range 1064°C to 1250°C.

As a conclusion, this phenomenon of droplet pinning, occurring even for high contact angles (~170°), is independent of the substrate roughness, and takes place even on mirror polished zirconia. Therefore, pinning effect seems to be an intrinsic peculiarity of the reactive liquid Au-1Ti / ZrO_2 substrate system. As it has been reported by Tomsia et al[28], the main reason is that in the interaction between liquid metals and solid surfaces at high temperatures during the process of wetting, ridges are formed on the solid surface that can greatly slow or even stop the spreading of the liquid. Thus, more work is needed to determine the main factors governing this phenomenon in the reactive Au-Ti / ZrO_2 system.

Figure 77 gives also top view images of zirconia substrate after wetting experiments. In the case of the sample for which we observed spreading (Figure 77a), the darkening of zirconia is more pronounced than in the case of the sample without spreading presented in Figure 77b (In both cases the contact time between liquid droplets and zirconia was 21 min).

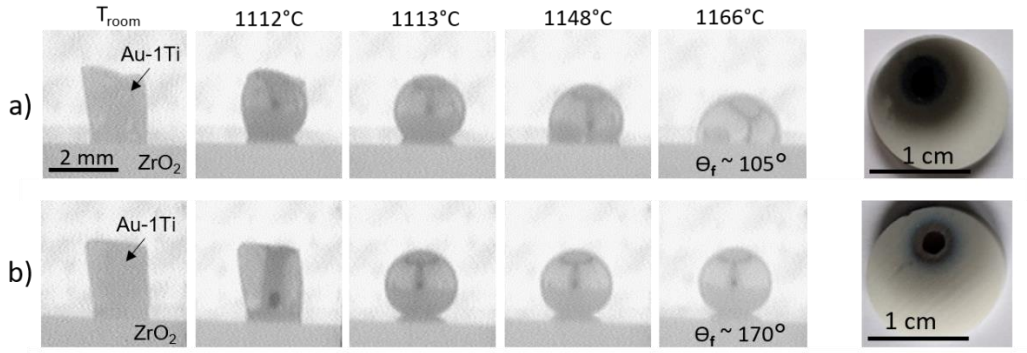

Figure 77: Selected images of two Au-1Ti alloy / raw zirconia (R_a = 0.5 µm) samples, heated simultaneously up to 1250°C with a heating rate of 20°C/min.

A last wetting experiment was performed with Au-1Ti alloy on polished zirconia (R_a = 0.2 µm) which consists of heating up to 1170°C with a heating rate of 20°C/min followed by an isothermal holding for 10 min at 1170°C and rapid cooling. Unfortunately, due to a technical problem, the recording was not performed during this experiment. An optical image of the cross-section of this Au-1Ti alloy on polished zirconia substrate sample after 14 min of contact in liquid state, in the temperature range 1080°C-

1170°C is given in Figure 78a. The solidified droplet presents a spherical cap form. The contact angle θ of this droplet on ceramic substrate was calculated from the volume V and the base radius R of the spherical cap by using the relation: $V = \pi R^3(2 - 3\cos\theta + cos^3\theta)/3$.

The calculated value of the contact angle of the Au-1Ti alloy on polished zirconia (θ ~ 73°) is close to the contact angle of Gold-ABA® (Au-3Ni-0.6Ti) alloy on the same substrate and in the same temperature range (θ = 86° - see Figure 73). This means a relative good wetting of Au-1Ti alloy on zirconia with an equilibrium contact angle that might be lower than 86°.

The contact between liquid Au-1Ti alloy and zirconia substrate during 15 min in the temperature range 1080-1170°C leads to the formation of a thin (~ 3 µm) and continuous reaction layer (Figure 78b), identified as Ti_xO_y phase.

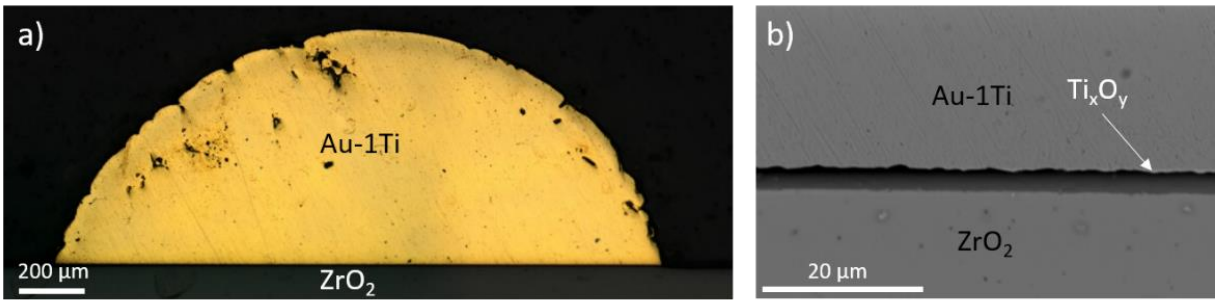

Figure 78: Optical (a) and SEM (b) images of the cross-section of Au-1Ti alloy / polished zirconia sample after an isothermal holding for 10 min at 1170°C (14 min of contact in liquid state).

c) *Wetting of zirconia by Au-2wt%Ti alloy*

Afterwards, the Ti content in Au was increased up to 2wt% and wetting study was performed by both sessile drop and dispensed drop methods.

Firstly, a preliminary experiment was carried out by following the Au-2Ti melting and spreading on raw zirconia (R_a = 0.5 µm) during heating up to 1250°C with a heating rate of 20°C/min.

Figure 79a gives some selected images of the droplet during spreading between 1115°C and 1125°C. At 1115°C, the entire piece of Au-2Ti melts and forms a spherical cap. This temperature is in good agreement with the liquidus temperature of Au-2Ti alloy given by the binary Ti-Au phase diagram (about 1110°C). The first contact angle measured at 1115°C is θ = 130°. The liquid alloy spreads rapidly: at 1125°C (1 min later), the contact angle θ = 82° is obtained and afterwards it remains constant during heating up to 1250°C and during cooling. However, spreading of the droplet is not continuous since successive jumps of the triple line are observed. Jumps are represented in Figure 79b on the graph

θ = f(t). This phenomenon (already observed for Au-1Ti alloy) clearly indicates a pinning of the triple line on zirconia substrate even for Au-2Ti alloy.

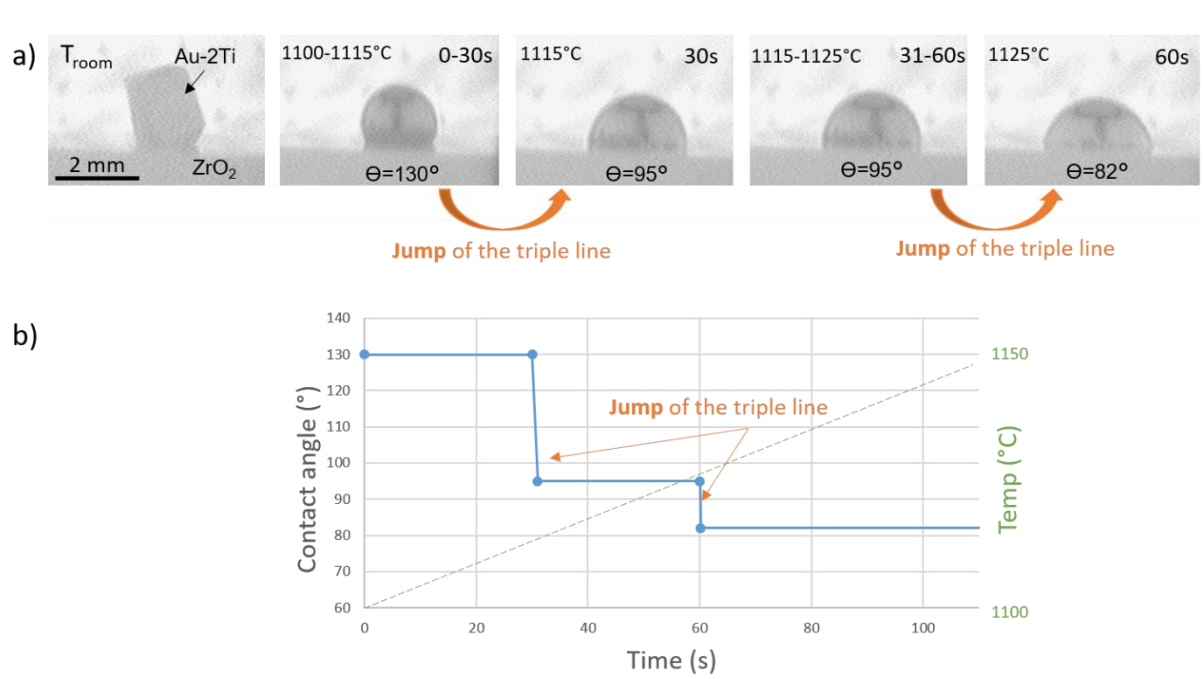

Figure 79: Selected images of the droplet (a) and variation of the contact angle θ and temperature with time (b) during spreading of Au-2Ti alloy on raw zirconia substrate (R_a = 0.5 µm) between 1115°C and 1125°C.

In order to evaluate the effect of substrate roughness on the pinning phenomenon of Au-2Ti droplet, a wetting experiment at 1170°C for 15 min with a heating rate of 20°C/min was performed on mirror polished zirconia (R_a < 30 nm).

Figure 80a shows in situ images of the sample during sessile drop experiment, at room temperature and during the isothermal holding at 1170°C. Figure 80b presents the variation of the contact angle with holding time at 1170°C. Once again, the spreading of the Au-2Ti droplet on zirconia is non-monotonic and occurs by successive jumps. Moreover, at about 250 and 850s, we can observe that the left contact angle is different from the right one. These two phenomena highlight the pinning of the triple line, despite the fact that this is a reactive system. The lower contact angle θ observed at 1170°C on polished zirconia is 57°. This value of θ obtained on mirror polished zirconia (R_a < 30 nm) is lower than that obtained on raw zirconia (R_a = 0.5 µm), θ = 82°.

Thus, pinning of the triple line occurs regardless of zirconia surface roughness, and occurs even if the titanium content in the Au-Ti alloy is increased from 0.6 to 2 wt%. Notice that the equilibrium contact angle of Au-2Ti alloy on zirconia might be lower than 57°.

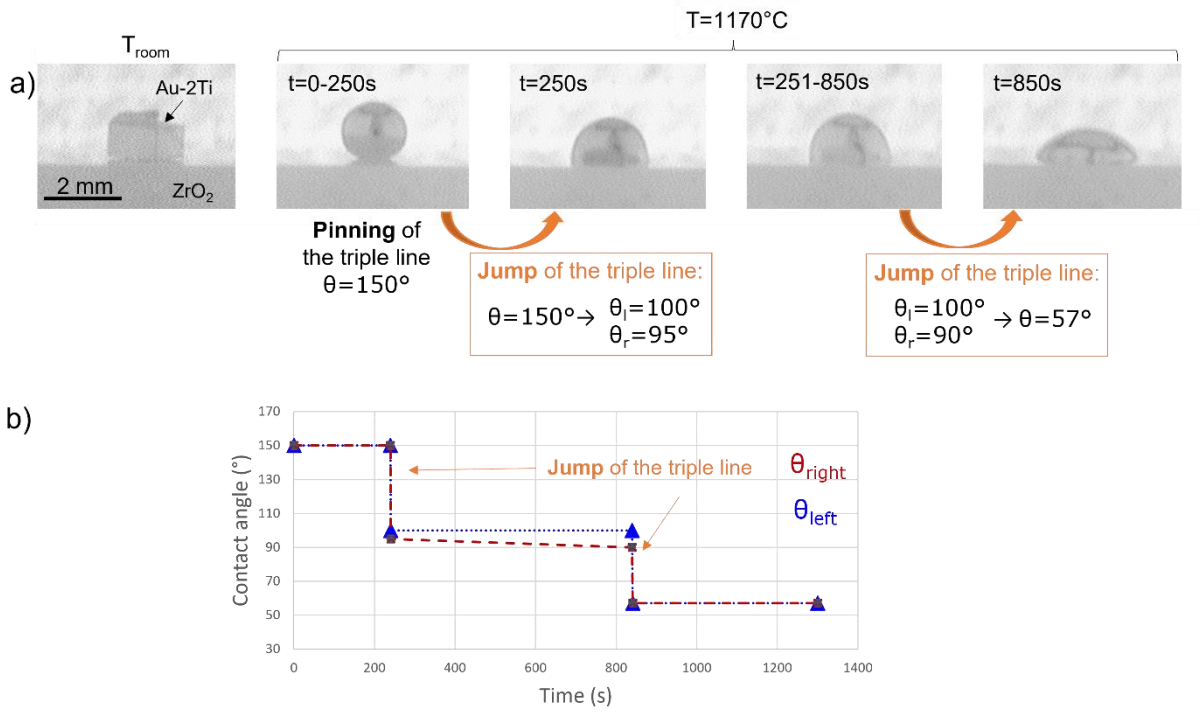

Figure 80: In situ images of the sample during sessile drop experiment for Au-2Ti alloy / mirror polished zirconia (R_a < 30 nm) substrate system at room temperature and during the isothermal holding at 1170°C (a). Variation of the contact angle with the holding time at 1170°C (b).

In order to study the impact of temperature on Au-2Ti alloy spreading on polished zirconia (R_a = 0.2 µm), dispensed drop experiments were performed for about 15 min during several isothermal holdings: 1140, 1170 and 1200°C. Recording was performed with a CCD camera (50 frames/s). For these three experiments, spreading of Au-2Ti occurs very rapidly and the first image recorded after the drop deposition (20-40 ms) gives the first observed contact angle, which remains constant with time during about 10 min. The final contact angles obtained at 1140, 1170 and 1200°C are respectively 87°, 89° and 87°. Therefore, according to these results obtained from dispensed drop experiments, in the range 1140-1200°C, temperature has no impact on Au-2Ti spreading on ZrO_2. Moreover, contact angle does not evolve with time. Note that these contact angle values (87 to 89°) obtained with dispensed drop technique on polished zirconia (R_a = 0.2 µm), are similar to the lowest value (82°) obtained at 1125°C on raw zirconia (R_a = 0.5 µm) but significantly higher than the lowest value (57°) obtained at 1170°C on mirror polished zirconia (R_a < 30 nm), by using the sessile drop method. These results strongly suggest that once again, the triple line is blocked, avoiding wetting of the alloy on ceramic because of the pinning phenomenon.

Figure 81 gives optical and SEM micrographs of Au-2Ti / polished ZrO_2 substrate sample after wetting experiment performed at 1170°C for 10 min. Note that, the total contact time between alloy in liquid state and zirconia substrate, including the cooling time down to melting temperature of the alloy, is

13 min. After the wetting experiment, the droplet was detached from zirconia substrate. It is shown that the droplet has a homogenous bulk microstructure, composed of acicular $TiAu_4$ precipitates, formed during cooling between the solvus of δ-Au phase and room temperature, dispersed into the δ-Au solid solution matrix. Indeed, during cooling, the solubility of Ti in δ-Au phase decreases significantly with temperature (see Figure 71) and thus δ-Au solid solution becomes depleted in Ti and, as a result,$TiAu_4$ needles precipitate inside the δ-Au matrix.

Notice on Figure 81b a border (indicated by a yellow dotted line) that separates two orientations of $TiAu_4$ needles. This border corresponds to the initial grain boundary of the δ-Au solid solution at temperatures above its solvus curve. Note also that at room temperature, the Ti contents in δ-Au and $TiAu_4$ phases are about 1 and 20 at%Ti respectively. Given the fact that the Ti content in the Au-2wt%Ti alloy corresponds to about 5at%, the molar fractions of δ-Au and $TiAu_4$ phases at equilibrium would be about 0.75 and 0.25 respectively.

Figure 81c shows that a continuous and consistent Ti_xO_y reactive layer about 3 µm thick is observed at the substrate / droplet interface. Fracture between droplet and substrate mainly occurs at the zirconia / Ti_xO_y interface, and occasionally inside the reaction layer.

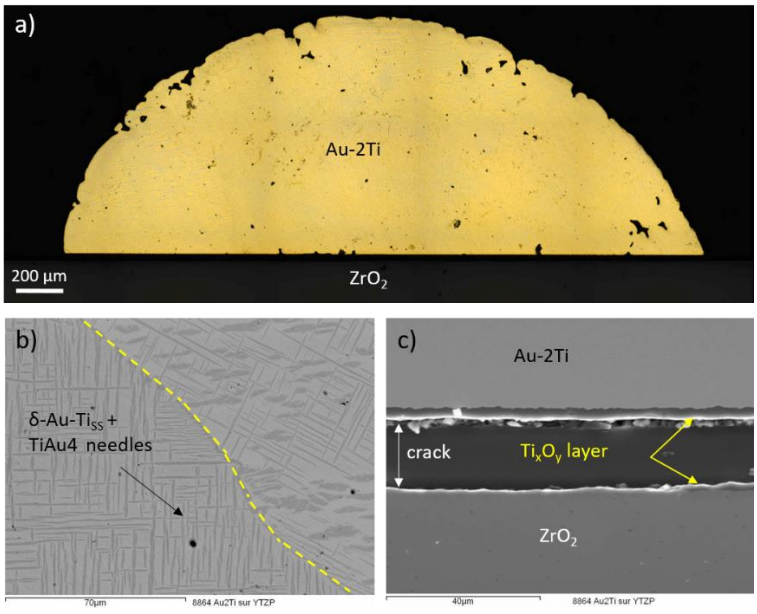

Figure 81: Optical (a) and SEM (b-c) micrographs of Au-2Ti alloy / ZrO_2 sample after wetting experiment performed at 1170°C during 13 min in liquid state on polished ZrO_2 substrate.

d) Wetting of zirconia by Au-3wt%Ti alloy

Afterwards, titanium content in gold was increased up to 3wt%. First, a preliminary experiment was performed by a prepared in situ Au-3Ti wt% alloy, by wrapping a piece of Ti with a gold sheet placed

on the zirconia substrate. This experiment was performed with a high heating rate (10°C/min) until 1190°C, in order to avoid, as much as possible, the dissolution of solid Ti in liquid Au during heating from the melting point of Au (1064°C) to the liquidus of Au-3wt%Ti alloy (about 1120°C). Indeed, as it will be seen below, this dissolution can lead to the transformation of liquid into δ-Au solid solution and thus to a solidification during heating. Figure 82a shows in situ images of Au-3Ti on zirconia sample at different stages of heating. At 1086°C and 1190°C, a part of the massive piece of Ti is detected on the left of the drop, resulting in two different contact angles at the left and the right of the drop. Figure 82b shows the variation of the left and right contact angles (θ_l and θ_r) and temperature as a function of time for the wetting of zirconia by this prepared in situ Au-3Ti wt% alloy. Both contact angles decrease rapidly first, and then slowly to attain the final contact angles θ_l = 57° and θ_r =71°at 1190°C.

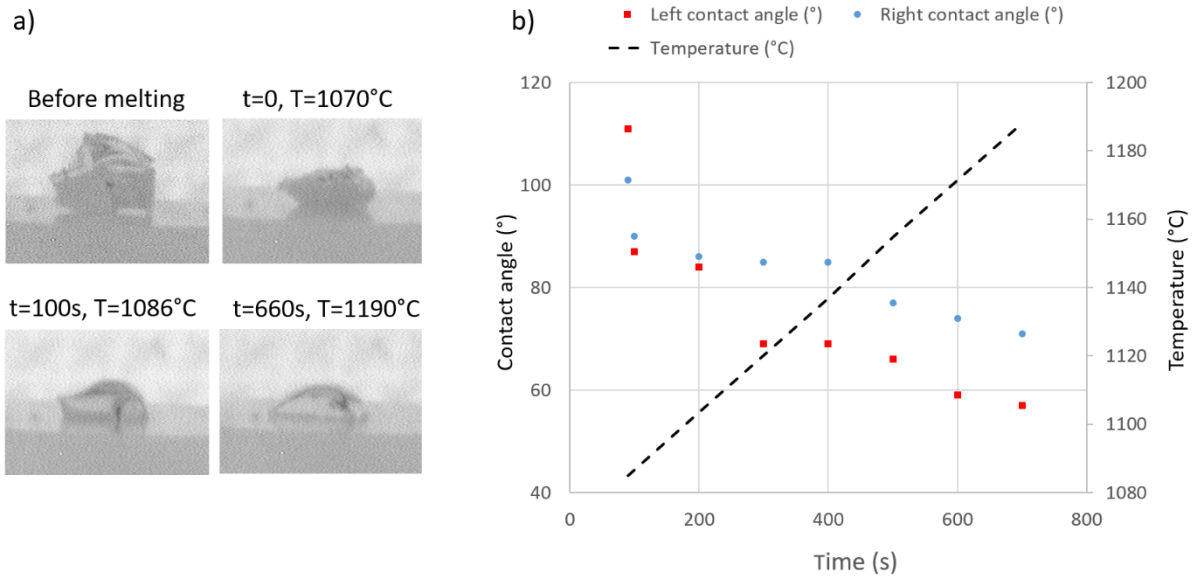

Figure 82: In situ images of Au-3Ti on zirconia sample at different stages of heating (a). Variation of the left (θ_l) and right (θ_r) contact angles and temperature as a function of time.

A second experiment was carried out with an Au-3Ti prepared in situ alloy, with successive isothermal holdings at 1070°C, 1087°C and 1148°C. In situ images of the sample, taken at different temperatures are presented in Figure 83. A first isothermal holding for 20 min is performed at 1070°C in order to determine if an isothermal solidification occurs rapidly at this temperature. Indeed, at 1070°C, the content of Ti in the liquidus and solidus of δ-Au solid solution are about 0.2 and 0.5 wt%Ti respectively (see Figure 71) thus the final state of the Au-3wt%Ti system corresponds to the δ-Au solid solution (the solubility limit of Ti in the δ-Au phase at 1070°C is about 3 wt%Ti). However, even after 20 min at 1070°C, an almost spherical cap of liquid phase is still observed. This means that the bulk piece of Ti is not completely dissolved in the liquid gold (Ti concentration in the liquid alloy is lower than 1 wt%) or

the interdiffusion process in Ti / δ-Au / liquid Au-Ti system is not rapid. The observed contact angle after 20 min at 1070°C is about 60°.

When the temperature is increased up to 1087°C, at the beginning the liquid alloy is enriched with Ti (by Ti dissolution) and in less than 4 min at 1087°C we observe the solidification of the droplet. This observation is in agreement with the Au-Ti phase diagram, which shows that at 1087°C, the solubility limit of Ti in Au-Ti liquid solution is less than 3 wt%. At 1087°C, the content of Ti in the liquidus and solidus of δ-Au solid solution are about 1 and 1.4 wt%Ti respectively and the solubility limit of Ti in δ-Au phase is about 3.2 wt% Ti. This means that an increase in temperature by only 17°C leads to a significant increase of the interdiffusion process in Ti-Au system. This observation is in agreement with the very high activation energy of interdiffusion in Ti-Au system (Q > 450 kJ/mol) reported in the literature [29].

Note that this behavior was not observed when heating the Au-3wt%Ti alloy up to 1190°C with a high heating rate (10°C/min) because the time of the Ti dissolution and interdiffusion process during heating, from the melting point of Au (1064°C) to the liquidus point of Au-3Ti (~ 1120°), was less than 6 min and thus not sufficient to lead to a significant solidification of the alloy by interdiffusion. Afterwards, when the temperature increases once again up to 1148°C, the formation of a liquid Au-Ti droplet is observed few minutes later, the whole Ti piece is dissolved in Au and a steady contact angle $\theta_f = 44°$ is attained. This observation is in good agreement with the binary Au-Ti phase diagram showing that the solubility limit of Ti in liquid Au at 1148°C (~ 3.6 wt%) is higher than the Ti content in the Au-Ti alloy (3 wt%).

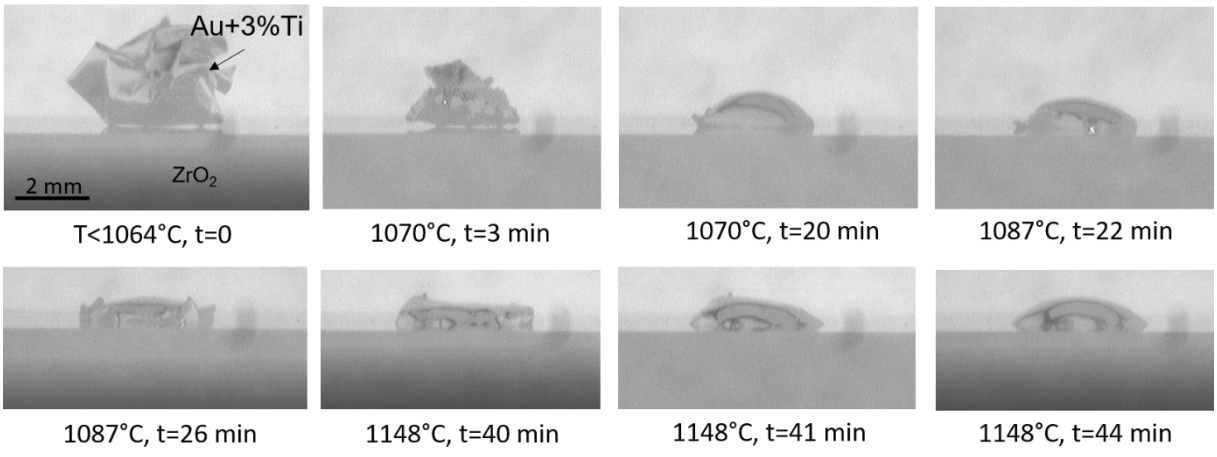

Figure 83: Selected images of Au-3Ti prepared in situ alloy / zirconia sample taken during successive isothermal holdings at 1070°C, 1089°C and 1148°C.

These results show that wetting of zirconia by liquid gold is significantly improved when some Ti is added and the contact angle of Au-Ti alloys on zirconia decreases when the Ti content in the alloy increases. This observation is in good agreement with experimental results of Kristalis et al.[30] who studied the wetting of alumina by Ni-Pd-Ti alloys and reported that the contact angle decreases from about 100° to 50° when the Ti content increases from 2 to 25 at%.

An optical image of the cross-section of the Au-3wt%Ti alloy on zirconia substrate after about 50 min of contact in liquid state, in the temperature range 1064-1148°C, is given in Figure 84a. Figure 84b clearly shows the formation of a reaction product at the Au-Ti alloy / zirconia interface. The interfacial layer has a homogeneous thickness of about 1-3 µm and analysis of this layer shows that it consists of Ti_xO_y phase. Figure 84c gives a SEM image of the bulk microstructure of the solidified droplet. It consists of fine $TiAu_4$ needles inside a δ-Au solid solution matrix which is consistent with the binary Ti-Au phase diagram.

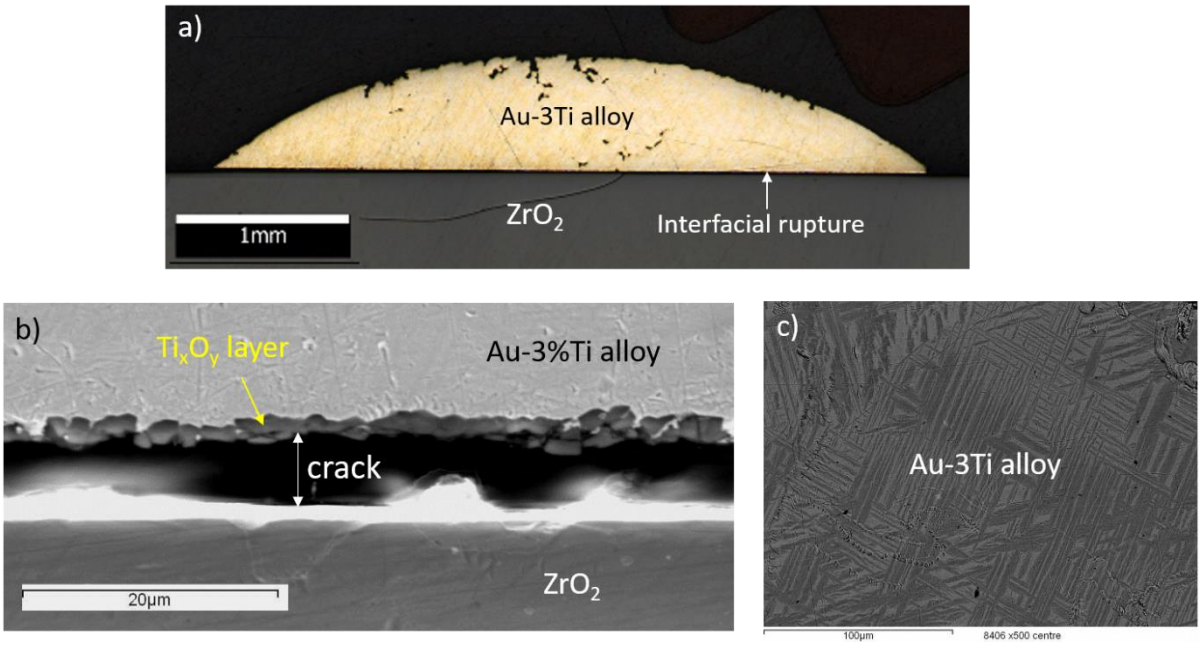

Figure 84: Optical (a) and SEM (b, c) images of a cross-section of the Au-3wt%Ti alloy on zirconia substrate after about 50 min of contact in liquid state, in the temperature range 1064-1148°C.

e) Wetting of zirconia by Au-4wt%Ti alloy

Finally, wetting of zirconia substrate by Au-4Ti (wt%) alloy was investigated with a pre-elaborated alloy.

Spreading kinetics was studied at 1170°C corresponding roughly to the liquidus temperature of Au-4Ti alloy. In order to limit spreading of the liquid alloy before reaching the isothermal holding temperature,

the sample was heated at the maximal heating rate allowed by the furnace (20°C/min). The goal is to begin the isothermal spreading kinetics from the highest possible contact angle.

Figure 85a gives some images of Au-4Ti alloy / zirconia system at room temperature and at 1170°C. This figure shows that a change in the form of the alloy occurs when the temperature attains 1170°C and, after 30s at 1170°C it takes the form of a spherical cap. The variation of contact angle and droplet base radius of Au-4Ti alloy on zirconia, during the isothermal holding at 1170°C, is presented in Figure 85b. We can see that the contact angle decreases first rapidly during about one minute, and then the spreading rate of the drop decreases significantly. The final contact angle θ_f ~ 47° is reached after 6 min. Spreading kinetics follows a typical reactive spreading curve: no jump of the triple line is observed. Moreover, six other experiments of zirconia wetting by Au-4Ti alloy were performed at 1170°C, and all the final contact angles are similar (θ_f ~ 47°). The fact that the final contact angle for 7 experiments is practically the same, strongly suggests that the equilibrium contact angle of Au-4Ti alloy on zirconia substrate at 1170°C is about 47° (no pinning phenomenon occurs during reactive spreading of Au-4wt%Ti alloy on zirconia).

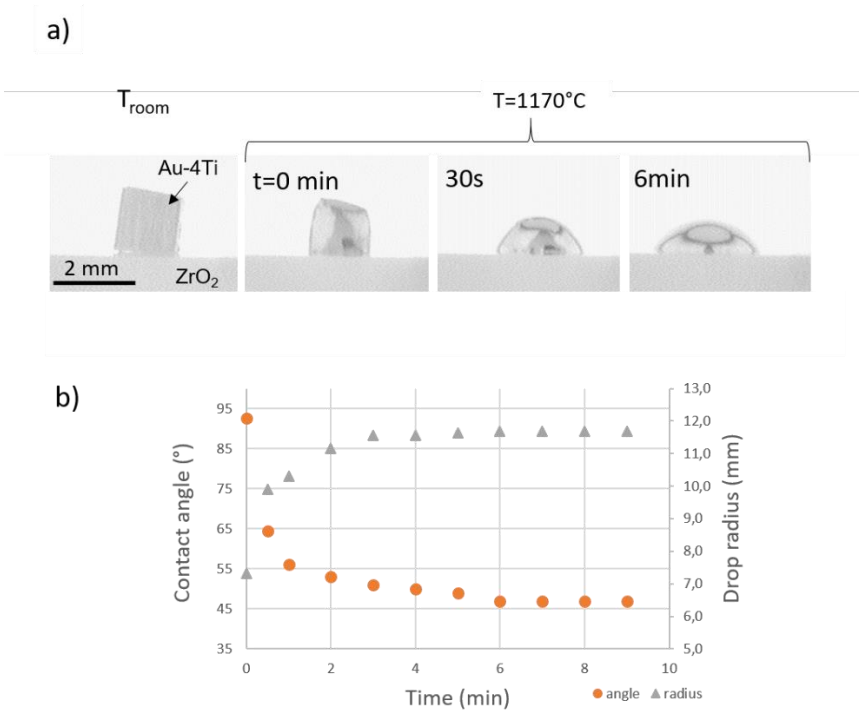

Figure 85: Selected images of the Au-4Ti alloy / zirconia system at room temperature and at 1170°C (a). Variation with time of contact angle and droplet base radius of Au-4Ti alloy on zirconia during the isothermal holding at 1170°C (b).

At the end of this thermal cycle, the obtained droplet has a circular shape, and the Au-Ti alloy is detached from the zirconia substrate. The droplet is placed on the zirconia substrate and after *embedding* the sample in an *epoxy resin*, it is cut in order to characterize a cross section of the sample.

Figure 86a shows a relatively homogeneous bulk microstructure of the Au-4Ti solidified droplet. The microstructure of this alloy is drastically different from that of Au-1Ti, Au-2Ti and Au-3Ti alloys (Figure 78, Figure 81 andFigure 84). Indeed, Figure 86a and b show the formation of large $TiAu_4$ primary dendrites in the solidified Au-4Ti droplet which was not the case for the other three alloys. According to the Au-rich side of the Ti-Au phase diagram represented in Figure 86d, the solidification path of Au-4wt%Ti alloy can be described as below:

- Precipitation of primary dendrites of $TiAu_4$ compound when the temperature decreases from 1172°C (point A) to 1123°C (point B).

  At 1123°C ± 3°C the peritectic transformation: $liq_P + TiAu_4 \rightarrow \delta\text{-}Au_C$ occurs until the total consumption of the liquid phase. The contents of Ti at points P and C are close to 3.5 wt% (12at%) and 4 wt% (14 at%) respectively.
- When the temperature decreases between 1123°C and room temperature, the solubility limit of Ti in the δ-Au solid solution decreases from about 3.5 to 0.3 wt%. Consequently, during cooling, the δ-Au solid solution becomes depleted in Ti and, as a result, the secondary $TiAu_4$ phase precipitates, forming $TiAu_4$ needles in the matrix (δ-Au phase) as it is shown by the SEM micrograph in Figure 86b.

SEM image of the alloy / substrate interface (Figure 86c) shows the formation of a homogeneous reaction layer of about 4 µm thick. In this image, it is clearly seen that the failure occurs at the Ti_xO_y reaction layer / zirconia interface.

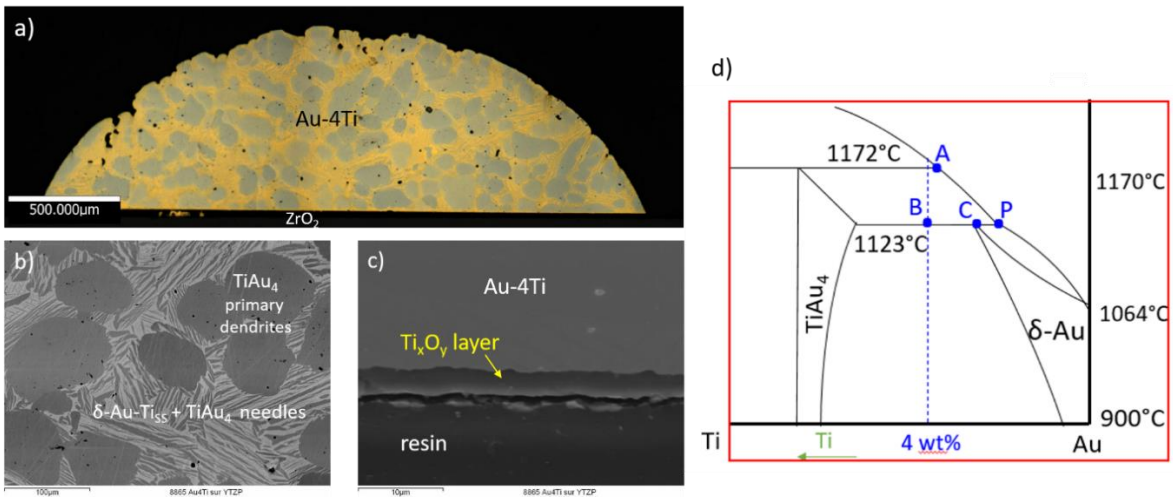

Figure 86: Optical (a) and SEM micrographs (b and c) of a cross section of the Au-4Ti alloy / zirconia sample after an isothermal holding at 1170°C for 10 min. Schematic representation of the Au-rich region of the Ti-Au phase diagram (d).

f) Conclusion

Pure liquid gold does not wet zirconia, the contact angle being much higher than 90°.

Wetting study of zirconia by the Au-Ti alloys was investigated, with titanium content ranging from 0.6 to 4 wt%. The addition of a few percent of Ti in Au allows the wetting of zirconia, thanks to the formation of the wettable Ti_xO_y reaction layer at Au / ZrO_2 interface. Contact angle (θ) of Au-Ti alloys on zirconia decreases when the Ti content increases, until attaining θ ~ 47° at 1150°C for 4 wt%Ti.

Pinning of the triple line of liquid Au-Ti alloys on zirconia is observed for Ti content less than or equal to 3 wt%, even in the very high contact angle range (160° - 170°), despite the fact that Au-Ti alloy / zirconia is a reactive system.

At the zirconia / Au-Ti alloy interface, a thin (0.5 µm – 4 µm), homogeneous and continuous Ti_xO_y reaction layer is formed. The thickness of this layer increases when the Ti content in the alloy increases.

2.3.2.2. Interfacial reactivity between zirconia and Au-xTi alloys (0.6 < x < 4 wt%): mechanisms of formation and growth of the reaction product layer

Wetting study of zirconia by the Au-xTi alloys (0.6 < x < 4 wt%) shows that a homogeneous reaction layer is formed at the alloy / zirconia interface, regardless of the Ti content in the alloy.

Recall that morphology and thickness of the reaction layer, formed at the interfaces between the substrates to be assembled and the brazing alloy, have a primary role on mechanical behavior of the brazed joint. Therefore, it is very important to carefully analyze the formation of interfacial product, as well as to study its evolution in time. For this purpose, we investigated the mechanisms of formation and growth of the Ti_xO_y reactive layer, the growth kinetics of this layer at a fixed temperature for a given Ti content in Au-Ti alloy, as well as the influence of Ti content in the alloy on the growth kinetics.

a) Determination of Ti_xO_y growth interface

Firstly, microscopic analysis of the Ti_xO_y reaction product layer was carried out in order to propose a growth mechanism of this layer. Figure 87 gives an example of observation of the zone close to the triple line, in the case of Au-1Ti droplet in contact with zirconia for 14 min in the temperature range 1064-1170°C. Notice that the reaction layer at the triple line goes beyond the droplet about 18 µm. This is certainly due to the shrinkage of the droplet during its solidification and not to the lateral growth of the wettable Ti_xO_y reaction layer that takes place in the front of the triple but at micrometric scale

(this lateral growth is a clear marker of reactive wetting presented in chapter 1). As it has been seen above, this lateral growth of the reaction layer leads to the spreading of Au-Ti alloy over zirconia substrate. In Figure 87, it is clearly seen that the Ti_xO_y reaction layer is completely situated above the zirconia substrate surface, identified on this micrograph with a yellow dotted line. This experimental fact clearly indicates that the growth of the Ti_xO_y reaction product takes place at the Ti_xO_y layer / alloy interface (as it was the case for the Ag-4Ti / ZrO_2 system – section 2.3.1.a). This growth occurs by reaction between Ti dissolved in the liquid Au-Ti alloy and oxygen of ZrO_2 substrate arriving at the growth interface by diffusion through the reaction layer:

$$yO_d + x(Ti)_{Au} \rightarrow Ti_xO_y \qquad (5)$$

with O_d referring to oxygen diffusing in the reaction layer and $(Ti)_{Au}$ referring to the dissolved titanium in the liquid Au-Ti alloy.

This reactive mechanism is in agreement with the fact that only trace of Zr was detected in the droplet by EDX analysis, i.e. the growth of Ti_xO_y mainly occurs by reaction (5) and not by reaction $ZrO_2 + (Ti)_{Au} \rightarrow Ti_xO_y + (Zr)_{Au}$, where $(Zr)_{Au}$ denotes Zr atoms dissolved in liquid Au.

This means that an oxygen diffusion profile exists through the zirconia substrate, i.e., the stoichiometry of zirconia varies from ZrO_2 in the bulk zirconia (far from the interface) to ZrO_{2-x} (at zirconia substrate / reaction layer interface).

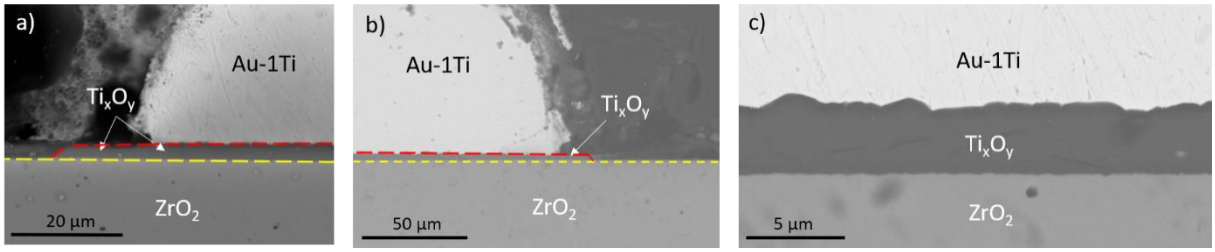

Figure 87: SEM micrographs of a cross section of Au-1Ti / ZrO_2 sample showing the relative position of the Ti_xO_y reaction layer in the region close to the triple line after 14 min of contact time between the liquid alloy and zirconia in the temperature range 1064-1170°C.

b) Influence of reaction time on the growth kinetics of Ti_xO_y layer

In order to determine the growth kinetics of the Ti_xO_y reaction layer at Au-Ti alloy / ZrO_2 interface, we have performed isothermal holdings at 1170°C for 0, 1, 10 and 37 min with the pre-elaborated Au-2Ti alloy which was selected for its intermediate Ti content. For these experiments, the maximal permitted heating rate (20°C/min) was used in order to decrease as much as possible the interaction time t_1

between the melting point of the alloy (~ 1130°C) and 1170°C (t_1 = 2 min). The duration time during cooling from 1170° to 1130°C is $t_2 \approx 1$ min. Therefore the interaction time in liquid state during heating and cooling steps is $t_i = t_1 + t_2 \approx 3$ min and thus the corresponding durations of Au-Ti alloy in the liquid state during isothermal holdings for 0, 1, 10 and 37 min are 3, 4, 13 and 40 minutes respectively. Figure 88 gives SEM micrographs of the Au-2Ti / zirconia interface after these different isothermal holdings at 1170°C. In all cases, the interfacial layer is relatively homogeneous in thickness. For the two short isothermal holdings (0 and 1 min), the droplet alloy is integral with the zirconia substrate, whereas for the long isothermal holdings (10 and 37 min) the samples are fractured and the fracture is located at the reactive layer / zirconia interface.

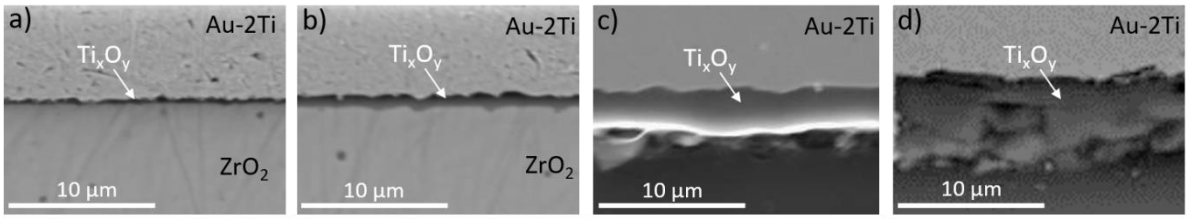

Figure 88: SEM micrographs of the Au-2Ti / zirconia interfaces after isothermal holdings at 1170°C for 0 (a), 1 (b), 10 (c) and 37 min (d) respectively.

Table 16 gives the average thicknesses of reaction product layer obtained after different holding times at 1170°C. The average layer thickness increases from 0.3 µm to 6.5 µm when the holding time increases from 0 to 37 min. (Note that from a mechanical point of view, a short time in liquid state is recommended in order to obtain a thin submicronic Ti_xO_y layer).

Holding time at 1170°C (min)	0	1	10	37
Ti_xO_y thickness e(µm)	0.3 ± 0.1	1 ± 0.3	3 ± 0.3	6.5± 0.5

Table 16: Thicknesses of the reaction layer formed at the Au-2Ti/zirconia interface during isothermal holdings at 1170°C.

A simple mass balance shows that the formation of a layer of TiO oxide (density ρ = 5 g/cm^3) or TiO_2 oxide (ρ = 4.2 g/cm^3)[31] 1 µm thick needs a very small quantity of Ti to be consumed (about 0.02 wt%Ti). Therefore, the maximal consumption of Ti content corresponding to the formation of a Ti_xO_y reaction layer 6.5 µm thick is only 0.13 wt%Ti, much lower than the initial content of Ti in Au-Ti alloy (2 wt%Ti). It can thus be concluded that during the reaction between Au-2Ti alloy and zirconia substrate, for reactions time lower than 40 min, the Ti content in the alloy remains almost constant. EDX analysis of the droplet supports these calculations since the titanium content detected by semi-quantitative analysis is almost equal to Ti content initially contained in the alloys.

In Figure 89, the average thickness of the reaction layer is plotted versus the square root of holding time at 1170°C. This figure shows that the Ti_xO_y thickness (e) varies linearly with the square root of the holding time (i.e., the growth kinetics of Ti_xO_y phase follows a parabolic law). This result suggests that the growth kinetics of Ti_xO_y phase layer is limited by diffusion of oxygen and thus the thermodynamic equilibrium is attained at Ti_xO_y phase / Au-Ti alloy interface (i.e. the equilibrium of reaction (5) at this interface is attained), as well as at ZrO_2 / Ti_xO_y interface.

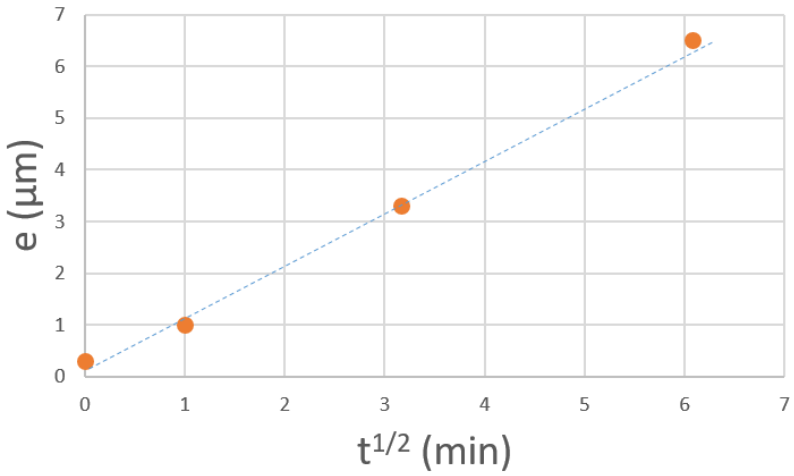

Figure 89: Thickness (e) of Ti_xO_y phase layer, formed at Au-2Ti / ZrO_2 interface, as a function of the square root of holding time at 1170°C. The straight line represent the linear fit of the data for $e = k.t^{1/2}$.

c) Influence of Ti content in Au-Ti alloy on the growth kinetics of Ti_xO_y layer

The second series of experiment is focused on the effect of the Ti content in Au-Ti alloy on the growth kinetics of Ti_xO_y layer at the same temperature and for the same reaction time. The titanium contents in the Au-Ti alloys are 1, 2 and 4 wt%. For this experiment, three pieces of Au-Ti alloys (Au-1Ti, Au-2Ti and Au-4Ti) on zirconia substrates are simultaneously placed in the furnace to ensure that they follow the same thermal cycling. Temperature is increased very quickly (20°C/min) up to 1170°C, then maintained at 1170°C for 10 min and finally rapidly decreased at room temperature.

Figure 90a shows top views of samples after heat treatment. We notice that the diameter of dark zirconia around each droplet increases with Ti content in the Au-Ti alloy. The dark zone corresponds to the area affected by oxygen diffusion from bulk zirconia to react with Ti at the substrate / alloy interface.

Figure 90b gives SEM micrographs of cross sections of the three samples showing the Ti_xO_y reaction layers formed at the Au-xTi alloys / zirconia interface. Ti_xO_y thickness slightly increases with Ti content,

from 3.1 to 3.8 µm. Therefore, a low content of titanium from the Au-Ti alloy is consumed to form the Ti_xO_y reaction product layer.

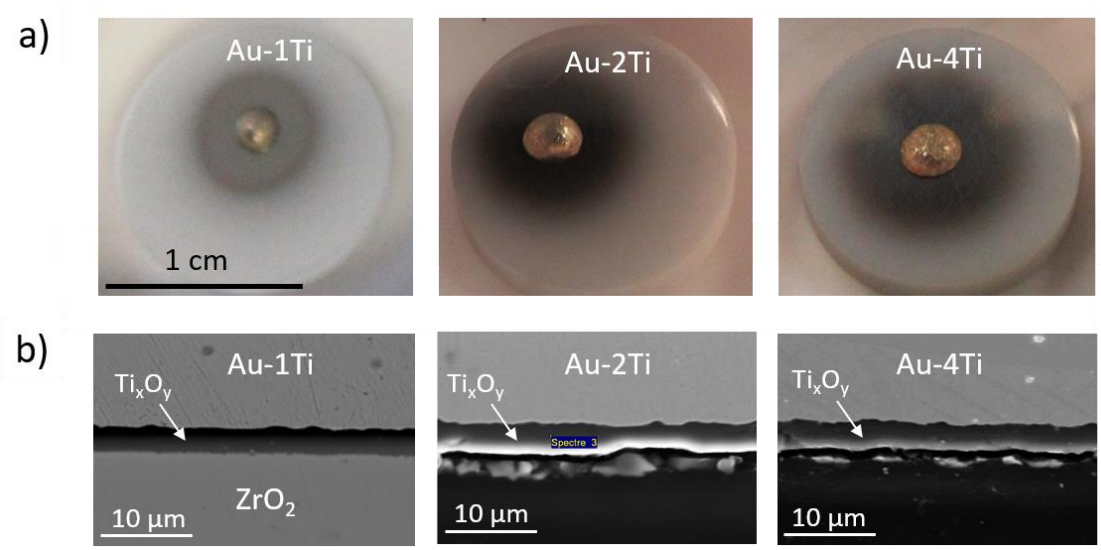

Figure 90: Top views of three Au-xTi alloys / zirconia samples (a) and SEM micrographs of cross sections of these samples after an isothermal holding at 1170°C for 10 min.

The fact that the growth kinetics of the Ti_xO_y reaction layer does not increase significantly when the Ti content in the alloy increases by a factor 4 is analyzed below.

Figure 91 gives a schematic representation of the Ti concentration (in blue line) and oxygen concentration (in red line) in the zirconia / Au-Ti alloy system during the growth of Ti_xO_y layer. Recall that the growth of this layer occurs at Ti_xO_y / Au-Ti alloy interface (noted interface 2), according to the reaction (5): $yO_d + x(Ti)_{Au} \rightarrow Ti_xO_y$.

First, we describe the oxygen diffusion profile from bulk zirconia, through the reaction product layer until the Au-Ti alloy. In ceramic substrate, oxygen concentration (C_O) is considered constant far from the interface 1 ($C_O = C_O^0$). Approaching the substrate / alloy interface, zirconia becomes depleted in oxygen in the "zone affected by oxygen diffusion", which corresponds to the dark zone shown in Figure 90a. The concentration of oxygen at zirconia / Ti_xO_y layer (noted interface 1), $C_O = C_1$ is lower than C_O^0.The oxygen diffuses through Ti_xO_y layer to react with Ti at interface 2. In the reaction product layer, oxygen concentration slightly decreases from interface 1 to interface 2 from C_2 to C_3 (C_3 is equal to the oxygen concentration at the thermodynamic equilibrium of reaction (5), noted C_O^*; the corresponding Ti concentration at this interface is noted C_{Ti}^*). Given the fact that the solubility of oxygen in liquid Au-Ti alloys is very low[24], a significant oxygen concentration jump is observed at the Ti_xO_y / Au-Ti alloy interface (interface 2) from C_3 $(= C_O^*)$ to C_4 $(= C_O^* \approx 0)$. Moreover, as the diffusion

coefficients of oxygen and titanium in the liquid Au-Ti alloys (D_{liq} ~ 5.10^{-9} m^2/s [32]) are several orders of magnitude higher than the diffusion coefficient of oxygen through the solid phases (here Ti_xO_y phase), the value of C_{Ti}^* is very close to the concentration of Ti in the bulk droplet (i.e. $C_{Ti}^* \approx C_{Ti}^0$).

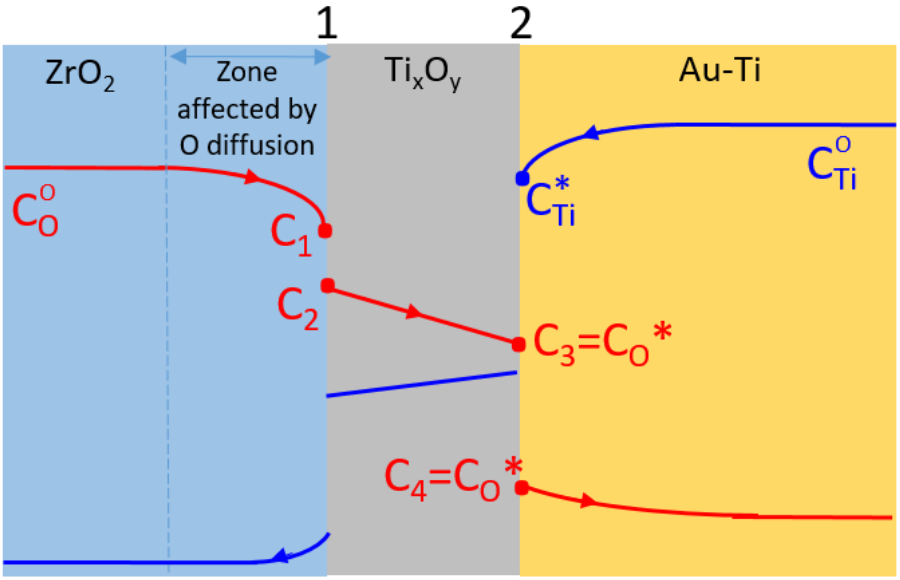

Figure 91: Schematic representation of the Ti concentration (in blue line) and oxygen concentration (in red line) in the zirconia / Au-Ti alloy system during the growth of Ti_xO_y reaction layer.

As we saw in the last paragraph, a very low content of Ti from the Au-Ti alloy is consumed to form the Ti_xO_y reaction product layer. In other words, the Ti concentration in the bulk Au-Ti alloy (C_{Ti}^0) remains substantially constant during the growth process of the reactive layer and equal to the initial Ti concentration in the droplet ($C_{Ti}^{bulk} \approx C_{Ti}^0$). Ti dissolved in the Au-Ti alloy is consumed at interface 2, by reaction with O to form the Ti_xO_y layer. A gradient of Ti concentration is observed between interfaces 2 and 1. In zirconia substrate, there is a slight Ti diffusion (mainly at the grain boundary) so Ti concentration is very low in ZrO_2.

Finally, the condition of equilibrium of reaction (5) at a given temperature can be expressed by the following relation:

$$(a_O^*)^y . (a_{Ti}^*)^x = \boldsymbol{exp}\left(\frac{\Delta_f \boldsymbol{G}_{\mathrm{ox}}^0}{\boldsymbol{RT}}\right) \qquad (6)$$

$\Delta_f G_{\mathrm{ox}}^0$ is the standard Gibbs free energy of formation of Ti_xO_y oxide from pure oxygen gas at pressure equal to 1 bar and pure liquid Ti at temperature T. a_O^* and a_{Ti}^* are the thermodynamic activities of oxygen and titanium in the liquid alloy at interface 2.

By assuming that the Au-based ternary Au-Ti-O alloy is a diluted liquid solution in titanium and oxygen, the activities of O and Ti can be expressed as a function of their molar fractions (x_i) by the following expressions:

$$a_O^* = \gamma_O^\infty x_O^* \quad \text{and } a_{Ti}^* = \gamma_{Ti}^\infty x_{Ti}^* \approx \gamma_{Ti}^\infty x_{Ti}^0 \qquad (7)$$

γ_O^∞ and γ_{Ti}^∞ are the activity coefficients of O and Ti at infinite dilution in liquid Au. x_O^* and x_{Ti}^* are the molar fractions O and Ti in the liquid alloy at interface 2, while x_{Ti}^0 is the initial molar fraction of Ti in the liquid Au-Ti alloy. Note that x_{Ti}^0 varies from about 0.02 to 0.14 when the initial weight percent of Ti in the Au-Ti alloy varies from 0.6 to 4 wt%Ti.

From equations (6) and (7), we can deduce the activity (a_O^*) and the molar fraction (x_O^*) of oxygen in the liquid alloy at interface 2 as a function of thermodynamic quantities and initial content of Ti in Au-Ti alloy.

At this stage, it is important to point out that the growth kinetics of Ti_xO_y oxide layer is limited by the diffusion of oxygen and the driving force of diffusion process through the Ti_xO_y layer is the difference between the chemical potential of oxygen (μ_O) at interface 1 - zirconia / Ti_xO_y ($\mu_{O,1}$) and that at interface 2 - Ti_xO_y / alloy ($\mu_{O,2}$). This difference is given by the following relation:

$$\Delta\mu_O = \mu_{O,1} - \mu_{O,2} = \mathrm{RTln}\left(\frac{a_{O,1}}{a_{O,2}}\right) \qquad (8)$$

$a_{O,1}$ is the activity of oxygen in Ti_xO_y (*and in zirconia*) at interface 1 (zirconia / Ti_xO_y) and $a_{O,2}$ is the activity of oxygen in Ti_xO_y (*and in the alloy*) at interface 2 (Ti_xO_y / alloy). The activity $a_{O,2} = a_O^* = \gamma_O^\infty x_O^*$ depends only on the initial content of Ti in the liquid alloy and thus the three quantities $\mu_{O,2}$, a_O^* and x_O^* decrease when the Ti content in the alloy increases.

The fact that the growth kinetics of Ti_xO_y oxide layer does not increase significantly with the Ti content in the alloy means that the difference $\Delta\mu_O = \mu_{O,1} - \mu_{O,2}$ increases only slightly with Ti content, which suggests that the chemical potential (activity) of oxygen at interface 1 is much higher than that at interface 2.

2.3.3. Conclusion

Zirconia wetting by the Ag-Ti, Au-Sn-Ti and Au-Ti alloys was investigated. A good wetting of zirconia by these alloys was obtained, thanks to the formation of a wettable Ti_xO_y reaction product layer at the zirconia / alloy interface. Thus, spreading of M-Ti alloys (M = Ag, Au-Sn, Au) on zirconia

corresponds to a reactive spreading. For low Ti content in the alloys (Ti < 3 wt%), pinning of the triple line is observed, avoiding continuous spreading of the alloy on ceramic substrate.

In the case of Au-Sn-Ti and Ag-Ti alloys, a thick reaction product layer, up to 50 µm, is formed at the zirconia / alloy interface. Moreover, preliminary brazing experiments show that Au-Sn and Ag matrix are not appropriate to zirconia / titanium brazing.

In the case of Au-Ti alloys, homogeneous, continuous and thin reaction layer of about 0.3 – 6.5 µm is formed at the interface. The study of reaction layer formation and its growth kinetics was performed. The product layer grows at the Ti_xO_y layer / alloy interface by reaction between oxygen diffusion from ZrO_2 substrate through the reaction layer and Ti dissolved in the Au-Ti alloy. The limiting step of the layer growth is the oxygen diffusion process.

Based on these wetting results and the interfacial reactivity analysis, we determined the more interesting alloys for the rest of the study, that is the wetting and reactivity with the titanium substrate (next section), and brazing of zirconia to titanium (next chapter). The more promising alloys for zirconia-to-titanium brazing are the Au-Ti alloys, with a low titanium content (lower than 4 wt%). Indeed, in addition to a good wetting of zirconia by Au-Ti alloys (as by other M-Ti alloys), the formation of a thin and homogeneous reaction layer at the zirconia / Au-Ti alloy interface is very promising for zirconia / titanium assembly in order to obtain satisfying mechanical properties of the joint.

3. Wetting and reactivity of Ti with pure Au

After studying wetting and interfacial reactivity between zirconia substrate and different candidate liquid braze alloys, it is necessary to study wetting and reactivity between the second substrate (Ti) and the selected Au-Ti alloys, with the aim of brazing zirconia to titanium with pure gold.

This section deals with wetting and reactivity of titanium metallic substrate by liquid gold in the temperature range 1066-1125°C. Given the solubility limit of titanium in liquid gold at these temperatures, ranging from 0.2 to 3.2 wt%, we use pure gold as filler metal and not Au-Ti alloys.

3.1. Wetting study of Ti by liquid Au

Titanium wetting by liquid gold was studied by the dispensed drop method under high vacuum (10^{-6} mbar) in the metallic furnace of the SIMAP laboratory. Measurement of the contact angle θ is mainly performed with a CCD camera with a frequency ranging from 25 to 100 frames/s. For a specific

experiment, a rapid camera (1500 frames/s) was used to capture, during the 50 first milliseconds, the very beginning stage of gold spreading on titanium substrate.

First, we describe titanium wetting by liquid gold at the intermediate temperature 1100°C. Then, spreading kinetics at different temperatures 1077, 1100, and 1125°C are also presented. Finally, the impact of titanium surface state on spreading kinetics at a given temperature is discussed.

3.1.1. Wetting of Ti by liquid Au at 1100°C

The Ti substrate chosen for this experiment is the same as the substrate chosen for brazing experiments (raw Ti – see Chapter 2). The initial stage of wetting of Ti by pure liquid Au at 1100°C is recorded with a rapid camera (1500 frames/s). Spreading kinetics of liquid gold on titanium substrate is plotted in Figure 92a and some corresponding in situ images (see points 1 to 10) are presented in Figure 92b. The very rapid spreading of the Au droplet occurs during the first 10 ms of contact: the contact angle decreases from about 120° to 42° in 10 ms. During this short stage, oscillations of the dispensed drop on Ti substrate are observed. From 10 ms, the contact angle is stabilized at its equilibrium value $\theta \sim 42°$ which corresponds to the initial contact angle of liquid gold on titanium substrate at 1100°C.

This first stage of wetting of liquid gold on titanium, down to a contact angle of about 42° in 10 ms can be attributed to the non-reactive wetting of liquid gold on titanium substrate. Indeed, it is well known in the literature that the non-reactive wetting of liquid metal on solid surface occurs in some milliseconds of contact[1]. Then, spreading of the liquid droplet can continue, in the case of a reactive system, with a lower spreading kinetics depending on interfacial interactions between liquid metal and solid substrate.

a)

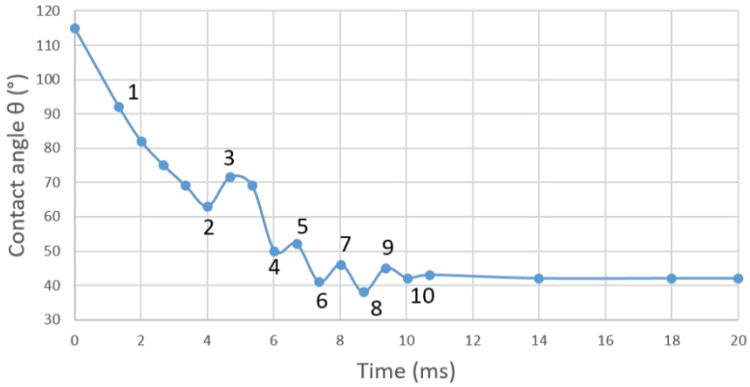

b)

Point	1	2	3	4	5
Time (ms)	1,3	4,0	4,7	6,0	6,7
					
Point	6	7	8	9	10
Time (ms)	7,4	8,0	8,7	9,4	10
				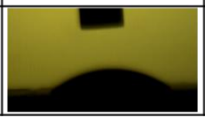	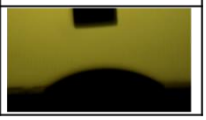

Figure 92: Variation with time of the instantaneous contact angle during spreading of pure liquid Au over Ti substrate at 1100°C (a) and some corresponding in situ images (b).

In order to determine the spreading mechanism occurring in the liquid Au / Ti system, a wetting experiment of gold on titanium substrate at 1100°C was repeated and recorded with a CCD camera (50 frames/s) during 1h10min. Figure 93 gives some selected images of the dispensed droplet. On the first recorded image (20 ms), the contact angle measures θ ~44°. This value is in good agreement with that obtained during the wetting experiment followed by the rapid camera. Afterwards, the contact angle decreases down to 30° in 7s. This contact angle could be attributed to the contact angle on the reaction product in contact with the Au-Ti liquid phase, i.e., the δ-Au solid solution phase. During the isothermal holding the droplet spreads slowly and after 1h10 of contact, gold does not spread on titanium anymore and the contact angle is θ ~ 16°. After 1h at 1100°C, the temperature was increased to 1120°C in about 10min. During this period, a significant spreading of the droplet occurs and thus the contact angle significantly decreases from about 16° to a very low contact angle. This point will be discussed here below.

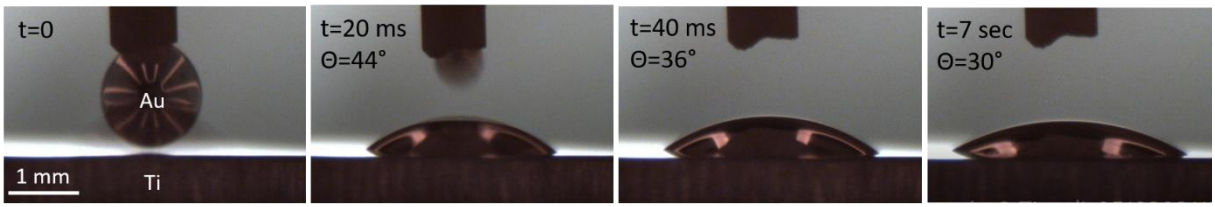

Figure 93: Some selected images during spreading of a pure liquid gold droplet on Ti substrate at 1100°C followed by CCD camera (50 images/s).

3.1.2. Impact of temperature on spreading kinetics

In order to investigate the temperature impact on spreading kinetics followed by the dispensed drop method, wetting of titanium by liquid gold was studied at the three temperatures 1077°C, 1100°C and 1125°C, in the view to understand the reaction mechanisms occurring below and above 1120°C which is close to the peritectic temperature T_P = 1123°C ± 3°C (see Figure 71). Wetting experiments were performed by the dispensed drop method.

Figure 94a-b give the variation with time of the contact angle during spreading for the three droplets. It is important to note that the first measured contact angle after 10ms of spreading at 1125°C (θ = 25°) is significantly lower than the first measured contact angles at 1077°C (θ = 46°) and 1100°C (θ = 39°). Moreover, these figures show that spreading kinetics increases with temperature.

At 1077°C and 1100°C, contact angles decrease first rapidly during the 30 first seconds, then slowly until a final contact angle. Contact angles respectively decrease from 47° to 38° and 39° to 27° in the time range 0.5s-180s. (Another sessile drop experiment shows that contact angle at 1066°C decreases from 54° to 50° between 11s and 180s of contact in liquid state).

Spreading kinetics at 1125°C is actually much higher: contact angle decreases from 25° to 11° between 10ms and 2.5s.

All these spreading kinetics are characteristic of reactive wetting (spreading times much longer than 10 ms). In the liquid Au / solid Ti system, two types of reactivity occur simultaneously:

- Dissolution of titanium substrate into liquid gold. When temperature increases from 1077°C to 1100°C, the solubility limit of titanium in gold increases from ~2 to 5 at%. Thus when temperature increases, the contact angle can evolve also due to the dissolution effect. Note however that the apparent contact angle θ_{app} measured in situ is lower than the equilibrium contact angle θ_{eq} formed at the triple line because of the substrate dissolution.

- Formation of a wettable reaction product at the Ti solid / Au liquid interface. According to the schematic Au-rich corner of the Ti-Au binary phase diagram illustrated in Figure 94c, at temperature interval between 1064°C and 1123°C (peritectic temperature), the reaction product in contact with the Au-Ti liquid phase is the δ-Au solid solution, thus the contact angle would correspond to that of Au on the δ-solid solution. While for the temperature range 1123°C-1172°C, the reaction product in contact with the liquid Au-Ti alloy will be $TiAu_4$ compound, thus the measured contact angle will correspond to the equilibrium contact angle on this compound.

In order to confirm that this drastic difference in spreading kinetic of Au on Ti below and above 1123°C is due to the difference of solid formed at the interface (δ-Au at T_1 below 1123°C± 3°C and $TiAu_4$ at T_2 above 1123°C± 3°C), wetting experiments should be performed on pre-elaborated δ-Au solid solution and $TiAu_4$ compound.

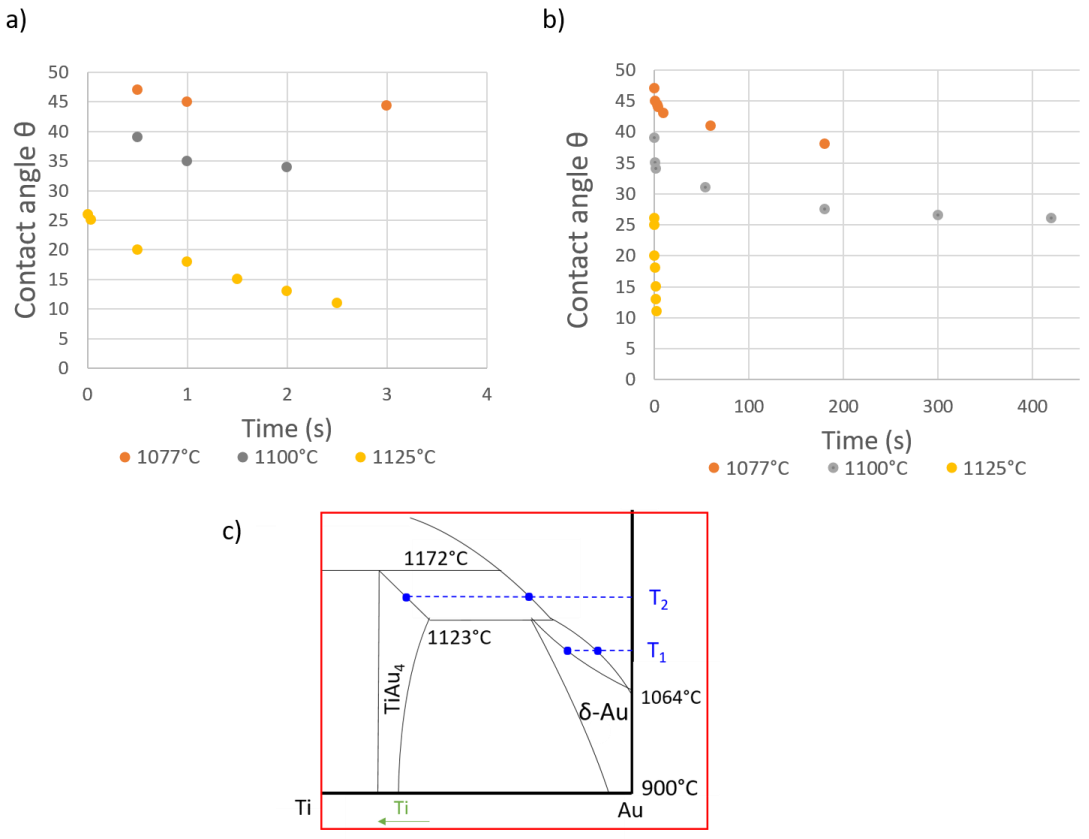

Figure 94: Variation with time of the contact angle during spreading of pure gold on Ti substrate at 1077°C, 1100°C and 1125°C - dispensed drop method (a, b). Schematic of Au-richer corner of binary Ti-Au phase diagram (c).

3.1.3. Impact of surface oxidation and roughness of Ti substrate on spreading kinetics

It is well known that metallic titanium is covered with a native oxide layer. This surface oxide layer, as well as substrate roughness, may have an impact on titanium wetting. Note that XPS analysis shown that native oxidation layer on raw titanium substrate is composed of TiO_2 and Ti_2O_3 oxides, and the total thickness of this layer is 6.4 nm. By polishing the substrate just before vacuuming (about 1h before XPS analysis and wetting experiment), the oxide layer thickness decreases down to 0.8 nm. In order to study the influence of both surface oxidation and roughness of the titanium substrate on the wetting process, liquid Au droplets have been deposited at 1100°C on:

- raw titanium substrate (R_a ~ 800 nm),
- fine polished titanium substrate (R_a ~ 70 nm),
- coarse polished titanium substrate (R_a ~ 600 nm).

Figure 95 gives the variation of contact angle θ with spreading time on the raw, fine and coarse polished titanium substrates.

Figure 95a presents spreading kinetics during 30 min of spreading. The contact angles decrease first rapidly from 43° to 29° during the 10 first seconds, then decrease slowly in the range 10s - 30min. . This figure clearly shows that, whatever the titanium surface state (oxidation state and roughness), spreading kinetics are practically the same.

Figure 95b is a focus on spreading kinetics during the 10 first seconds of spreading. First values of the contact angle on each substrate (35-45°) are relatively close and correspond to the wetting of a metallic surface (Ti)[1]. Thus, the wetting of Ti by pure liquid Au at 1100°C is practically independent of the roughness surface of Ti substrate and of the presence of a nanometric native Ti oxide layer at the surface. It means that the nanometric oxide layer is instantaneously dissolved into liquid gold and thus does not affect the spreading kinetics.

As a conclusion, the surface state of titanium substrate (oxidation and roughness) has no significant impact on the titanium wetting by liquid gold at 1100°C.

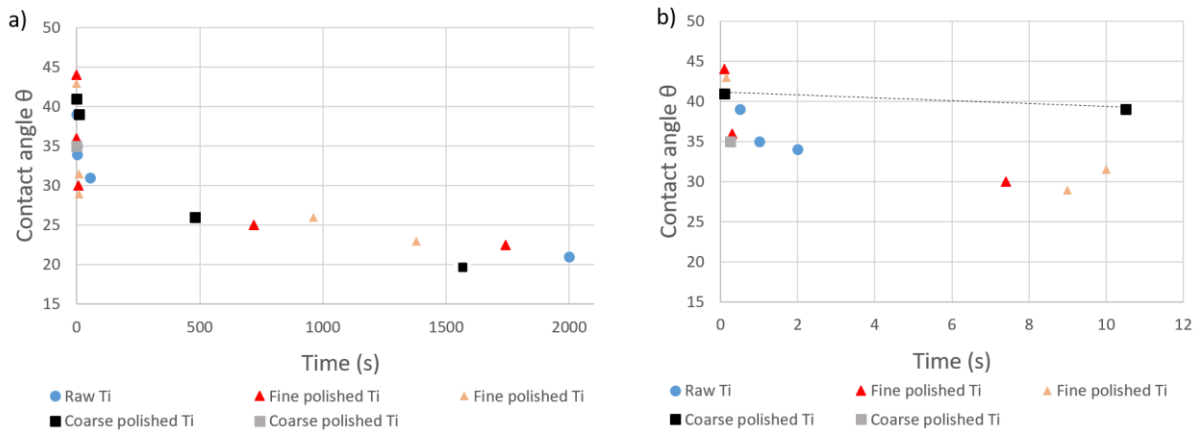

Figure 95: Variation of contact angle θ with spreading time during wetting of pure liquid gold on the raw, fine and coarse polished titanium substrates at 1100°C. The corresponding roughness are R_a ~ 800, 70 and 600 nm respectively.

3.2. Interfacial reactivity between liquid Au and solid Ti

Reactivity between liquid gold and solid titanium was studied in the temperature range 1077-1100°C thanks to deposited Au droplets on the Ti substrate providing isothermal reactions.

In this paragraph, we will first present the growth kinetics of Ti-Au intermetallic compounds at the intermediate temperature 1100°C for the contact durations 15, 60, 120 and 240 min. Based on the obtained experimental results, a schematic evolution of the Au / Ti system will be presented and a growth mechanism of reaction layers will be proposed.

In a second time, we will investigate the reactivity between liquid gold and solid titanium at 1077°C for 3 min of contact, because it is under these conditions that ZrO_2 / Au / Ti brazing will be studied in detail in chapter 4.

3.2.1. Interfacial reactivity between liquid Au and solid Ti at 1100°C for different contact times

a) Introduction

Reactivity between liquid gold and solid titanium, in particular the growth kinetics of the five solid intermediate phases formed at 1100°C (that is the four Ti-Au intermetallic compounds and the δ-Au phase) is investigated after 15, 60, 120 and 240 min of contact in liquid state. Figure 96 gives the Ti-Au binary phase diagram with a schematic zoom of the Au rich-region.

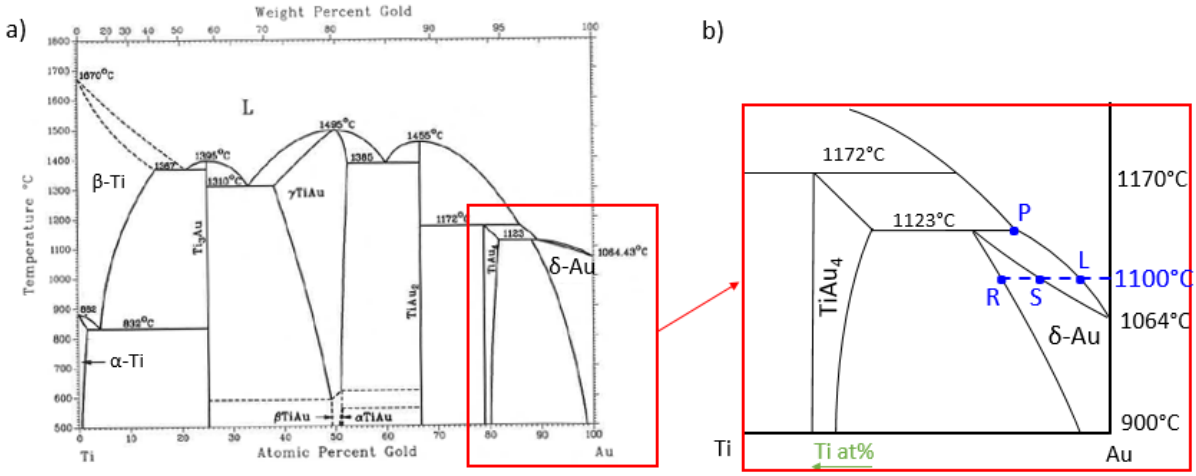

Figure 96: Binary Ti-Au phase diagram[25] with a schematic zoom on the Au-rich region.

At this stage, it is important to point out that the sequence of phase formation in the solid Ti / liquid Au diffusion couple at T = 1100°C can be described as below:

Solid Ti / Ti_3Au / TiAu / $TiAu_2$ / $TiAu_4$ / δ-Au / **Liquid Au-Ti** (9)

Given the fact that the thickness (e) of the first end-member (Ti) of the diffusion couple (e_{Ti} = 2 mm) is much higher than that of the second end-member, Au (e_{Au} < 500 µm), this sequence will remain as it is until the total consumption of the liquid Au-Ti. During this period, as we will see later, the thicknesses of all intermediate phases increase with the isothermal holding time at the expense of Ti and Au end-members.

After the total consumption of the liquid Au-Ti, the δ-Au solid solution becomes the second end-member of the diffusion couple as described below:

Solid Ti / Ti_3Au / TiAu / $TiAu_2$ / $TiAu_4$ / **δ-Au solid solution** (10)

Thus, starting from this moment (noted t* in the following), the thickness of δ-Au phase will decrease with the holding time. Moreover, the driving force of IMCs growth in the new diffusion couple (10) being different from that in the couple (9), a change in the growth rate of IMCs layers will also occur.

b) Experimental results and discussion

The cross-section of the solidified droplet deposited at 1100°C and maintained at this temperature for 15 min is presented in Figure 97. The droplet, which was detached from the substrate after the experiment, was replaced on it.

On this micrograph, it can be seen that the Ti / droplet interface is clearly located under the initial surface of the titanium substrate (which is marked by a yellow dashed line). The distance between this line and the lowest part of the sample varies from 25 µm in the middle of the droplet to 45 µm at the edge of the droplet. This observation confirms that a significant dissolution of Ti in liquid Au occurs during the spreading process, i.e. during the contact between liquid Au and solid Ti. Moreover, triple line observation reveals a non-planar shape of the Ti / droplet interface close to the triple line, of about 250 µm long, which is a characteristic profile of dissolutive wetting[33]. This distance also corresponds to the measured spreading distance of the triple line (change in the drop base radius) occurring between 20 ms and 15 min of contact.

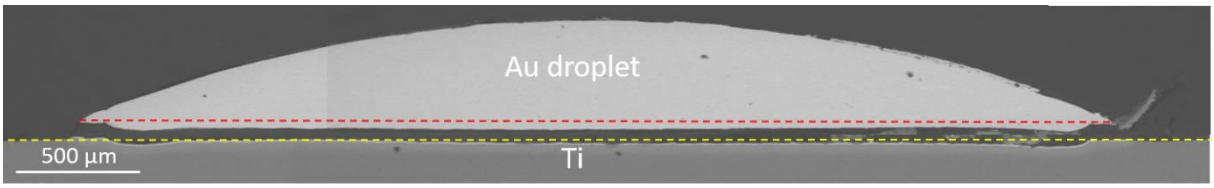

Figure 97: SEM cross-section of a solidified droplet deposed at 1100°C on Ti substrate for 15 min.

Figure 98 gives two enlarged SEM images of the titanium substrate / gold droplet interface of the solidified drop maintained at 1100°C for 15 min presented above.

A significant Au amount is detected in Ti substrate in the region close to Ti / Au interface over about 50 µm wide (Figure 98a), corresponding to gold diffusion in titanium, occurring both in volume and especially at the grain boundaries. Gold diffusion in titanium substrate will be investigated and discussed in detail in the case of Ti / ZrO_2 brazing with pure gold (see chapter 4 paragraph 3.3.2).

At the Ti / droplet interface, the four Ti-Au intermetallic compounds (IMCs) Ti_3Au, TiAu, $TiAu_2$ and $TiAu_4$, given by the Ti-Au binary phase diagram are observed, with a wavy shape and a total thickness of about 14 µm (see Figure 98b).

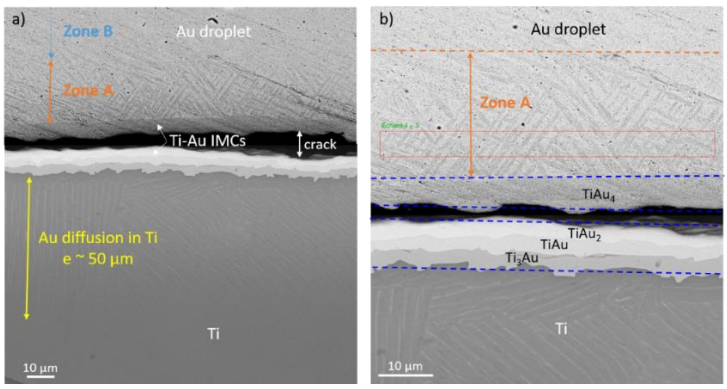

Figure 98: SEM micrographs of the Ti substrate / Au droplet interface after the solidification of the droplet deposited at 1100°C for 15 min.

In the solidified droplet, above $TiAu_4$ layer, a relatively homogeneous layer, 20-30 µm thick, named "Zone A" in Figure 98, containing large needle-shape $TiAu_4$ precipitates (thicker than ~2 µm) is observed. EDX analysis indicates that the average Ti content in this zone is about 12 at%, which is significantly higher than the solubility limit of Ti into liquid Au at 1100°C (~ 5 at% - point L in Figure 96b). Moreover, this average Ti content is very close to the solubility limit of Ti into solid δ-Au at 1100°C (~ 11 at.% - point R in Figure 96b). These results strongly suggest that δ-Au solid solution is formed in zone A during the isothermal holding at 1100°C.

Knowing that at 1100°C, the δ-Au phase is stable in the composition range ~ 6 – 11 at% Ti (between points S and R in Figure 96b) and the solubility limit of Ti in δ-Au phase drastically decreases with temperature from ~ 11 at% at 1100°C to ~ 1 at% Ti at room temperature, the δ-Au solid solution becomes depleted in Ti during cooling. As a result, $TiAu_4$ phase precipitates in the shape of large needles inside the δ-Au matrix.

Over this δ-Au layer of about 25 µm (i.e. over the Zone A), the rest of the droplet (about ~400 µm height in its center), named "Zone B", is composed of a homogeneous microstructure with no visible needle at the SEM scale. After 15 min of contact at 1100°C, this zone B represents an important volume proportion of the droplet. EDX analyses indicate that the average Ti content in this zone is about 6 at%, which is very close to the solubility limit of Ti into liquid Au at 1100°C. Thus, at the end of the isothermal holding at 1100°C, the zone B consists of liquid gold containing some Ti in solution.

SEM images of the cross-sections of the droplets maintained for 60, 120 and 240 min in contact with titanium substrate at 1100°C (see appendix 2), show similar behavior with the sample held for 15 min, i.e., gold diffusion in titanium and formation of the five Ti-Au solid phases (the four IMCs and the δ-Au phase). Note however that the thicknesses of these layers grow with the contact time. Table 17 summarizes the diffusion distances of Au in Ti substrate, the average total thicknesses of Ti-Au IMCs, as well as the thickness of δ-Au phase (corresponding to Zone A) after different isothermal holdings at 1100°C.

Contact time (min)	**15**	**60**	**120**	**240**
e(Au diffusion in Ti) ± 10 (µm)	50	100	150	210
e(Ti-Au IMCs) ± 3 (µm)	14	19	22	30
e(Zone A) ± 10 (µm)	25	50	100	500

Table 17: Diffusion distances of Au in Ti substrate, thicknesses of Ti-Au IMCs and δ-Au layers measured on the cross-sections of the Au droplets deposited on Ti at 1100° for contact times equal to 15, 60, 120 and 240 min.

For the samples with a contact time of 60, 120 and 240 min, the large $TiAu_4$ needles inside the δ-Au matrix (i.e. zone A) are observed above the IMCs layer respectively over about 50, 100 and 500 µm wide. For the three samples, EDX analyses in this region give an average Ti content of ~11 at%. According to the Ti-Au phase diagram, these results clearly suggest the formation of δ-Au phase during the different isothermal holdings at 1100°C. Notice that the droplet maintained at 1100°C for 240 min is entirely composed of large $TiAu_4$ needles inside δ-Au matrix (zone A). This means that, all the Au-Ti liquid (i.e., the second end-member of the diffusion couple (9)) is consumed due to the interdiffusion process and thus to the growth of IMCs and δ-Au phase formed in the Ti / liquid Au couple. Therefore the state of this sample (240 min at 1100°C) corresponds to reaction times higher than t* and thus δ-Au phase (and Ti) is consumed at the expense of IMCs.

In summary, for reaction times $t < t^*$, the thickness of δ-Au layer increases, while for $t > t^*$ it decreases.

Besides, for the three samples with a holding time of 60, 120 and 240 min, EDX analyses at the top of the drops give ~ 9 at%Ti whereas for a holding time of 15 min it gives 6 at%Ti. These results suggest that an isothermal solidification of the whole Au-Ti droplets on titanium substrate occurs for a contact time lower than 1h, i.e. $t^* < 1h$. Note however that much finer chemical analyses of the samples are necessary in order to determine more precisely the value of t*.

The average value of the total thickness (e) of the Ti-Au intermetallic layer versus the square root of holding time at 1100°C is plotted in Figure 99. This figure shows that the growth kinetics of Au-Ti IMCs follows a parabolic law:

$$e = e_0 + k.t^{1/2}$$

with *e* the thickness of the layer, *k* the growth rate constant and *t* the time. e_0 ~ 9 µm corresponds to the value of *e* at t = 0.

This result suggests that the growth of IMCs is limited by the diffusion process through the reaction layer. The growth rate constant k is equal to $2.3.10^{-7}$ $m/s^{0.5}$, i.e. $k^2 = 5.2 .10^{-14}$ m^2/s. The value of k^2 at 1100°C evaluated in this study is higher by more than one order of magnitude than values of k^2 reported in the literature, at lower temperatures, by Taguchi et al.[29] ($2.8.10^{-15}$ m^2/s at 877°C) and Kumar et al.[34] ($5.6.10^{-15}$ m^2/s at 900°C).

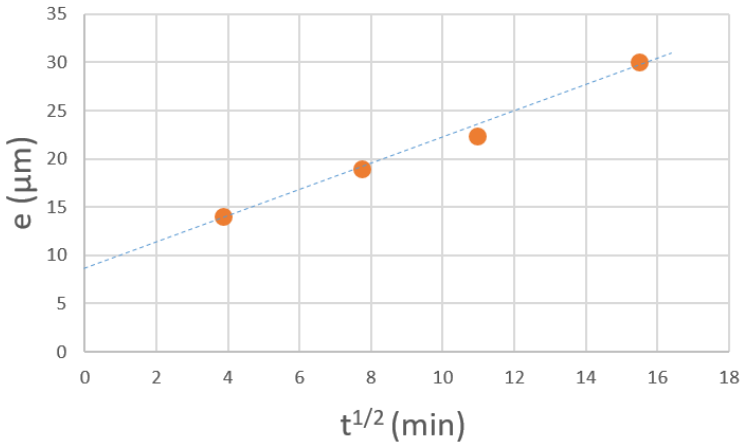

Figure 99: Variation of the total thickness (e) of the Ti-Au IMCs as a function of square root of holding time at 1100°C. The straight lines represent the linear fit of the data for $e = k.t^{1/2}$.

c) Schematic evolution of the Au / Ti system and growth mechanism of reaction layer

In light of the present microstructural study conducted on Au droplet on Ti substrate, a growth mechanism of reaction layer is proposed.

From a thermodynamic point of view, nucleation and growth of the four Ti-Au IMCs (i.e. Ti_3Au, TiAu, $TiAu_2$ and $TiAu_4$) and the δ-Au phase occur at Ti / liquid Au interface. Currently, for most of binary systems, the sequence of formation and growth of intermediate phases at reactive interfaces is not yet known and this is also the case for the binary Au-Ti system. For Au-Ti system, this is a complex process until the formation and growth of five successive and continuous reaction layers as it was experimentally observed in this study. Nevertheless, it is well known from the literature that the growth kinetics of all reaction layers in Au / Ti system follow a parabolic growth law at temperature range 837 - 900°C[29,34]. These results strongly suggest that the rate controlling step of the growth process at higher temperatures (here at 1100°C) is the interdiffusion process through the reactive layers. Thus, the thermodynamic equilibrium is attained at all reactive interfaces of the Au / Ti system at 1100°C. Under these conditions, a quasi-steady state of the system is achieved except for liquid Au because its concentration in Ti increases over time until the saturation (about 5 at%Ti at 1100°C). From this moment, the growth of the five reactive layers occurs by interdiffusion process and reaction at interfaces and it is controlled by the diffusion through the reactive layers.

A schematic representation of the whole system, when the quasi-steady state at 1100°C is attained, is given in Figure 100, where the thicknesses of different reactive layers are given arbitrary. This figure also gives a schematic variation of molar fraction of Ti (x_{Ti}) through the reactive system (purple dotted lines). The concentrations of Ti at reactive interfaces are given by the binary Au-Ti phase diagram. The

molar fractions of Au in different phases are not indicated in this figure. Over time, the interdiffusion of Ti and Au atoms through this reactive system leads to the growth of solid phases (Ti-Au IMCs and δ-Au), to Ti enrichment of liquid Au as well as to Au enrichment of solid Ti.

Notice that there is a competition between growth and regress of different phases at their left and right reactive interfaces. Indeed, for instance, the growth and regress of $TiAu_2$ compound at its left (interface 3) and right side (interface 4) - see Figure 100, occur according to the following reactions:

Interface 3: $Au_d + TiAu \rightarrow \mathbf{TiAu_2}$ (growth) (3a)

$\mathbf{TiAu_2} + Ti_d \rightarrow 2TiAu$ (regress) (3b)

Interface 4: $TiAu_4 + Ti_d \rightarrow 2\mathbf{TiAu_2}$ (growth) (4a)

$2Au_d + \mathbf{TiAu_2} \rightarrow TiAu_4$ (regress) (4b)

Au_d and Ti_d designate the Au and Ti atoms diffusing through the reactive system.

Thus, the growth kinetics of $TiAu_2$ compound is very complex and results from the combination of Au and Ti interdiffusion fluxes and the four reactions above at interfaces 3 and 4. In order to simplify, let assume for instance that the diffusion coefficient of Ti is much higher than that of Au. In this hypothetical case, the reactions 3a and 4b are negligible and the $TiAu_2$ layer grows at the interface 4 by reaction 4a and regress at the interface 3 by reaction 3b. Note that, in the particular case, when two reactive layers grows and regress in a diffusion couple, the growth laws of each layers are given by analytical expressions (see for example the work of Philibert et al.[35] or chap. 1 § 4.4). When more than two reactive layers are formed, the problem becomes much more complex.

The evolution of the diffusion profile of Ti in liquid Au droplet can be evaluated by considering that the molar fraction of Ti at liquid / δ-Au interface remains constant over time and equal to ~ 5 at%Ti (point L in Figure 96b) and the initial Ti content in liquid Au droplet is equal to 0. A characteristic diffusion time (t_D) in the droplet can be estimated by the relation $t_D \sim L^2/D$ where L is a characteristic diffusion distance and D the diffusion coefficient of Ti in liquid Au at 1100°C. By taking $D \sim 5.10^{-9}$ m^2/s [32] and L = droplet height < 500 µm = 5.10^{-4} m (see Figure 97), we calculate the necessary time $t_D < 50$ s (~1 min) for the saturation of liquid Au with Ti, which is much lower than the contact time of Au on Ti (>15 min).

Thus, we can consider that the whole liquid droplet is almost saturated in Ti just after about one minute following the melting of Au. This result is in agreement with the EDX analysis showing that the Ti concentration in Au is almost constant over the zone B corresponding to the liquid phase in the droplet.

When liquid gold is fully consumed, that is IMCs and δ-Au phase layers extend all over the whole droplet, the new diffusion couple becomes δ-Au phase / Ti. In this case, the thickness of δ-phase layer decreases over time, to the benefit of IMCs that will normally grow faster than before the total consumption of the liquid.

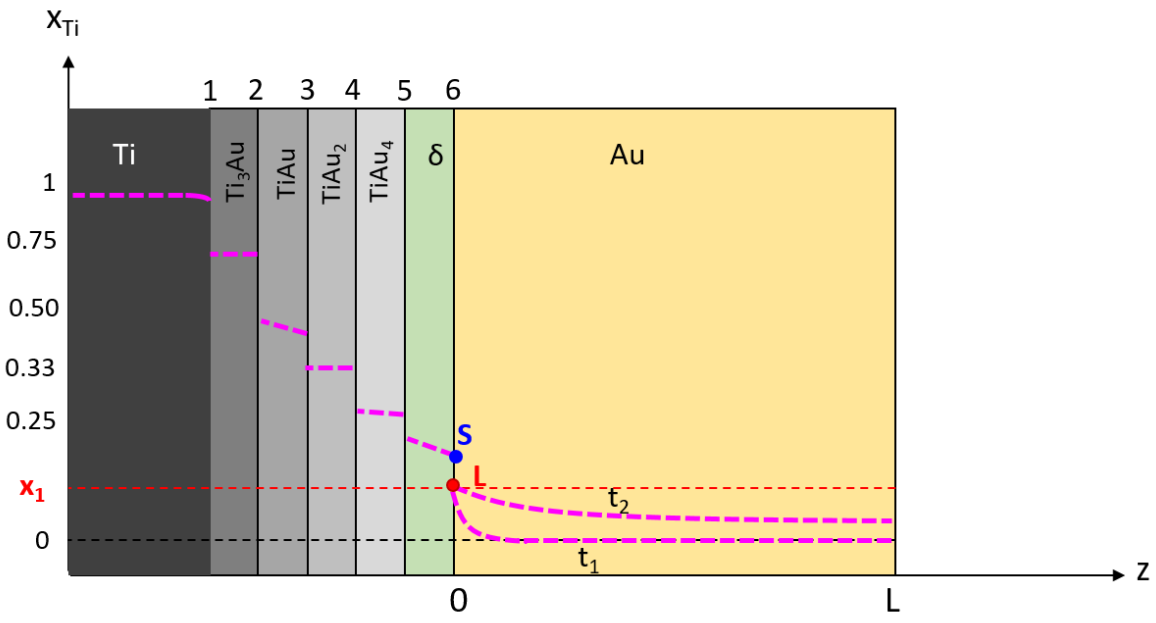

Figure 100: Schematic representation of Ti content through the different reactional layers formed between Au droplet and Ti substrate at 1100°C.

3.2.2. Interfacial reactivity between liquid Au and solid Ti at 1077° for 3 min

The deposited droplet at 1077°C and maintained in liquid state for 3 min, which is of particular interest to us for the brazing study (chapter 4), was selected to be analyzed by SEM. A SEM micrograph of a cross section of the droplet / Ti sample is presented in Figure 101. The droplet / substrate interface is clearly located under the titanium surface of about 20 µm, marking a rapid titanium dissolution. Once again, dissolution in more pronounced on the periphery of the droplet, near the triple line over about 100 µm. This distance also corresponds to the spreading distance during dissolutive / reactive wetting corresponding to the difference of drop base radius between 20 ms and 3 min of contact.

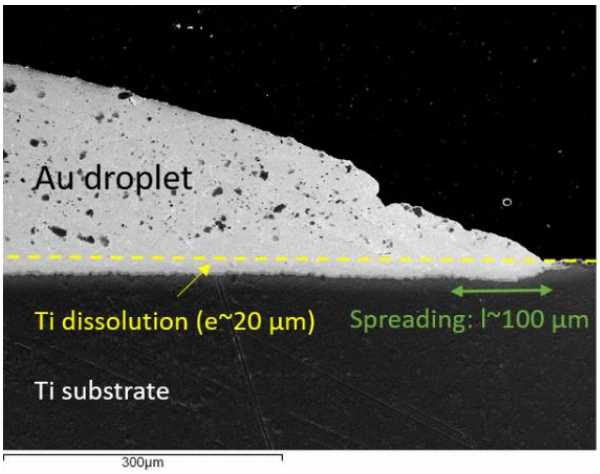

Figure 101: SEM image of a cross-section of the droplet/Ti sample deposed at 1077°C for 3 min.

On the SEM micrograph of the titanium / droplet interface (Figure 102b), gold diffusion in titanium at the grain boundaries is observed over a distance of about 15 µm. The formation of four wavy Ti-Au intermetallics layers, with a total average thickness of about 10 µm is revealed in Figure 102a. The $TiAu_4$ layer is not easily visible because of the bad quality of the sample preparation (cross-section polishing) but this observation is supported by EDX analyses. Large $TiAu_4$ needles are not observed in the droplet. The hand-polishing of this sample limits the microstructural observation of the successive layers which compose the Ti / droplet interface.

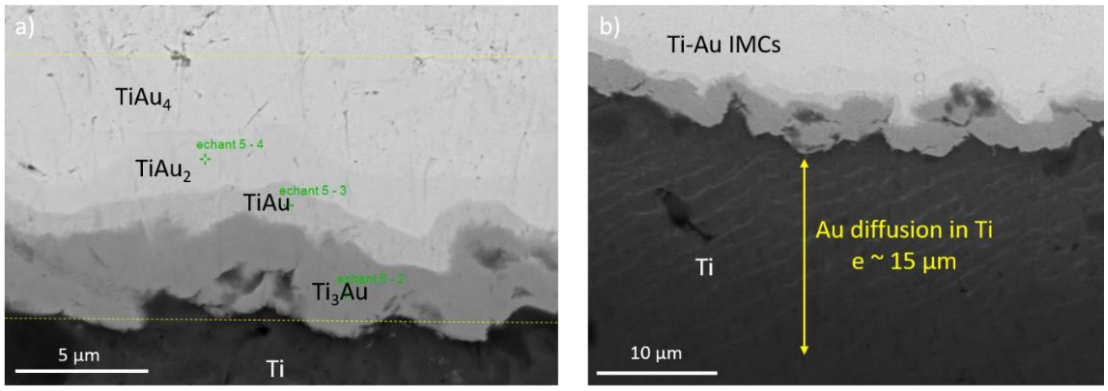

Figure 102: SEM micrograph of the Au droplet / Ti interface deposed at 1077°C for 3min, showing the Ti-Au IMCs (a) and Au diffusion in Ti substrate (b).

In order to observe the reaction zone with more details, in particular the IMCs / δ-Au and δ-Au / liquid Au interfaces, the cross-section was abraded with the FIB technology, machining a very well polished slit by the ion beam (Figure 103a and b). The sample is tilted inside the SEM to observe the wall of the slit, presented in Figure 103c and d. The four Ti-Au intermetallics compounds are also well observed. Ti_3Au and TiAu have a thickness of the order of micrometer, whereas $TiAu_2$ and $TiAu_4$ are thicker (~ 4 µm each).

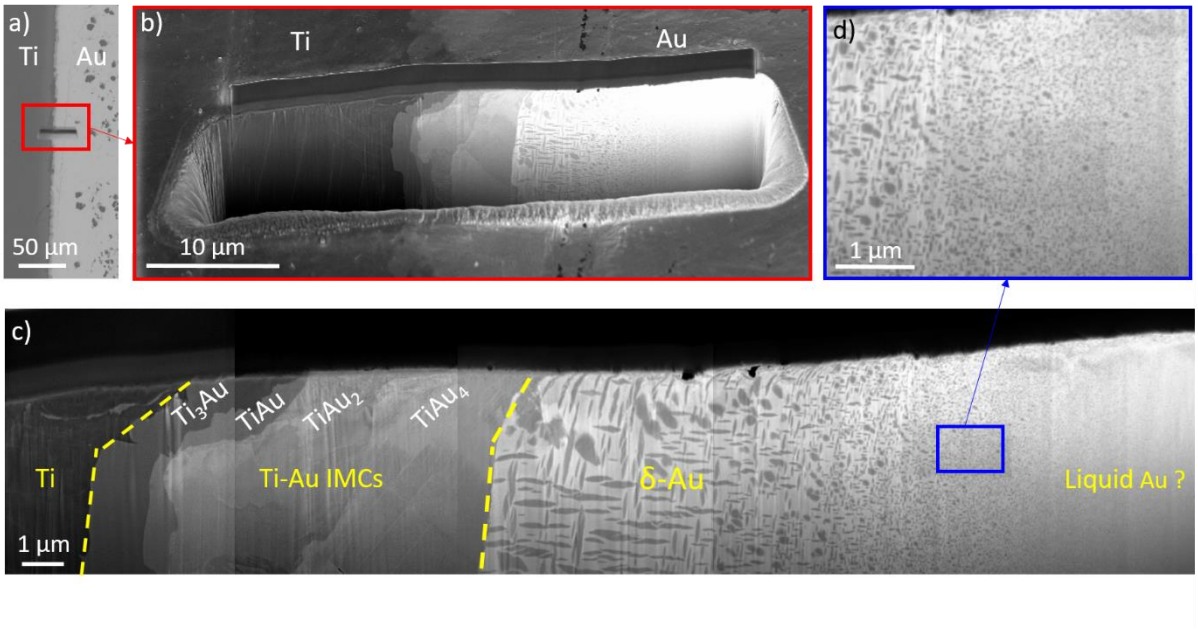

Figure 103: SEM micrographs of the Au droplet / Ti substrate interface abraded with the FIB technology: zone abraded by FIB (a, b), SEM images stitching of the whole Ti / Au interface showing the Ti-Au IMCs and δ-Au phase (c), and zoom on the droplet at about 10 µm of the IMC / δ-Au interface.

In Figure 103c, the interface between IMCs and δ-Au phase is then clearly distinguished. At the right side of the IMCs (i.e. in the δ-Au phase), small needles-shape $TiAu_4$ precipitates, of about 1-2 µm long and 0.2 µm large are visible over a zone about 6 µm wide. The size of the $TiAu_4$ precipitates decreases away from the IMCs / δ-Au interface, and submicronic $TiAu_4$ particles are observed over about 7 µm wide. From about 13 µm away of the IMCs / δ-Au interface, these precipitates are not visible at the SEM scale anymore. The δ-Au / liquid Au interface at 1077°C could not be easily identified because the difference in Ti content between liquid and solid δ-Au phases in equilibrium at this temperature is less than 1 at%, thus no significant change in the microstructure would be expected when crossing this interface. However, in a zone of about 15 µm wide starting from the IMCs / δ-Au interface, several EDX analyses give a Ti content of at least 11 at%, whereas the Ti content in the rest of the droplet is much lower. Indeed, starting from ~20 µm of the Ti / IMCs interface until the top of the droplet, the Ti content is almost homogeneous and is about 4-5 at%. Thus, we can consider that the solid δ-Au layer formed at 1077°C after 3 min of contact is about 15-20 µm thick, so the majority of the droplet is composed of liquid gold containing some Ti in solution. Notice that the 4-5 at%Ti given by the EDX analyses is significantly higher than the solubility limit of Ti in Au at 1077°C (~1 at% Ti). This difference could be due to the measurement error of the semi-quantitative EDX analysis technique as well as to the accuracy of the binary Ti-Au phase diagram in the Au-rich corner. Indeed, only three experimental values of liquidus and solidus compositions of the δ-Au phase are determined in the temperature range between 1064 and 1123°C[25].

3.3. Conclusion

In this section, wetting and interfacial reactivity between liquid gold and titanium in the temperature range 1066-1125°C were studied.

Concerning wetting study, several conclusions can be drawn.

First of all, titanium surface oxidation and titanium roughness have no impact on spreading kinetics of liquid gold on titanium substrate at 1100°C neither on the final contact angle.

Second, non-reactive wetting was observed during the 10 first milliseconds of contact between liquid gold and solid titanium at 1100°C. The initial contact angle of about 40° obtained in about 10 ms corresponds to the equilibrium contact angle of liquid Au on Ti substrate. After 10 ms, reactive and dissolutive wetting occurs, and spreading kinetics increases with temperature.

Finally, at temperature between 1066°C and the peritectic temperature T_P = 1123°C± 3°C, the contact angle θ decreases first rapidly and then slowly, until almost stabilization after about 3 min of spreading at the values θ = 50° at 1066°C and θ = 27° at 1100°C. The final contact angle corresponds to the equilibrium contact angle of liquid Au on δ-Au solid solution phase. At temperatures above T_P = 1123°C± 3°C, the contact angle decreases very rapidly in some seconds until almost perfect wetting of gold on titanium. During the spreading process, dissolution of Ti as well as formation of four reactive phases at Au / Ti interface occur. The final contact angle corresponds to the equilibrium contact angle of liquid Au on $TiAu_4$ intermetallic phase. However, the reaction rate is so rapid that, after about 30s at 1125°C, the entire liquid droplet reacts with titanium leading thus to the formation of intermetallic compounds (IMCs).

Interfacial reactivity between liquid gold and solid titanium was studied for the first time by the dispensed drop method at 1100°C and 1077°C. As expected, dissolution of titanium substrate under the droplet is observed and all stable phases provided by the binary Ti-Au phase diagram, i.e. four IMCs ($TiAu_3$, TiAu, $TiAu_2$, $TiAu_4$) and δ-Au solid solution phase, are formed with layered morphology and grow by interdiffusion process. The four IMCs layers present wavy interfaces, whereas the δ-Au phase layer has a relatively homogeneous thickness and, after cooling, presents a dual phase microstructure: δ-Au phase containing needles-shape $TiAu_4$ precipitates.

The growth kinetic of IMCs layer was investigated at 1100°C for the contact times 15, 60, 120 and 240 min. The total thickness of IMCs layers increases from 14 to 30 µm when the holding time increases from 15 to 240 min and the growth kinetics follows a parabolic law.

The thickness of the δ-Au phase layer is difficult to estimate because the jump of Ti content at the δ-Au phase / liquid Au-Ti interface is very low (~ 1 at%). However, we can assure that large $TiAu_4$ needles are observed over a zone in the range 25-500 µm wide (corresponding to the whole droplet height) when the holding time increases from 15 to 240 min. Nevertheless, according to EDX analyses, from about 1h of contact between Au and Ti, all the liquid is consumed to form the solid phases (IMCs and δ-Au phase) leading thus to an isothermal solidification of the droplets.

In the particular and interesting case of liquid Au in contact with solid Ti for 3 min at 1077°C, the total IMCs layer is about 10 µm thick, and no large $TiAu_4$ needle (visible at 1100°C for longer contact time) is observed. Small $TiAu_4$ precipitates are observed over a zone of 10-20 µm wide, suggesting that the majority of the droplet consists of liquid gold containing Ti content in solution.

Finally, a solid-state diffusion of Au into Ti substrate is observed over a distance increasing with the contact time, in the range 25 - 210 µm for 15 – 240 min of contact at 1100°C, and ~15 µm at 1077°C for 3 min.

4. Conclusions

In this chapter, we studied wetting and interfacial reactivity of the zirconia and titanium substrates under high vacuum (~10^{-6} mbar) in order to assemble them subsequently by brazing. We started to investigate first zirconia wetting because most liquid metals or metallic alloys do not wet zirconia. On the contrary, titanium substrate is well wetted by liquid metals or metallic alloys except when metallic surfaces are oxidized.

Therefore, wetting of zirconia by alloys containing zirconium and titanium active elements in order to improve zirconia wetting was studied. For both active elements, three noble metal matrix M were explored: M = Au-20Sn (low melting point alloy), Ag and Au.

A good wetting of zirconia by the three M-Zr alloys was obtained. At the alloy / zirconia substrate interface, a micrometric ZrO_2 reaction layer is formed. The growth of this layer occurs at the reaction layer / liquid alloy interface by oxygen diffusion from zirconia substrate and Zr dissolved in the alloy.

However, Ag-3Zr alloy is not adapted to ZrO_2 / Ti brazing configuration due to the high Ti activity in Ag: Ti from the substrate dissolves and diffuses into the liquid Ag and reacts with ZrO_2, leading to a thick reaction layer (~32 µm). Au-Sn-Zr alloy poses a significant problem due to Sn oxidation and needs to increase the temperature up to more than 1000°C for deoxidation under vacuum. The reaction product layer formed with Au-Zr alloy is relatively thick (until 15 µm) and presents a faceted morphology, thus not desirable to achieve a successful brazing, with high mechanical strength of the joint. Thus, the alloys containing Zr as active element were not selected for the brazing study.

Concerning the M-Ti alloys, a good wetting of zirconia is also obtained, due to the formation of a wettable Ti oxide layer at the alloy / zirconia interface. Preliminary brazing experiments show that Ag and Au-Sn matrix are not suitable for zirconia / titanium brazing contrary to Au matrix. Zirconia wetting by the Au-Ti alloys was therefore investigated in detail in this chapter with Ti content ranging from 0.6 to 4 wt%, in the temperature range 1064-1270°C.

Contact angle of Au-Ti alloys on zirconia decreases with titanium content in the filler metal until attaining $\theta \sim 44°$ at 1170°C with 4 wt% of Ti in Au. For the low Ti content in Au (Ti ≤ 2 wt%), a pinning of the triple line is observed despite the fact that the Au-Ti / zirconia is a reactive system. In some cases, contact angle remains very high (160-170°), and in other cases, Au-Ti alloy spreads zirconia by successive jumps of the triple line.

Generally, ZrO_2 / Au-Ti interfaces are strong, except for some samples with a long duration in liquid state where interfacial failures are observed.

At the zirconia / M-Ti alloy interface, a wettable Ti_xO_y layer is formed. The growth of this layer occurs at the Ti_xO_y / alloy interface by reaction between oxygen diffusing from the zirconia substrate and Ti dissolved in Au-Ti alloy. This reaction product layer is continuous, homogeneous and thin (0.3 – 4 µm), which is promising for zirconia-to-titanium brazing.

Therefore, we chose to focus our research on Au-Ti active alloy. In particular, the selected filler metal for the brazing study is pure gold since titanium is provided from the Ti metallic substrate.

For this reason, wetting and reactivity of titanium by liquid gold were presented and discussed in this chapter. A very good wetting was observed, the contact angle being lower than 45° and wetting does not depend on the roughness and the native oxidation of Ti substrate. Spreading kinetics increases with temperature in the range 1066-1125°C.

For temperatures lower than the peritectic temperature T_P = 1123 ± 3°C, the dissolutive and reactive wetting leads to the formation of five solid phases at the Ti substrate / liquid gold interface: four Ti-Au intermetallic compounds (Ti_3Au, TiAu, $TiAu_2$ and $TiAu_4$) and the δ-Au solid solution phase and the contact angle corresponds to the equilibrium contact angle of δ-Au phase in contact with liquid Au-Ti alloy. The thicknesses of theses phases grow with contact time between liquid Au and solid Ti and the growth kinetics of IMCs layer at 1100°C follows a parabolic law. At 1100°C, from about 1h of contact all the liquid is consumed, leading to an isothermal solidification of the droplet.

References of chapter 3

1. N. Eustatopoulos, M.G. Nicholas & B. Drevet. *Wettability at high temperatures*. (Pergamon materials series, 1999).

2. X. M. Xue, Z. T. Sui & J. T. Wang, Effect of zirconium on wettability of alumina and zirconia by silver-indium base alloy. *J. Mater. Sci. Lett.* **11**, 1514–1517 (1992).

3. A. V. Durov, Y. V. Naidich & B. D. Kostyuk, Investigation of interaction of metal melts and zirconia. *J. Mater. Sci.* **40**, 2173–2178 (2005).

4. H. Bian, Y. Zhou, X. Song, S. Hu, B. Shi, J. Kang & J. Feng, Reactive wetting and interfacial characterization of ZrO2 by SnAgCu-Ti alloy. *Ceram. Int.* **45**, 6730–6737 (2019).

5. W. Fu, A. Passerone, H. Bian, S. Hu, Y. Zhao, & X. Song, M. Wang & F. Valenza. Wetting and interfacial behavior of Sn–Ti alloys on zirconia. *J. Mater. Sci.* **54**, 812–822 (2019).

6. Luigia Muolo, M., Ferrera, E., Morbelli, L. & Passerone, A. Wetting, spreading and joining in the alumina–zirconia–Inconel 738 system. *Scr. Mater.* **50**, 325–330 (2004).

7. N. Iwamoto & H. Yokoo, Joining of zirconia to metals using Zr-Cu alloy. *Eng. Fract. Mech.* **40**, 931–940 (1991).

8. T. H. Chuang, M. S. Yeh & Y. H. Chai, Brazing of zirconia with AgCuTi and SnAgTi active filler metals. *Metall. Mater. Trans. A* **31**, 1591–1597 (2000).

9. A. Koltsov, Physico-chimie du brasage de AlN : mouillage et réactivité. [PhD, Grenoble INPG] (2005).

10. W. B. Hanson, K. I. Ironside & J. A. Fernie, Active metal brazing of zirconia. *Acta Mater.* **48**, 4673–4676 (2000).

11. S. W. Park, H. Lee, B. H. Lee, T. H. Kim, K. I. Kim, S. A. Hong, M. Kim, S. Hyun, G. H. Ryu & K. T. Kim, Effect of Interface Microstructure on Joint Strength of Zirconia/Titanium Alloy Brazed with Amorphous Zr-Ti-Ni-Cu Active Filler Metal. *Metals* **10**, 718 (2020).

12. Y. Liu, J. Hu, Y. Zhang & Z. Guo, Interface microstructure of the brazed zirconia and Ti-6Al-4V using Ti-based amorphous filler. *Sci. Sinter.* **45**, 313–321 (2013).

13. Jiang, G., Mishler, D., Davis, R., Mobley, J. P. & Schulman, J. H. Zirconia to Ti-6Al-4V braze joint for implantable biomedical device. *J. Biomed. Mater. Res. B Appl. Biomater.* **72B**, 316–321 (2005).

14. J. J. Pak, M. L. Santella & R. J. Fruehan, Thermodynamics of Ti in Ag-Cu alloys. *Metall. Trans. B* **21**, 349–355 (1990).

15. H. Okamoto & T. B. Massalski, The Au−Nb (Gold-Niobium) system. *Bull. Alloy Phase Diagr.* **6**, 134–136 (1985).

16. C. De Gonzalez & E. A. Garcia, Determination of the diffusion coefficients of oxygen in zirconium by means of XPS. *Appl. Surf. Sci.* 211–219 (1990).

17. A. J. Marzocca, F. Povolo & G. H. Rubiolo, Self-diffusion coefficient of a-zirconium. *J. Mater. Sci. Lett.* **6**, 431–433 (1987).

18. M. Kilo, C. Argirusis & M. A. Taylor, Experimental and theoretical investigation of oxygen diffusion in stabilised zirconia. *Radiat. Eff. Defects Solids* **157**, 1077–1083 (2002).

19. M. Kilo, C. Argirusis, M. A. Taylor & G. Borchardt, Cation self-diffusion of 44Ca, 88Y, and 96Zr in single-crystalline calcia- and yttria-doped zirconia. *J Appl Phys* **94**, 6 (2003).

20. D. S. Cheong, Self diffusion of cation in yttria stabilized zirconia single crystal. *J. Korean Cryst. Growth Cryst. Technol.* **19**, 237–241 (2009).

21. P. Kritsalis, B. Drevet, N. Valignat, N. Eustathopoulos, Wetting transitions in reactive metal/oxide systems. **30**, 6 (1994)

22. R. Voytovych, F. Robaut & Eustathopoulos. The relation between wetting and interfacial chemistry in the CuAgTi/alumina system. *Acta Mater.* **54**, 2205–2214 (2006).

23. P. Protsenko, A. Terlain, V. Traskine & N. Eustathopoulos. The role of intermetallics in wetting in metallic systems. *Scr. Mater.* **45**, 1439–1445 (2001).

24. O. J. Kleppa & L. Topor. Thermochemistry of binary liquid gold alloys: The systems (Au + Cr), (Au + V), (Au + Ti), and (Au + Sc) at 1379 K. *Metall. Trans. A* **16**, 93–99 (1985).

25. J.L. Murray, The Au-Ti (Gold-Titanium) system. *Bull. Alloy Phase Diagr.* **4**, 278–283 (1983).

26. D. Chatain, F. Chabert, V. Ghetta & J. Fouletier. New Experimental Setup for Wettability Characterization under Monitored Oxygen Activity: I, Role of Oxidation State and Defect Concentration on Oxide Wettability by Gold. *J. Am. Ceram. Soc.* **76**, 1568–1576 (1993).

27. Y. V. Naidich, A. V. Durov, B. D. Kostyuk & A. V. Shevchenko. Wetting and brazing zirconia ceramic with alloys of the CuGaTi system. *Powder Metall. Met. Ceram.* **38**, 367–368 (1999).

28. E. Saiz, A. P. Tomsia & R. M. Cannon, Triple line ridging and attachment in high-temperature wetting. *Scr. Mater.* **44**, 159–164 (2001).

29. O. Taguchi, T. Watanobe, Y. Yamazaki & Y. Iijima. Reaction diffusion in the Au-Ti System between 1110K and 1150K. in *Defect and diffusion forum*. **194–199,** 1569–1574 (Scitec Publications, 2001).

30. P. Kritsalis, B. Drevet, N. Valignat, N. Eustathopoulos, Wetting transitions in reactive metal/oxide systems. **30**, 6. (1994)

31. P. Blanchart, Dioxyde de titane - Propriétés et applications. *Verres Céramiques* (2019)

32. G.H. Geiger & D. R. Poirier. *Transport Phenomena in Metallurgy*. Addison-Wesley Publshing Company (1973).

33. J. A. Warren, W. J. Boettinger & A. R. Roosen, Modeling reactive wetting. *Acta Mater.* **46**, 3247–3264 (1998).

34. A. K. Kumar & A. Paul, Interdiffusion studies in bulk Au–Ti system. *J. Mater. Sci. Mater. Electron.* **21**, 1202–1206 (2010).

35. J. Philibert. Reactive diffusion in thin films. in *Applied Surface Science*. **53,** 74–81 (1991).

Chapter 4 : Study of zirconia to titanium brazing

Contents

1. Introduction

This chapter is dedicated to the zirconia / titanium brazing with pure gold, where the main focus is given to the physico-chemical mechanisms of interactions between Au-Ti alloy (Ti being provided by the dissolution of the metallic substrate in pure Au) and the substrates (ZrO_2 and Ti). The goal of the brazing study is to propose a robust brazed assembly. In order to achieve a high hermeticity of the joint, which is a key parameter for the biomedical application, the formed zirconia / braze and titanium / braze interfaces have to be strong with no defect like voids or failures. It is therefore crucial to identify the sensitive brazing parameters, as well as to control the growth kinetics of the reaction layers formed at both interfaces.

First, a preliminary study of zirconia-to-zirconia brazing and zirconia-to-titanium brazing is performed using the industrial active brazing alloy Gold-ABA® (Au-3Ni-0.6Ti wt%) known to join ceramic to metal with success, in order to identify the potential of Au-Ti filler metal (section 2).

The third section of this chapter deals with physico-chemical characterization of the joint. In order to understand the joining process from a metallurgical point of view, solid and liquid state interactions are investigated. First, the impact of several brazing parameters on the joint microstructure, such as the Au foil thickness, the temperature and duration in liquid state of Au-Ti alloy, is studied in order to propose an optimized brazing configuration. Once the brazing parameters fixed, a deep analysis of the joint microstructure (bulk Au-Ti alloy and two reactional interfaces) is performed for the purpose of discussing the reactional mechanisms involved during brazing process as well as the rate-limiting step(s).

Finally, the fourth section of this chapter is dedicated to mechanical characterization of the joint, which is performed by tensile tests. For the first time, a relationship between mechanical properties of brazed assemblies and the vacuum level (i.e. oxygen partial pressure) in the furnace is established.

For the main brazed samples, experiments were carried out in sandwich configuration by placing a metallic foil (Au-3Ni-0.6Ti or Au) between titanium (the bottom substrate) and zirconia (the upper substrate) discs (diameter of 15 mm and height of 2 mm) used as received, without any specific surface treatment (see chapter 2). Samples before and after brazing process are presented in Figure 104. A metallic weight of 20 g is placed on the assembly to ensure proper contact between the braze and the substrates during the brazing process, corresponding to a surface mass of about 12 g/cm^2. Some fine

microscopic analyses and the whole mechanical characterization of the joints were performed with tensile test specimens which will be presented in section 4.

The assembly is placed in the LPA metallic furnace (Figure 104), also used for the wetting study by sessile drop technique (chapter 3). Thus, experimental conditions, in particular vacuum level (~ 5.10^{-6} mbar) and oxygen partial pressure (P_{O2}) are the same for both wetting and brazing experiments. An example of a sample after brazing is given in Figure 104c.

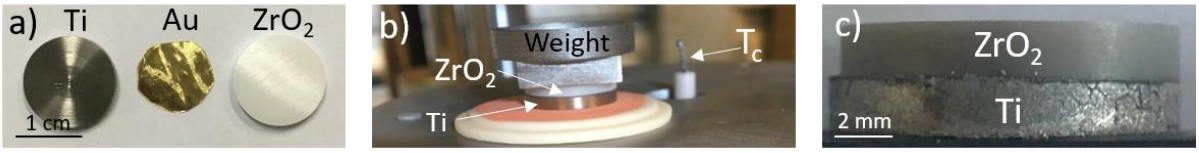

Figure 104: ZrO_2 / Au / Ti sample before and after brazing: Ti, ZrO_2 and Au discs (a), Sample before brazing in the furnace (b), Sample after brazing (c).

Figure 105 presents a schematic brazing thermal cycle used for the entire brazing study, defined from the wetting experiments in Au-Ti / zirconia system. The brazing cycle is composed of a slow temperature ramp at a heating rate of 5°C/min from room temperature to 500°C not to induce a violent heating to the furnace at low temperature range. Then, the heating rate is increased to 10°C/min until the brazing temperature ranging from 1064°C to 1170°C. The duration of the isothermal holdings varies from 1 min to 15 min, depending on the experiment, and sometimes up to 60 min. Finally, a free cooling of the furnace is carried out. At high temperature, cooling rate is very high (about 50°C/min above 800°C) and decreases drastically at low temperatures (about 2°C/min below 500°C).

During brazing process, the following reactions occur:

- Solid state reactions at Ti substrate / alloy interface below Au melting point (1064°C) or Au-3Ni-0.6Ti solidus (1003°C).
- Liquid state reactions at both Ti / alloy and zirconia / alloy interfaces above Au melting point or Au-3Ni-0.6Ti liquidus.

Note that the major difference between reactive solid / solid and solid / liquid systems is that, in the case of solid / liquid couples, a significant dissolution of the solid in the liquid phase can occur during the first contact until a total covering of the interface by the reaction product. Moreover, the activation energy of diffusion process in solids being very high, the solid-state reactions become significant only at relatively high temperatures.

Note also that, at the end of the brazing cycle, during cooling, the solidified braze bonds zirconia and titanium substrates. Therefore, substrates are not able to shrink independently, thus causing thermomechanical stresses in the assembly. These stresses are particularly important in the case of dissimilar brazing, because zirconia and titanium have different mechanical properties, especially very different thermal expansion coefficients (see chapter 2).

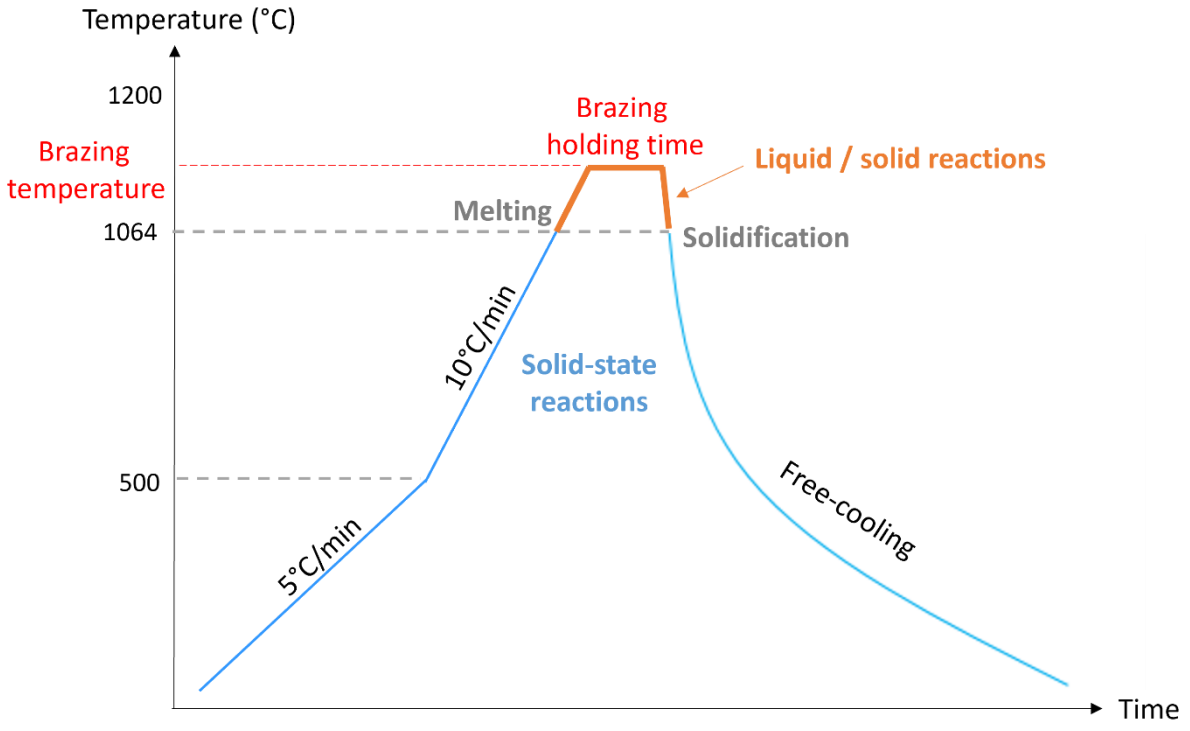

Figure 105: Schematic thermal cycle of brazing used for the study.

2. ZrO_2 / ZrO_2 and ZrO_2 / Ti brazing by an industrial reactive braze (Gold-ABA®)

2.1. Introduction

In this section, preliminary brazing tests of similar brazing (zirconia / zirconia) and dissimilar brazing (zirconia / titanium) were carried out using an industrial active brazing alloy containing Ti active element named Gold-ABA®. The composition of this alloy is Au-3Ni-0.6Ti wt%.

As it has been seen in chapter 3, this alloy shows a good behavior in sessile drop configuration on zirconia, namely:

- The formation of a circular drop at 1040°C and a relatively good wetting with a final contact angle θ ~ 85°, after 7 min of contact in liquid state on polished zirconia in the temperature range 1040-1170°C. This wetting behavior could be sufficient for ceramic / metal brazing in sandwich configuration.
- A good adhesion of the solidified droplet on zirconia after wetting experiments, for a liquid phase duration below 30 min.
- The formation of a homogeneous, continuous and thin Ti_xO_y reaction layer (less than 2 µm) at the droplet / substrate interface.
- No failure in the ceramic under the droplet, neither at the interface nor in the reaction layer.

Note that in general, pinning phenomenon observed in sessile drop configuration, could not occur in brazing for sandwich configuration except for solid surfaces with high roughness.

2.2. Similar brazing of zirconia by the Au-3Ni-0.6Ti alloy

Remember that we talk about similar brazing when both of the substrates to be joined have the same nature. First of all, a similar brazing of zirconia by the Au-3Ni-0.6Ti alloy was performed, with a Gold-ABA® foil of 100 µm thick, in order to evaluate the potential of the Au-Ti alloy with a low Ti content in brazing configuration, at the zirconia / alloy interface. After the thermal cycle of 30 min in liquid phase in the temperature range 1040 - 1100°C, both zirconia substrates became grey and they were well assembled. The sample resisted manual torsional and tensile forces. Brazed assembly was encapsulated in epoxy resin, cut in half and polished in order to observe a cross section of the joint. Figure 106a shows an optical micrograph of the sample. The joint is homogeneous, well filled and has no apparent defect like voids or cracks. A SEM observation of alloy / zirconia interface is presented in Figure 106b. A thin Ti_xO_y layer, non-homogeneous in thickness, in the range 0 - 1 µm, is observed at the interface. However, the SEM resolution does not allow to confirm whether this reaction product layer is continuous (with locally a nanometric thickness) or discontinuous. Notice that, as already seen in chapter 3, this reaction product is wettable by liquid gold, which is a necessary condition for brazing.

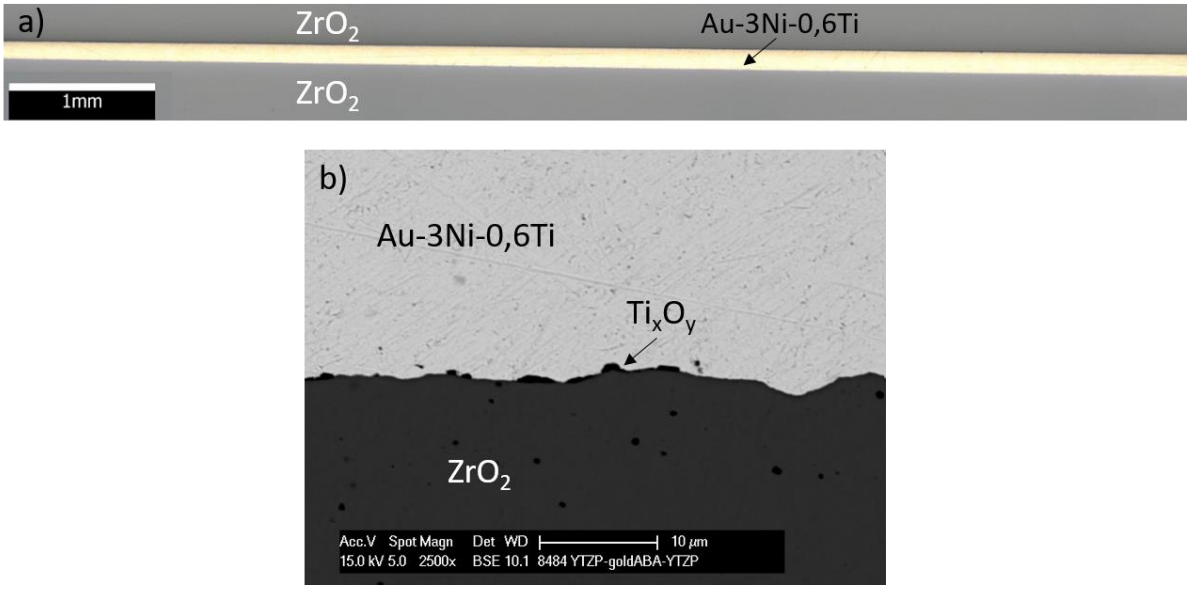

Figure 106: Micrograph of a cross section of ZrO_2 / Au-3Ni-0.6Ti / ZrO_2 joint obtained by brazing during 30 min in liquid state in the temperature range 1040 - 1100°C (a), SEM micrograph of the ZrO_2 / Au-3Ni-0.6Ti interface showing Ti_xO_y reaction product (b).

To conclude, Au-3Ni-0.6Ti alloy is an adapted filler alloy for zirconia to zirconia brazing. Moreover, a low titanium content (0.6 wt%) leads to the formation of a thin Ti_xO_y reaction layer at the Au-Ti alloy / zirconia interface, which is promising for zirconia to titanium brazing with pure gold.

2.3 Zirconia to titanium brazing by the Au-3Ni-0.6Ti alloy

A zirconia / titanium brazing test was conducted at 1064°C for 10 min with an Au-3Ni-0.6Ti foil of 100 µm thick. The assembly was successfully brazed.

On the SEM picture of the cross section presented in Figure 107, a relatively homogeneous microstructure of the joint is observed. Notice the presence of large $TiAu_4$ needles formed inside the δ-Au-Ni-Ti solid solution matrix. The precipitation of $TiAu_4$ phase inside the δ-Au-Ni-Ti matrix occurs during cooling of δ phase due to the fact that the solubility of Ti in δ phase drastically decreases with the temperature (see chapter 3 - solidification of Au-Ti alloys).

At the titanium / gold interface, a thick and continuous reaction layer is observed. This layer is composed of the four Au-Ti intermetallic compounds (IMCs) given by the Au-Ti binary phase diagram (Figure 11396). The formation of these IMCs is due to the reaction between Ti in solid state and Au in both solid and liquid states. At the zirconia / alloy interface, a submicronic wettable reaction layer that consists of titanium oxide is formed.

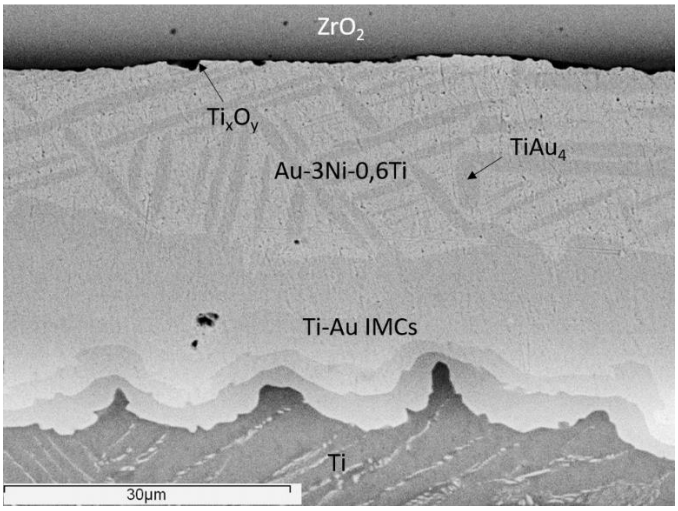

Figure 107: SEM micrograph of ZrO_2 / Au-3Ni-0.6Ti (Gold-ABA® alloy) / Ti joint obtained by brazing at 1064°C for 10 min.

A leak of liquid alloy out of the joint occurred during brazing, because titanium substrate was very well wetted by the Au-3Ni-0.6Ti alloy. This process issue led to a heterogeneous thickness of the joint, ranging from about 30 µm to 60 µm (Figure 108). This first test permitted to highlight that, for a single thermal cycle, Ti-Au IMCs thickness depends on gold thickness. Indeed, when the joint thickness (IMCs + δ phase) increases from 30 to 60 µm, the IMCs thickness decreases from ~22 to ~16 µm. This preliminary result prompted us to study the impact of gold thickness on the joint microstructure, and in particular on the Ti-Au IMCs thickness.

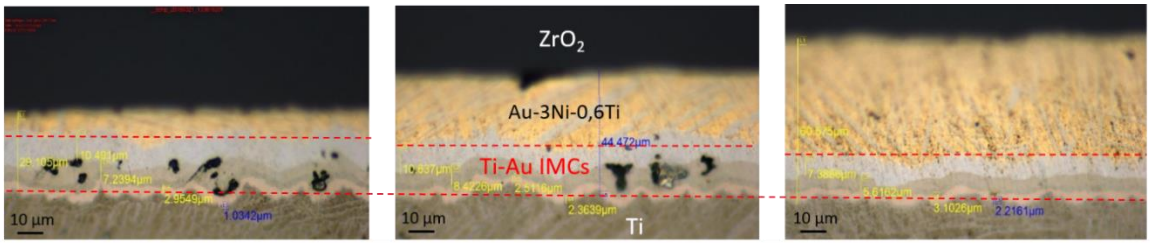

Figure 108: Optical micrographs of different parts of a single ZrO_2 / Au-3Ni-0.6Ti (Gold-ABA® alloy) / Ti joint obtained by brazing at 1064°C for 10 min showing a variable total thickness of the joint and IMCs.

2.4. Conclusion

The industrial Au-3Ni-0.6Ti alloy is an adapted filler metal for zirconia-to-zirconia and zirconia-to-titanium brazing. At the zirconia / braze interface, the low titanium content in the alloy (0.6 wt%) leads to the formation of a thin wettable Ti_xO_y reaction layer, which is necessary to perform a successful brazing . At the titanium / alloy interface, a homogeneous layer, which consists of four Ti-Au IMCs is formed. These preliminary results are promising for zirconia-to-titanium brazing using pure gold.

3. Physico-chemical study of ZrO_2 / Ti joint brazed by a gold foil

3.1. Introduction

This zirconia / titanium brazing study is focused on biomedical application. For this reason, using nickel in the filler metal is not desirable, so we chose not to continue brazing experiments with the commercial Gold-ABA® (Au-3Ni-0.6Ti) alloy. Therefore, zirconia to titanium brazing was performed using a pure gold foil as filler metal. Titanium active element is provided from the Ti metallic substrate by dissolution in liquid Au. Indeed, the solubility limit of titanium into liquid gold in the temperature range 1080°C-1100°C varies from about 2 at% (0.5 wt%) to 5 at% (1.5 wt%). Wetting study and similar brazing of zirconia with the Au-3Ni-0.6Ti alloy showed that low Ti content into gold (between 0.6 and 1 wt%) is sufficient to form a strong interface between Au-Ti alloy and zirconia, with the formation of a thin and wettable Ti_xO_y reaction layer at the interface. Moreover, preliminary experiments of zirconia / titanium brazing with pure gold show a good mechanical behavior of the joint. Therefore, we studied in detail the zirconia / titanium brazing using pure gold as filler metal.

In this section the impact of different physico-chemical parameters on the reactivity at the substrates / alloy interfaces and on the joint microstructure will be presented and discussed in order to select the optimal brazing parameters (§ 3.2). For the optimized ZrO_2 / Au / Ti brazed samples, fine characterizations of the interfaces will be detailed in order to study the reactional mechanisms in the ZrO_2 / Au / Ti system (§ 3.3).

3.2. ZrO_2 / Ti brazing using a pure Au foil: influence of different parameters

3.2.1. Introduction

In this section, we study first the influence of the initial thickness of the gold foil on the total thickness of Au-Ti intermetallics as well as on the microstructure of the formed joint (§ 3.2.2). Afterwards, we study the influence of the brazing temperature and the brazing time on the whole joint microstructure and especially on the morphology and the thickness of the wettable Ti_xO_y layer formed at zirconia / gold interface (§ 3.2.3 and 3.2.4). Moreover, the reactivity between Ti substrate and solid Au during heating up to the brazing temperature is studied and its influence on the subsequent evolution of the interfacial system is discussed (§ 3.2.5).

Based on this systematic study, the optimal brazing parameters (gold thickness, brazing temperature and holding time) are selected.

3.2.2. Impact of gold thickness on the total thickness of intermetallic layers and on the joint microstructure

a) Introduction

It is well established that intermetallics (IMCs) are brittle phases and thus they could be detrimental to the mechanical behavior of the joint. Therefore, it could be very advantageous to limit as much as possible the IMCs thickness, provided that a very continuous layer is obtained at the interface[1]. Moreover, it is also well known that a homogeneous microstructure of the joint, without formation of large precipitates, is advantageous for the mechanical properties of the joint. Therefore, the impact of gold thickness on the total thickness of IMCs and on the joint microstructure was investigated in order to determine the reactional mechanisms occurring during brazing.

For this purpose, four ZrO_2 / Au / Ti samples were brazed at intermediate temperature of 1100°C for 10 min, with Au foils of 25, 50, 100 and 150 µm thick. After the brazing experiments, all samples were analyzed by optical and electron microscopy. Consequently, the most appropriate filler metal thickness will be proposed.

b) Experimental results

The four assemblies were successfully brazed. Optical images of cross sections of the joints, presented in Figure 109, show a good general aspect of the joints with a perfect filling without significant voids or defects. Moreover, the IMCs reaction product layer presents homogenous average thickness everywhere at the interface. Note that, as it is indicated by the binary Au-Ti phase diagram (Figure 113), the stable phases that can be formed between liquid Au and solid Ti in the temperature range 1070°C-1120°C are the intermetallics Ti_3Au, TiAu, $TiAu_2$, $TiAu_4$ and the solid solution δ-Au (containing up to ~10 at% Ti at 1070°C to ~12 at % Ti at 1120°C).

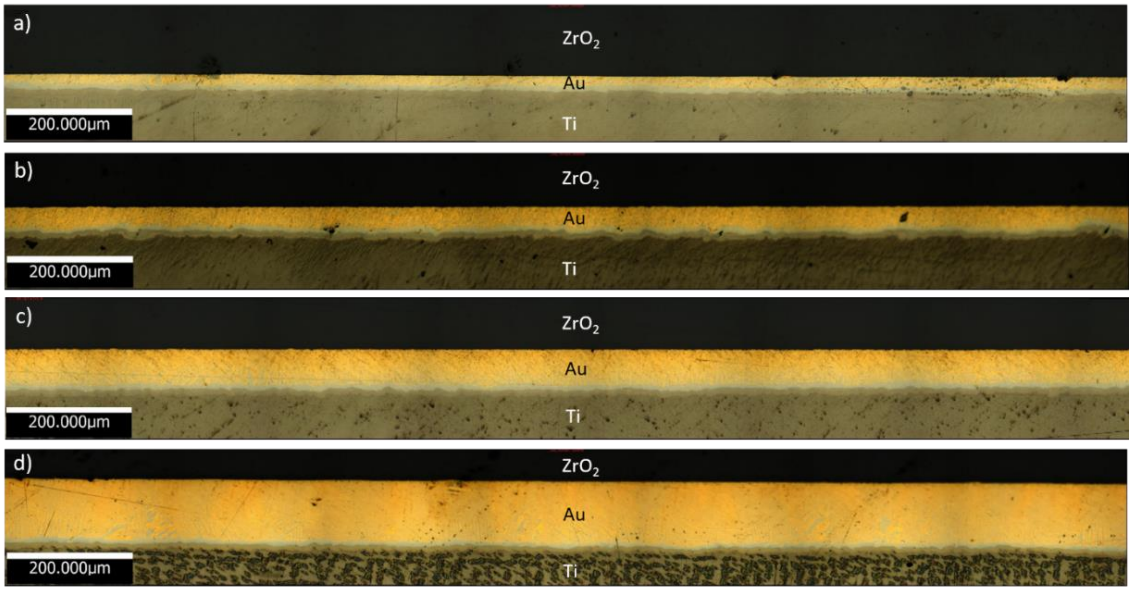

Figure 109: Optical micrographs of ZrO_2 / Au / Ti joints obtained by brazing at 1100°C for 10 min with different Au foils thicknesses a) 25 µm, b) 50 µm, c) 100 µm, d) 150 µm.

Figure 110 gives an assembled image of all brazed joints performed with Au foils 25, 50, 100 and 150 µm thick. It can be seen that the total thicknesses of the joints formed between Ti and ZrO_2 (i.e. Ti-Au IMCs + δ-Au thicknesses) are ranging from ~ 34 µm to 134 µm. Moreover, this figure clearly shows that the total IMCs thickness decreases respectively from ~24 µm to ~14 µm with increasing total joint thickness. In all images, it can be noted the presence of $TiAu_4$ needles inside gold matrix especially in the region close to the intermetallics.

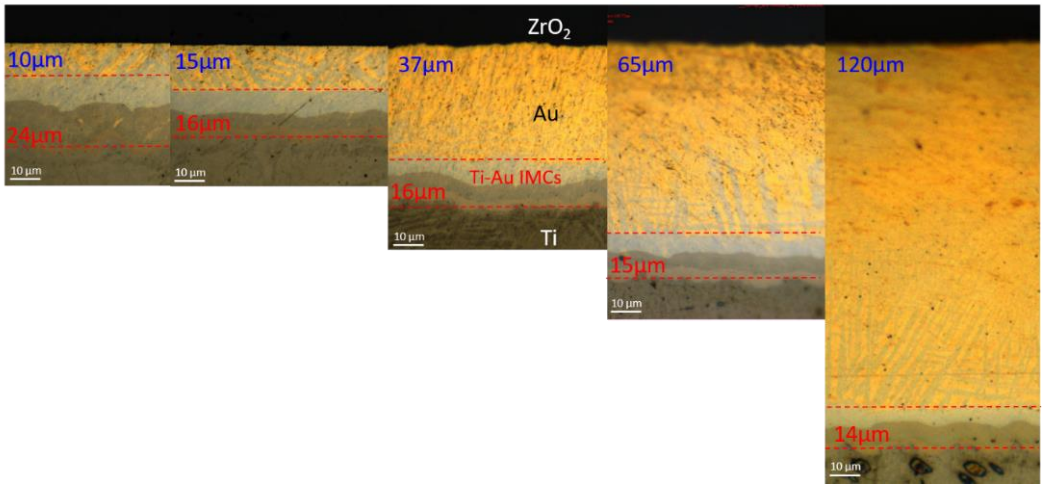

Figure 110: Optical micrographs of ZrO_2 / Au / Ti joints obtained by brazing at 1100°C for 10 min with different Au foils thicknesses.

For better understanding of the interactions occurring at 1100°C for 10 min in the liquid Au / solid Ti system, we characterized by SEM the joint microstructure obtained with the three higher Au thicknesses 50, 100 and 150 µm.

First of all, Figure 111 shows SEM pictures of a typical microstructure of the joint brazed with a gold foil of intermediate thickness 50 µm. A homogeneous joint, with no visible defect is obtained (Figure 111a). In the Ti metallic substrate, near IMCs, we notice the presence of precipitates containing gold which clearly testifies gold diffusion in titanium over about 60 µm in depth, that seems to be mostly grain boundary diffusion. This phenomenon will be discussed in detail in section 3.3.2.

The bulk microstructure of the joint is composed of a gold matrix containing large $TiAu_4$ precipitates (Figure 111b). A reaction layer is observed at Au / Ti interface over the entire length of the joint, with a constant average thickness of 18±2µm (Figure 111a and b). Four Ti-Au IMCs are detected inside the reaction layer (Ti_3Au, TiAu, $TiAu_2$ and $TiAu_4$) in agreement with the binary Ti-Au phase diagram presented in Figure 113. The composition of these IMCs will be analyzed in detail further in this chapter.

The thicknesses of the three IMCs richer in Ti are quite similar, whereas $TiAu_4$ is twice thicker.

Figure 111c clearly shows that a submicronic, not homogeneous in thickness, Ti_xO_y reaction layer is formed at Au / ZrO_2 interface. The formation of this layer is due to the reaction between zirconia and Ti atoms diffusing through liquid gold from Ti / Au interface to Au / ZrO_2 interface. Note that, as it has been seen in chapter 3, this Ti oxide reaction product is wettable by liquid Au-Ti alloy, which is a necessary condition to perform a good brazing. Notice also that the reaction layer formed in the case of ZrO_2 / Ti brazing with an Au foil 150 µm thick, is also submicronic and not homogeneous in thickness.

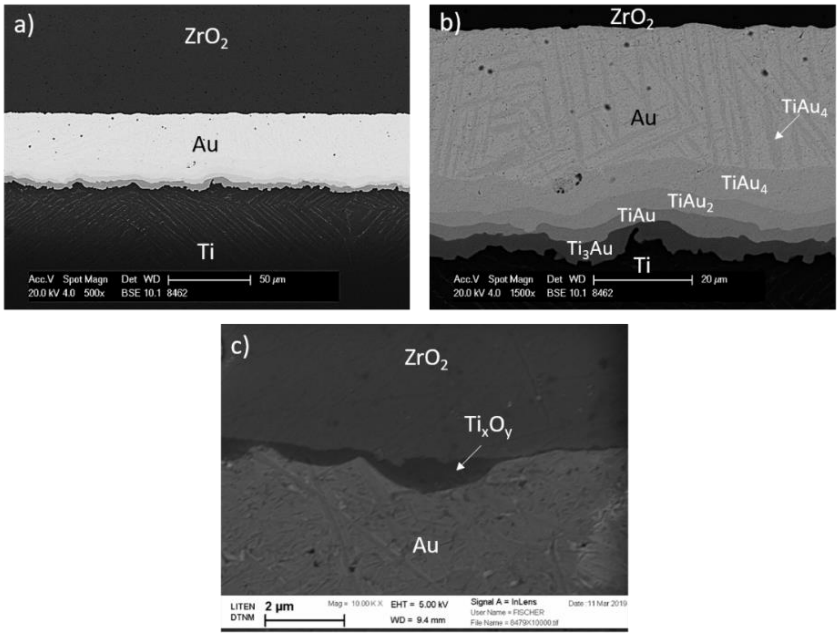

Figure 111: SEM micrographs of a cross section of ZrO_2 / Au / Ti joint obtained by brazing at 1100°C for 10 min (a and b), SEM micrograph of the ZrO_2 / Au interface showing the Ti_xO_y reaction product (c). Gold foil 50 µm thick.

In Figure 112, we compare the microstructure of three joints obtained by using three different gold thicknesses (50, 100 and 150 µm) and brazed under the same conditions (at 1100°C for 10 min). Semi-quantitative analyses of large zones in the joint give the average content of Ti in different areas of the joint situated outside the IMCs region (Figure 112d).

All analyses indicate an average Ti content lower than 10 at% and the difference of Ti content between different zones is relatively low. However, a concentration gradient of Ti can be detected, ranging from ~ 9 at% Ti at the IMC side to ~ 5 at% Ti at the zirconia side.

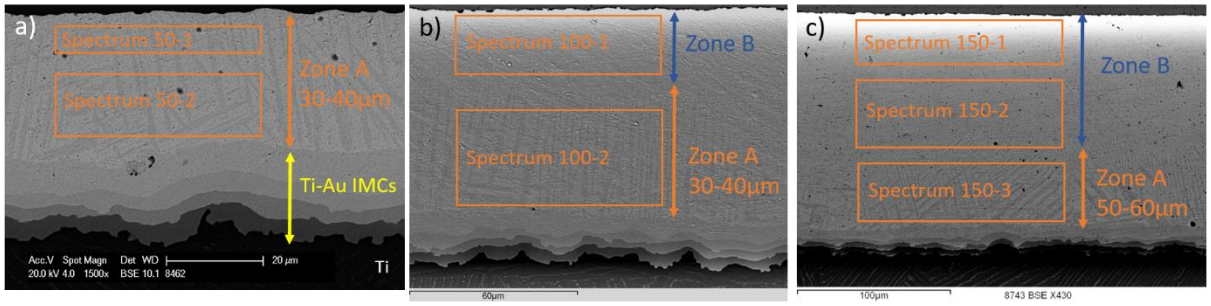

d)	e(Au)=50µm		e(Au)=100µm		e(Au)=150µm	
	Spectrum	Ti (at %)	Spectrum	Ti (at %)	Spectrum	Ti (at %)
	50-1	7	100-1	5	150-1	5
	50-2	8	100-2	8	150-2	6
	-	-	-	-	150-3	9

Figure 112: SEM micrographs of ZrO_2 / Au / Ti joints obtained by brazing at 1100°C for 10 min with different Au foil thicknesses a) 50 µm, b) 100 µm, c) 150 µm and d) results of respective EDX analyses.

From Figure 112, it can be seen that, for samples brazed with Au foils 100 µm (Figure 112b) and 150 µm thick (Figure 112c), the part of the joint situated between Ti_xO_y and IMCs layers, is composed of two microstructural zones (noted A and B):

- At the IMCs side, a relatively homogeneous layer, 40-60 µm thick, containing large $TiAu_4$ needles inside a gold matrix (zone A). The average Ti content in this zone is about 8-9 at%, which is significantly higher than the solubility limit of Ti into liquid Au at 1100°C (~ 5 at%) – see Figure 113. These results strongly suggest that at this temperature, δ-Au solid solution is well formed between Ti and liquid Au (together with four IMCs described above). Note that at 1100°C, the δ-Au phase is stable in the composition range between ~ 6 and 11 at% Ti and the solubility limit of Ti in δ-Au phase drastically decreases with the temperature from ~ 11 at% at 1100°C to ~ 1 at% Ti at room temperature (see Figure 113). Thus, during cooling, the δ-Au solid solution becomes depleted in Ti and, as a result,$TiAu_4$ phase precipitates in the form of large needles inside the δ-Au matrix.

- At the zirconia side, a homogeneous zone with no $TiAu_4$ needle detected in the micrograph scale, is observed (zone B). This zone is composed of Au containing ~ 5 at% of Ti, which is just below the solubility limit of Ti into liquid Au at 1100°C. It can thus be concluded that, at brazing temperature, this zone is composed of liquid gold containing Ti in solution.

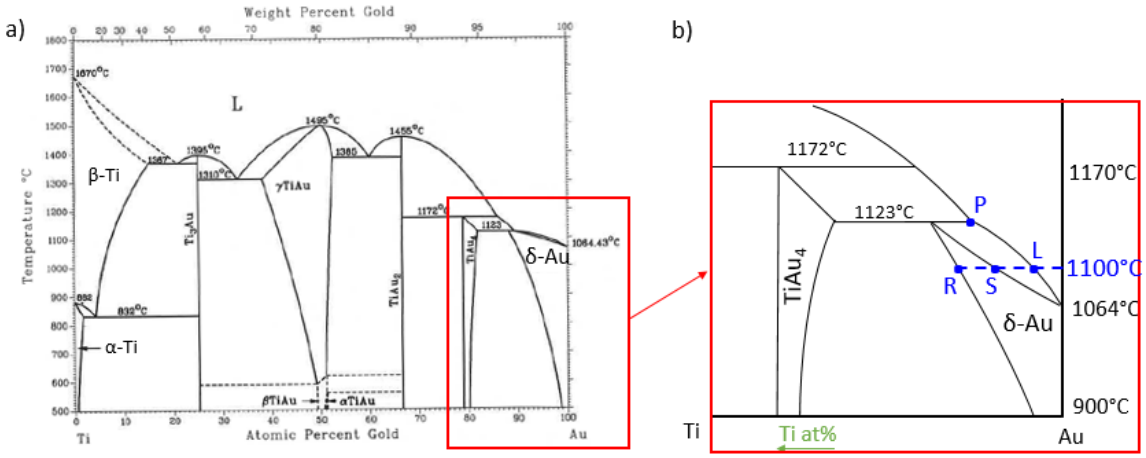

Figure 113: Ti-Au binary phase diagram[2] (a), schematic zoom on the Au-rich region (b).

c) Analysis and discussion

As already mentioned in chapter 3 (§ 3.2.1.), the same reasoning leads to the description of the sequence of phase formation in the solid Ti / liquid Au diffusion couple at T = 1100°C as presented below:

Solid Ti / Ti_3Au / TiAu / $TiAu_2$ / $TiAu_4$ / δ-Au / **Liquid Au-Ti** (1)

Given the fact that the thickness (e) of the first end-member (Ti) of the diffusion couple (e_{Ti} = 2 mm) is much higher than that of the second end-member, Au (e_{Au} < 150 µm), this sequence will remain as it is until the total consumption of the liquid Au-Ti. During this period, as we will see later, the thicknesses of all intermediate phases increase with the isothermal holding time at the expense of Ti and Au end-members.

After the total consumption of the Au-Ti liquid, the δ-Au solid solution becomes the second end-member of the diffusion couple as described below:

Solid Ti / Ti_3Au / TiAu / $TiAu_2$ / $TiAu_4$ / **δ-Au solid solution** (2)

Thus, starting from this moment (noted t* in the following), the thickness of δ-Au phase will decrease with the holding time. Moreover, the driving force of IMCs growth in the new diffusion couple (2) being different from that in the couple (1), a change in the growth rate of IMCs layers will also occur.

For the sample brazed with a gold foil 50 µm thick (Figure 112a), the part of the joint situated between Ti_xO_y and IMCs layers, of about 30-40 µm thick, is entirely composed of large $TiAu_4$ needles in Au-Ti matrix, i.e. of δ-Au phase (zone A). The average Ti content is about 7-8 at% everywhere in the Au-Ti joint (except IMCs) which corresponds to the average Ti content in δ-Au phase at 1100°C. This means that, at brazing temperature, all the Au-Ti liquid (i.e. the second end-member of the diffusion couple (1)) is consumed due to the interdiffusion process and thus to the growth of IMCs and δ-Au phase formed in the Ti / liquid Au couple. Therefore the state of this sample, at the end of isothermal holding for 10 min at 1100°C, corresponds to reaction times higher than t* and thus δ-Au phase (and Ti) is consumed at the expense of IMCs (i.e. t* < 10 min for brazing at 1100°Cwith a gold foil 50 µm thick).

In summary, for reaction times t < t* the thickness of δ-Au layer increases while for t > t* it decreases.

The total consumption of the liquid phase during interdiffusion at constant temperature is often used for practical purposes such as for example the Transient Liquid Phase Bonding (TLPB) process. In TLPB the desired goal is to increase the melting temperature of the joint by performing isothermal solidification. However, in the case of brazing process, the isothermal solidification is not wanted. Moreover, the growth of very irregular reactive layers (for example in the form of large dendrites) can lead to the formation of bridges between the two solids to be joined and thus to the formation of isolated liquid pockets. This configuration might cause defects such as voids at the interface and could be harmful for the mechanical properties of the joint.

Note finally that the main difference between the brazing configuration and sessile drop configuration (discussed in chapter 3), with respect to liquid Au / solid Ti interactions, is the initial thickness e_{Au} (or height h_{Au}) of the liquid gold. Indeed, in brazing configuration the liquid thickness is uniform and varies between 25 and 150 µm, whereas in the case of sessile drop experiments the liquid height is not uniform with a maximal height at the center of the droplet of about 500 µm. Consequently, the values of t* will be different; for exemple at 1100°C: t* < 10 min for brazing configuration with e_{Au} = 50 µm and t* ~ 60 min for sessile drop configuration with h_{Au} = 500 µm (see chapter 3, § 3.2.1).

d) Conclusion

The impact of the gold thickness on zirconia to titanium brazing was studied at 1100°C for 10 min with four gold thicknesses: 25, 50, 100 and 150 µm.

In general, the joints were successfully brazed. However, voids were detected in the thinner joints (25 and 50 µm) at the zirconia side. After brazing, the joint microstructure is composed of four Au-Ti

intermetallics (IMCs) layers at the Ti side, one submicronic Ti oxide (Ti_xO_y) layer on the zirconia side and another large intermediate region containing the δ-Au solid solution and $TiAu_4$ precipitates.

When the initial thickness of Au increases from 25 to 150 µm, the total thickness of the joint increases from about 34 to 134 µm while the total thickness of IMCs decreases from about 24 to 14 µm. Knowing that IMCs are brittle compounds, it is recommended to limit their thickness by using a relatively thick gold filler metal (at least 50 µm).

The intermediate region (between Ti_xO_y and Ti-Au IMCs) is composed of two zones:

- At the IMCs side, a δ-Au solid solution containing large $TiAu_4$ needles, thick of 40-60 µm. This zone consists of δ-Au phase at the end of isothermal holding.
- At the zirconia side, a δ-Au solid solution with an average Ti content lower than the solubility limit of Ti in liquid Au. This zone consists of liquid Au-Ti phase at the end of isothermal holding.

When the joint is too thin (typically below 50 µm), all the liquid is consumed causing a solidification of the joint during isothermal holding at the brazing temperature, which generates defects like voids at the δ-Au solid solution / Ti_xO_y interface. Moreover, this leads to a faster growth kinetics of IMCs which are brittle phases and thus could be detrimental to the mechanical behavior of the joint.

Therefore, it is desirable to braze ZrO_2 and Ti with a relatively thick Au foil (higher than 50 µm) in the temperature range 1070-1123°C. Moreover, a short duration in liquid state is also advised in order not to consume all the liquid gold at the brazing temperature. Based on these results, the gold thickness is set at 100 µm for the rest of the brazing study.

3.2.3. Impact of temperature on the joint microstructure

In order to provide an optimized thermal cycle, the impact of temperature on interfacial reactivity and joint microstructure was studied. The gold foil was 100 µm thick. The joint microstructures of two samples brazed at 1080°C and 1100°C for 17 min in liquid phase, with a total thickness of 70 µm, are compared in Figure 114.

For both samples, the four Ti-Au IMCs are observed at the Ti / joint interface, with a total thickness of about 16 µm for each case (Figure 114a2 and b2).

In the same way, for the two samples, the part of the joint situated between Ti_xO_y and IMCs layers, is composed of two microstructural zones (Figure 114a1 and a2), one containing large needle-shaped $TiAu_4$ precipitates inside a δ-Au phase matrix (zone A) and one, at the zirconia side, without visible $TiAu_4$ needles (zone B). However, the thickness of these zones varies with brazing temperature. Indeed,

for the joint brazed at 1080°C, the width of the zone A is about 40-50 µm (Figure 114a1), whereas it is thinner (30-40 µm) for the brazing performed at 1100°C (Figure 114a2). Thus, at the end of brazing, almost all the liquid gold is consumed at 1080°C (the remained liquid corresponds to the zone B and is less than 10 µm thick) while at 1100°C, the joint contains about 20-30 µm of liquid before cooling. This result is in agreement with the fact that the solubility limit of Ti in liquid gold at 1080°C (~1at%) is significantly lower than at 1100°C (~5 at%).

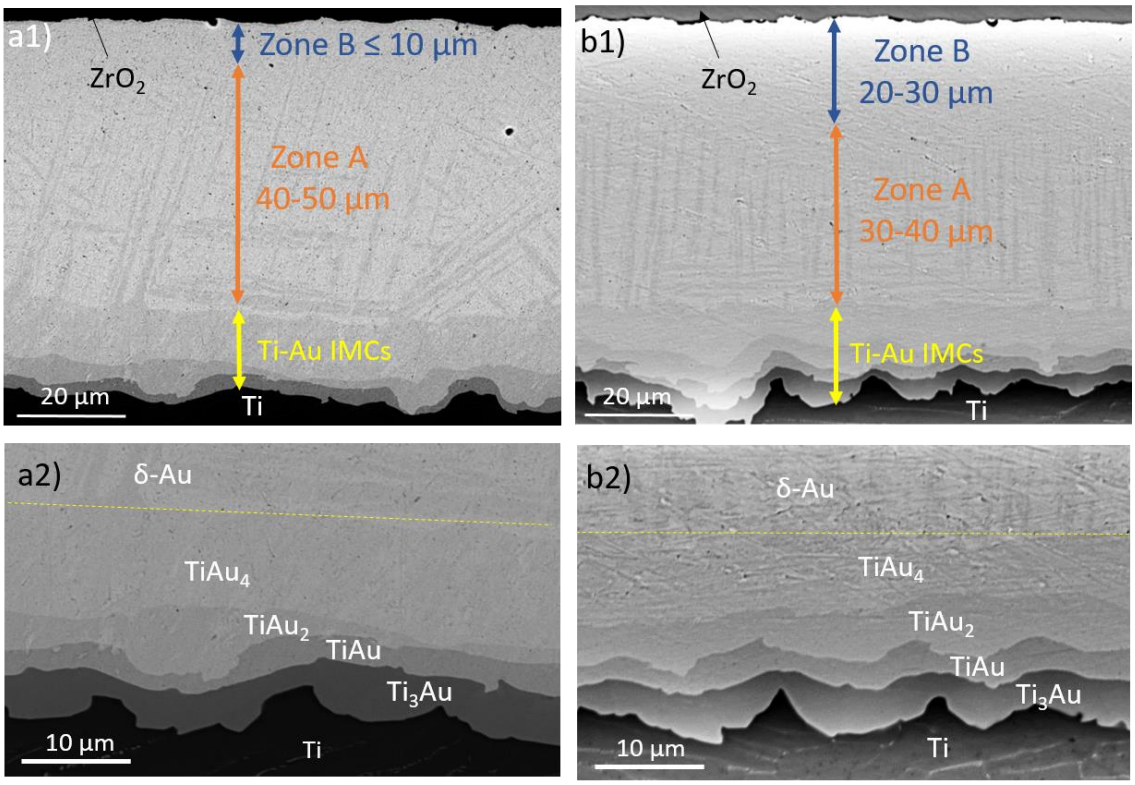

Figure 114: SEM micrographs of ZrO_2 / Au / Ti joints obtained by brazing for 17 min in liquid state a) at 1080°C (general view (a1) and Ti / Au interface (a2)) and b) at 1100°C (general view (b1) and Ti / Au interface (b2)). Gold foil 100 µm thick.

Figure 115 gives SEM micrographs of the ZrO_2 / Au interfaces for two samples brazed at 1080°C and 1100°C for 17 min in liquid state. At the zirconia side, for the lower temperature (Figure 115a), the Ti_xO_y layer is continuous and relatively homogeneous, measuring 300-700 nm everywhere whereas at high temperature, the Ti_xO_y layer has a non-homogeneous thickness ranging from almost 0 to 2 µm (Figure 115b)

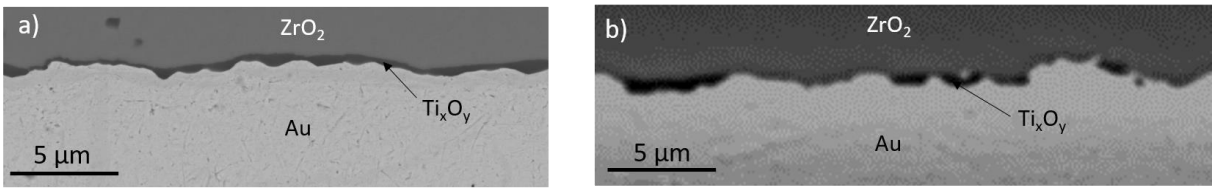

Figure 115: SEM micrographs of ZrO_2 / Au interface obtained by brazing for 17 min in liquid state at 1080°C (a) and 1100°C (b). Gold foil 100 µm thick.

As a conclusion, in the range 1080 – 1100°C, brazing temperature has no significant impact on IMCs thickness. However, given the fact that the solubility limit of Ti into liquid Au at 1080°C is lower than at 1100°C, the thickness of the δ-Au phase layer formed during the brazing process (containing the large $TiAu_4$ needles at room temperature) is thicker at 1080°C than at 1100°C.

Concerning the Ti_xO_y layer formed at Au / ZrO_2 interface, a low brazing temperature is recommended in order to form a relatively homogeneous and submicronic reaction layer that is preferable from a mechanical point of view.

3.2.4. Impact of holding time on the joint microstructure

The impact of brazing holding time (more specifically the liquid phase duration) on the IMCs thickness and joint microstructure was investigated at 1080°C for 3, 17 and 60 minutes. When the holding time increases, two significant changes are noticed on the IMCs thickness and joint microstructure (Figure 116).

First, at Ti / joint interface, the total thickness of Ti-Au IMCs layer increases from about 14 to 24 µm when the holding time increases from 3 to 60 min (Figure 116d).

Second, the thickness of the δ-Au phase layer formed at 1080°C (and containing large $TiAu_4$ needles at room temperature) increases also significantly with brazing time. Indeed, for a duration in liquid phase of 3 min, the large needle-shaped $TiAu_4$ precipitates are not observed at the micrograph scale, and by zooming at the IMCs / joint interface, smaller needles are visible over a zone about 10 µm wide (Figure 116a).

After 17 min in liquid state (Figure 116b), large needle-shaped $TiAu_4$ precipitates are observed over an area about 40 - 50 µm wide, corresponding to almost all the joint zone between Ti-Au IMCs and Ti_xO_y layer. Therefore, after only 17 min at 1080°C, the joint is almost solidified with the formation of intermetallic compounds and a thick solid-solution δ-Au phase layer.

After one hour of brazing at 1080°C, these large $TiAu_4$ precipitates are observed over the entire zone between IMCs and Ti_xO_y. This means that the liquid gold (which is an end-member of Ti / Au diffusion couple) is totally consumed well before the end of brazing process, leading thus to an isothermal solidification of the joint at 1080°C.

Thus, for a long brazing duration (say longer than 30 min at 1080°C), before cooling, the entire joint will be composed of intermetallics and δ-Au solid solution, which becomes a new end-member of the diffusion couple.

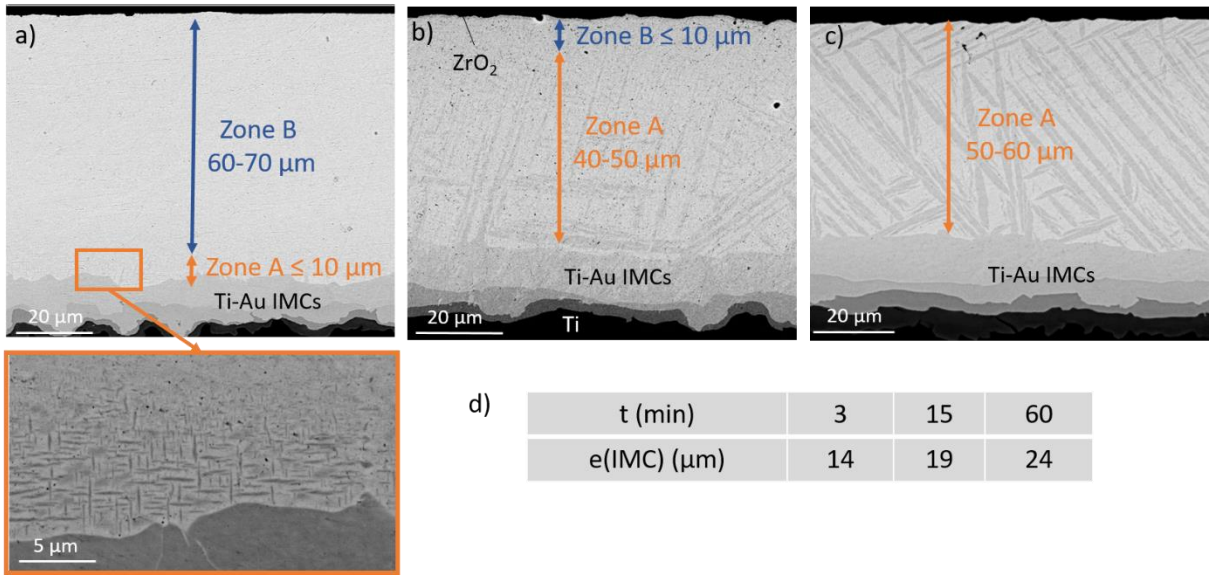

d)

t (min)	3	15	60
e(IMC) (µm)	14	19	24

Figure 116: SEM micrographs of ZrO_2 / Au / Ti joints obtained by brazing at 1080°C for a) 3 min, b) 17 min and c) 1h in liquid state. Gold foil 100 µm thick.

Figure 117 gives SEM micrographs of the ZrO_2 / Au interfaces for the three samples brazed at 1080°C for 3, 17 and 60 minutes in liquid state respectively. This figure shows that, in all cases, the Ti_xO_y layer is continuous and its thickness increases significantly with the holding time. For the holding times of 3 and 17 min the thickness measures 200-400 nm and 300-700 nm respectively whereas for 60 min it is a homogeneous layer about 1 µm thick.

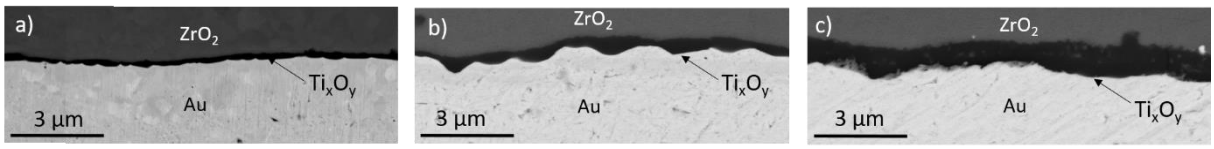

Figure 117: SEM micrographs of ZrO_2 / Au interface obtained by brazing at 1080°C for a) 3 min, b) 17 min and c) 1h in liquid state. Gold foil 100 µm thick.

Figure 118 gives SEM micrographs of titanium substrate near the Ti / Au interface of ZrO_2 / Au / Ti joints obtained by brazing at 1080°C for 3, 17 and 60 min in liquid state. These micrographs clearly show that the diffusion distance of gold at the titanium grain boundaries increases with the brazing holding time. The visible Au diffusion distance at the micrographs scale is respectively about 30, 50 and 100 µm.

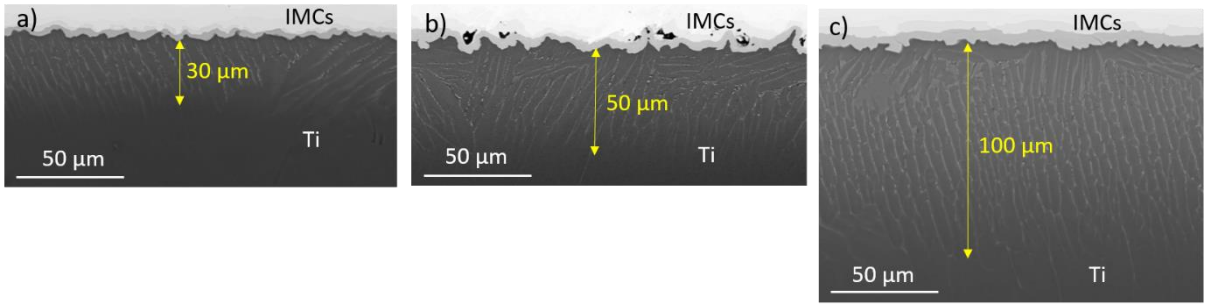

Figure 118: SEM micrographs of Ti / IMCs interface for the ZrO_2 / Au / Ti joints obtained by brazing at 1080°C for a) 3 min, b) 17 min, c) 1h in liquid state, showing diffusion distances of Au through grain boundaries of the Ti substrate.

To conclude, the brazing holding time has a strong impact on the joint microstructure, in particular on the thickness of the Ti-Au IMCs and δ-Au solid solution phase as well as on the thickness and morphology of the Ti_xO_y layer. It has also a significant impact on the gold diffusion distance in titanium substrate. For a very short brazing time (3 minutes in liquid state at 1080°C), using a gold foil of 100 µm thick, the IMCs and δ-Au solid solution layers are relatively thin (respectively ~15 µm and ≤ 20 µm) so the majority of the joint at the end of the brazing process is composed of liquid gold (containing a few titanium content in solution). When the holding time increases, the thicknesses of these layers increase as well through additional consumption of the liquid gold (and solid Ti). At 1080°C, after 17 min in liquid state, almost all the liquid gold is consumed and after 1 h, the entire joint is solidified. As it was detailed in paragraph 3.3.2, this isothermal solidification is not wanted in brazing process because it generates defects in the joint. Therefore, for a ZrO_2 / Au / Ti brazing at 1080°C with a gold foil of 100 µm thick, a short liquid phase duration (< 17 min) is a necessary condition to perform a good brazing.

3.2.5. Study of Ti / Au reactivity at solid state during heating

In the previous sections, we studied the influence of some parameters such as the thickness of Au foil, the temperature and the liquid phase duration on the total thickness of Au-Ti intermetallics as well as on the microstructure of the joint. However, interactions between gold and titanium can also occur during heating, before gold melting. These solid-state interactions become significant only at relatively high temperatures.

With a view to determine the impact of solid-state reactions during heating on the joint evolution, a thermal cycle, similar to brazing cycle, was performed under the melting point of gold. A ZrO_2 / Au / Ti sample was heated up to 1050°C with a heating rate of 8°C/min and immediately cooled at room temperature. At the end of the experience, there is no contact point between zirconia and gold, and

ceramic stays totally white showing that no chemical reaction occurs at the zirconia/gold interface. Figure 119 gives optical and SEM micrographs of the Ti / Au interface after this thermal cycle. Figure 119a clearly shows that Au / Ti contact is punctual, with reactive areas only at some interfacial regions, leading to the local formation of a reaction product consisting of Ti-Au intermetallic compounds (IMCs). Depending on titanium surface state, the total area of reactive interfacial zones, measured from the cross section, varies significantly. Indeed, when a chemical etching of the Ti substrate was performed in order to remove the native Ti oxide layer, the area of reactive interface represents around 65% of the total interface, whereas in the case of raw titanium used after a simple cleaning, the interaction area represents only about 25% of the total interface.

In both cases, the thickness of the reaction product is not homogeneous. In the reactive zones, the average value is about 14µm and can reach 20µm. Four IMCs layers are detected in the reaction product: $TiAu_4$, $TiAu_2$, TiAu and Ti_3Au, i.e. all the stable intermetallics given by the phase diagram of the binary Au-Ti system.

Note that, as it was already described above, the average thickness of the reaction layer at Au / Ti interface after brazing for 10 min at 1100°C is uniform all over the joint (Figure 109) despite the fact that, during heating up to 1050°C, the thickness of IMCs by solid-state diffusion varies drastically from 0 at certain zones (no contact at Au / Ti interface) to about 20 µm at other zones (Figure 119a). These results, reproduced several times, strongly suggest that the IMCs formed by solid-state reaction are partially or totally dissolved in pure liquid gold (just after melting point) until the local concentration of Ti in the dissolution zone attains the solubility limit of Ti in liquid Au at 1100°C (about 5 at% - see Figure 113). Thus, when gold melts, there is a competition between dissolution and growth of the IMCs at the interface. As a result, we can conclude that solid-state reactions at Ti / Au interface, occurring during heating, have no significant impact on the further evolution of the interfacial system during brazing process (solid Ti / liquid Au interactions).

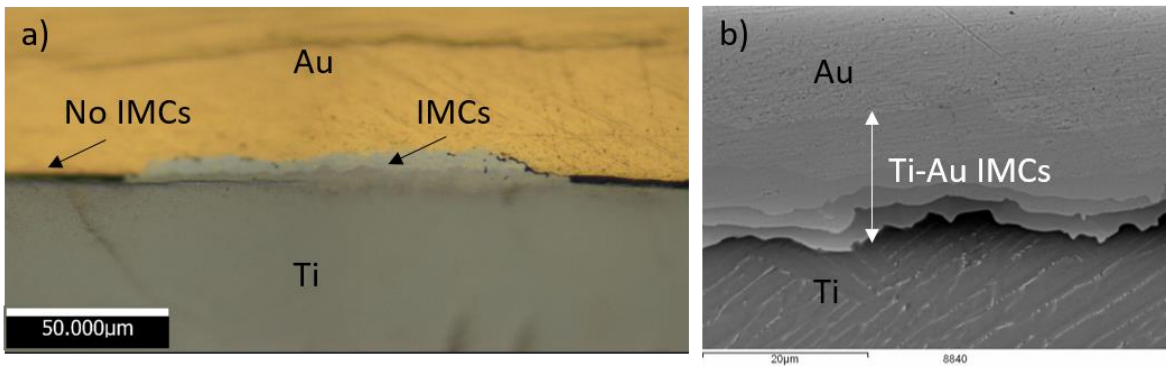

Figure 119. a) Optical and b) SEM micrographs of Au / Ti interface obtained after heating up to 1050°C with a heating rate of 8°C/min and immediately cooled at room temperature, showing the local formation of IMCs at the interface.

3.2.6. Conclusion

ZrO_2 / Ti brazing is performed with pure gold foils thanks to Ti active element, which is provided by the Ti substrate. Ti in liquid gold is provided first by dissolution of Ti substrate and/or IMCs formed during heating and afterwards by diffusion through continuous Au-Ti intermetallic compounds layers formed at Ti / Au interface. Meanwhile, Ti diffuses through the liquid gold towards the ZrO_2 / Au interface where it reacts with zirconia and forms the wettable reaction product Ti_xO_y leading thus to a good wetting of zirconia by the liquid metal.

The impact of several brazing parameters on interfacial reactions was studied in order to understand the reactional mechanisms occurring during brazing, and to propose an optimized brazing process. First, it was shown that gold thickness has a influence on Au-Ti intermetallic compounds thickness and also on the joint microstructure. Brazing ZrO_2 and Ti using thin gold foils (25-50 µm) may cause a total consumption of liquid gold (which is an end-member of Ti / Au diffusion couple), i.e. isothermal solidification. Thus, at the brazing temperature, the entire joint is composed of intermetallics and δ-Au solid solution (which becomes the new end-member of the diffusion couple), and in the worst case only of Ti-Au intermetallics (total consummation of δ-Au). Therefore, it is strongly suggested to braze ZrO_2 and Ti with a thick gold foil (~100 µm) and for a short duration (some minutes) in the temperature range 1070-1100°C. Moreover, the short duration is also recommended to form a homogeneous submicronic Ti_xO_y layer at the zirconia / gold interface. Finally, it was shown that, during heating up to the melting temperature of gold, solid-state reactions occur at the Ti / Au interface and leads to local formation of Ti-Au IMCs of total thickness 0 – 20 µm which depends on the presence (or not) of native Ti oxide at this interface. However, these IMCs could be partially or totally dissolved in pure liquid gold so that, after brazing (i.e. after liquid state reactions), IMCs layer has a relatively homogeneous thickness everywhere at the interface. Thus, titanium surface state (raw Ti or etched Ti) has no significant impact on brazed joint microstructure.

3.3. ZrO_2 / Ti brazing using a pure Au foil 100 µm thick at 1080°C

3.3.1. Introduction

Based on the experimental results presented in the previous section (parametric study), the optimized brazing conditions are set. Therefore, ZrO_2 / Ti brazing is performed under high vacuum with a gold thickness of 100 µm, using a raw titanium substrate (with no etching). Brazing temperature and liquid phase duration are limited at 1080°C for 3 min.

Recall that, under these brazing conditions, the bulk microstructure of the joint shows a large zone containing less than about 5 at% Ti (zone B in Figure 116a), which means that a large quantity of liquid Au-Ti alloy remains at the end of the isothermal holding at the brazing temperature. Moreover, under these conditions:

- Ti-Au IMCs have relatively thin thicknesses and $TiAu_4$ needles are smaller compared to those obtained with a thin Au foil (25 µm).
- The Ti_xO_y reaction layer formed at the Au / ZrO_2 interface is a relatively homogeneous and thin layer (200 – 400 nm).

In this section, a more in-depth study of the joint microstructure and interfacial reactions at both substrates / joint interfaces is carried out in the case of zirconia / titanium brazing performed with these experimental conditions.

Physico-chemical investigation was performed on tensile specimens cross sections, in order to reproduce the same brazing conditions as for the samples used for the mechanical characterizations (described in the next section), in particular the filler Au metal size (thickness and width), the external pressure applied on the joint and the same oxygen partial pressure P_{O2} (i.e. the proximity of the joint to a getter and/or graphite tool).

Firstly, characterizations of the brazed joint by FEG SEM will be detailed. Then, TEM observations and EDX analyses of the ZrO_2 / Au interface will be presented, in particular the Ti_xO_y reaction product layer. The impact of oxygen partial pressure P_{O2}, in the furnace during brazing, on the Ti_xO_y product layer formation and growth will be discussed. Finally, reactional mechanisms occurring at Ti / liquid phase interface as well as phase transformations taking place during cooling of the joint will be presented and discussed.

3.3.2. Physico-chemical characterization of the brazed joint

Being the reference brazing conditions of the thesis, several ZrO_2 / Au / Ti samples were brazed at 1080°C for 3 min with a 100 µm thick Au foil. All of the joints have an excellent general aspect, with no defect like voids or cracks. The only imperfection observed is the thickness heterogeneity of the formed joint. Indeed, for one tensile specimen, the resulting gold thickness varies from 30 to 160 µm despite the fact that braze Au preforms are 100 µm ± 15 µm thick. Nevertheless, despite this thickness variation still high, sealing of the joints is observed.

A cross section of a reference brazed joint was performed in order to be analyzed by FEG SEM and TEM. The Esprit 2.3. Software from Bruker was used to collect and treat the data. First, a general view of the joint is given in Figure 120a with the Au map (in yellow, Figure 120b) and Ti map (blue color, Figure 120c). The joint has a homogeneous thickness of about 80 µm and the bulk microstructure is uniform with no visible $TiAu_4$ needle at the scale of this micrograph.

Notice the thin and continuous Ti_xO_y reaction layer at the Au / ZrO_2 interface, characterized by a drastic and local increase in Ti content. At the Ti / Au interface, the Ti and Au contents change over Ti-Au IMCs layers. A significant Au amount is detected in Ti substrate in the region close to IMCs, corresponding to gold diffusion in titanium.

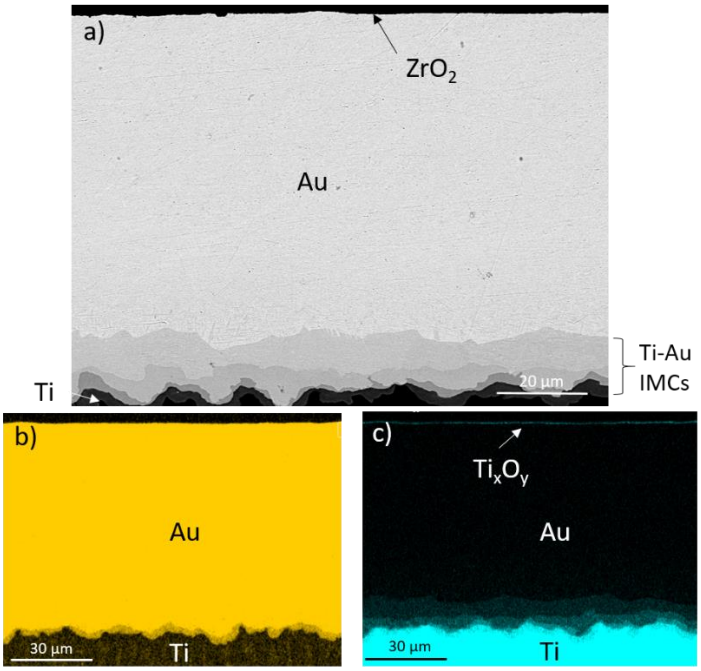

Figure 120: SEM micrograph (a) and EDX analysis (b, c) of ZrO_2 / Au / Ti joints obtained by brazing at 1080°C for 3 min, showing Au (b) and Ti (c) mapping.

a) Diffusion of Au in Ti substrate and consequences on Ti microstructure

The gold diffusion in metallic substrate, introduced in section 3.2.4., is investigated in depth in Figure 121. In Ti substrate, near the IMCs, solid-state diffusion of Au into Ti is observed over a distance of about 50 µm (Figure 121a, d and e). Au diffusion occurs both in volume and especially at the grain boundary, where small precipitates containing Au are observed at SEM (Figure 121b) and TEM scales (Figure 121c), having a stick shape of a few micrometers long, and a diameter of about 200 nm.

Figure 121d presents the Au diffusion profile over 120 µm in depth, averaged on 60 µm in width. Au content in α-Ti solid solution decreases from about 4 to 0 at% moving away from the IMCs / Ti interface.

The fact that the average Au content in α-Ti near the Ti / IMCs interface reaches 4 at %, strongly suggests that locally, at the region close to the grain boundary, Au content could be significantly higher than 4.2 at% Au, which corresponds to Au content in β-Ti at 832°C (eutectoid transformation) indicated by the point E on the Ti-rich side of the Au-Ti phase diagram (Figure 121f). Therefore a gold concentration gradient exists inside Ti grains (at least for grains far from the Ti / IMCs interface), from the center of the grains to the grain boundary. If we assume that the small precipitates are not formed during isothermal holding at 1080°C but during cooling, then at grain-scale, the Au content varies from the grain boundary to the grain center, in the range 0 - C_S, where C_S is the Au concentration of point S (Figure 121f) at 1080°C which corresponds to about 7 at% Au.

Thus, after cooling from 1080°C to room temperature, and according to the local concentration of gold in β-Ti phase (Figure 121f), the microstructure of Ti substrate near the IMCs is mainly composed of α-Ti grains with Ti_3Au precipitates localized at the grain boundary and eutectoid mixture ($\alpha\text{-}Ti^e + Ti_3Au^e$). Note however that it cannot be excluded that Ti_3Au compound (or other IMCs) may precipitate at the grain boundaries of β-Ti phase during the isothermal holding at 1080°C. An in-depth study of the precipitates composition would allow to confirm if TiAu, $TiAu_2$ and $TiAu_4$ are formed or not at the grain boundaries of β-Ti phase during the isothermal holding at 1080°C.

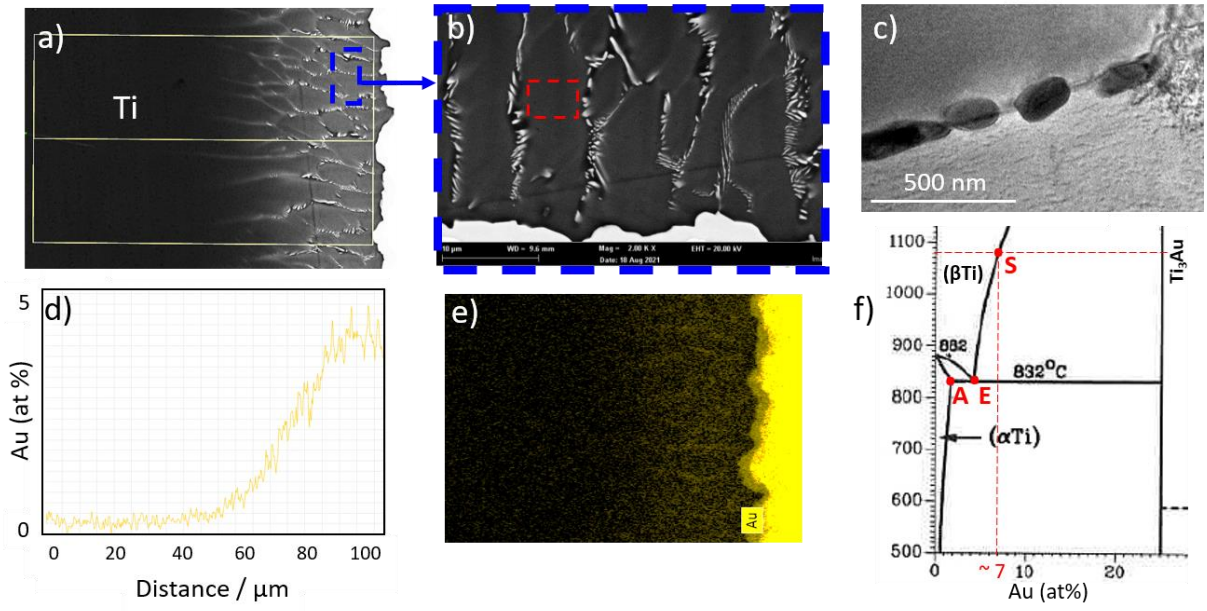

Figure 121: SEM micrograph of the titanium substrate near the Ti / IMCs interface (a), SEM micrograph showing white precipitates in Ti substrate (b), TEM observation of the precipitates formed at the grain boundaries of β-Ti phase (c), Au diffusion profile over ~ 120 µm (d), Au mapping showing solid-state diffusion of Au into Ti (e), Ti-rich side of the Au-Ti phase diagram[2] (f).

b) *Microstructure of Au / Ti interface*

Figure 122 gives secondary electron and back-scattered electron micrographs of the Au / Ti interface for two different zones. The four Ti-Au intermetallic compounds Ti_3Au, TiAu, $TiAu_2$ and $TiAu_4$ are observed, with an average thickness of about 14 µm. The wavy layers have different thicknesses: Ti_3Au and TiAu have a similar thickness of about 2 µm (ranging from 1 to 5 µm), $TiAu_2$ is a bit thicker ~3 µm (ranging from 2 to 7 µm), whereas $TiAu_4$ is well thicker (~ 8 µm ranging from 3 to 10 µm). The interface between δ-Au and $TiAu_4$ is rather flat compared to the other wavy interfaces situated between $TiAu_4$ and Ti. Moreover, very fine $TiAu_4$ needles are observed in δ-Au matrix, near the IMCs layer (Figure 122a) and the eutectoid microstructure in the titanium is highlighted (Figure 122b).

EDX spectra of the four Ti-Au layers are overlapped and presented in Figure 122c. Only Ti and Au elements are detected, and the Ti content decreases from Ti substrate to the joint. Figure 122d presents Ti and Au contents of each layer with the accuracy of 1 at%, measured by EDX in the SEM observation conditions 20 kV, WD : 9,5 mm. The measured concentrations are very close to the theoretical values.

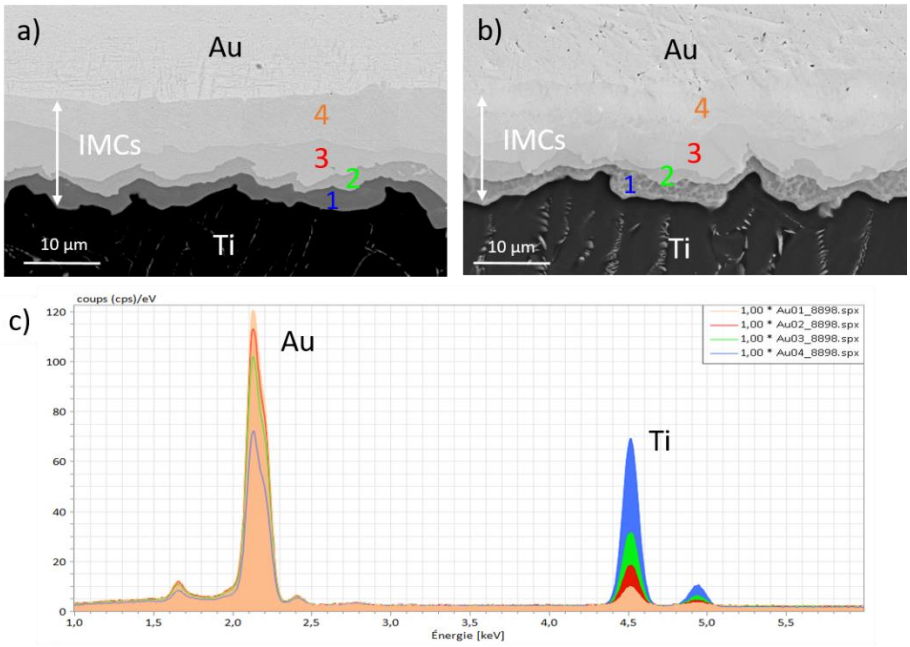

d)

Layer	Ti at%	Au at%	Possible phase
1	75	25	Ti_3Au
2	49	51	TiAu
3	32	68	$TiAu_2$
4	17	83	$TiAu_4$

Figure 122. Backscattered electrons (a) and secondary electrons micrographs (b) of the Ti / Au interface showing the four Ti-Au intermetallics (IMCs), overlapped EDX spectra of the four IMCs (c) and Ti and Au contents of the four Ti-Au layers at the Au / Ti interface, measured by EDX (d).

Figure 123 gives Ti content profile, performed by EDX with a pixel size of 190 nm, over the successive layers forming the Ti / Au interface. Between intermetallic compounds, a jump of Ti content is observed, in good agreement with the Ti-Au binary phase diagram. Ti content in each layer is almost homogeneous, with a slight concentration gradient lower than 5 at%. On the right part of the Ti profile, Ti content into gold varies in the range 5-10 at%, which is characteristic of the δ-Au solid solution formed isothermally during the hold at the brazing temperature (1080°C), and leading during cooling to the formation of $TiAu_4$ needles in a δ-Au matrix (with a very low amount of Ti at room temperature). The average concentration of Ti in this layer (about 7 at%) is in agreement with the Ti-Au phase diagram showing that the concentration range of Ti content in δ-Au solid solution is about 5 to 10 at% at 1080°C.

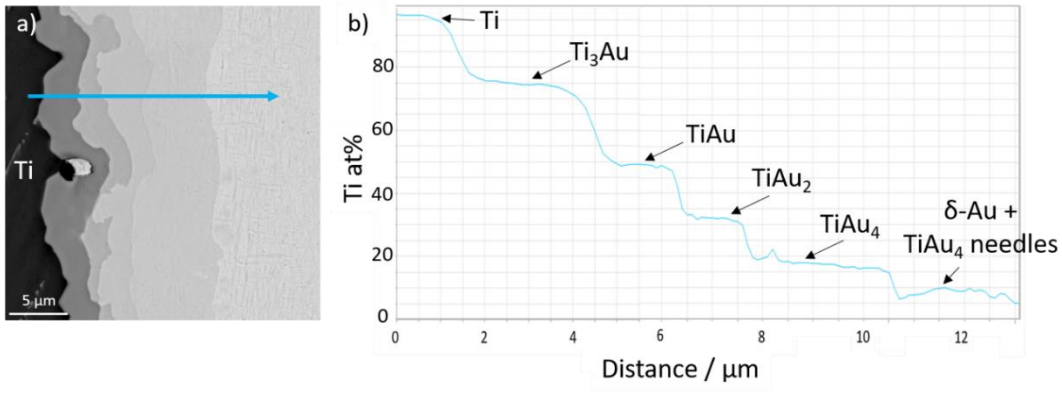

Figure 123. SEM micrograph of the Ti / Au interface after brazing at 1080°C for 3 min (a), Ti content profile performed by EDX along the blue arrow from Ti substrate to δ-Au solid solution phase (b).

A thin slice (~100 nm thick) was extracted at the Ti / Au interface by FIB (focused ion beam), in order to observe this interface by TEM (transmission electron microscopy), especially IMCs grains and interfaces between IMCs phases. Unfortunately, the thin slice was not extracted from the overall thickness of IMCs, so we could not achieve the desired analyses and thus only the Ti_3Au layer is observed at Ti / Ti_3Au interface (Figure 124). This layer is composed of coarse grains, about 2-3 µm, in the size of the Ti_3Au layer thickness. On the left side of Figure 124, we can also observe submicronic Ti_3Au precipitates at the grain boundaries of Ti substrate.

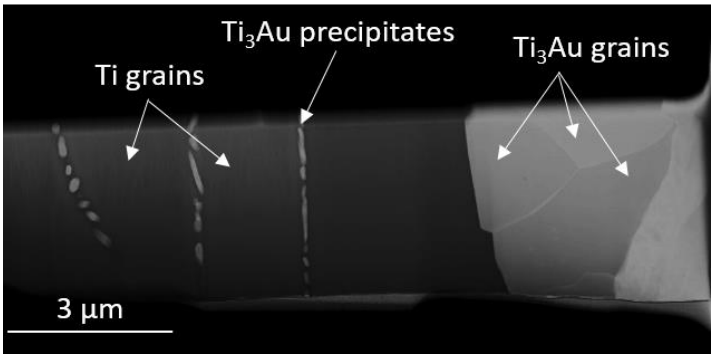

Figure 124. TEM micrograph of the Ti / Au interface showing Ti and Ti_3Au grains (after brazing at 1080°C for 3 min).

c) Microstructure study of the ZrO_2 / Au interface

After analyzing the Ti side of the braze joint, the second joint / substrate interface is investigated, that is zirconia / gold interface and especially the Ti_xO_y reaction product layer.

As it will be presented in the fourth section of this chapter, the partial pressure of oxygen (P_{O2}) in the furnace during brazing process has a significant impact on the mechanical properties of the brazed joints. Indeed, the presence of Zr getters in the furnace during brazing leads to a significant modification of the mechanical response of the brazed assemblies. A microstructural modification of the ceramic / gold interface and in particular the Ti_xO_y layer, could be at the origin of this effect. For this reason, the zirconia / gold interface formed in both brazing conditions (with and without getter) is precisely characterized by SEM and TEM.

Figure 125 gives typical SEM images of the Au / ZrO_2 interfaces, for samples brazed without getter (Figure 125a) and with getter (Figure 125b). These images show that Ti_xO_y layer is continuous with a homogeneous thickness of 200-400 nm everywhere at the interface. This reaction layer exhibits an almost scallop-shaped morphology, a signature of nucleation and growth of Ti_xO_y crystal grains forming the layer. No significant difference between the two interfacial layers is observed at the SEM scale.

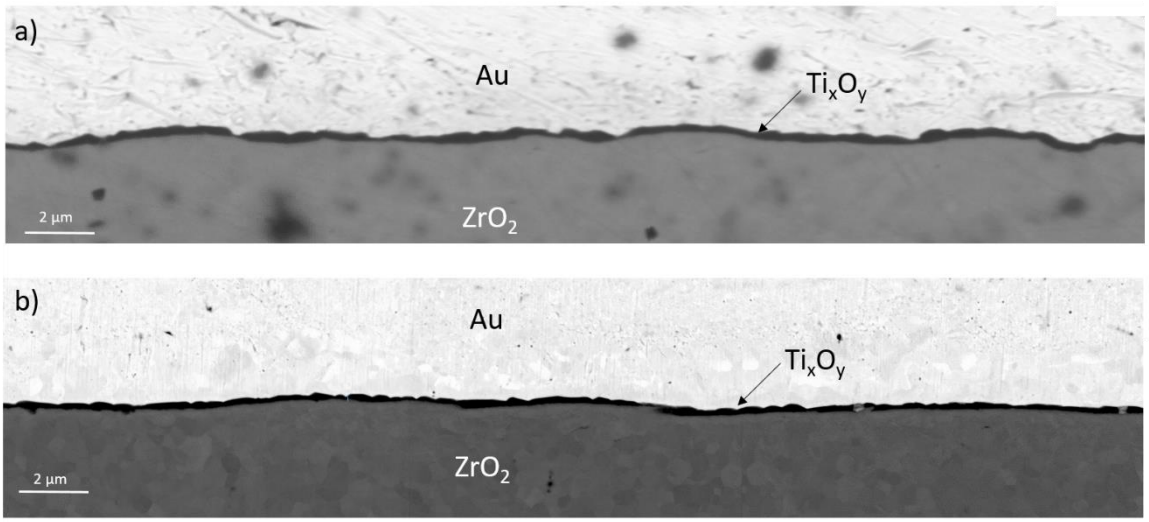

Figure 125: SEM micrographs-stitching of the ZrO_2 / Au interface after brazing at 1080°C for 3 min performed without (a) and with getter (b).

Regarding the submicronic dimension of the Ti_xO_y layer, TEM analysis was performed in order to characterize the reaction product layer, as well as zirconia and gold near the reaction layer. For the purpose of comparing this interface in both brazing conditions, namely with and without getter, a thin

slice of ~100 nm of thickness was extracted at the zirconia / gold interface for each sample by FIB (focused ion beam). In a view of a comparative study by EDX (Energy dispersive X-rays spectroscopy) and EELS (Electron energy loss spectroscopy), the thicknesses of both thin slices should be as close as possible. For this reason, the extracted thin slices foils were stick together and polished at the same time (Figure 126). The two thin foils are thus simultaneously introduced in the TEM and analyzed in the same conditions.

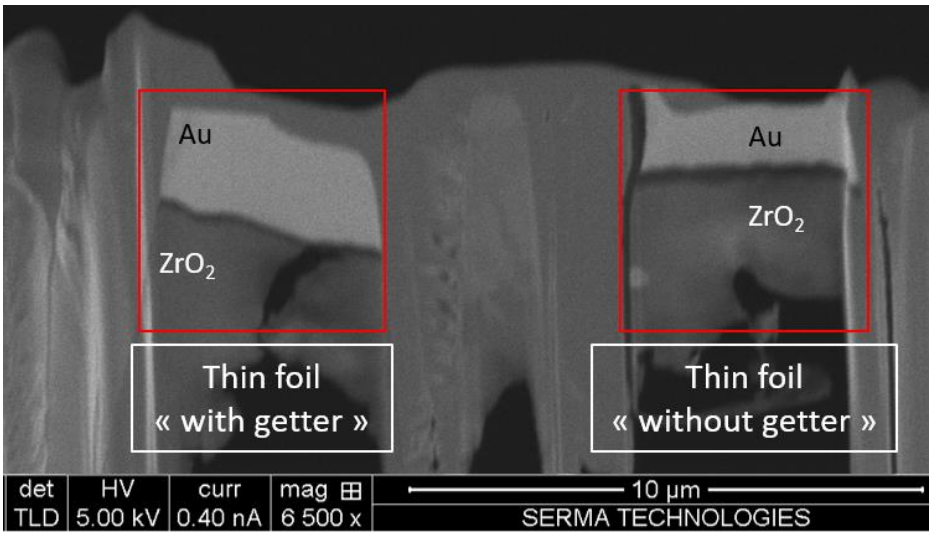

Figure 126: In-lens SEM micrograph of thin slices extracted at ZrO_2 / Au interface (samples brazed with and without getters) obtained after FIB finishes.

Figure 127a-d gives bright field images of the zirconia / gold interfaces without getter (a and b) and with getter (c and d) of the thin slices presented above.

Figure 127a-b shows that, for the sample performed without getter, the Ti_xO_y layer is homogeneous in thickness. Moreover, it clearly shows the granular morphology of the Ti_xO_y layer with a grain height (h) equal to the thickness (e) of the layer and a length (l) greater than e. This result is in agreement with SEM observation given in Figure 125a.

In the case of the sample performed with getter, the grain size of the Ti_xO_y layer is also relatively homogeneous in thickness (Figure 127c-d) but it is difficult to distinguish the grains of this layer. However, TEM observation of another sample brazed with getter (Figure 127e-f) shows a scallop-form of Ti_xO_y layer, composed of a single grain in thickness, with an average length of about 0.7µm. This result strongly suggests that disparity in the layer morphology could be due to the location of the observations, rather than to the oxygen partial pressure used during brazing of the analyzed samples. The bulk microstructure of zirconia is composed of "coarse grains" measuring 100-900 nm. In both cases (samples brazed without getter - low P_{O2} or with getter - very low P_{O2}), small grains of zirconia (< 50 nm) are observed in a zone very close to the Ti_xO_y layer (200-400 nm thick). This zone is often in

contact with the Ti_xO_y layer and it always extends at a distance of less than 1 µm from the zirconia / Ti_xO_y interface. No difference of composition is observed between small and coarse grains. This could be due to the tetragonal-to-monoclinic transformation of zirconia at low temperatures (70° to 130°C)[3] accelerated by the mechanical constraints induced at Au / ZrO_2 interface during cooling of the brazed samples. However, more work is needed to understand the phenomena leading to the formation of the small grains of zirconia at this interface.

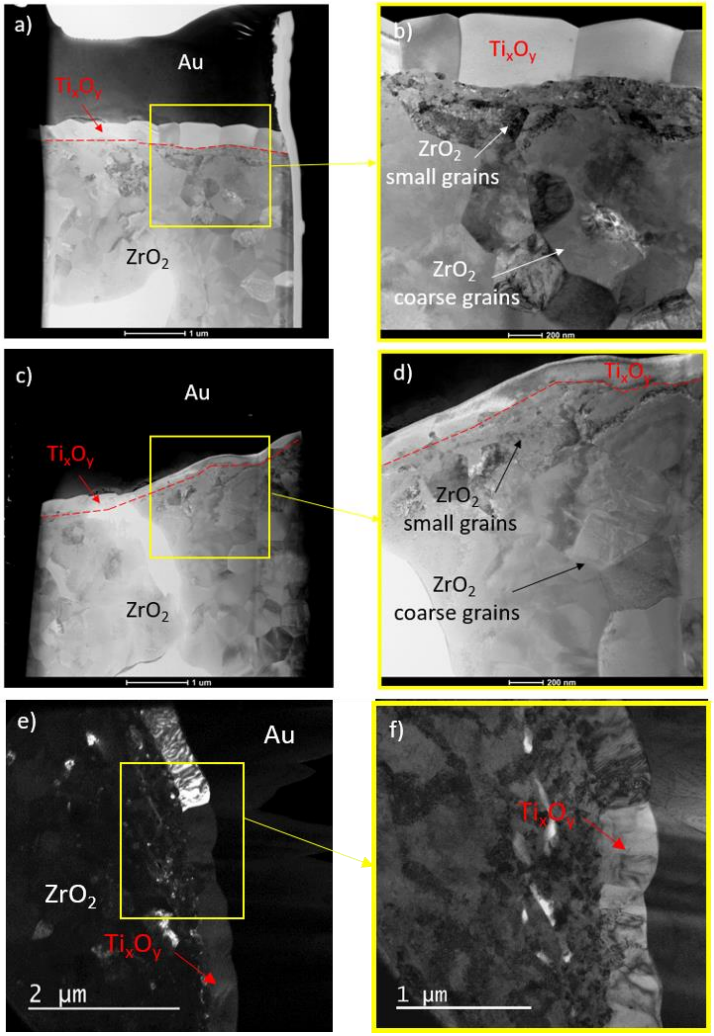

Figure 127: TEM micrographs of the ZrO_2 / Au interface of three samples brazed at 1080°C for 3 min : sample 1 (a-b) was performed without getter whereas samples 2 (c, d) and 3 (e, f) with getter. The extracted thin slices of samples 1 and 2 were stick together and polished at the same time (see Figure 126) and are simultaneously introduced in the TEM.

Semi-quantitative chemical analyses of samples presented in Figure 128a-d were performed. Figure 128a and b give Au, O, Ti and Zr concentration profiles through the Ti_xO_y layer, averaged over 100 nm of thickness (marked by the red rectangles) from Au joint to zirconia substrate, for the samples respectively brazed without and with getter. In both Ti_xO_y reaction layers, no trace of zirconium is detected and Ti and O concentrations are quite similar (around 50 at%), suggesting that the formed reaction layer could be TiO oxide which is stable within a large oxygen concentration range (see Figure

31, chapter 1 - Ti-O phase diagram). Note that very low gradients of Ti and O concentrations are observed through the reaction layer when brazing without getter (Figure 128a), whereas significant gradients are observed through the Ti_xO_y layer when brazing with getter (Ti and O concentrations vary of about 10 at% between Au / Ti_xO_y and Ti_xO_y / ZrO_2 interfaces) - Figure 128b. However, a second diffusion profile, performed on another zone of the Ti_xO_y layer of the same sample after brazing with getter, shows that no concentration gradient is observed through this layer (see appendix 3). Thus, the difference could be attributed also to the location of the observed zone and not necessarily to oxygen partial pressure during brazing. Note that, as it has been mentioned before, the thickness of Ti_xO_y layer is not homogeneous and it is similar for both brazing cases with and without getter - (see Figure 128) and thus, in the case of TEM analysis, it could depend on the location of the analyzed zone.

Therefore, no significant difference of thickness, morphology and composition of Ti_xO_y layer is observed for samples brazed with and without getter.

Finally, it should be pointed out that these semi-quantitative chemical analyses show a high Zr content in gold (about 7at%) which is in total contradiction with a simple mass balance for reaction between ZrO_2 and Ti leading to the formation of a Ti oxide layer less than 1 µm thick. This point will be discussed in detail in the next paragraph.

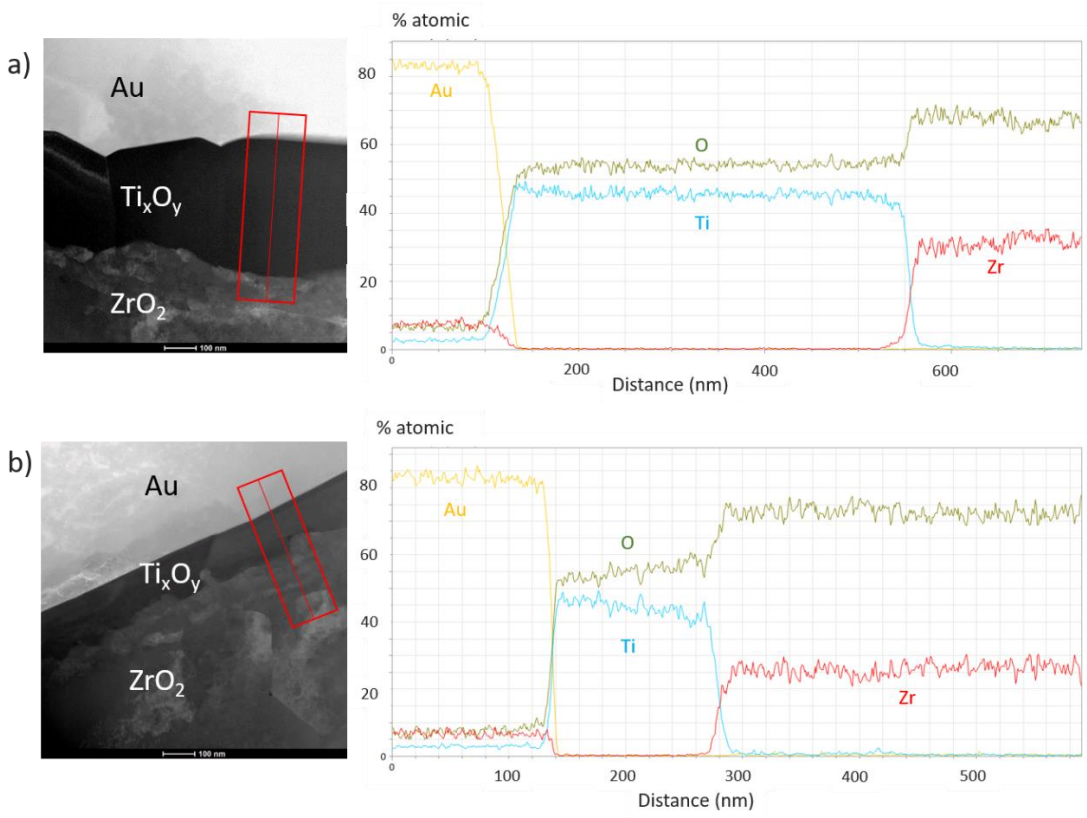

Figure 128: EDX profile over the Ti_xO_y reaction layer of samples brazed at 1080°C for 3 min without getter (a) and with getter (b).

Electron diffraction patterns of both Ti_xO_y layers, when brazing without and with getter, show that these layers are crystallized. However, from the obtained diffraction patterns, it was not possible to determine the precise nature of these layers and therefore more work and in-depth analyses is needed to achieve this goal.

EELS (electron energy loss spectroscopy) spectrum of Ti_xO_y layers presented in Figure 129, analyzed near the Ti_xO_y / Au interface (zone marked with a green square) and near the Ti_xO_y / ZrO_2 interface (marked with a red square), as well as the diffraction patterns of these zones, show for both samples that, Ti_xO_y layer is composed of a single phase whatever the analyzed zone. Moreover, EELS analyses clearly show that Ti_xO_y layer for both samples (brazed with and without getter) consists of the same chemical nature phase. Compared to EELS spectra of Ti_xO_y taken from literature[4], the number and form of ELNES peaks (energy loss near edge structure) and the relative peak height suggest either a Ti_2O_3 or TiO stoichiometry and exclude TiO_2 (well-marked double peak for L_2 and L_3 of Ti as well as for O K in TiO_2).

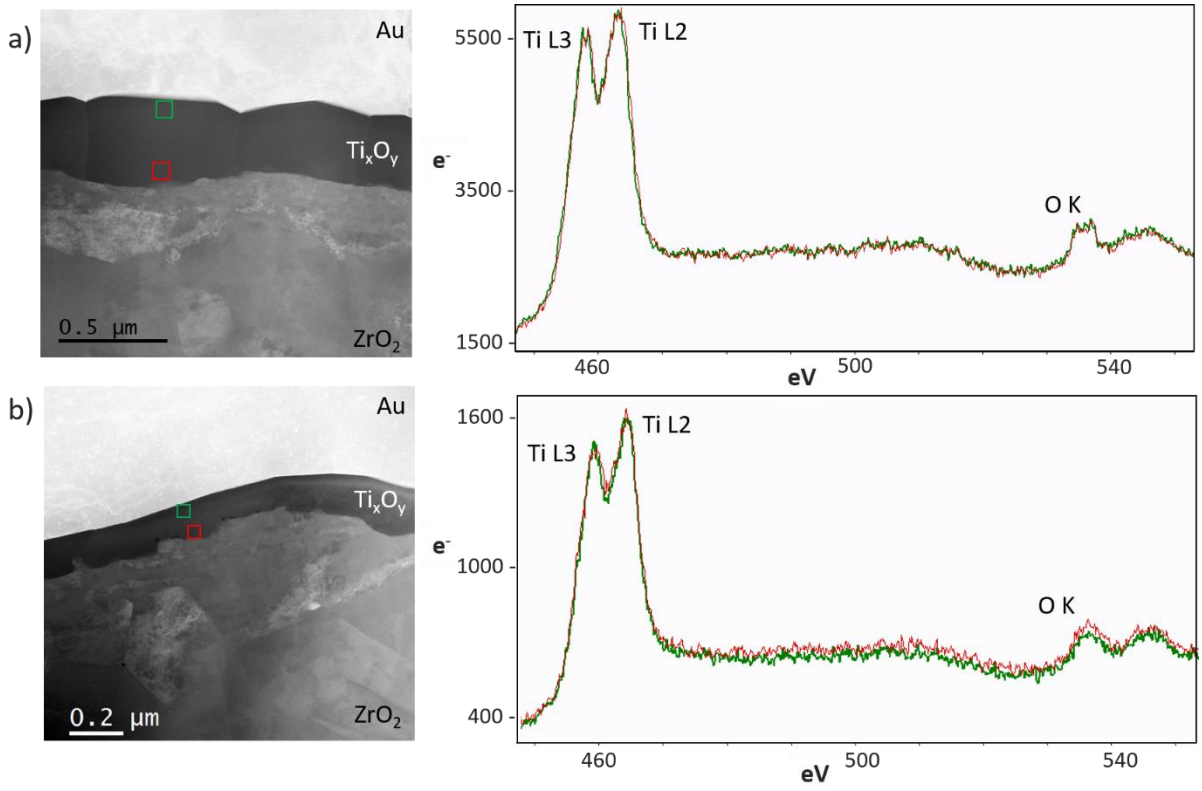

Figure 129: TEM micrographs and EELS spectra in two areas (green-square near the Ti_xO_y / Au interface, red-square near the Ti_xO_y / ZrO_2 interface) of Ti_xO_y reaction layers of samples brazed at 1080°C for 3 min without getter (a) and with getter (b).

Figure 130 gives a cartography of Ti element in zirconia near the Ti_xO_y layer, on two different zones. For both brazing conditions (with and without getter), Ti diffusion is observed in zirconia substrate over a distance of about 300 nm. Ti diffusion occurs both in volume and especially at the grain boundaries.

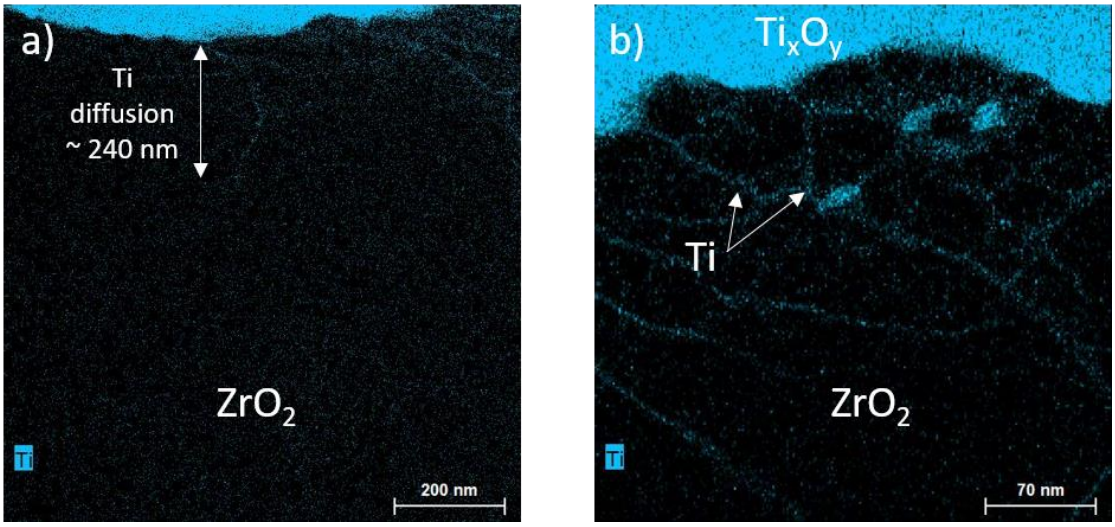

Figure 130. EDX mapping of Ti element in ZrO_2 near Ti_xO_y reaction layer.

d) Microstructure study of the joint

Figure 131 gives a diffusion profile of Ti over Au layer performed by EDX with a pixel size of 200 nm. Ti content in gold is continuous and decreases from about 6 at% at IMC / Au interface to about 1-2 at% at the Au / ZrO_2 interface. Notice on the right part of the diffusion profile, a sharp increase of Ti content, which corresponds to the Ti oxide reaction product layer formed at the gold / zirconia interface.

According to these semi-quantitative analyses and the Ti-Au phase diagram, during isothermal holding at 1080°C, the joint is composed of Au-Ti IMCs, the δ-Au solid solution at the Ti side, and liquid gold containing some at% Ti at the zirconia side. However, no jump of Ti content is observed in the Ti concentration profile in the region between $TiAu_4$ layer and Ti oxide layer (marked by the red dotted line in Figure 131). Moreover, the joint microstructure from $TiAu_4$ to Ti oxide layer seems to be continuous at this scale while it was not continuous in the case of Figure 116a and Figure 123 where small $TiAu_4$ needles were observed only in an area close to IMCS about 10 µm wide. In any case, it is very difficult to detect a practical jump of Ti concentration at the solid δ-Au / liquid Au-Ti interface because the Ti contents of both interfacial phases at equilibrium at 1080°C are very close (~ 2.5 and 1.5 at% Ti for solid δ-Au and liquid Au-Ti phases respectively). However, knowing that the Ti content range in δ-Au phase at 1080°C is ~ 2.5 to 10 at % Ti, and assuming the Ti content profile in Figure 131 as being correct, we can estimate that the thickness of solid δ-Au layer is not very thick (< 30 µm), so

the majority of the joint between $TiAu_4$ layer and Ti_xO_y layer consists, at the end of the isothermal holding at 1080°C, of liquid gold with Ti in solution. This configuration is strongly recommended to achieve a good brazing without defect.

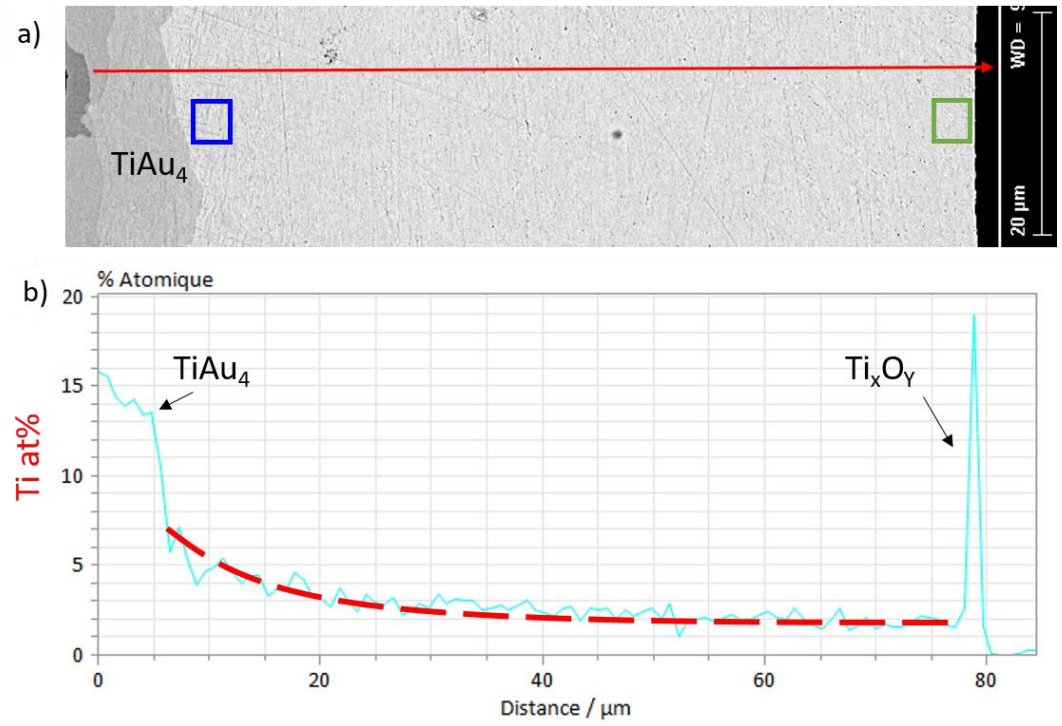

Figure 131: Ti concentration profile across the joint from $TiAu_4$ to ZrO_2 for a sample brazed at 1080°C for 3 min.

It is important to note that brazing time at 1080°C must be limited in order to avoid isothermal solidification of the joint, corresponding to a total consumption of liquid gold. Thus, for an extended duration at 1080°C, the δ-Au phase may be formed on the entire joint, including at the joint / zirconia interface, which can generate defects.

Note finally that EDX analysis of the sample, brazed at 1080°C for 3 minutes, shows that the Zr content in the joint is ~10 and 3.5 at% Zr in two regions situated at a distance of ~7 and 20 µm from the Ti_xO_y / Au interface and it continues to decrease down to ~ 0.8 and 0.4 at% Zr in the regions situated at a distance of ~30 and 15 µm from the IMCs / δ-Au interface. The estimated average content in the joint is about 2.1 at% Zr. Similar Zr contents were measured also by EDX analysis (see appendix 4) for two other samples brazed at 1080°C for 17 and 60 min. The semi-quantitative analysis of Zr content has been performed by peak deconvolution (without reference samples) taking into account the K-ray of Zr (at 15.8kV) which does not overlap any other peak. Indeed, the L-rays of Zr overlap the M-rays of Au between 1.6 and 3 keV, which makes peak deconvolution more complex.

Thus, the uncertainty of these analyses can be high and consequently should be considered only as qualitative values. Indeed, a simple mass balance for Zr element during the brazing process shows that the average Zr content in the joint should be much lower than 2.1 at% Zr. The maximum Zr content in the joint can be evaluated by considering the following reaction between zirconia and Ti leading to the formation of a stoichiometric TiO oxide layer 0.5 µm thick:

$$ZrO_2 + (Ti)_{Au} \rightarrow 2TiO + (Zr)_{Au}$$

where $(Ti)_{Au}$ and $(Zr)_{Au}$ designate respectively Ti and Zr dissolved in liquid Au.

Knowing the molar volumes of ZrO_2 (21.7 cm^3/mol), TiO (12.8 cm^3/mol) and liquid Au (10.2 cm^3/mol) [5,6], it can be easily calculated that the average content of Zr in the liquid Au (~ 70 µm thick) due to the formation of a TiO layer 0.5 µm thick is equal to ~ 0.3 at% Zr. This value is almost one order of magnitude lower than that estimated by EDX analysis (2.1 at% Zr).

e) Conclusion

In this section, a fine microstructural analysis of the joint brazed at 1080°C for 3 min was presented.

At titanium / gold interface, the four Ti-Au intermetallics compounds given by the binary phase diagram are formed, with an average thickness of about 14 µm. Au diffusion is observed in titanium substrate over a distance of about 60 µm leading to the formation of Ti_3Au precipitates at the grain boundaries of Ti.

At the zirconia / Au interface, a submicronic (200 - 400 nm) and continuous reaction layer of a titanium oxide is formed. This layer consists of one single crystallized titanium oxide. No significant difference of Ti_xO_y (morphology, thickness, composition) is observed when samples are brazed with getter (low oxygen partial pressure, P_{O2}) or without getter (higher P_{O2}).

The microstructure of the joint in the zone situated between Ti-Au IMCs / Au and Au / ZrO_2 interfaces should be constituted of δ-Au and $TiAu_4$ phases. However, at the SEM scale, the $TiAu_4$ phase is observed only at a region ~ 10 µm width near the Au-Ti IMCs in the form of needle-like precipitates within the δ-Au phase matrix.

At the brazing temperature (1080°C) the zone situated between $TiAu_4$ layer and Ti_xO_y layer is constituted of δ-Au and Au-Ti liquid phases which both transform during cooling in Ti-depleted δ-Au phase (containing ~ 1at% Ti at room temperature) and $TiAu_4$ precipitates.

No significant difference was observed between samples brazed with and without getter, neither at Ti side nor at ZrO_2 side.

3.3.3. Schematic evolution of the ZrO_2 / Au / Ti system and growth mechanism of reaction layers

In light of the present microstructural study conducted on ZrO_2 / Au / Ti brazed joint, a mechanism of joint formation over time is proposed at the isothermal hold of brazing.

As previously discussed, whether Ti reacts or not in solid-state with Au during heating below gold melting, as soon as Au melts (at 1064°C), there is dissolution of Ti and/or IMCs in liquid Au. This dissolution occurs until over-saturation of Ti in liquid Au near the Ti / Au interface, that is, Ti content in liquid Au at the interface exceeds the solubility limit (about 1.5 at%Ti at 1080°C).

From a thermodynamic point of view, there is then nucleation and growth of the four Ti-Au IMCs (i.e. Ti_3Au, TiAu, $TiAu_2$ and $TiAu_4$) and the δ-Au phase. As already mentioned in chapter 3, for most of binary systems, the sequence of formation and growth of intermediate phases at reactive interfaces is not yet known and this is the case also for the binary Au-Ti system. For Au-Ti system, this is a complex process until the formation and growth of five successive and continuous reaction layers as it was observed experimentally. Nevertheless, it is well known from the literature that the growth kinetics of all reaction layers in Au-Ti system follow a parabolic growth law at temperature range 837 - 900°C [7,8]. These results strongly suggest that the rate controlling step of the growth process at higher temperatures (here at 1080°C) is the interdiffusion process through the reactive layers. Thus, the thermodynamic equilibrium is attained at all the reactive interfaces of Au-Ti system at 1080°C. Under these conditions, a quasi-steady state of the system is achieved except for liquid Au because its concentration in Ti increases over time until the saturation (about 1.5 at%Ti at 1080°C). From this moment, the growth of the five reactive layers occurs by interdiffusion process and reaction at interfaces is controlled by the diffusion through the reactive layers.

A schematic representation of the whole system, when the quasi-steady state at the brazing temperature is attained, is given in Figure 132a where the thicknesses of different reactive layers are given arbitrary. This figure gives also a schematic variation of molar fraction of Ti (x_{Ti}) through the reactive system (purple dotted lines). The concentrations of Ti at reactive interfaces are given by the binary Au-Ti phase diagram. The molar fractions of Au, Zr and O are not indicated in this figure. Over

time, the interdiffusion of Ti and Au atoms through this reactive system leads to the growth of solid phases (IMCs and δ-Au), to Ti enrichment of liquid Au as well as to Au enrichment of solid Ti.

Notice that there is a competition between growth and regress of different phases at their left and right reactive interfaces. This point has been discussed in detail in chapter 3. In the particular case, when two reactive layers grow and regress in a diffusion couple, the growth laws for each layer are given by analytical expressions (see for example the work of Philibert et al.[9] or chap. 1 § 3.4). When more than two reactive layers are formed (as it is the case here), the problem becomes much more complex.

The evolution of the diffusion profile of Ti in liquid Au can be easily evaluated by considering that the molar fraction of Ti (x_{Ti}) at liquid / δ-Au interface remains constant over time (thermodynamic equilibrium at the interface) and equal to ~ 2 at% Ti ($x_1 = 0.02$ – point L in Figure 132a) and the initial content of Ti in liquid Au is constant (in our case $x_0 = 0$). Figure 132b gives the concentration distributions of a diffusing species at various times in a sheet of width equal to 2L, with initial uniform concentration C_0 and fixed surface concentration C_1 as a function of L, time (t) and diffusion coefficient (D) assumed concentration independent [10]. By using this numerical solution applied to the diffusion of Ti in liquid Au with a width L, the liquid Au will be saturated at about 90% with Ti (i.e. $x_{Ti}(t) > 0.9.x_1 = 0.018$) at a time t such as $Dt/L^2 \approx 1$ (see Figure 132b).

By taking the diffusion coefficient of Ti in liquid gold $D \sim 5.10^{-9}$ m^2/s [11] and $L < 100$ µm $= 10^{-4}$ m, we calculate the necessary time $t < 2$ s for the saturation of liquid Au with Ti, which is much lower than the brazing time (180 s). Thus, we can consider that the whole liquid Au layer is almost saturated in Ti just during the first seconds following the melting of Au. This result is in agreement with the EDX analysis (Figure 131) showing that the Ti concentration in Au is almost constant over a zone about 40 µm width corresponding to the liquid phase at brazing temperature. Note finally that the time required to saturate Au in Ti depends on Au thickness, thus, the thinner the Au layer, the faster the saturation.

When liquid gold is fully consumed, that is IMCs and δ-Au phase layers represent the whole thickness of the joint, the new diffusion couple becomes δ-Au phase / Ti. In this case, the thickness of δ-Au phase layer decreases over time, to the benefit of IMCs that will normally grow faster than before total consumption of the liquid.

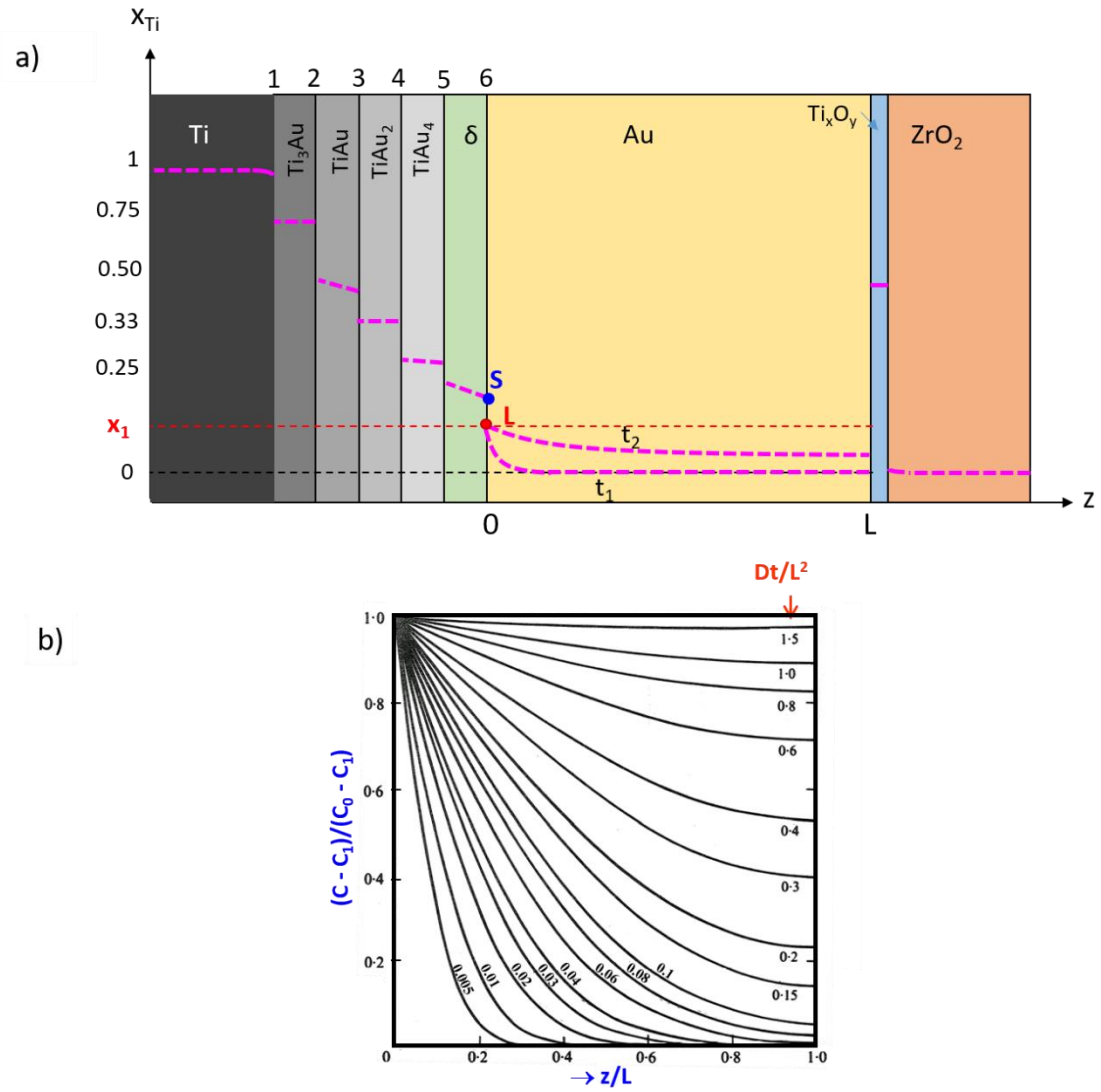

Figure 132: Schematic representation of Ti content through the different layers composing the brazed joint (a), Concentration distributions at various times in a sheet (width equal to 2L) (b), -L < z < L, with initial uniform concentration C_0 and fixed surface concentration C_1. Numbers on curves correspond to values of Dt/L^2. D is the diffusion coefficient assumed concentration independent[10].

3.4. Summary and conclusion

In this section, ZrO_2 / Ti brazing is performed with pure gold foils thanks to Ti active element, which is provided by the Ti substrate. Ti in liquid gold is provided first by dissolution of Ti substrate and/or Au-Ti intermetallic compounds (IMCs) formed during heating and afterwards by diffusion through continuous Au-Ti IMC layers formed at Ti / liquid Au interface. Meanwhile, Ti diffuses through the liquid gold towards the ZrO_2 / Au interface where it reacts with zirconia and forms the wettable reaction product Ti_xO_y leading thus to a good wetting of zirconia by the liquid metal.

The impact of several brazing parameters on interfacial reactions was studied in order to understand the reactional mechanisms occurring during brazing, and to propose an optimized brazing process.

First, it was shown that gold thickness has an influence on Au-Ti intermetallic compounds thickness and also on the joint microstructure. Brazing ZrO_2 and Ti using thin gold foils (25-50 µm) may cause a total consumption of liquid gold (which is an end-member of Ti / Au diffusion couple), i.e. isothermal solidification. Thus, at the brazing temperature, the entire joint is composed of intermetallics and δ-Au solid solution (which becomes the new end-member of the diffusion couple), and in the worst case only of Ti-Au intermetallics (total consummation of δ-Au). Therefore, it is strongly suggested to braze ZrO_2 and Ti with a thick gold foil (~100 µm) and for a short duration (some minutes) in the temperature range 1070-1100°C. Moreover, the short duration is also recommended to form a homogeneous submicronic Ti_xO_y layer at the zirconia / gold interface.

Finally, it was shown that, during heating up to the melting temperature of gold, solid-state reactions occur at the Ti / Au interface and lead to local formation of Ti-Au IMCs of total thickness 0-20µm which depends on the presence (or not) of native Ti oxide at this interface. However, these IMCs could be partially or totally dissolved in pure liquid gold so that, after brazing (i.e. after liquid state reactions), IMCs layer has a relatively homogeneous thickness everywhere at the interface. Thus, titanium surface state (raw Ti or etched Ti) has no significant impact on brazed joint microstructure.

Based on the experimental results presented in the parametric study, a fine microstructural analysis (by FEG-SEM and TEM) of the joint brazed with optimal parameters, that is with a gold foil of 100 µm and brazed at 1080°C for 3 min, was presented.

At titanium / gold interface, the four Ti-Au intermetallics compounds given by the binary Ti-Au phase diagram are formed, with an average thickness of about 14 µm. Au diffusion is observed in titanium substrate over a distance of about 60 µm leading to the formation of Ti_3Au precipitates at the grain boundaries of Ti.

At the zirconia / Au interface, a submicronic (200 - 400 nm) and continuous reaction layer of titanium oxide is formed.

The microstructure of the joint in the zone situated between Ti-Au IMCs / Au and Au / ZrO_2 interfaces is constituted of δ-Au and $TiAu_4$ phases. However, at the SEM scale, the $TiAu_4$ phase is observed only at a region ~ 10 µm width near the Au-Ti IMCs in the form of needle-like precipitates within the δ-Au phase matrix. At the brazing temperature (1080°C) this zone (situated between $TiAu_4$ layer and Ti_xO_y layer) is constituted of δ-Au and Au-Ti liquid phases which both transform during cooling in Ti-depleted δ-Au phase (containing ~ 1at% Ti at room temperature) and $TiAu_4$ precipitates.

No significant difference was observed between samples brazed with and without getter, neither at Ti side nor at ZrO_2 side.

4. Mechanical characterization of the brazed joints

4.1. Introduction

The satisfying zirconia to titanium brazing results with a 100 µm gold foil at 1080°C for 3 min encourage us to perform tensile test in order to quantify the mechanical strength of the joints. Given the fact that the main scope of this thesis was the physico-chemical aspect of ZrO_2 / Ti brazing (wetting, interfacial reactivity and microstructure of the joint), only one brazing parameter is investigated in this mechanical study: the partial oxygen pressure in the furnace during brazing which clearly appeared to be a crucial parameter on the mechanical behavior of the brazed joints. The influence of other parameters such as gold thickness, brazing temperature and holding time on the mechanical properties of the joint has not been studied during this thesis.

Batches of tensile specimens are brazed in the metallic furnace with and without zirconium getter. Zirconium has the ability to trap on its surface reactant gases in the temperature range 900°C-1850°C and in particular the oxygen. Oxygen is dissolved in zirconium, decreasing the oxygen partial pressure in the furnace during brazing. Other sample batches are brazed in a graphite furnace, imposing a very low chemical potential of oxygen.

4.2. Tensile test

Figure 133a gives a schematic picture of a tensile specimen cross section, composed of two slug pieces of zirconia and a titanium ferrule as substrates, the filler metal being in the form of two gold rings 100 µm thick. Tensile specimen, as well as tensile test method, are based on the ASTM F19-64 standard, which describes the procedures for conducting tension and vacuum tests on metal / ceramic brazed joints. Figure 133b and c give pictures of four samples placed in the furnace and brazed simultaneously. On Figure 133b, are shown the specimens and their graphite brazing tool while on Figure 133c, we can see the samples brazed with zirconium getter. Zirconium sheets, cut and wound on themselves, are placed near the samples to be brazed. Getters are maintained with a zirconium crown encircling the sample. The goal of zirconium getter is to decrease the oxygen partial pressure (P_{O2}) of the thermal chamber, especially near the joints.

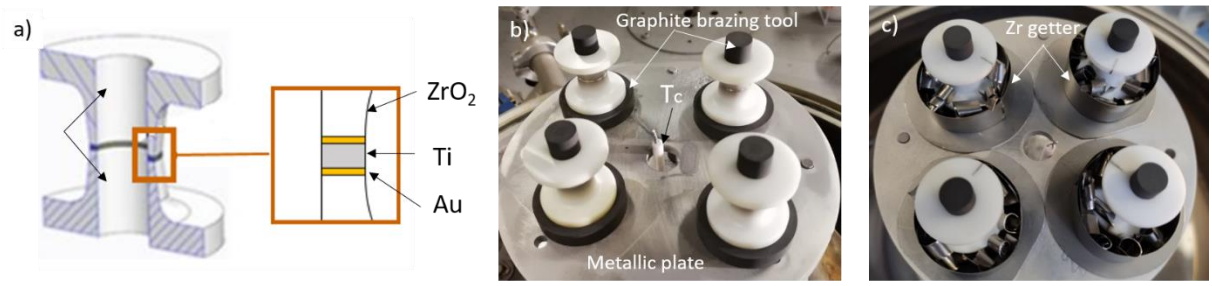

Figure 133: Cross section of a schematic brazed specimen (a), photography of a batch of 4 brazed specimens placed in the metallic furnace without (b) and with getter (c).

14 samples were brazed in a graphite furnace and 5 samples in a metallic furnace with getter. In both cases, the oxygen partial pressure (P_{O2}) is extremely low. 6 samples were brazed in a metallic furnace without getter, with a higher oxygen partial pressure.

Before tensile test, sealant of each sample is controlled thanks to a helium leak test. Most samples (93%) passed the test that means they have a leak rate lower than 10^{-8} mbar.L.s^{-1}. Notice that sealant is a key property of the brazed joint for the concerned biomedical application.

Then, tensile test is performed recording the force applied to the test piece by the traction machine over displacement. We could not measure the specimen elongation because we did not have extensometer adapted to the joint dimensions. We measured the maximal force supported by the sample (in N). From this value, knowing the brazed surface (35.2 mm^2), we calculated the rupture stress of the specimens (in MPa). The overall rupture stress results are summarized in Figure 134.

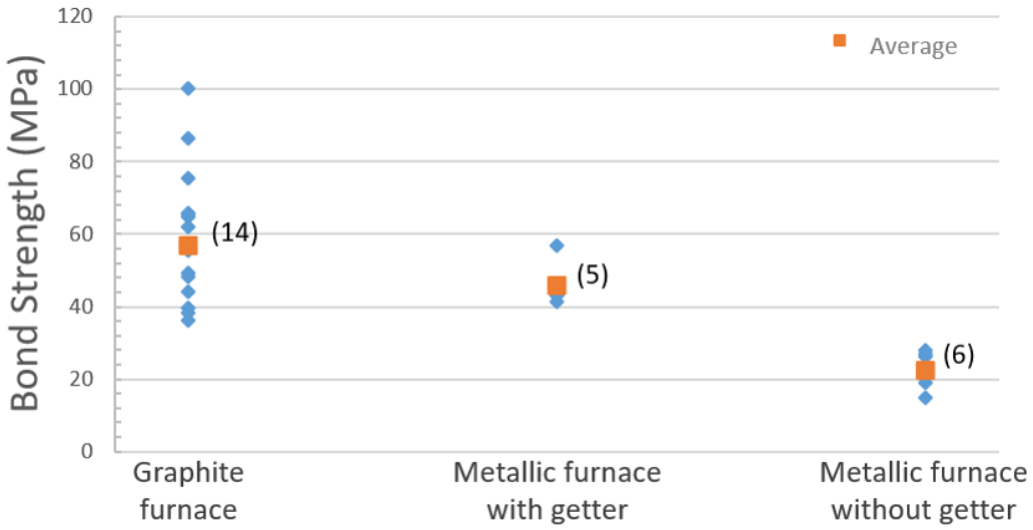

Figure 134: Graph representing bond strength of the whole tensile specimens brazed under different oxygen partial pressure conditions. The number of samples is given in parenthesis and orange squares indicate the average values of bond strength.

The average bond strengths for samples brazed in graphite furnace and in metallic furnace with getter and without getter are respectively 56, 50 and 26 MPa. These values are relatively high and largely sufficient for the target application. An important outcome is the gap between fracture stress of samples brazed with a low P_{O2} (graphite furnace and metallic furnace with getter), and those obtained with a higher P_{O2} (metallic furnace without getter). Indeed, the average value is twice higher in the first case, and all the samples brazed with a low P_{O2} have a higher fracture stress than samples brazed in metallic furnace without getter (higher P_{O2}). Notice also a large dispersion of results in the case of graphite furnace, which can be attributed to the larger number of values.

4.3. Fracture surface analysis

After tensile tests, fracture surfaces of the samples are observed in order to detect the fracture zone of the joint. Figure 135a and b gives pictures of representative brazed samples, as part of this thesis, with and without getter. At first glance, fracture surfaces look similar: the major part of the surface is composed of Ti-Au IMCs, and a minor part of Ti_xO_y. Titanium oxide and Ti-Au intermetallics are observed on both sides of the broken specimens, thus, fracture occurs mainly in the reaction layers (and not at the gold / reaction layer or substrate / reaction layer interfaces). All the samples have the same aspect, with a fracture localized both in Au-Ti IMCs, and in Ti_xO_y layer (representing about 5-30 % of the entire surface).

Brazed specimens presented defects, such as a gold drop on zirconia substrate out of the braze surface, due to an overfull joint. Note that gold drop is randomly located inside (Figure 135a) or outside (Figure 135b) the brazed crown, sometimes showing a cohesive fracture in zirconia, characteristic of a good adhesion at the interface. During an internship that supported this mechanical study, specimens without gold drops were brazed[12]. Figure 135c gives the fracture surface of a sample brazed under these conditions. Optical characterizations show that half of the samples have a fracture exclusively in the IMCs layer. However, these optical observations are not at all sufficient to confirm if the failure initiation occurs at the Ti / Au interface. Thus, more work is needed to characterize these brazed samples with a particular configuration.

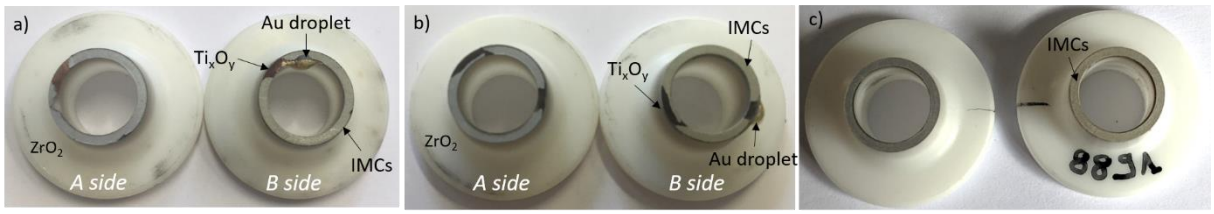

Figure 135: Pictures of representative broken samples brazed in metallic furnace a) with getter, b) without getter, c) with getter, no gold drop and improved tensile tool[12].

Figure 136 gives some schematic representations of the broken sample. Figure 136a presents a schematic cross section of the specimen with the two brazed joints. The red line represents the fracture zone, mainly occurring in the Ti-Au IMCs layers and partially in the Ti_xO_y layer, thus separating the sample in two pieces, in the following called A side and B side.

Figure 136b shows the two pieces (A and B sides) once the broken sample is separated. The blue arrows represent the directions of the top views taken over the two fracture surfaces (A and B sides), seeing in both cases a majority of IMCs and a small part of titanium oxide layer as it is schematized in Figure 136c.

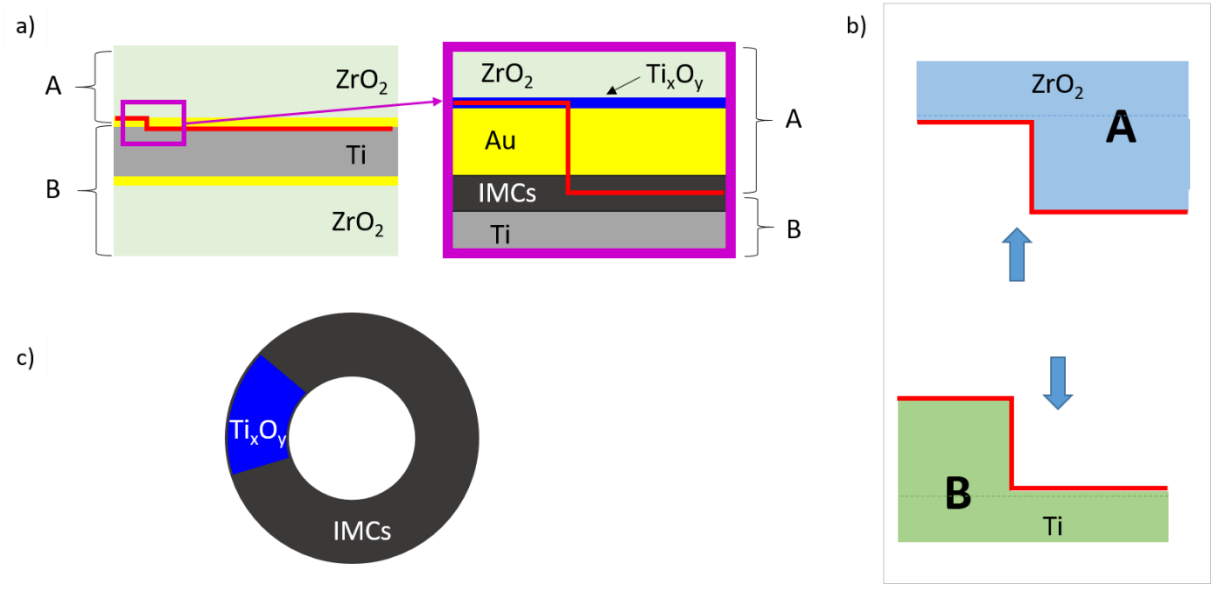

Figure 136: Schematic representations of a brazed specimen: cross section (a), broken sample, the blue arrows indicate the direction of the top views taken over both A and B sides (b), top view of the fracture surface (c).

Fracture surfaces of the samples presented in Figure 135 are observed by SEM. Two image- stitchings of the sample brazed with getter (see Figure 135a) taken over A and B sides are shown in Figure 137 (and B side of the sample brazed without getter (see Figure 135b) is presented in appendix 5). Both images clearly delimit the IMCs zone and the Ti_xO_y zones of the fracture surfaces.

In the following, we will present first, closer analyses of the IMCs zone, and afterwards the Ti_xO_y zone will be investigated.

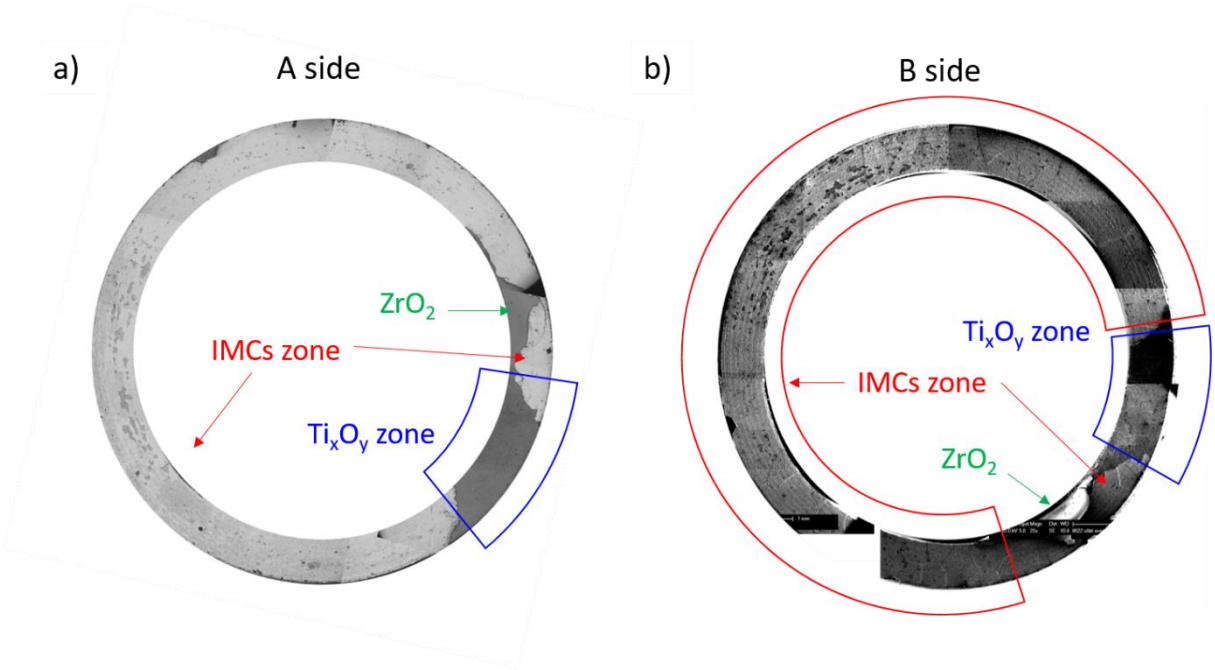

Figure 137: SEM image-stitchings of representative fracture surfaces, a) A side and b) B side of a sample brazed with getter in the metallic furnace (see Figure 136 for definition of A and B sides of the brazed sample).

a) Analysis of the IMCs zones of the fracture surfaces

In order to accurately locate the fracture in the IMCs zone, A and B sides of the samples are observed and analyzed by SEM and EDX.

Figure 138 gives SEM pictures of the specimens brazed with getter. The fracture surfaces are quite unusual because characteristics of ductile and fragile fracture are not seen. Intergranular fracture is the most likely fracture mode. IMCs zone is composed of two phases, with a predominant one representing at least 90% of the surface, spotted with another phase.

Looking at the predominant phase marked in red color (Figure 138a, c and d), grains of about 10 µm are observed on A side (Figure 138d), whereas smaller grains of about 5 µm are observed on B side (Figure 138c). Moreover, EDX analysis shows that A side is composed of ~20 at% Ti and 80 at% Au that corresponds to $TiAu_4$ intermetallic compound, while B side contains ~32 at% Ti and 68 at% Au, corresponding to $TiAu_2$ compound. This means that, in this zone, fracture is located at the $TiAu_2$ / $TiAu_4$ interface.

The minor phase marked in blue color on Figure 138b (B side) is also analyzed by EDX. Ti_3Au and Ti (enriched in Au) are detected on B side, and Ti_3Au is analyzed on the opposite fracture surface (A side), showing that fracture is located at the Ti_3Au / Ti interface.

These morphological and semi-quantitative analyses, performed on a few samples, show that fracture occurs in the Ti-Au IMCs layers. More precisely the fracture takes place at the $TiAu_2$ / $TiAu_4$ interface for the major portion of the IMCs zone surface (> 90 % of the surface), and at the Ti_3Au / Ti interface in a much lower proportion, whatever the brazing conditions (with or without getter) and the fracture stress value (ranging from ~ 15 to 100 MPa).

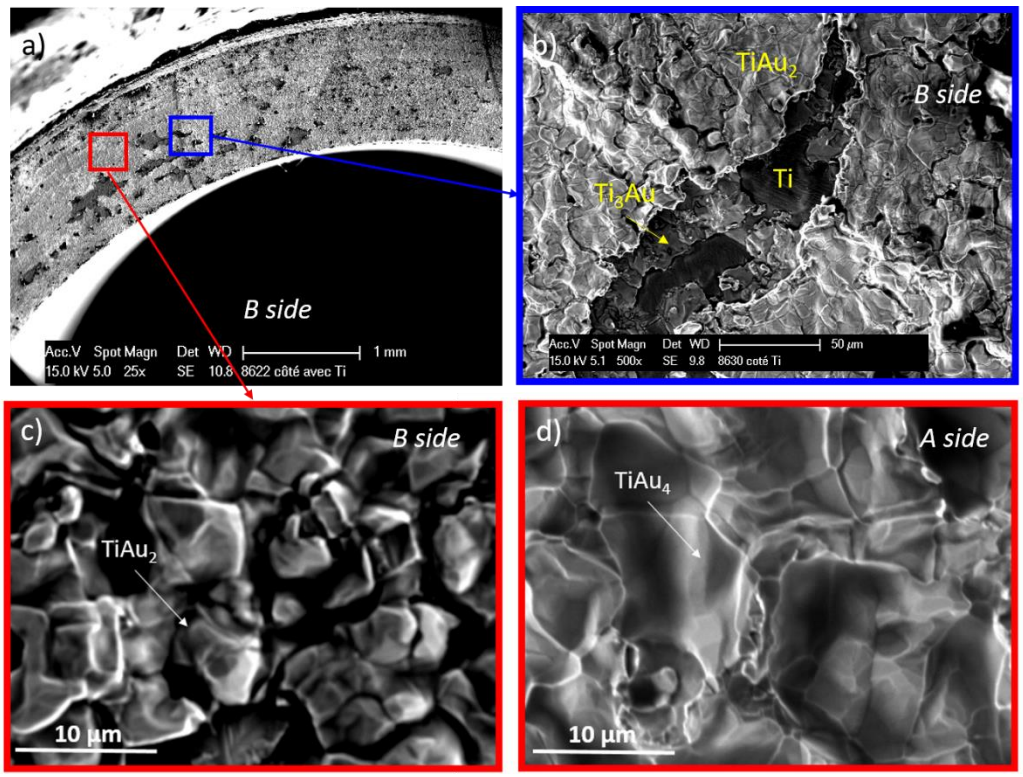

Figure 138: SEM micrographs of B side (a, b, c) and A side (d) of the IMCs zone of the fracture surface presented in Figure 137 (sample brazed with getter in the metallic furnace).

In order to determine if the oxygen partial pressure (P_{O2}) has any significant influence on the IMCs fracture surface type, the morphology of $TiAu_2$ grains observed on B side are compared for two samples brazed with and without getter respectively (Figure 139). Figure 139 shows that in both cases, the grains size and the general aspect of the fracture surfaces are similar. However, notice that voids of 2-10 µm are observed only on the sample brazed without getter. Moreover, these porosities are detected over the whole rupture surface of this sample, except for an area of about 200 µm wide near the graphite brazing tool (where the P_{O2} should be locally lower) located on the left side of Figure 139d. This result suggests that more work is needed to determine if the oxygen partial pressure in the furnace can impact Ti-Au IMCs.

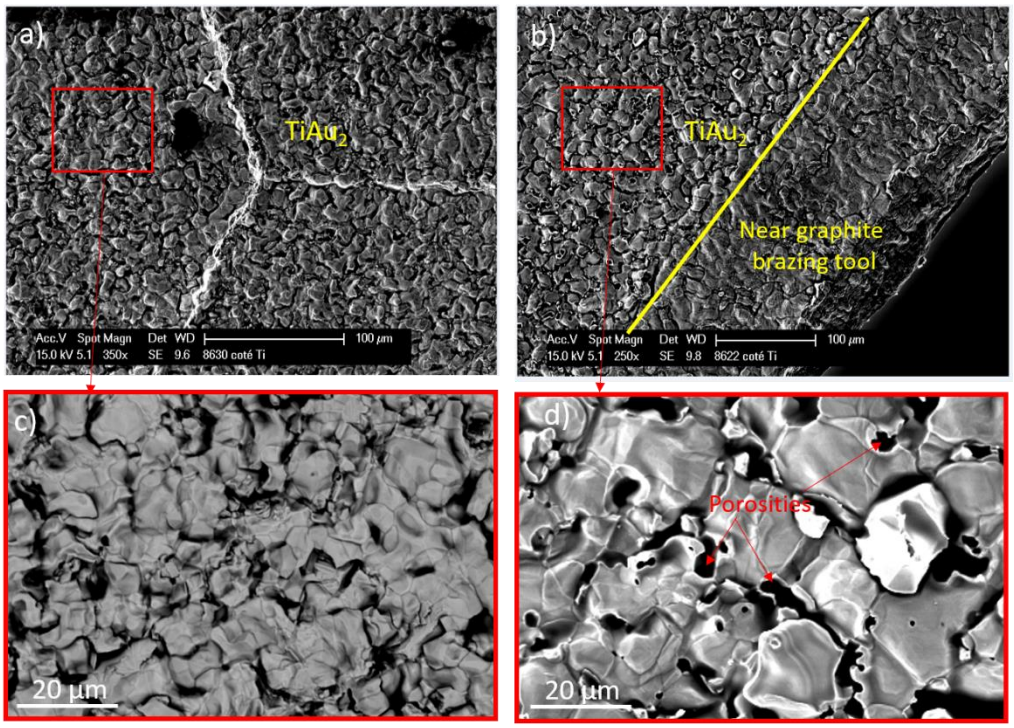

Figure 139: Fracture surface micrographs (B side) of samples brazed in metallic furnace with getter (a, c), and without getter (b, d).

b) *Analysis of the Ti_xO_y zones of the fracture surfaces*

After examination of IMCs area of fracture surfaces, the Ti_xO_y zone of the fractured surface of a sample brazed with getter is observed with SEM.

The fracture surface of the B side presented area in Figure 140 contains Ti_xO_y zone on the left and also IMCs zone on the right side of the pictures, delimited with a yellow dotted line. The strips on Ti_xO_y surface correspond to machining strips of zirconia, formed during ceramic shaping.

The Ti_xO_y zone is composed of two areas: *a darker area* marked "Ti_xO_y area" and *a lighter one* marked "Au rich area" on Figure 140c which reveals a rupture located at two areas.

EDX analysis of the *darker area* reveals a high oxygen amount (~50 at%), some titanium and a low Au amount. Thus, the darker area consists of Ti_xO_y (the Au signal detected comes from the gold joint under the Ti_xO_y layer). Indeed, the thickness of the Ti_xO_y reaction product layer is 200-400 nm, so the interaction bulb penetrates in the Au joint under the reaction layer.

EDX spectrum of the *lighter area* indicates low Ti and O contents (~10 at% each), and a high Au content. In this case, the affected volume by electrons is mostly located in the Au layer (the joint) under Ti_xO_y layer, which means that the titanium oxide is very thin in the lighter areas. Thus, the lighter area reveals a fracture occurring in the Ti_xO_y layer very close to the Ti_xO_y / Au interface.

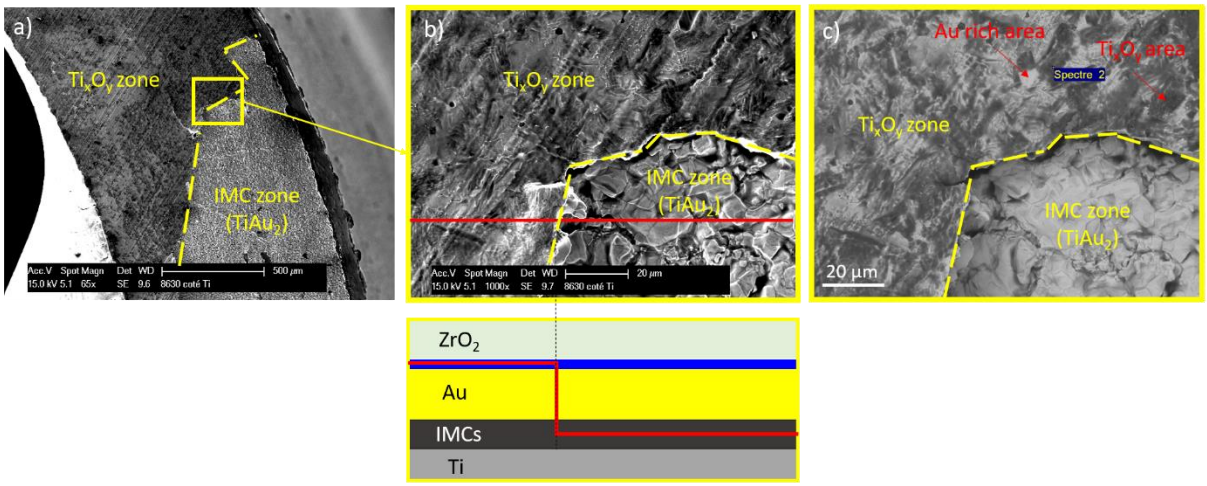

Figure 140: Fracture surface micrographs of the Ti_xO_y zone and IMCs zone (B side of the sample brazed with getter) (a), in secondary electrons (b), in backscattered electrons (c).

The fracture surface observation of the A side of Ti_xO_y zone is presented in Figure 141. This fracture surface also has a dual-phase structure, clearly observed by backscattered electrons microscopy (Figure 141b). EDX analysis and secondary electron imagery (Figure 141c) show that Ti_xO_y and zirconia are observed, in similar proportions.

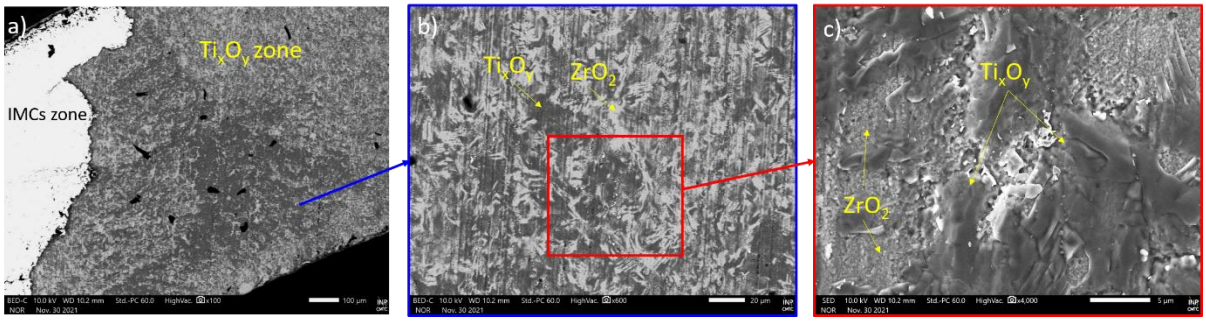

Figure 141: Fracture surface micrographs of the Ti_xO_y zone (A side of the sample brazed with getter) (a), in backscattered electrons (b), in secondary electrons (c).

Therefore, the observations and EDX analyses of both fracture surfaces of Ti_xO_y zone (A and B sides, respectively presented in Figure 141 and Figure 140) allow to conclude that fracture occurring in Ti_xO_y zone is located at Ti_xO_y / zirconia interface and also near Ti_xO_y / gold interface in similar proportions.

To conclude, after the tensile test, fracture occurs both at Ti / Au interface (IMCs zone representing at least 70 % of the surface) and at ZrO_2 / Au interface (Ti_xO_y zone) whatever the brazing conditions (with or without getter) and the fracture stress value (ranging from ~15 to 100 MPa). Note however that experimental results obtained by C. Godinot during her internship[12] without Au droplet and an optimized tensile tool, show that, *at optical scale*, fracture occurs only in IMCs zone for half of the samples. Nevertheless, these results should be confirmed in the future at least by SEM analyses of the fractured surfaces.

The morphological and semi-quantitative analyses, performed on a few samples, show that fracture occurring in Ti-Au IMCs zone is precisely located at the $TiAu_2$ / $TiAu_4$ interface for more than 90% of the IMCs zone surface and at the Ti_3Au / Ti interface in a much lower proportion. These analyses show also that the fracture occurring at the ZrO_2 / Au interface, is located at ZrO_2 / Ti_xO_y and inside Ti_xO_y layer very close to Ti_xO_y / Au interface.

4.4. Conclusion

The ZrO_2 / Au / Ti joints brazed with a 100 µm gold foil at 1080°C for 3 min in liquid state were mechanically characterized by tensile test. Most of the samples (93%) have a leak rate lower than 10^{-8} mbar.L.s^{-1} before tensile test, which is a key parameter for the concerned biomedical application. Good mechanical strength of the joint is obtained with the average rupture strength of about 56 MPa measured on 19 samples (brazed in graphite furnace and metallic furnace with getter). However, a large dispersion of experimental results is noticed, with a standard deviation of about 17 MPa. The oxygen partial pressure (P_{O2}) in the furnace during brazing has a significant influence on mechanical properties of the joint. Indeed, when brazing is performed in a graphite furnace or when Zr getters are added in the metallic furnace (very low P_{O2}), the mechanical strength of the joints is twice higher than for the joints obtained by brazing in a metallic furnace without getter (higher P_{O2}).

The fracture surface of a few broken samples were analyzed. Whatever the brazing conditions (P_{O2} in the furnace) or the tensile strength of the sample, fracture occurs both at ZrO_2 / Au interface and at the Au-Ti IMCs zone (in large proportion, higher than 70 %). At ZrO_2 side (ZrO_2 / Au interface), the failure is complex. At titanium side (Au-Ti IMCs zone), the failure is also complex, with some fracture areas at Ti / Ti_3Au interface, and the major part of the fracture localized at the $TiAu_2$ / $TiAu_4$ interface.

5. Conclusions

In this chapter, brazing study of ZrO_2 / Ti with pure gold was performed. First of all, successful tests of zirconia / zirconia and zirconia / titanium brazing with the commercial braze named Gold-ABA® (Au-3Ni-0.6Ti alloy) led to the formation of filled joints with strong interfaces. Then, zirconia / titanium brazing with pure gold was investigated, and the impact of several brazing parameters such as gold foil thickness (in the range 25 -150 µm), brazing temperature (between 1080 and 1100°C), holding time (from 3 to 60 min) and oxygen partial pressure in the brazing furnace was studied.

The ZrO_2 / Au / Ti joint is formed thanks to Ti dissolution and diffusion in liquid Au, leading thus to the formation of a titanium oxide reaction layer at the zirconia / gold interface. Oxygen is provided by the zirconium substrate, becoming sub-stoichiometric near the joint. This reaction product layer formed at liquid Au / ZrO_2 interface is wettable by liquid gold, which is a necessary condition to obtain a good brazing.

At the Ti / Au interface, the four Ti-Au intermetallics (IMCs) given by the binary Ti-Au phase diagram (Ti_3Au, TiAu, $TiAu_2$ and $TiAu_4$) and the δ-Au solid solution phase are formed. The very rapid growth of IMCs and δ-Au phase in Ti / Au system leads to a rapid consummation liquid Au. Thus, as it was seen in this chapter, a thin Au foil, a high temperature and a long brazing duration (for instance an isothermal holding of 10 min at 1100°C, using a gold foil thinner than 25 µm) lead to an isothermal solidification of the joint, (i.e. a total consumption of liquid gold) causing defects in the joint like voids at the zirconia side.

Therefore, to ensure hermeticity and good mechanical strength of the brazed joint, using a thick Au foil (~ 100 µm) and a short duration in liquid phase (~ 3 min at 1080°C) is recommended. In these brazing conditions, the total average IMCs thickness is about 14 µm and the zone constituted of δ-Au phase (containing micrometric needle-like $TiAu_4$ precipitates at room temperature) is thinner than 30 µm. Thus, at the end of the brazing isothermal holding, the joint is composed of a high amount of the Au-based, Au-Ti liquid alloy. The resulting solidified joint has a homogeneous structure without voids or other defects.

The second interest of a short duration in liquid phase concerns the Ti_xO_y layer morphology, which is homogeneous, 200 – 400 nm thick, and continuous everywhere at the ZrO_2 / Au interface, that is desirable from a mechanical point of view. In contrary, a longer brazing holding time (~ 15 min) leads to an irregular growth of the titanium oxide reaction layer, in the range 200 nm – 2 µm.

Tensile tests showed a high rupture stress of the brazed joints with an average of 56 MPa measured on 19 samples brazed in graphite furnace and metallic furnace with getter, that is satisfying for the target medical application. For the first time, a relationship between oxygen partial pressure (P_{O2}) in the brazing furnace and mechanical behavior of the joint has been unambiguously established experimentally. The obtained rupture stress for samples brazed in a graphite furnace, as well as in a metallic furnace with getter (assuring an extremely low partial pressure of oxygen) is twice higher than the rupture stress resulting from brazing in a metallic furnace without getter (under a higher partial pressure of oxygen). In-depth physico-chemical analyses of cross sections of the entire brazed joints by MEB FEG and of the ZrO_2 / Au interface by TEM, did not allow to detect significant microstructural

differences between samples brazed in metallic furnace with getter (very low P_{O2}) and without getter (higher P_{O2}). Moreover, fracture surfaces are similar for both cases, with a mixed fracture mainly located in the Au-Ti IMCs (at the $TiAu_2$ / $TiAu_4$ interface), and in a small proportion at the ZrO_2 / Au interface in the Ti_xO_y layer.

References of chapter 4

1. N. Eustatopoulos, M.G. Nicholas & B. Drevet. *Wettability at high temperatures*. (Pergamon materials series, 1999).

2. J. L. Murray, The Au-Ti (Gold-Titanium) system. *Bull. Alloy Phase Diagr.* **4**, 278–283 (1983).

3. J. Chevalier, B. Cales & J. M. Drouin, Low-Temperature Aging of Y-TZP Ceramics. *J. Am. Ceram. Soc.* **82**, 2150–2154 (2004).

4. Huang et al. Nanoscale research letters. (2010).

5. *Smithells metals reference book* (Butterworth-Heinemann, 1998).

6. Ya. I. Gerasimov, A.N. Krestovnikov & A.S. Shakhov. *Chemical Thermodynamics of non ferrous metallurgy*. **3** (1965).

7. A. K. Kumar & A. Paul. Interdiffusion studies in bulk Au–Ti system. *J. Mater. Sci. Mater. Electron.* **21**, 1202–1206 (2010).

8. O. Taguchi, T. Watanobe, Y. Yamazaki & Y. Iijima. Reaction diffusion in the Au-Ti System between 1110K and 1150K. in *Defect and diffusion forum*, **194–199** 1569–1574 (Scitec Publications, 2001).

9. J. Philibert, Reactive Diffusion. *Defect Diffus. Forum* **66–69**, 995–1014 (1991).

10. J. Crank. *The mathematics of diffusion*. (Oxford University Press, Ely House, London W.I, 1975).

11. G.H. Geiger & D. R. Poirier. *Transport Phenomena in Metallurgy*. (1973).

12. C. Godinot. Technical report CEA/LITEN/DTCH/LCA/2021/22. (2021).

General conclusions and prospects

The main objectif of this thesis was to perform a zirconia-to-titanium brazing in sandwich configuration for the cochleair implant application. It consists firstly of selecting active alloys or metals suitable for brazing, and secondly of recommending brazing conditions in a view to achieve an hermetic and mechanically strong dissimilar joint.

In the literature, very few ZrO_2 / Ti brazing studies using biocompatible braze are conducted. However, it is well known that the addition of a few percent of active element in the filler metal (Ti or Zr for instance) leads to the formation of a wettable reaction layer at the zirconia / filler metal interface. Wetting of both substrates by the braze is a necessary condition to obtain an intimate contact between substrates and liquid metal and therefore to perform a successful brazing.

The first part of this work deals with an experimental study of wetting and interfacial reactivity of zirconia and titanium substrates, performed by the sessile drop and dispensed drop techniques under high vacuum.

First, we studied the wetting of zirconia by active brazing alloys containing zirconium and titanium active elements. For both active elements, three noble metal matrix M were explored: M = Au-20wt%Sn (low melting point alloy), Ag and Au. A good wetting of zirconia by these active alloys was obtained. The good wetting of M-Zr alloys on zirconia is due to the formation of a wettable micrometric ZrO_{2-y} reaction layer at the M-Zr / zirconia interface. The growth of this layer occurs at the reaction layer / liquid alloy interface by oxygen diffusion from zirconia substrate and Zr from the alloy. The good wetting of M-Ti alloys on zirconia is due to the formation of a wettable submicronic Ti oxide layer at the M-Ti alloy / zirconia interface. The growth of this layer occurs at the Ti_xO_y / alloy interface by reaction between oxygen diffusing from the zirconia substrate and Ti dissolved in Au-Ti alloy.

Study of reactivity in wetting and brazing configurations at the braze / zirconia interface shows that Au-Ti alloy is the best candidate to pursue the wetting and brazing studies. Thus, zirconia wetting by the Au-Ti alloys was investigated in detail with Ti content ranging from 0.6 to 4 wt%, in the temperature range 1064-1270°C. Contact angle θ of Au-Ti alloys on zirconia decreases with titanium content in the filler metal until attaining $\theta \sim 44°$ at 1170°C with 4 wt% of Ti in Au. For low Ti content in Au ($Ti \leq 2$ wt%), a pinning of the triple line is observed despite the fact that the Au-Ti / zirconia is a reactive system. In some cases, contact angle remains very high (160-170°), and in other cases, Au-Ti alloy spreads zirconia by successive jumps of the triple line.

The Ti_xO_y reaction product layer formed at the Au-Ti alloy / zirconia interface is continuous, homogeneous and thin (0.3 – 4 µm), which is promising for zirconia-to-titanium brazing.

Therefore, we chose to focus our research on Au-Ti active alloy. In particular, the selected filler metal for the brazing study is pure gold since titanium is provided from the Ti metallic substrate. For this reason, spreading kinetics and reactivity of titanium (the second substrate to be assembled) by liquid gold were investigated.

A very good wetting of Ti substrate by liquid Au was observed, the contact angle being lower than 45°. Wetting does not depend on the roughness neither on the native oxidation of Ti substrate. Spreading kinetics increases with temperature in the range 1066-1125°C. For temperatures lower than the peritectic temperature T_P = 1123 ± 3°C, the dissolutive and reactive wetting leads to the formation of five solid phases at the Ti substrate / liquid Au interface: four Ti-Au intermetallic compounds (Ti_3Au, TiAu, $TiAu_2$ and $TiAu_4$) and the δ-Au solid solution phase. The contact angle corresponds to the equilibrium contact angle of the liquid Au-Ti alloy on the δ-Au phase. The thicknesses of theses phases grow with the contact time between liquid Au and solid Ti, and the growth kinetics of IMCs layer at 1100°C follows a parabolic law. At 1100°C, from about 1 h of contact, all the liquid is consumed, leading to an isothermal solidification of the droplet.

The second part of this work deals with zirconia-to-titanium brazing under high vacuum in sandwich configuration using a pure gold foil. The impact of several brazing parameters such as gold foil thickness (in the range 25 -150 µm), brazing temperature (between 1080 and 1100°C), holding time (from 3 to 60 min) and oxygen partial pressure was studied.

The ZrO_2 / Au / Ti joint is formed thanks to Ti dissolution and diffusion in liquid Au, leading to the formation of a titanium oxide reaction layer at the zirconia / gold interface. Oxygen is provided by the zirconium substrate, becoming sub-stoichiometric near the joint. A low amount of Zr from the ceramic substrate is dissolved in the joint. The Ti_xO_y reaction product layer formed at liquid Au / ZrO_2 interface is wettable by liquid gold, which is a necessary condition to obtain a successful brazing. At the Ti / Au interface, the four Ti-Au intermetallics (IMCs) given by the binary Ti-Au phase diagram (Ti_3Au, TiAu, $TiAu_2$ and $TiAu_4$) and the δ-Au solid solution phase are formed. The very rapid growth of IMCs and δ-Au phase in Ti / Au system leads to a rapid consummation of liquid Au. In worst-case, a total consumption of liquid gold leads to an isothermal solidification of the joint at brazing temperature, causing defects in the joint like voids at the zirconia side.

This parametric study allows to offer some recommendations for the brazing process to ensure hermeticity and good mechanical strength of the brazed joint: using a thick Au foil (~ 100 µm) and a short duration in liquid phase (~ 3 min at 1080°C). In these brazing conditions, the total average IMCs thickness is about 14 µm and the zone constituted of δ-Au phase (containing micrometric needle-like $TiAu_4$ precipitates at room temperature) is thinner than 30 µm. Thus, at the end of the brazing isothermal holding, the joint is composed of a high amount of the Au-based, Au-Ti liquid alloy. The resulting solidified joint has a homogeneous microstructure without voids or other defects.

The second interest of a short duration in liquid phase concerns the Ti_xO_y layer morphology, which is homogeneous, 200 – 400 nm thick, and continuous everywhere at the ZrO_2 / Au interface, that is desirable from a mechanical point of view. In contrary, a longer brazing holding time (~ 15 min) leads to an irregular growth of the titanium oxide reaction layer, in the range 200 nm – 2 µm.

This study was completed by tensile tests leading to an average rupture stress of 56 MPa (measured on 19 samples). For the first time, a relationship between the oxygen partial pressure (P_{O2}) in the brazing furnace and the mechanical behavior of the joint has been unambiguously established experimentally. The obtained rupture stress for samples brazed in a graphite furnace, as well as in a metallic furnace with getters (assuring an extremely low P_{O2}) is twice higher than the rupture stress resulting from brazing in a metallic furnace without getter (under a higher P_{O2}). In-depth physico-chemical analyses of cross sections of the entire brazed joint by MEB FEG and of the ZrO_2 / Au interface by TEM, did not allow to detect significant microstructural differences between samples brazed in metallic furnace with getters (low P_{O2}) and without getters (higher P_{O2}). Moreover, fracture surfaces are similar for both cases, with a mixed fracture mainly located in the Au-Ti IMCs (at the $TiAu_2$ / $TiAu_4$ interface), and in a small proportion at the ZrO_2 / Au interface in the Ti_xO_y layer.

To conclude, we can propose some research prospects to this thesis work:

- Deepen the wetting study of titanium by pure gold, in particular by performing dispensed drop experiments on pre-elaborated δ-Au solid solution and $TiAu_4$ compound.
- Extend the studies of wetting, interfacial reactivity and brazing to other biocompatible substrates: for instance TA6V, alumina-zirconia composites ZTA (which do not undergo hydrothermal aging), etc…
- Investigate the capillary infiltration of Au (or Au-Ti alloys) in the ZrO_2 / Ti joint, and especially explore the role of pinning phenomenon on liquid infiltration kinetics (application to brazing in capillary configuration).

- Perform in-depth analyses (TEM, XRD, XPS) of the ZrO_2 / Au interface in order to identify the nature of the Ti_xO_y oxide layer.
- Understand the origin of small grains of ZrO_2 near Ti_xO_y reaction layer, and highlight its potential influence on the mechanical properties of ZrO_2 / Au interface.
- Identify the potential influence of the oxygen partial pressure in the furnace on the composition of Ti substrate, Ti_xO_y and Au-Ti intermetallic phases, as well as on the mechanical properties of theses phases and different interfaces.
- Carry out a thorough mechanical study in different test configurations in order to define a criterion of failure initiation.
- Investigate the feasibility of metallic deposit on titanium substrate in order to obtain, after the brazing process, a thin and homogeneous intermetallic layer that allows a controlled Ti diffusion through this layer.

Appendix

Appendix 1: Phase diagrams of the binary Au-Zr, Ag-Zr and Ag-Ti systems

The binary phase diagrams of the Au-Zr, Ag-Zr and Ag-Ti systems are used in this work to determine the thermal cycle of the sessile drop experiments, and also to analyse the microstructure of the solidified droplets.

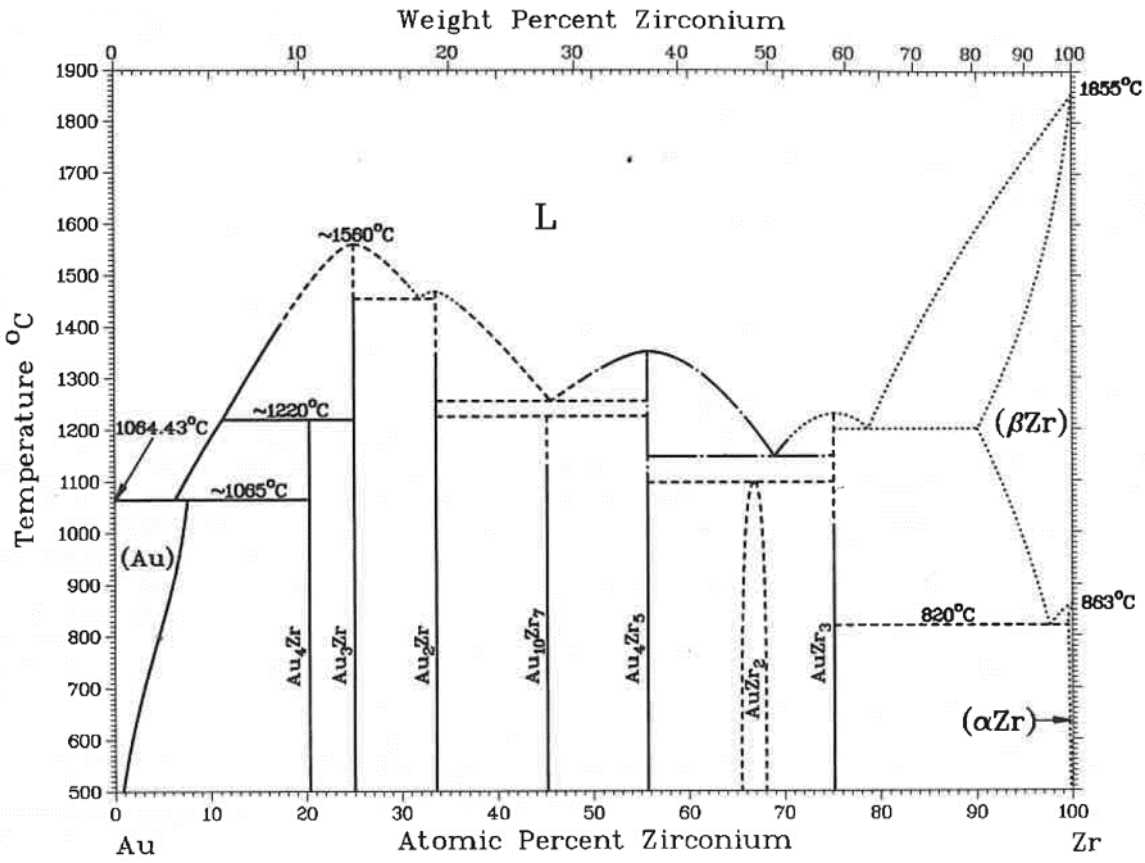

Figure 142: Au-Zr binary phase diagram[1]

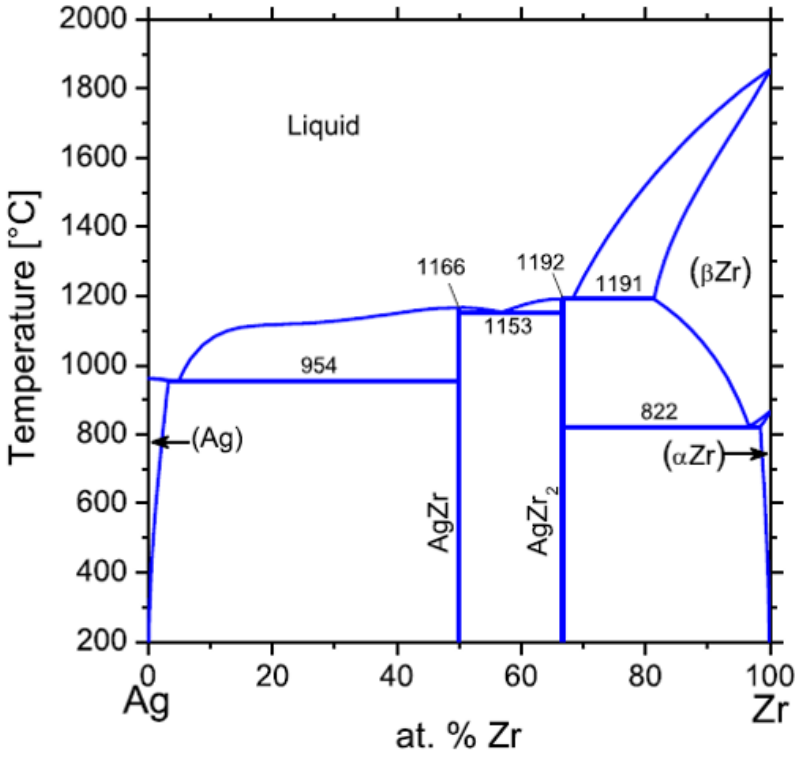

Figure 143: Ag-Zr binary phase diagram[2]

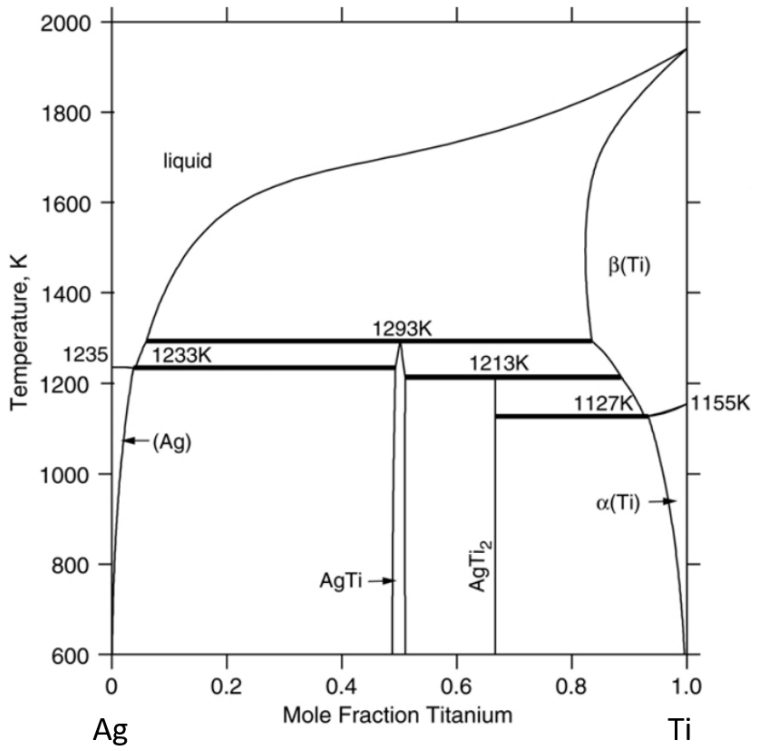

Figure 144: Ag-Ti binary phase diagram[3]

Appendix 2: SEM images of cross sections of liquid Au droplets maintained for 60, 120 and 240 min in contact with Ti substrate at 1100°C

In chapiter 3 section 3.2.1, reactivity between liquid gold and solid titanium, in particular the growth kinetics of the five solid intermediate phases formed at 1100°C and the Au diffusion distance in Ti substrate are investigated after 15, 60, 120 and 240 min of contact in liquid state. Figure 145 gives SEM cross sections of the solidified droplets maintained for 60, 120 and 240 min at 1100°C.

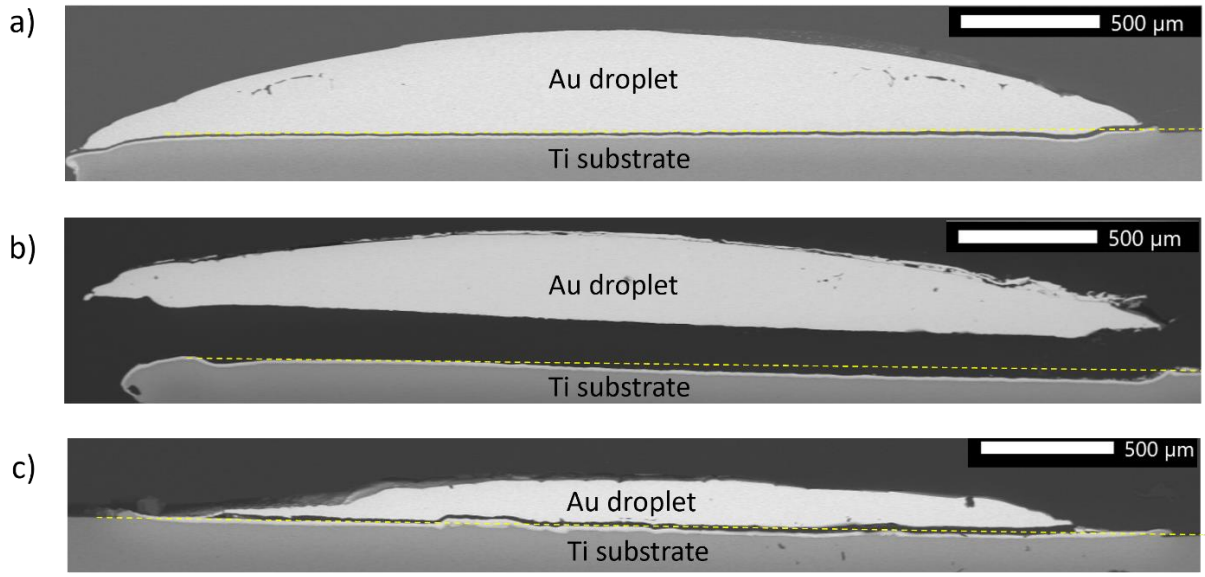

Figure 145: SEM images of cross sections of liquid Au droplets maintained for a) 60, b) 120 and C) 240 min at 1100°C in contact with Ti substrate

Figure 146 gives SEM pictures of these Au droplets / Ti substrates interfaces, showing the 5 intermediate phases (δ-Au and Ti-Au intermetallics) and the Au diffusion in Ti substrate. The thickness of theses layers has been measured and is reported in table 17 (p. 135).

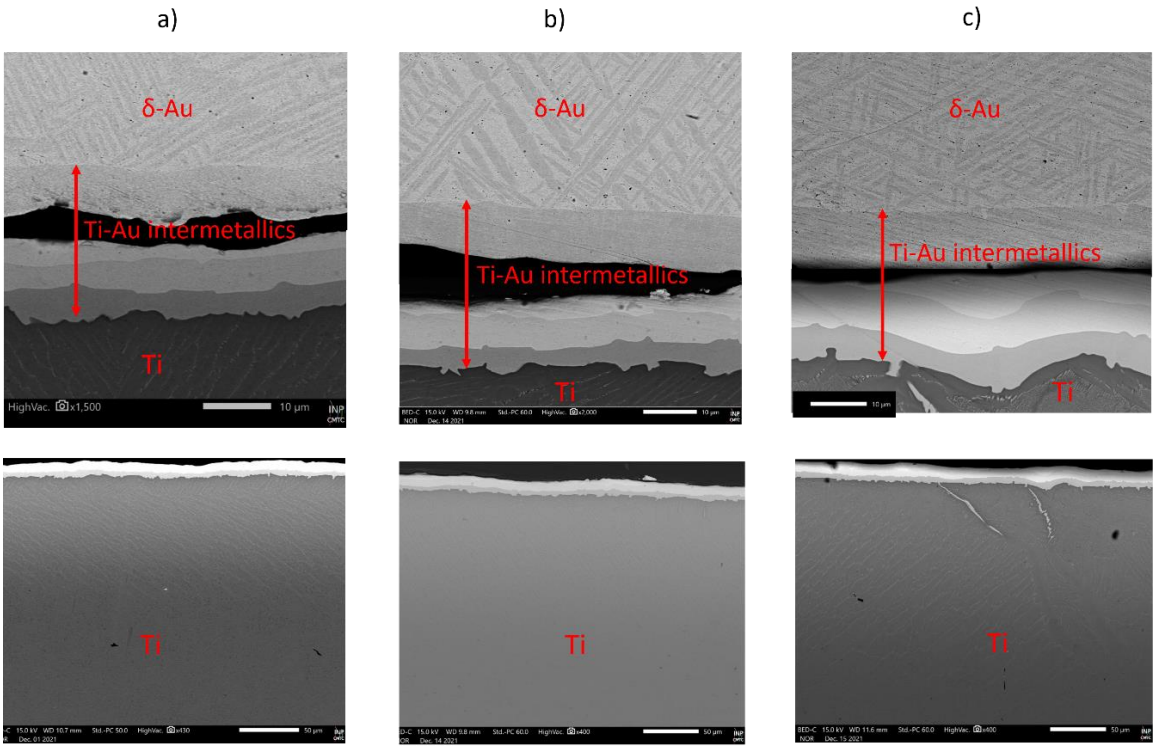

Figure 146: SEM pictures of the Au - Ti interfaces after a) 60, b) 120, c) 240 min of contact in liquid state at 1100°C

Appendix 3: EDX diffusion profile over Ti_xO_y layer (at ZrO_2 / Au interface) performed on a cross section of a brazed sample with getter at 1080°C for 1 min.

In chapiter 4 section 3.3.2.c), a physico-chemical characterization of brazed joints at 1080°C for 1 min (3 min at liquid state) is presented and analyzed, in particular the ZrO_2 / Au interface. EDX diffusion profiles over Ti_xO_y layers of samples brazed without getter (low P_{O2}) and with getter (very low P_{O2}) are compared.

It is noticed that very low gradients of Ti and O concentrations are observed through the reaction layer when brazing without getter (figure 128a), whereas significant gradients are observed through the Ti_xO_y layer when brazing with getter (Ti and O concentrations vary of about 10 at% between Au / Ti_xO_y and Ti_xO_y / ZrO_2 interfaces in figure 128b).

A diffusion profile on another zone of the Ti_xO_y layer of the same sample after brazing with getter is performed. Figure 147 gives Au, O, Ti and Zr concentration profiles through the Ti_xO_y layer, averaged over 100 nm of thickness (marked by the red rectangles) from Au joint to zirconia substrate, for the sample brazed with getter. This figure shows that there is no significant gradient of Ti and O contents over the Ti_xO_y layer.

This additional analysis confirms that the difference of Ti and O profiles (over the Ti_xO_y layer at ZrO_2 / Au interface), observed in figure 128 between samples brazed with and without getter, is due to the location of the analyzed zones and not necessarily to the difference in the partial pressure of oxygen during brazing.

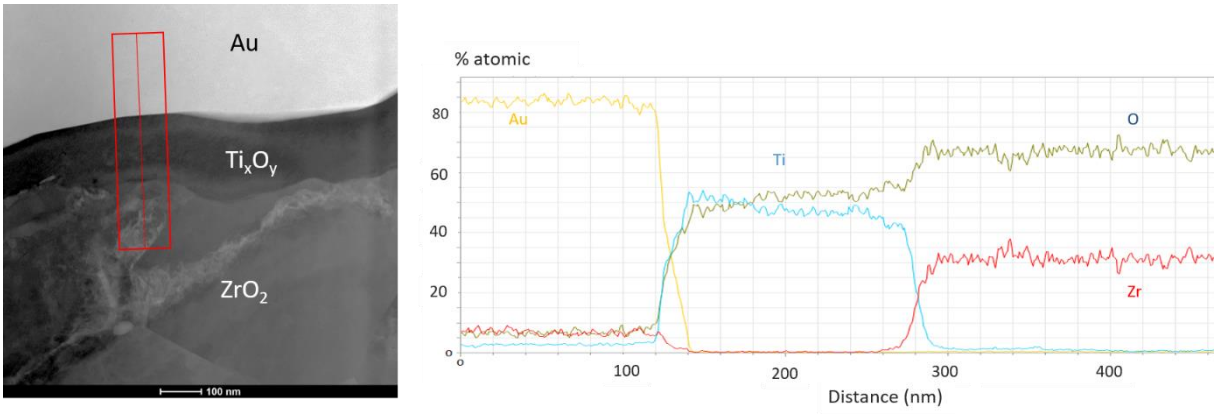

Figure 147: TEM micrograph of the Au / ZrO_2 interface of a sample brazed at 1080°C with getter for 3 min in liquid state, and EDX profile over the Ti_xO_y reaction layer.

Appendix 4: EDX analysis of ZrO_2 / Au / Ti joints, brazed at 1080°C for 3, 17 and 60 min in liquid state (with a 100 µm Au foil).

EDX analyses of the ZrO_2 / Au / Ti samples brazed at 1080°C for 3, 17, and 60 min in liquid state with a 100 µm Au foil are performed. A representative EDX spectra (of sample brazed for 17 min in liquid state), presented in Figure 148, clearly shows the presence of Zr element in the joint. The semi-quantitative analysis of Zr content has been performed by peak deconvolution (without reference samples) taking into account the K-ray of Zr (at 15.8kV) which does not overlap any other peak. Indeed, the L-rays of Zr overlap the M-rays of Au between 1.6 and 3 keV, which makes peak deconvolution more complex.

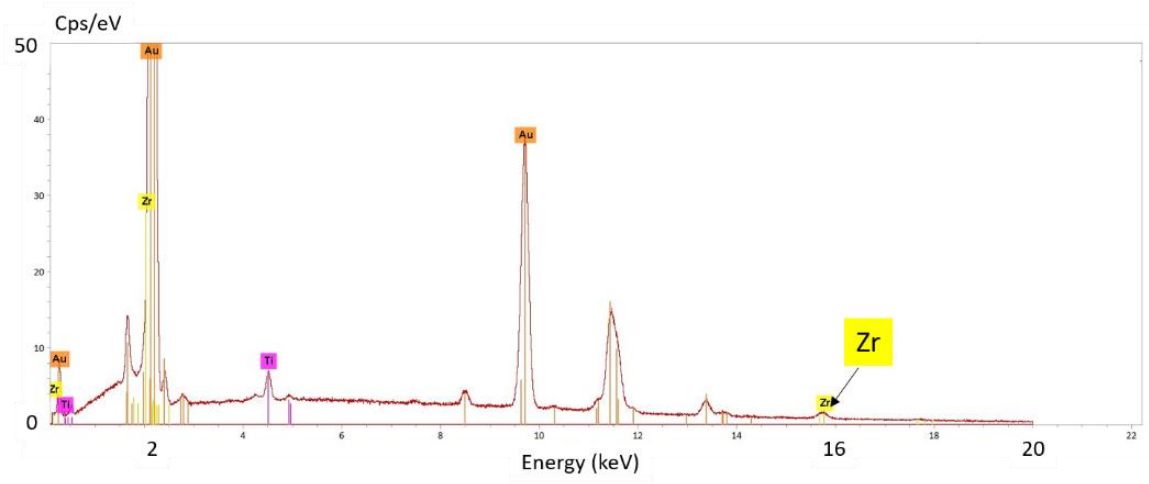

Figure 148: EDX spectra of a ZrO_2 / Au / Ti joint (sample brazed at 1080°C for 17 min in liquid state, 100 µm foil) showing the the K-ray of Zr.

Zirconium and titanium contents were measured by EDX analysis for the three samples brazed at 1080°C for 3, 17 and 60 minutes in different zones of the joint, presented in Figure 149. Zr element is detected all over the joints with a content, decreasing from the ZrO_2 side to the IMCs in the range 15 - 0.5 at%.

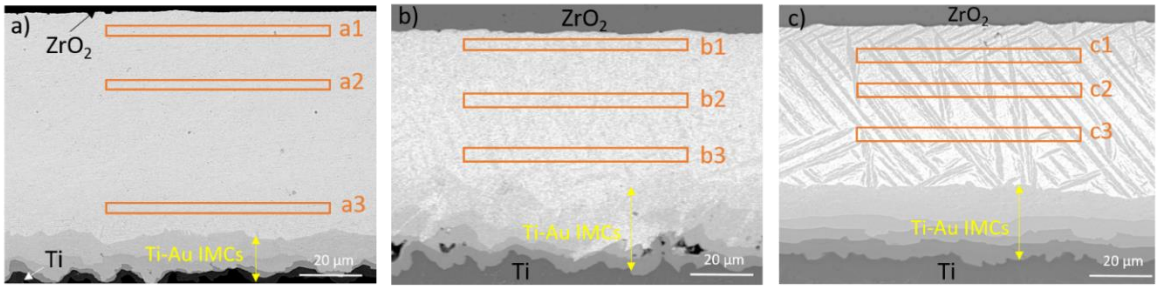

Liquid state duration: **3min**			Liquid state duration: **17min**			Liquid state duration: **1h**		
Spectra	Ti (at%)	**Zr (at%)**	Spectra	Ti (at%)	**Zr (at%)**	Spectra	Ti (at%)	**Zr (at%)**
a1	2	**10**	b1	6	**15**	c1	10	**8**
a2	3	**3**	b2	7	**6**	c2	10	**2**
a3	5	**< 1**	b3	10	**< 1**	c3	11	**< 1**

Figure 149: SEM micrographs of ZrO_2 / Au / Ti joints obtained by brazing at 1080°C for a) 3min, b) 17min, c) 60min with a 100 µm Au foil, and results of EDX analyses.

Appendix 5: Fracture surface analysis of a tensile specimen brazed without getter (at 1080°C, 3 min in liquid state, 100 µm foil)

In chapter 4 section 4.3., the fracture surface of tensile specimens brazed at 1080°C with and without getter for 3 min in liquid state are observed in order to detect the fracture zone of the joint. Figure 135a and b gives pictures of representative samples respectively brazed with and without getter. The fracture surfaces of these samples are observed by SEM. Two image- stitchings of the sample brazed with getter taken over A and B sides are shown in Figure 137. In this appendix, SEM image-stitching of the sample brazed without getter (B side), presented in Figure 150, clearly delimits the intermetallics (IMCs) zone and the Ti_xO_y zones of the fracture surfaces. The major part of the surface is composed of Ti-Au IMCs (named "IMCs zone"), and two minor parts of Ti_xO_y (named "Ti_xO_y zone"). Titanium oxide and Ti-Au IMCs are observed on both sides of the broken specimen, thus, fracture occurs mainly in the reaction layers (and not at the gold / reaction layer or substrate / reaction layer interfaces).

Thus, samples brazed with and without getter have the same aspect, with a fracture localized both in Au-Ti IMCs, and in Ti_xO_y layers.

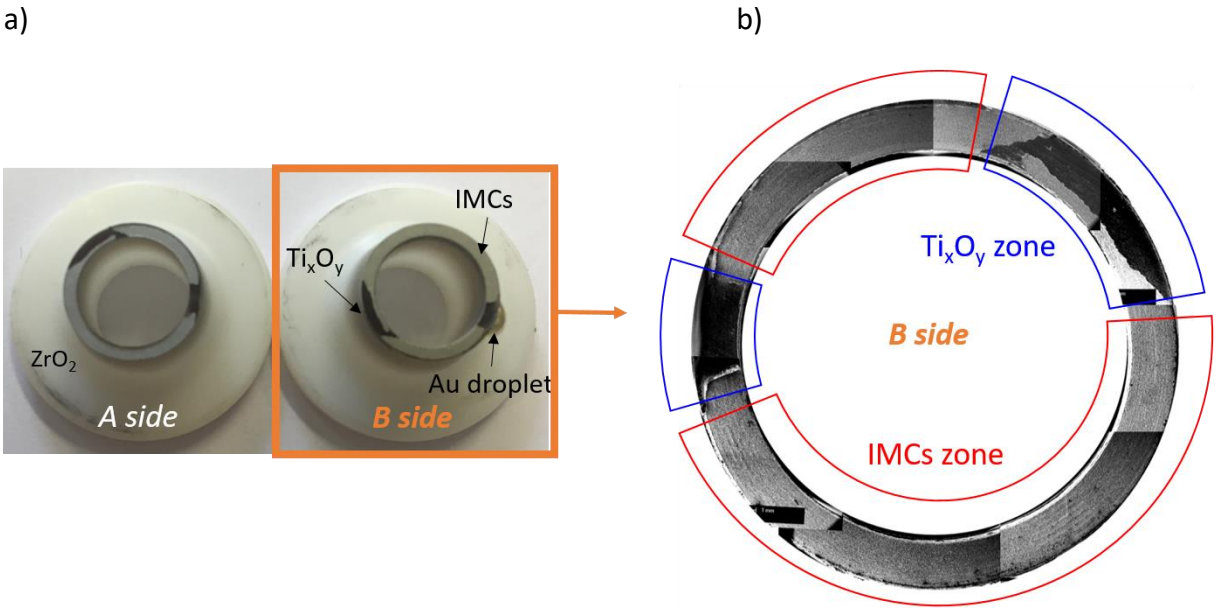

Figure 150: Fracture surface of a ZrO_2 / Ti tensile specimen brazed without getter (1080°C, 3 min in liquid state, Au foil 100 µm). a) top view photo of the broken sample, b) SEM image stitching of the B side.

Appendix references

1. T. B. Massalski, H. Okamoto & J.P. Abriata, The Au-Zr (Gold-Zirconium) system. *Bull. Alloy Phase Diagr.* **6**, 519–522 (1985).

2. H-M. Hsiao, S. M. Liang, R. Schmid-Fetzer & Y. Yen 'Thermodynamic assessment of the Ag-Zr and Cu-Zr binary systems. *Calphad* **55**, 77–87 (2016).

3. M. Li, C. CLi, F. Wang & W. Zhang Experimental study and thermodynamic assessment of the Ag–Ti system. *Calphad* **29**, 269–275 (2005).

Résumé

Dans ce travail, nous avons étudié les aspects physico-chimiques de l'assemblage ZrO_2 / Ti par brasage pour une application biomédicale (implants cochléaires), avec l'appui de la caractérisation fine (MEB, MEB-FEG, MET) pour analyser les produits réactionnels.

Dans une première partie, nous avons réalisé une étude expérimentale du mouillage et de la réactivité interfaciale des substrats zircone et titane, en mettant en œuvre les techniques de la «goutte posée» et de la «goutte déposée». Tout d'abord, nous avons investigué le mouillage de la zircone par des alliages de brasage réactifs et biocompatibles (Ag-A, Au-Sn-A et Au-A, A étant l'élément actif Ti ou Zr) entre 1066°C et 1270°C. Tous ces alliages permettent un bon mouillage de la zircone. Une étude approfondie a été effectuée avec les alliages Au-xTi (0,6 < x < 4 % massique) puisqu'ils sont les meilleurs candidats pour le brasage zircone / titane en terme de réactivité interfaciale. En effet, la couche réactionnelle Ti_xO_y mouillable formée à l'interface zircone / alliage est homogène, continue et fine (0.3 – 4 µm). Ensuite, le mouillage du titane par l'or pur a été étudié entre 1077°C et 1125°C. L'étalement non réactif de l'or sur le titane, observé durant les 10 premières millisecondes, est suivi d'un étalement réactif (dissolution et formation d'un produit réactif à l'interface) beaucoup plus long. Un très bon mouillage est obtenu quel que soit l'état de surface du substrat Ti (avec ou sans oxyde natif).

Dans une seconde partie, le brasage ZrO_2 / Ti avec l'or pur a été investigué. Le joint ZrO_2 / Au / Ti est créé grâce à la formation de produits réactionnels aux deux interfaces. A l'interface Ti / Au, quatre intermétalliques Ti-Au (Ti_3Au, TiAu, $TiAu_2$ and $TiAu_4$) et la solution solide δ-Au sont observés. La dissolution du Ti du substrat et la diffusion de Ti dans Au liquide, conduisent à la formation d'un oxyde Ti_xO_y mouillable à l'interface ZrO_2 / Au. L'oxygène est fourni par la zircone qui devient sous-stœchiométrique proche du joint. L'effet de plusieurs facteurs tels que l'épaisseur de la brasure, la température de brasage, le temps de maintien et la pression partielle d'oxygène, a été étudié dans le but de proposer des paramètres de brasage optimaux. Cette étude a été complétée par des essais de traction qui ont conduit à une contrainte à rupture moyenne de l'ordre de 56 MPa. Une relation entre la pression partielle d'oxygène dans le four de brasage et le comportement mécanique du joint a été établie expérimentalement pour la première fois.

Summary

This work deals with physico-chemical aspects of zirconia-to-titanium joining by brazing for a biomedical application (cochlear implant), mainly supported by microscopy analyses (SEM, FEG-SEM, TEM) of interfacial reaction products.

In a first section, we performed an experimental study of wetting and interfacial reactivity of zirconia and titanium substrates, using the «sessile drop» and «dispensed drop» methods. First, wetting of zirconia by the biocompatible active brazing alloys (Ag-A, Au-Sn-A and Au-A, A being Ti or Zr active element) was studied, in the temperature range 1066°C - 1270°C. Zirconia is well wetted by all these selected alloys. A comprehensive study was conducted with the Au-xTi (0.6 < x < 4 wt%) alloys, as they are the best candidates for zirconia-to-titanium brazing in terms of interfacial reactivity. Indeed, the wettable Ti_xO_y reaction product layer formed at the ZrO_2 / alloy interface is homogeneous, continuous and thin (0.3 – 4 µm). Then, wetting study of titanium substrate with pure gold was performed in the temperature range 1077 – 1125°C. The non-reactive wetting of Au on Ti, observed during the first ten milliseconds, is followed by a much longer reactive spreading stage occurring by dissolution and formation of a reaction product layer at the interface. Good wetting of Ti is obtained, whatever the surface state of the substrate (with or without native oxide).

In a second section, ZrO_2 / Ti brazing with pure gold was investigated. The joint is created thanks to the formation of reaction products at both interfaces. At Ti / Au interface, four Ti-Au intermetallic compounds (Ti_3Au, TiAu, $TiAu_2$ and $TiAu_4$) and the δ-Au solid solution are observed. Ti dissolution and diffusion into liquid Au lead to the formation of a wettable Ti_xO_y layer at the ZrO_2 / Au interface. Oxygen is provided by zirconia, becoming sub-stoichiometric near the joint. The impact of several factors such as filler metal thickness, brazing temperature, holding time and oxygen partial pressure was investigated in order to propose optimum brazing parameters. This brazing study was supported by tensile tests, leading to an average rupture stress of about 56 MPa. For the first time, a relation between the oxygen partial pressure in the brazing furnace and the mechanical properties of the joint was experimentally established.